Characterisation of bacterial multiple inositol polyphosphate phosphatases relevant to the animal feed industry

Monika Aleksandra Ziętek

PhD Thesis

School of Biological Sciences

University of East Anglia

September 2017

Word count: 64045

Registration Number: 100070975

Abstract

Phytases are enzymes that degrade phytate, the main storage form of phosphorus in plants. Animal feed industries use plant-based feed with abundant phytate content. Without the supplementation with phytases, the animals would not be able to access the phosphorus in the form of phosphate stored in the phytate molecule.

This thesis describes research carried out to characterise a group of bacterial phytases from *Bacteroides thetaiotaomicron, Bifidobacterium infantis* and *Bifidobacterium pseudocatenulatum* with comparisons to an existing commercial phytase, Quantum Blue. The enzymatic properties, product profiles, binding and thermostability were examined and the structure of the binding site at various stages of the catalytic cycle was investigated with the aid of active site mutagenesis. X-ray structure of the active site mutant helped elucidate the structure of the intermediate and product-bound forms of the *Bifidobacterium infantis* phytase. Further mutagenesis experiments examined the function of disulphide bridges in the enzyme.

The experimental results described in this work provide novel insights into the hydrolysis of phytate by bacterial phytases, the conformational changes during the catalytic cycle and the contribution of disulphide links to thermostability of the enzyme. These results lay the foundations of the work toward optimisation of phytases for use by the industry of the animal feed supplements.

Acknowledgments

I would like to extend my sincere gratitude to my supervisors, Dr Charles Brearley and Dr Andrew Hemmings, for their unending support and guidance throughout my PhD and for the vast amount of scientific knowledge and expertise they shared with me. I am also grateful to AB Vista, the industrial sponsor of my project.

Thank you to Dr Gabriella Kelemen for the advice, believing in me and helping me persevere.

Thank you to my lab mates and colleagues from Bio for their support, shared knowledge and good times. Special shoutouts to Saannya Sequeira, Elena Tan and Sundeep Kaur for the comic relief.

Last but not least, I would like to thank my partner Greg and my Grandma: dziękuję za Wasze niewyczerpane wsparcie, cierpliwość i zrozumienie podczas mojego doktoratu.

List of Abbreviations

abbreviation	meaning
ATP	Adenosine triphosphate
Bl	*Bifidobacterium longum* subsp. *infantis* ATCC 15697 phytase
Bp	*Bifidobacterium pseudocatenulatum* phytase
BPP	Beta-propeller phytase
Bt	*Bacteroides thetaiotaomicron* phytase
D1, D2, D1D1	Bl phytase disulphide knock out mutants
ddH_2O	double distilled water
DSC	Differential Scanning Calorimetry
DSF	Differential Scanning Fluorimetry
FTU	One phytase unit is the amount of enzyme needed for the release of 1 µmol of inorganic orthophosphate from the substrate in one minute under the standard reaction conditions of pH 5.5 and 37°C.
HAP	Histidine acid phosphatase
HAE	Subgroup of the HAP phytases with HAE proton donor motif
HPLC	High-performance liquid chromatography
IP_1	*myo*-inositol monophosphate
IP_2	*myo*-inositol bisphosphate
IP_3	*myo*-inositol trisphosphate
IP_4	*myo*-inositol tetrakisphosphate
IP_5	*myo*-inositol pentakisphosphate
IP_6	*myo*-inositol hexakisphosphate, phytate, phytic acid
IS_6	*myo*-inositol hexasulphate
LB	Lysogeny broth
MINPP	Multiple inositol phosphate phosphatase
PAP	Purple acid phosphatase
SDS-PAGE	Sodium dodecyl sulfate polyacrylamide gel electrophoresis
QB	Quantum Blue phytase

Table of Contents

Table of Figures

List of Tables

1 Introduction

1.1 Environmental factors concerning phosphorus

Phosphorus is crucial for every organism as a key component of nucleic acids, cell signalling components, ATP and other cellular components necessary for survival (Abelson, 1999). In normal circumstances, it is abundantly present in soil in the form of mineral phosphates, and a fraction of this is available for soil-dwelling organisms to absorb. It then travels up the food chain, thus getting incorporated into all organisms. Aggressive farming strategies focused on maximising animal growth within shorter time and with lower costs necessitate the addition of external phosphorus to the soil for replenishment in the form of fertilizers. Phosphorus for fertilizers is sourced from phosphorus rock. By various estimates, it is suspected to be in risk of depletion by year between 2050 to 2410 (Steen, 1998; Gilbert, 2009; Cordell and White, 2011).

Plant uptake of phosphorus as phosphate is limited, and as such fertilizers often contain a phosphate as mono- or diammonium salt. Inositol hexakisphosphate, phytate, is the major storage form of phosphate in storage organs of plants such as seeds, beans and tuber. Phosphorus constitutes around 3-7 mg/g of dry weight of typical animal feed made of wheat or soybean seeds, and, of this phosphorus, phytate comprises around 75 +/- 10% (Raboy, 1997, 2003). Consequently, animal feedstuffs derived from plants contain high levels of phytate. Much of the phosphate, however, is not available for the nutrition of non-ruminant animals, because convention has it that the animals do not have enough of the enzymes in the right part of the digestive tract necessary to degrade phytate. Consequently, farmers supplement the plant-based animal feed with expensive phosphorus supplements or with enzymes, phytases, capable of mobilizing phosphate from phytate during passage of feed through the gastro-intestinal tract. In the absence of phytase addition to feed, a large proportion of phosphorus from feed is output to the environment as animal waste (Turner, Richardson and Mullaney, 2007; Gilbert, 2009).

It is widely assumed that phytate outputs to the environment are mineralised by phytases present in the environment. Possible sources of phytase in the environment are plants, bacteria, fungi as well as secreted mucosal phytases in the small intestine and gut

microbial phytases (Kumar *et al.*, 2010). Since beta-propeller phytases are largely abundant in soil, the *Bacillus* bacteria are a possible candidate for the organism responsible for the eutrophication of waterways resulting from animal waste phytate dephosphorylation (Lim *et al.*, 2007; Huang *et al.*, 2009). Extensive metagenomics experiments would be needed to verify which organisms in particular are present and expressing the candidate phytase genes in the areas with high phosphorus soil and water content (Neal *et al.*, 2017).

Several economic and environmental factors are drivers of practice to limit phosphorus usage and waste. As mentioned, phosphorus sources are limited and are depleting at a significant rate. In the meantime, phosphate rock mining often leaves behind toxic waste containing heavy metals, that tend to contaminate local groundwater unless thoroughly contained. Undigested phosphorus from animal farms adds to the water pollution. On top of this, the economic toll of waste phosphorus demands solutions for increasing the efficiency of that substance (Turner, Richardson and Mullaney, 2007; Tarayre *et al.*, 2016).

Due to its structure and strong negative charges, phytate chelates minerals and binds proteins easily. During digestion, this makes these nutrients unavailable (Konietzny and Greiner, 2004). The anti-nutritive effect of phytate in diet is further enhanced by phytate's ability to precipitate proteins, causing them to become insoluble and thus reduce their digestibility (Vohra and Satyanarayana, 2003). By complexing calcium ions, phytate and IP_5 can inhibit enzymes such as amylase, trypsin, acid phosphatase and tyrosinase, leading to decreased digestibility of nutrients such as starch (Harland and Morris, 1995; Sajjadi and Carter, 2004)

Various approaches can be employed to enable digestion of phytate and facilitate phosphorus uptake. One way is to investigate and optimise the phytate-digesting enzymes, phytases, added into animal feed. Indeed, there is a large phytase industry for feedstuffs which in 2010 was valued at circa $725 million and was projected to reach $1 billion by 2017 (Pandey, Negi and Socco, 2016). The inclusion of phytases has already proven beneficial in terms of economy, ecology as well as scientific progress. It is estimated that utilisation of phytase by the monogastric industries saves $3 billion a year in feed costs (*Understanding the value chain of phytate*, 2017).

1.2 Overview of phytate and phytases

Phosphorus in the form of phytate can be utilised by ruminant animals because of their specific microbial flora. Bacteria such as *Selenomonas ruminantium* and *Mitruokella jalaludinii* are ruminant bacterial species possessing high phytase activity, allowing for phytate digestion and improving availability of minerals in plant-based feed in ruminants (Lan *et al.*, 2011). At the same time, non-ruminant, monogastric, animals including humans, poultry and swine do not possess the molecular machinery allowing them to efficiently utilise phytate in any advantageous amounts (Holm, Kristiansen and Pedersen, 2002). As such, the phytate passes unabsorbed through the digestive system and especially in areas with intense farming environments, leads to phosphate pollution in ground waters (Sharpley, 1999).

Myo-inositol hexakisphosphate (*myo*-IP_6 or phytate) is one of the most abundant identified forms of organic phosphorus in the environment. It comprises up to 90% of phosphorus content in soils. The humic fraction of soils is the principal other organic fraction, but the composition of this humic fraction is wholly undefined. Other isomers of IP_6 such as *scyllo,* D-*chiro* and *neo* constitute around 1-50 %, 10 % and 1 % soil phosphorus content respectively (Giles, Cade-Menun and Hill, 2011). The prevalence of inositol hexakisphosphates in soil can be explained by their adsorption by ligand exchange between phosphate groups of IP_6 with reactive hydroxyls on the surface of rocks, as well as reacting with iron (Ognalaga, Frossard and Thomas, 1994).

Phytate is a salt of the phytic acid, whose chemical term is myo-inositol 1,2,3,4,5,6-hexakisphosphate (abbreviated to InsP6 or simply IP6). Phytases are a group of enzymes termed myo-inositol 1,2,3,4,5,6-hexakisphosphate phosphohydrolases. In nature, they mediate the breakdown of phytate by hydrolysis into myo-inositol pentakisphosphate (InsP5 or simply IP5) and phosphate (also called orthophosphate to underline the loss of all three hydrogen atoms from the phosphate group) (Turner, Richardson and Mullaney, 2007) as shown in Figure 1.1 below.

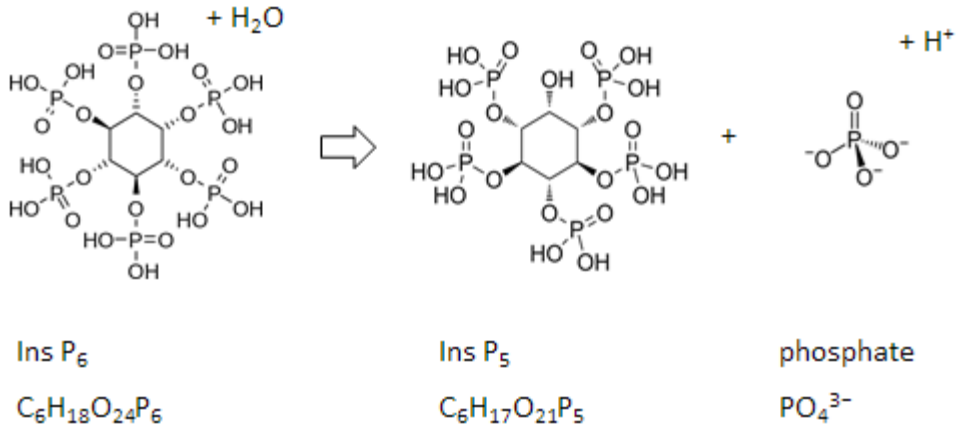

Figure 1.1 Outline of phytase-catalysed phytic acid hydrolysis.
Phytase catalyses the degradation of phytate (IP_6) into IP_5, releasing inorganic phosphate.

After the initial production of IP_5, the phytate degradation process continues further, releasing phosphate in a step-wise manner. This system uses the newly-formed products as substrates in the consecutive phosphate hydrolysis reactions.

The Nomenclature Committee of the International Union of Biochemistry recommend a particular way of numbering the phosphates in the inositol phosphate according to their position regarding the axial group. Following the D- and L- nomenclature, D- numbering of IP_6 begins on the carbon to the right of the axial phosphate position, as seen in Figure 1.2. The axial phosphate is always on position 2 in both D- and L- naming conventions. The D- numbering then proceeds anticlockwise around the inositol ring. The L- nomenclature begins to the left of the axial group and proceeds clockwise (Angyal, 1989; Majumder and Biswas, 2006).

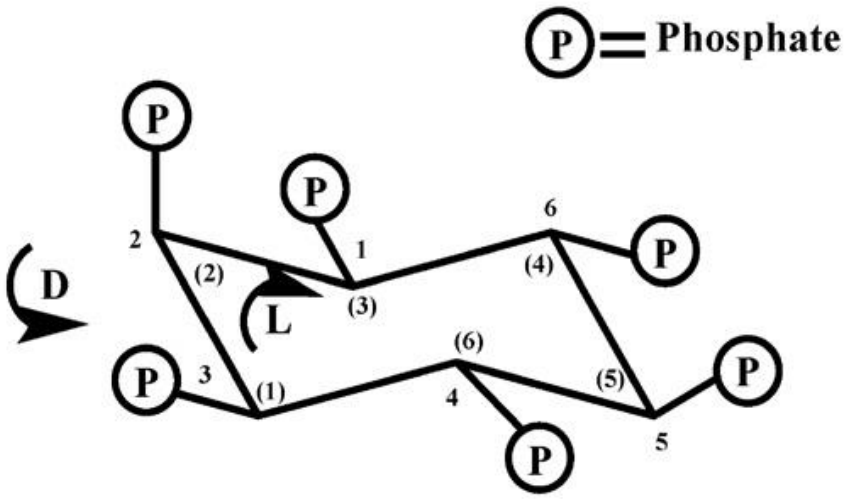

Figure 1.2 D- and L-nomenclature conventions of inositol phosphates.
D- nomenclature starts the numbering from the carbon to the right of the axial phosphate and continues anticlockwise. L- nomenclature begins on the carbon on the left of the axial group and proceeds clockwise (image from Sun *et al.*, 2017).

Similarly to the amino acid naming convention, whereby the symbol Ala in the biochemical work is taken to signify L-alanine ('IUPAC-IUB Joint Commission on Biochemical Nomenclature (JCBN). Nomenclature and symbolism for amino acids and peptides. Recommendations 1983.', 1984), the symbol Ins was proposed to refer to a *myo*-inositol phosphate with the D- numbering, unless the prefix L- is explicitly shown (Angyal, 1989; Majumder and Biswas, 2006). The stereospecific numbering is crucial to make clear the enantiomeric relationships. These are important in elucidating the metabolic pathways involving the inositol phosphates. The different enantiomers serve diverse physiological functions in the cell, including channel physiology, membrane dynamics and nuclear signalling (Irvine and Schell, 2001).

The *myo*-inositol hexakisphosphate isomer of IP_6 is the most abundant form of IP_6 in soil (Giles, Cade-Menun and Hill, 2011). Its most stable conformation is the 'chair' conformation, where the phosphate on carbon 2 is oriented axially and the remaining five phosphates are equatorial. This conformation has been likened to a turtle, which can be used as a visual mnemonic to keep nomenclature of IP_6 phosphates consistent, as shown in Figure 1.3 below (Agranoff, 2009).

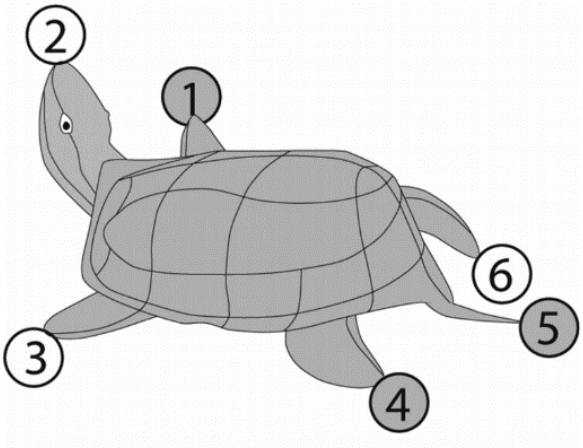

Figure 1.3 Agranoff's turtle – a visual mnemonic for consistent naming of inositol phosphates.
Phosphate on D1-position is the turtle's right flipper, with the head being the axial phosphate on 2-position (image from Agranoff, 2009).

With respect to phytase action, the axially oriented 2-phosphate is the only stable phosphate in *myo*-inositol hexakisphosphate, with the remaining five being scissile phosphates. The scissile phosphates can be removed by most phytases under the right conditions to some extent. The recalcitrant 2-phosphate can only be detached by a small group of phytases, mostly of the beta-propeller group (Wyss *et al.*, 1999; Shin *et al.*, 2001; Adeola and Cowieson, 2011).

As research into phytates and phytases progressed, increasing numbers of new members of these protein families were discovered. Each of those have different physiological functions and various interactions with one another. New insights are underway to improve the understanding of the phytases, their underlining mechanisms, substrates, products and the potential real-life applications (Turner, Richardson and Mullaney, 2007; Adeola and Cowieson, 2011).

1.3 History of phytases

Phytic acid was first mentioned in a scientific publication in 1903 and in 1907 the first scientific reference to a phytase enzyme was reported (as reviewed in Lei *et al.*, 2013; Turner, Richardson and Mullaney, 2007, pp. 61, 97). Phytin, the calcium and magnesium

salt of phytate, was shown to be abundant in the entire seeds of corn, oat and barley, while in wheat it was thought to localise only to the outer layers of the seed (Hart and Tottingham, 1909). Soon after, it was confirmed that a phytase enzyme is present in wheat bran, which degraded phytins into inorganic phosphate as well as several lower inositol phosphates (Anderson, 1915). Over the course of the twentieth century the research into phytases progressed slowly, due to the apparent lack of cost benefits of using phytase over supplemental phosphorus in farming practices (Shivange and Schwaneberg, 2017). Thus, farmers used large amounts of increasingly expensive inorganic phosphate supplementation to meet the dietary needs of the monogastric animals, which lead to progressive pollution of the environment with undigested phosphorus (Lei *et al.*, 2013).

In the meantime, multiple microorganisms were discovered to produce phytases to allow them to utilise phytate *in vivo.* For example, *Aspergillus, Penicillium* and *Mucor* species were found to produce phytases, with increasing production in conditions of limited inorganic phosphate (Shieh and Ware, 1968). In addition, between the 1960's and 1970's phytases were found to be produced by microorganisms such as *Aerobacter, Bacillus, Pseudomonas* and various plants (Irving and Cosgrove, 1974).

Fishmeal was a major source of protein for animal producers, however with the increasing global demands and food shortages, fishmeal gradually became less cost-effective. As aquaculture producers began to increasingly substitute the fish diets with plant-based feed (Rumsey, 1993; Fontaínhas-Fernandes *et al.*, 1999; Khan, Siddique and Zamal, 2013; Kushwaha, 2013), the need for phytase supplementation grew (Turner, Richardson and Mullaney, 2007, p. 97).

Eventually in 2008 the demand for phosphate-based fertilisers increased drastically in India and China. This, together with the record energy prices contributed to the cost of phosphorus production from phosphate rock to increase to 500 % of its 2007 value (Gilbert, 2009). Together with the raised environmental awareness and the worldwide introduction of agricultural pollution control, it brought phytases into the limelight.

1.4 Classification of phytases

Typically, enzyme classification is carried out according to the enzyme's *in vivo* function. Since up to recently, the *in vivo* function of phytases was largely unknown (Konietzny and Greiner, 2002), their classification as phytases was based on the *in vitro* behaviour of the enzyme (Turner, Richardson and Mullaney, 2007). Phytases belong to the group of phosphomonoesterases (EC 3.1.3). They show high diversity in size, catalytic mechanism, biochemical properties and structure – in particular, the active site elements (Oh *et al.*, 2004). There are different ways to further classify phytases, based on their exact mechanism of action, substrate specificity or size. These methods of classification are more or less arbitrary and in some cases contradict each other. Below is an attempt at classifying them according to standards presented in literature.

1.4.1 Phytase classification based on the structure of the active site and the catalytic mechanism

Enzymes displaying phytase activity can be divided into four groups based on their common biochemical and catalytic mechanisms, while maintaining a broad diversity of structures and active sites. These are histidine acid phosphatases (HAPs), cysteine phosphatases, beta-propeller phytases (BPP) and purple acid phosphatases (Turner, Richardson and Mullaney, 2007). These enzymes utilise different catalytic mechanisms to dephosphorylate IP_6 with optimal activities in various different conditions. Specifics of these classes are discussed in detail further in section 1.4.

1.4.2 Phytase classification based on the site of the initial phosphate hydrolysis

Phytases can be classified into four subgroups, depending on the specificity of the initial phytate hydrolysis. Hence, as recognised by the International Union of Pure and Applied Chemistry and the International Union of Biochemistry, the 3-phytases (EC 3.1.3.8)

catalyse the dephosphorylation of phytate starting on the position D3 on the inositol ring and are common in microorganisms. The 6-phytases begin the catalysis on position L6/D4 (EC 3.1.3.26) and commonly originate from seeds of higher plants (Turner, Richardson and Mullaney, 2007). However, there are a few unique phytases with other initiation positions. The lily pollen phytase begins its hydrolysis from the 5 position, which bears the same numbering whether the D- or L-nomenclature is used (Barrientos, Scott and Murthy, 1994) and the *E.coli* phytate-degrading enzyme P2 initiates the hydrolysis at the D6/L4 position (Greiner, Konietzny and Jany, 1993; Greiner, Carlsson and Larsson, 2000).

To date, no D1-phytases nor 2-phytases have been found as evidenced by literature searches as well as the databases of the NC-IUBMB (Nomenclature Committee of the International Union of Biochemistry and Molecular Biology, 2017) and BRENDA (BRENDA. The Comprehensive Enzyme Information System, 2017). The apparent absence of 2-phytases can be explained by the fact that the 2-phosphate is located axially, which makes it recalcitrant to cleavage by phytases. Phytases preferentially remove the equatorial phosphates (Wyss *et al.*, 1999) and it is rare for a phytase to be able to dephosphorylate the 2-phosphate at all (Adeola and Cowieson, 2011).

1.4.3 Phytase classification by broad and narrow substrate specificity

The nature of the substrate specificity of phytase and phosphatase enzymes differs not only between genera, but also between species within one genus. The differences are apparent despite the high degree of amino acid sequence homology between the fungal phytases mentioned below. For example, the HAP phytases of *Aspergillus niger* and *Escherichia coli* demonstrate narrow substrate specificity, with high specific activities against phytate and to a lesser extent lower inositol phosphates, and with minimal activities against other phosphate-containing substrates. When reacted with phytate, they accumulated IP_3s and IP_2s. Their reactivity with IP_1 was low (Wyss *et al.*, 1999).

On the other hand, the HAP phytases of *Aspergillus fumigatus* and *Aspergillus nidulans,* together with the pH 2.5 acid phosphatase of *A. niger* show broad substrate specificity, being able to catalyse dephosphorylation of a wide range of substrates not necessarily

related to phytate in structure. These phytases had the highest specific activities for fructose 1,6-biphosphate, phenyl phosphate, para-nitrophenyl phosphate and others. They showed a lesser degree of activity against phytase than the narrow substrate specificity phytases. However, when reacted with phytate, they showed lower accumulation of lower inositol phosphates than the narrow substrate specificity phytases, mainly accumulating Ins2P. Additionally, they cleaved Ins1P more readily (Wyss *et al.*, 1999).

The specificity of phytases for substrates reflects how actively they react with phytate, since the narrow-specificity phytases showed higher activity with phytate and *vice versa.* Despite these differences, when present in excess, the reactions of fungal and *E.coli* phytases had the same final product of phytate degradation, namely Ins2P. This demonstrates strong stereospecificity between the different phytases, while maintaining different preferences for the site of the initial hydrolysis (Wyss *et al.*, 1999).

While this thesis will discuss structural features of a particular histidine acid phosphatase from *Bifidobacterium longum* MINPP (*Bl*Minpp) in detail later, it is relevant here to note that residues 300 and 301 in the narrow substrate specificity *A. niger* phytase are conserved between other fungal phytases, showing either narrow or broad substrate specificity. Significantly, while residue 301 is a highly conserved lysine, the residue 300 varies with a certain trend. Most narrow specificity phytases that were investigated had an aspartate on residue 300, while the broad specificity phytases mostly had a glycine. However, residue 300 on the *A. niger* phytase is a lysine. Upon substitution mutation K300E the enzyme's specific activity against phytate was enhanced (Mullaney *et al.*, 2002).

Bacillus phytases, as members of the structurally different to HAP's group of beta-propeller phytases, do not fit well into the distinction of broad and narrow substrate specificities. They display high specificity for IP_6, however with lower specific activity than the narrow-substrate specificity HAP's (Shimizu, 1992; Kim, Kim, *et al.*, 1998), as shown in Table 1.1 below.

Organism	substrate specificity for IP_6	Specific activity (U/mg)	Specific activity (nKat/mg)
Aspergillus niger	narrow	102.5	1708.7
Aspergillus terreus	narrow	142-196	2367.1 - 3267.3
Aspergillus fumigatus	broad	23-28	383.4 - 466.8
Emericella nidulans	broad	29-33	483.4 - 550.1
Escherichia coli	narrow	811	13519.4
Bacillus spp DS11	narrow	20	333.4
Bacillus subtilis natto	narrow	8.7	145.0

Table 1.1 Substrate specificity and specific activity in relation to IP_6 of a representative selection of phytases.
Showing specific activity in enzyme units (amount of enzyme that releases 1 µmol of inorganic phosphate per minute) per mg of protein and nanokatals (amount of enzyme that releases 1 µmol of inorganic phosphate per second) per mg of protein (Shimizu, 1992; Kim, Kim, *et al.*, 1998; Wyss *et al.*, 1999).

It is possible to estimate the extent of an enzyme's substrate specificity using the Broad Substrate Specificity Estimator (BRASS). This method relates the existence of residues and motifs similar to that of the active site of the enzyme to the increased breadth of substrate specificity. Such 'duplicate' residues are thought to create electrostatically similar scaffolds for related substrates to bind and undergo catalysis. Indeed, this analysis was congruent with experimental data on four different enzymes (Chakraborty, Ásgeirsson and Rao, 2012).

The above techniques could be employed in manipulating phytases for use in the industry, where it might be necessary to alter or enhance the substrate specificity of the enzymes. Phytases with broad substrate specificities might be more suited for feed additives in animal nutrition due to them readily hydrolysing most phosphates of phytate (Wyss *et al.*, 1999). On the other hand, narrow substrate specificity phytases would be an advantage when introducing them into plants, to maintain the plants' metabolic pathways intact (Konietzny and Greiner, 2004).

1.4.4 Phytase classification by pH optima

Phytases with their pH optima of around pH 5 can be classed as acid phytases, while those with pH optima of around pH 8 are alkaline phytases. Most studied phytases fall within the acid phytase group and have a narrow pH optimum of between pH 4.5-6.0. An exception is the *A. fumigatus* phytase, which displays a broad pH optimum of pH 4.0-7.3. Presence of phosphate is known to strongly inhibit transcription and activity of phytases. The acid phytases are capable of accepting lower inositol phosphates as substrate in addition to phytic acid. In most cases if the reaction is allowed to proceed to completion, the final product of these phytases is Ins2P, with only rare occurrences of free *myo*-inositol (Wyss *et al.*, 1999; Konietzny and Greiner, 2002). Typically, the acid phytases show broad substrate specificity, being able to accept several phosphate containing compounds in addition to metal-free phytate (Oh *et al.*, 2004).

Alkaline phytases are less abundant. They tend to display narrow substrate specificities, being highly active against calcium-bound phytate (Oh *et al.*, 2004). Those with the pH in the range of 6.0-8.0 have been identified in bacteria. Phytases with the pH optima of around pH 8.0 have been found in legume seeds, lily pollen, cattail and rat intestine. These alkaline phytases often only accept IP_6, IP_5 and IP_4 as substrate, accumulating IP_3 as the end product (Konietzny and Greiner, 2002, 2004). However, the alkaline *Bacillus* phytase is capable of removal of all phosphates, yielding *myo*-inositol as the end product (Shin *et al.*, 2001).

1.4.5 Histidine acid phosphatase phytases

Histidine acid phosphatase (HAP) phytases are widely spread across kingdoms, being present in animals, plants and microorganisms (Turner, Richardson and Mullaney, 2007, p. 98). They share a common catalytic mechanism, conferred by the particular amino acid sequence making up their active site. The N-terminal HAP consensus sequence consists of the motif RHGXRXP (Ullah, Cummins and Dischinger, 1991; Van Etten *et al.*, 1991) and works in concert with the C-terminal motif HD or HAE. The amino acid sequences and sequence alignments are shown in Appendix 1 and 2.

1.4.5.1 HAP phytase general structure

HAP phytases show a conserved HAP fold consisting of a large alpha-beta domain and a smaller alpha-domain. The alpha-beta domain consists of a central six-stranded twisted beta-sheet with two alpha-helices flanking it on both sides. The active site lies in the large cavity on the interface of the two domains, with the central two of the alpha domain's several helices forming a part of it (Lim *et al.*, 2000; Ariza *et al.*, 2013). Furthermore, all HAP enzymes have a conserved disulphide bridge forming the C-terminal loop linker (Lee *et al.*, 2003; Böhm *et al.*, 2010), visible at the bottom of Figure 1.4 below .

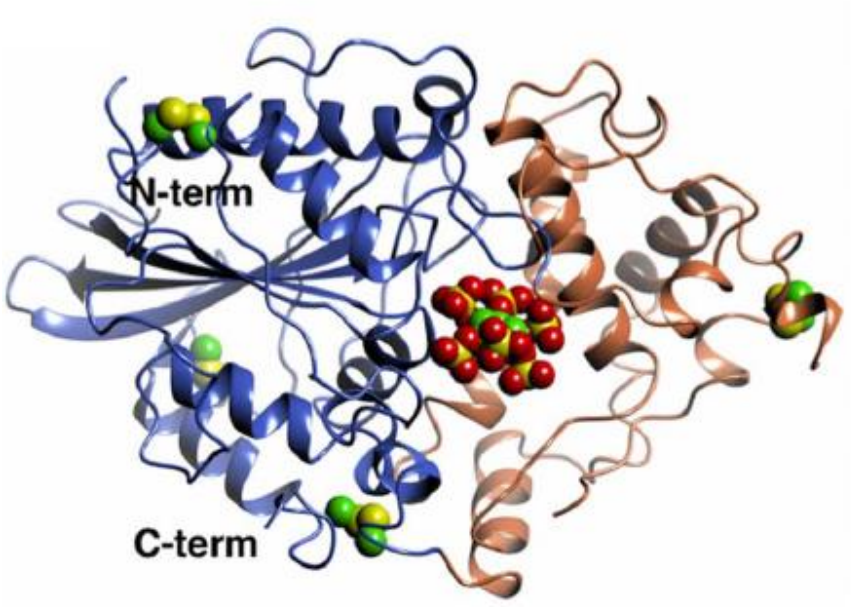

Figure 1.4 Ribbon representation of the structure of the *Hafnia alvei* HAP phytase in complex with inositol hexasulphate.
The alpha domain is shown in orange and the alpha-beta domain is shown in blue. The disulphide bridges are shown in green and yellow in ball formats (image from Ariza *et al*., 2013).

Except for the conserved C-terminal loop linker, the number and location of any other disulphides vary between HAPs (Böhm *et al.*, 2010). Cysteines and disulphides from the *A. ficuum* phytase were analysed spectroscopically using the Ellman's reagent. It was shown that all ten cysteines form disulphides and that the disulphide bridges are crucial not only for the structural stability, but also for the catalysis (Ullah and Mullaney, 1996). Similarly, the catalytic activity and conformational stability of phytase from *A. niger* were analysed in the presence and absence of a cysteine reducing agent DTT. A loss of activity followed the removal of the disulphide bonds, suggesting that disulphide bridges play an important role in catalytic ability of the enzyme as well as its structure (Wang, Meng and Zhou, 2004)

The *Klebsiella* HAP phytase has a total of three disulphide bridges involving all of its six cysteines (Böhm *et al.*, 2010). Its disulphides are fully conserved with the HAP glucose-1-phosphatase's disulphides (Lee *et al.*, 2003). The human prostatic acid phosphatase is a non specific phosphomonoesterase that has a very similar structure to the *Klebsiella*

phytase. It contains the C-terminal linker in addition to other disulphides absent from the *Klebsiella* phytase (Van Etten *et al.*, 1991; Böhm *et al.*, 2010).

Fungal HAP phytases show a conserved eight-cysteine motif, as is apparent from the cysteine distribution and the disulphide bridge pairing. It was shown to be essential in the formation of disulphide bonds and overall stability rather than catalysis, however it could indirectly impact catalysis by providing the structural scaffold that allows the maintenance of the active site. Furthermore, all phytases originating from the filamentous ascomycete group of fungi, such as *A. niger* and *A. fumigatus,* have an additional pair of conserved cysteines at the N-terminus, which are highly likely to form a disulphide bridge. As disulphide bridges are considered to confer structural stability and thermostability, it can be assumed that this additional conserved disulphide is responsible for the higher stability of *Aspergillus* phytases (Mullaney and Ullah, 2005).

1.4.5.2 HAP phytase catalytic mechanism

The catalytic mechanism of HAP phytases consists of two steps, illustrated in Figure 1.5 below. First, the ε2 nitrogen on the catalytic histidine from the conserved N-terminal RHGXRXP motif carries out a nucleophilic attack with its lone electron pair on a phosphorus of the substrate (Ostanin *et al.*, 1992). Thus, the substrate transfers a phospho group to the enzyme by forming a covalent bond. Meanwhile, the HAE or HD motif containing the proton donor glutamate or aspartate, respectively, provides the proton to the leaving group as a general acid. This allows the creation of the phosphohistidine intermediate. In the second step of catalysis the deprotonated active site glutamate or aspartate now acts as a general base after losing its proton, which allows it to attack a water molecule. This allows the activated water to interact with the phosphohistidine intermediate, breaking its phosphamide bond and freeing the phosphate group as the product: inorganic phosphate (Ostanin and Van Etten, 1993; Lindqvist, Schneider and Vihko, 1994; Porvari *et al.*, 1994; Liu *et al.*, 2004; Ariza *et al.*, 2013; Stentz *et al.*, 2014).

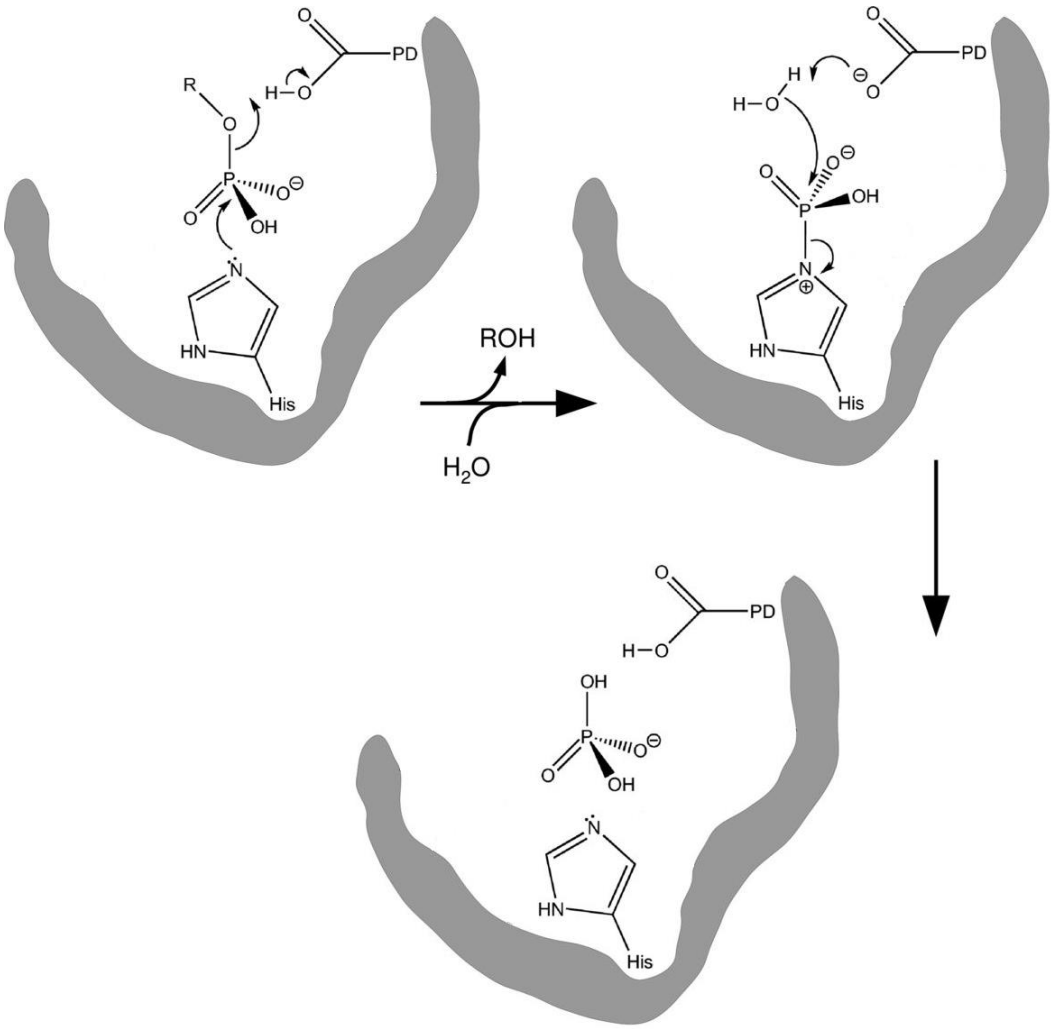

Figure 1.5 The two-step catalytic mechanism of histidine acid phosphatases.
The catalytic histidine on the enzyme conducts a nucleophilic attack on the phospho group of the substrate. A phosphohistidine intermediate is formed. The active site glutamate or aspartate residue acts as a proton donor, attacking a water molecule, which attacks the phospho group of the phosphohistidine to generate free phosphate. The phospho group disassociate from histidine, yielding free phosphate.

The need for the proton donor in the catalytic reaction can explain the acidic pH optima of the histidine acid phytases. Until recently, HAP phytases were known to rely on catalytic aspartate residue for proton donation. However, Stentz et al. (Stentz *et al.*, 2014) characterised a new type of HAP phytase produced by the human commensal gut bacteria *Bacteroides thetaiotaomicron*. This phytase was shown to have an HAE tripeptide in place of the typical HD motif, likely using glutamate instead of aspartate as proton donor during the catalytic reaction.

1.4.5.3 HAP phytase structure of the active site

Lim *et al.*, (2000) determined the crystal structure of an acid phosphatase from the periplasm of *E.coli.* The enzyme showed high substrate specificity for IP_6 and was known to exhibit an exceptionally high activity. Because of the high specificity, the acidic pH optima and the conserved active site sequence motif RHGXRXP, the enzyme was identified as an HAP phytase. The nucleophilic histidine of the active site was substituted with an alanine residue to create an inactive mutant. Crystals were soaked with phytate at pH 5.0, close to the optimum pH of the enzyme of 4.5. X-ray diffraction data was collected at 2.05 Å.

The side chains of the two conserved RHGXRXP motif arginines Arg 16 and Arg 20, along with the conserved downstream Arg 92, His 303 and the amide nitrogen of Asp 304 were shown to coordinate the binding of the scissile phosphate as shown in the Figure 1.6 below.

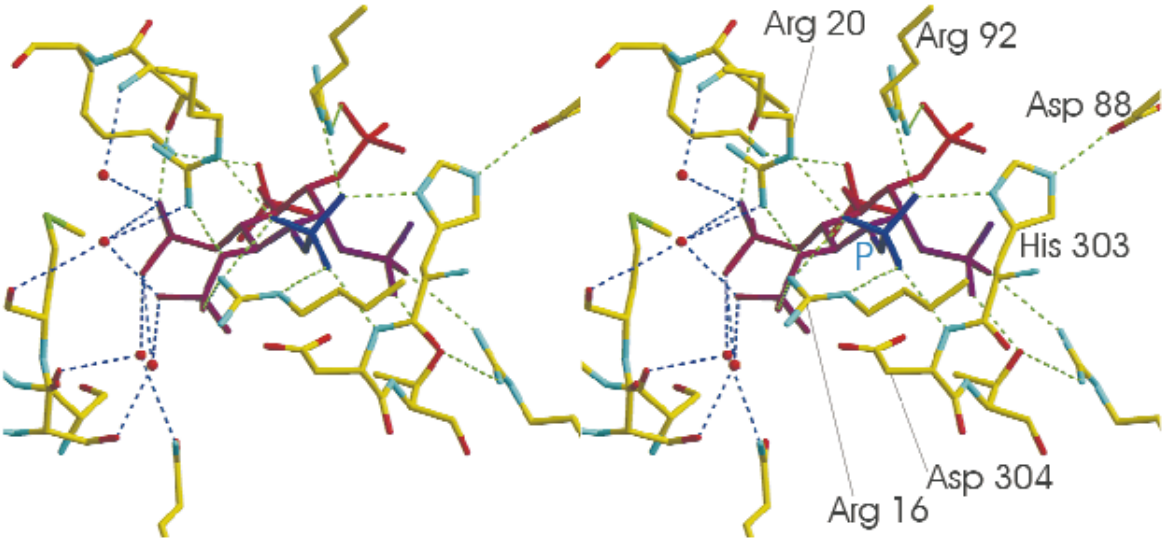

Figure 1.6 Active site structure of an inactive mutant of *E.coli* phytase with phytate bound.
The scissile phosphate at position L3 is coordinated by the side chains of conserved Arg 16, Arg 20, Arg 92 and His 303 and the amide nitrogen of Asp 304 (image from Lim *et al.*, 2000).

The residues taking part in coordination of phosphate in the active site are conserved in HAP phytases. This is shown by many published structures, for example the rat prostatic phosphatase at 3 Å (Schneider, Lindqvist and Vihko, 1993), human prostatic acid

phosphatase at 2.9 Å (Lacount, Handy and Lebioda, 1998), *Aspergillus niger* phytase at 2.4 Å (Kostrewa *et al.*, 1999) and a *Klebsiella* ASR1 phytase at 1.7 A ˚ (Böhm *et al.*, 2010).

Lim et al. (2000) also obtained the structure of the active enzyme with tungstate bound to the active site by growing crystals of protein containing 1.5 mM Na_2WO_4. The position of tungstate here was similar to the position of phosphate in the inactive enzyme structure with phytate. Therefore it could be a reliable model, allowing for visualisation of the native active site conformation with phosphate bound. The structure showed the side chain of the catalytic His 17 from the RHGXRXP motif being hydrogen bonded with the carbonyl oxygen of Gly 18, allowing the histidine to assume the position for a nucleophilic attack, as shown in the figure below.

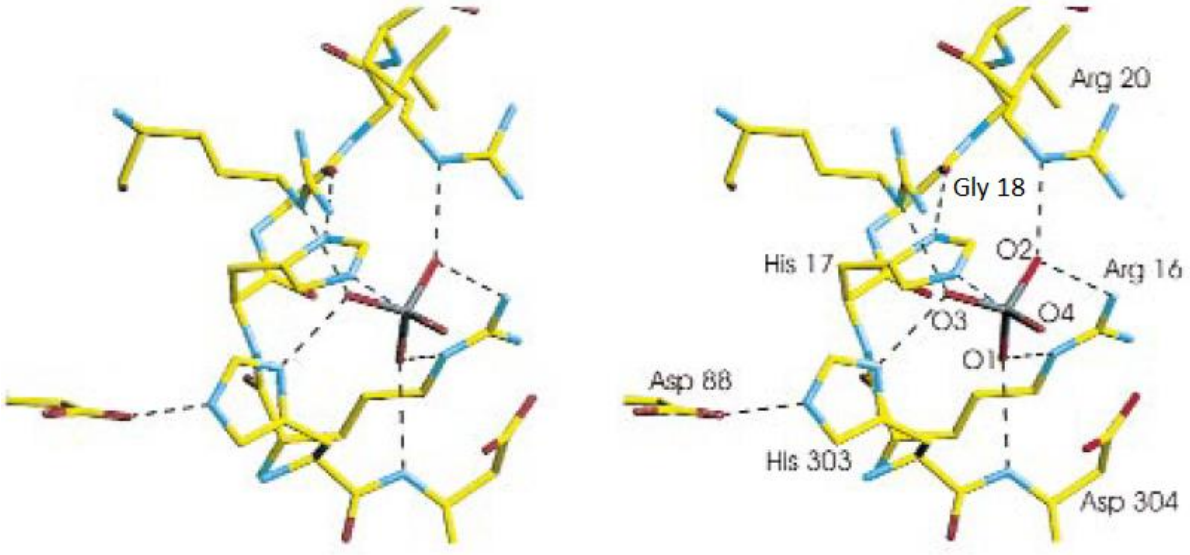

Figure 1.7 Tungstate binding to the active site of the *E.coli* phytase.
Carbonyl oxygen of Gly 18 hydrogen bonds to catalytic His 17, orienting it for a nucleophilic attack (modified image from Lim *et al.,* 2000).

The same phenomenon is reported in the 1.7 A ˚ resolution structure of an HAP *Klebsiella* phytase. The δN atom of the imidazole group of histidine creates a hydrogen bond with the backbone oxygen of glycine residue of the HGXRXP motif (Böhm *et al.*, 2010).

Previous studies by Greiner, Konietzny and Jany (1993) show the *E.coli* phytases to initiate hydrolysis preferentially at the D6/L4 position, and to a lesser extent at the D1/L3 position. Lim et al. (2000) obtained a structure of the inactive phytase with IP_6 bound with

its L3 phosphate positioned in the active site as shown in figure 4 above, suggesting that this would be the site of initiation of hydrolysis
in that case (Lim *et al.*, 2000).

Use of the inactive enzyme, and comparison of substrate-bound and apo enzyme, allowed Lim et al. to elucidate the conformational changes responsible for substrate binding. One such change occurs in the binding pocket, as shown in Figure 1.8 below.

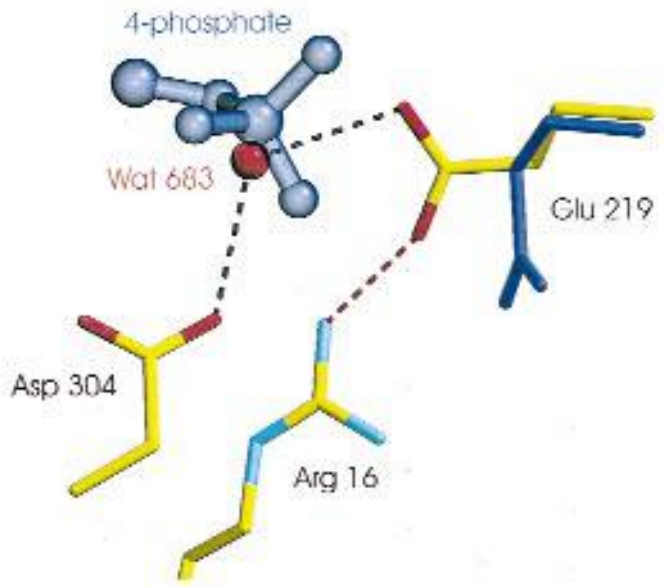

Figure 1.8 Conformational change in Glu 219 of *E.coli* phytase upon substrate binding. In the absence of substrate, Glu 219 points towards the center of the binding pocket and interacts with Asp 304 through a water molecule. With substrate bound, Glu 219 moves its side chain carboxylate away (image from Lim *et al.*, 2000).

At pH 4.5 and 5.0 in the apo enzyme, the carboxylate of the side chain of Glu 219 is directed towards the center of the binding pocket, causing a water-mediated interaction with Asp 304. This interaction prevents protonation of Asp 304. Upon substrate binding, the charge of the 4-phosphate repels Glu 219 carboxylate, towards Asp 325. The van der Waals force interactions with surrounding residues restrict the Glu 219 movement only to the side chain carboxylate group. This conformational change promotes proton donation by Asp 304.

However, at pH 6.6 the side chain of Glu 219 adopts the *holo* enzyme conformation, whether substrate is present or not. This could be explained by Asp 304 becoming deprotonated at a higher pH – for example, pH 6.6 – and this negative charge repels the

carboxylic group of Glu 219 (while normally the pKa of Asp is 3.9, the environment within the protein is influenced by the presence of other residues, effectively changing the pKa of the surroundings). It also casts doubt on the necessity of the Glu 219 conformational change for substrate catalysis in the *E.coli* phytase. Indeed, the crystal structures of the *Hafnia alvei* HAP phytase with and without substrate exhibited no such conformational change (Ariza *et al.*, 2013). This shows that the movement of Glu 219 (Glu 222 in *Hafnia* phytase) is not necessary for all HAP phytases, or that the conformational change in *E.coli* phytase was only due to pH changes.

1.4.5.4 MINPP

Multiple inositol polyphosphate phosphatases (MINPP) are enzymes that can be classified as a subgroup of HAPs. Homologues have been found in human, rat (Caffrey *et al.*, 1999), mouse (Chi *et al.*, 2000), chicken (Romano *et al.*, 1998), slime mould *Dictyostelium discoideum* (Eichinger *et al.*, 2005), plants (Mehta *et al.*, 2006) and microorganisms (Chi *et al.*, 1999). It is the only enzyme known to dephosphorylate IP_6 *in vivo* in mammals, although its substrates are mainly present in the cytosol, while the enzyme is largely located in the interior of the endoplasmic reticulum (Hidaka *et al.*, 2003).

MINPPs have a broad substrate specificity, being able to utilise not only phytate, but also 2,3-bisphosphoglycerate (Cho *et al.*, 2008), para-nitrophenylphosphate, fructose-1,6-bisphosphate and others (Tamayo-Ramos *et al.*, 2012). MINPPs are different from the majority of characterised HAP phytases in that while they also contain the conserved RHGXRXP motif, their proton donor is a glutamate in the HAE motif instead of aspartate in the HD motif (Stentz *et al.*, 2014). While the use of glutamate as a proton donor could explain the acidic pH optima of the HAE phytases, a MINPP from lily pollen exhibits the pH optimum of 8.0 against phytate and pH 7.0 against para-nitrophenyl phosphate (Mehta *et al.*, 2006). Hence, phytase classifications are arbitrary and occasionally contradict each other.

Sequence alignment of a representative group of MINPP phytases that includes organisms such as *Bt, Bp, Bl,* lily, barley, wheat, chicken, human and rat is shown in Appendix 2 in

Figure 9.5. It highlights the HAE catalytic motif as well as several fully conserved regions around the active site. Cysteine residues were highlighted to reflect possible sites of disulphide bridge formation, several of which are conserved to varying degrees.

1.4.6 Beta-propeller phytases

Beta-propeller phytases (BPP) are an entirely distinct group of phytases, unrelated to the others (Kim, Lee, *et al.*, 1998; Ha *et al.*, 2000). They were discovered by screening food-grade *Bacillus* bacteria for extracellular phytase activity (Kerovuo *et al.*, 1998) and by screening the soil of a cattle shed (Kim, Kim, *et al.*, 1998). To date, all BPP phytases originated from *Bacillus* and *Paenibacillus* species (Kumar *et al.*, 2017). Their pH optima fall between pH 6-8 (Kerovuo *et al.*, 1998; Kim, Kim, *et al.*, 1998) and the optimal temperature for activity was found to be 55 °C (Kerovuo *et al.*, 1998) and 70°C (Kim, Kim, *et al.*, 1998).

The naming conventions for the BPP phytases changed across the years. Some publications used the names PhyC, TS-Phy, PhyD, PhyL and PhyA (Turner, Richardson and Mullaney, 2007, p. 102). Nowadays, the name beta-propeller is inspired by the six-bladed propeller shaped structure consisting of beta-propeller sheets. The propeller structure was discovered by Ha et al. (Ha *et al.*, 2000) from a 2.1 Å crystal structure as depicted in Figure 1.9 below.

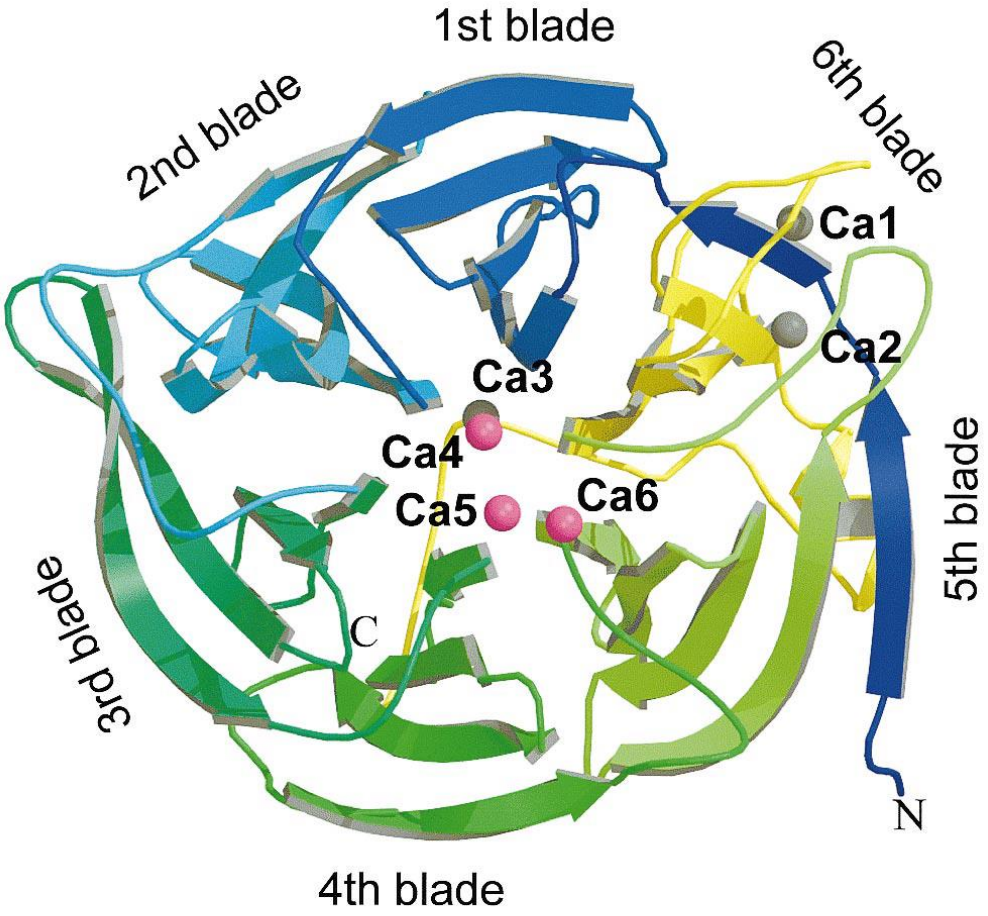

Figure 1.9 Ribbon diagram of a *B. amyloliquefaciens* beta-propeller phytase.
Ca1-3 are calcium ions conferring thermal stability. Ca4-6 are calcium ions conferring the calcium-dependent catalytic activity of the enzyme (image from Ha *et al.*, 2000).

Figure 1.9 above shows the ribbon diagram of the *B. amyloliquefaciens* phytase with the calcium ions bound in their respective binding sites. The propeller 'blades' are highly curved sheets with hydrophobic interactions in-between. Each blade contains four or five interconnected antiparallel beta-strands. The distinct central shaft that spouts the blades tightly binds water molecules in an ordered way. The enzyme was shown to have three distinct calcium binding sites conferring thermostability with high affinity. In fact, the affinity was strong enough to prevent dissociation after strict calcium-free buffer dialysis.

Three other calcium binding sites facilitate substrate catalysis. They exhibited low binding affinity. In the absence of calcium ions at the low affinity sites the enzyme showed no activity, which suggested that the low affinity calcium binding sites where part of the

active site. Further experiments with cadmium ion binding and mutagenesis of nearby glutamates confirmed this assumption (Ha *et al.*, 2000).

Shin et al. (Shin *et al.*, 2001) obtained a 1.8 Å crystal structure of the above phytase in complex with phosphate and calcium ions. It revealed two phosphates and four calciums bound tightly at the active site. Calcium binding was shown to be paramount for the enzyme activity. The catalytic mechanism of the enzyme was deduced using the crystal structure, mutagenesis and biochemical experiments.

The low affinity calcium binding sites are found at one end of the molecule, called 'top'. Figure 1.10 below illustrates a 'side' view of the molecule, making it easy to see the cleft. The shallow cleft is lined largely with negatively charged amino acid residues. Positively charged calcium ions bind to their three low affinity binding sites, creating an optimal electrostatic environment for the binding of phytate.

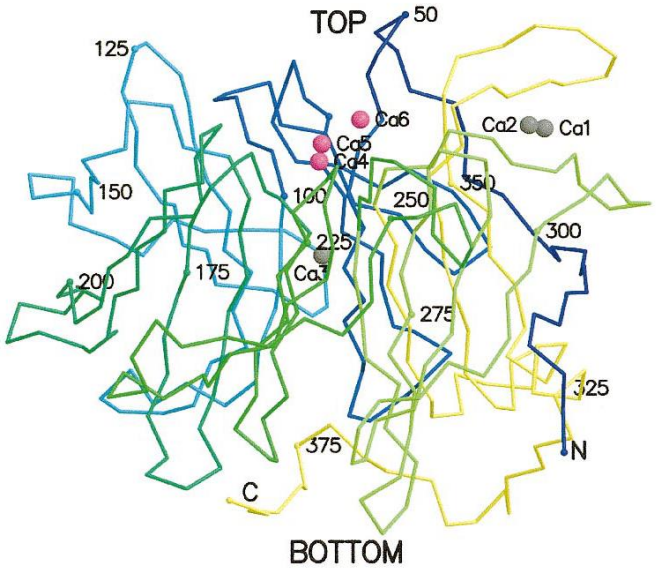

Figure 1.10 Structure of the *B. amyloliquefaciens* beta-propeller phytase.
Different colours signify each of the six propeller blades. The top of the molecule contains the catalytic site cleft (image from Ha *et al.*, 2000).

The low affinity calcium binding sites are not specific to calcium. In fact, molecules such as Mg^{2+} and Ba^{2+} were found to be able to bind to the calcium binding sites and activate the phytase about half as effectively as Ca^{2+} (Kim, Kim, *et al.*, 1998). It is a useful trait for

binding phytate in its natural environment, when it is often found chelating metal ions (Ha *et al.*, 2000). To bind substrate, one phosphate (Pho1) binds to the three calcium ions on top of the phytase molecule. In response to its binding, a fourth calcium ion becomes chelated by Pho1 near the Ca4-6 sites. If present, the second consecutive phosphate on the inositol ring (Pho2) directly interacts with several nearby residues that in response undergo disorder-to-order changes (Shin *et al.*, 2001).

Figure 1.10 below illustrates the proposed catalytic mechanism of beta-propeller phytases. Calciums Ca5 and Ca6 are bridged by a water molecule. This water molecule is proposed to conduct a nucleophilic attack on the Pho1 phosphorus atom of the substrate, creating an intermediate. A general acid (either a water molecule or the nearby lysine residue) donates a proton to the intermediate, cleaving the scissile phosphomonoester bond and freeing the inorganic phosphate from the inositol phosphate.

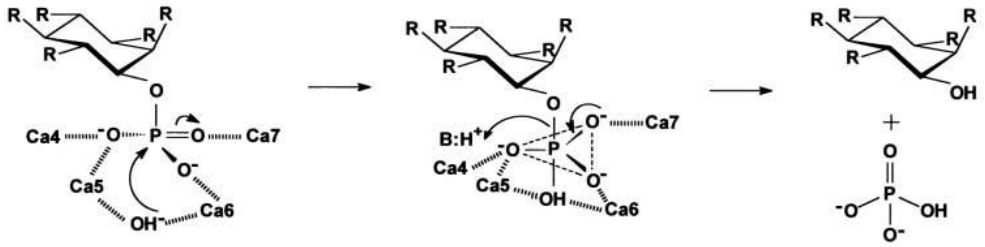

Figure 1.11 The catalytic mechanism of *B. amyloliquefaciens* beta-propeller phytase. Water molecule bridging Ca5 and Ca6 calcium ions carries out a nucleophilic attack on the phosphate. $B:H^+$ is a general acid acting as proton donor (image from Shin *et al.*, 2001).

The BPP enzymes were found to display alternate dephosphorylation of phosphates – hydrolysing every second phosphate rather than adjacent one. Hence, product profile analysis resulted in two different IP_3 products possible at the same time: Ins(2,4,6)P_3 and Ins(1,3,5)P_3 (Kerovuo, Ruovinen and Hatzack, 2000; Greiner and Farouk, 2007). This suggests that the enzyme preferentially recognises a substrate with two consecutive phospho groups over, cleaving one phosphate of the pair (Pho1), while the other phosphate (Pho2) works to increase the binding affinity (Shin *et al.*, 2001).

Notably, the BPP phytases were found to be able to remove all phosphate groups from the IP_6 molecule, including the axial phosphate on position 2 (Shin *et al.*, 2001). This is a

unique trait among phytases. Phytate dephosphorylation by the vast majority of phytases, when present in excess, results in *myo*-inositol 2-monophosphate (Ins2P) as the enzymes display a strong preference for the equatorial phosphates as opposed to axial (Wyss *et al.*, 1999). In addition to soil, beta-propeller phytases are abundant in water environments, where they are a major contributor to phytate-phosphorus cycling (Lim *et al.*, 2007; Huang *et al.*, 2009).

1.4.7 Cysteine phytases

Cysteine phosphatases are the most abundant phytate-degrading enzyme in ruminant animals (Li *et al.*, 2014). They were first identified in the obligatory anaerobic rumen bacterium *Selenomonas ruminantium* (Yanke, Selinger and Cheng, 1999). Because the gut flora in the ruminant animals changes during the feeding cycle, the phytases have different pH optima. Thus, this group of phytases shows pH optima in the range of about 4- 6.5, temperature optima at about 50-55 °C and are monomeric in nature (Yanke, Selinger and Cheng, 1999; Puhl, Greiner and Selinger, 2009; Huang *et al.*, 2011; Li *et al.*, 2014). Cysteine phytases are otherwise known as protein tyrosine phosphatases (Gruninger *et al.*, 2014).

The distinctive feature setting the cysteine phosphatases apart from the HAP and BPP phytases is the conserved cysteine-containing P loop near the active site. The active site is encoded by the motif HCXXGXXR(T/S), shared with the protein tyrosine phosphatases, a subgroup of CP phytases (Denu and Dixon, 1998). The motif forms a wide loop, capable of binding the IP_6 molecule, facilitated by the negative charge of IP_6 (Chu *et al.*, 2004; Turner, Richardson and Mullaney, 2007, p. 104). Figure 1.12 below illustrates the structure of a representative example of a cysteine phytase from *S. ruminantium*.

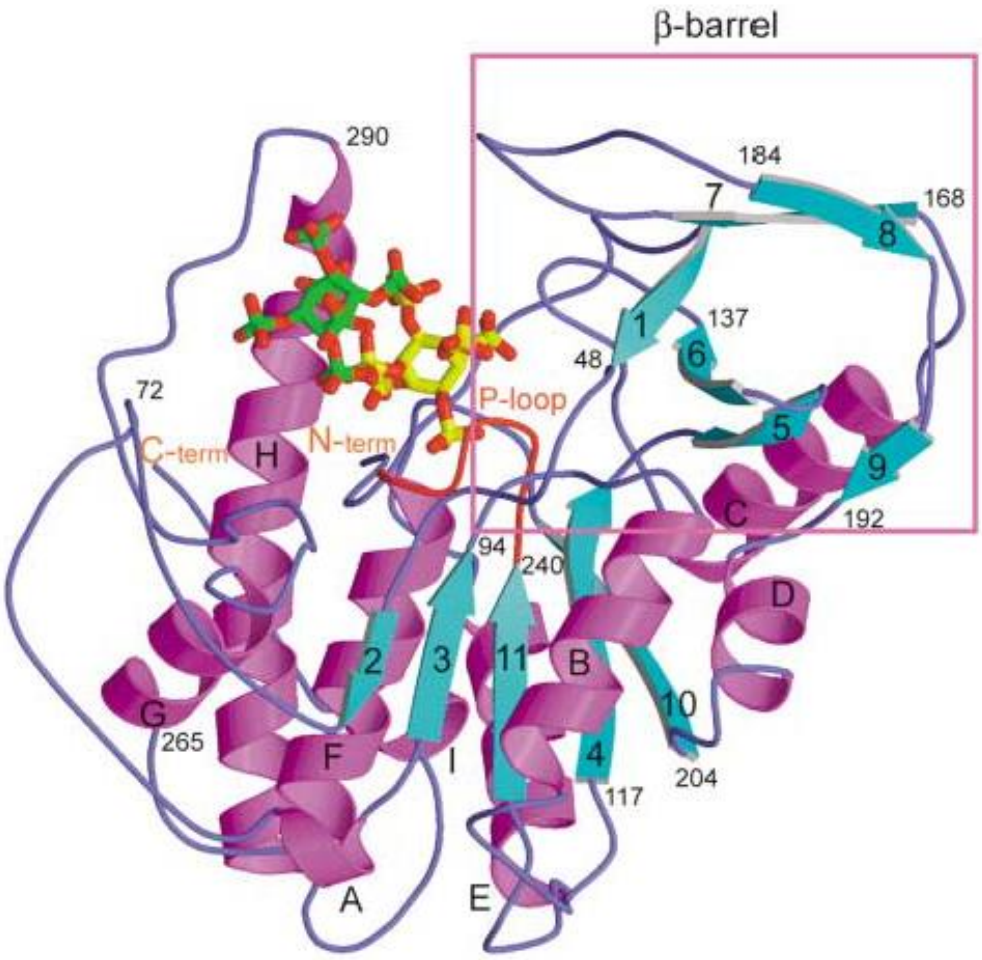

Figure 1.12 Structure of the *S. ruminantium* cysteine phytase with bound inositol hexasulfate, IS_6.
IS_6 bound at the active site is shown in yellow. The enzyme consists of two domains, a large and a small. The small one is shown in the box (image from Chu et al., 2004).

The *S. ruminantium* phytase consists of a large domain and a small domain. The large domain contains a twisted five stranded beta-sheet, flanked by two helices on one side and three helices on the other side. Two alpha-helices are positioned on the edge of the large domain, forming part of a shallow substrate binding pocket. Two loops support the structure of the binding site further. The P loop on the interface of the two domains contains the catalytic motif. Finally, the small domain consists of a five stranded beta barrel and a short beta strand, with a helix positioned on the edge of the domain. Using an inhibitor *myo*-inositol hexasulphate it was shown that the phosphate to be hydrolysed is held close to the sulfhydryl group of the cysteine. The structure of the *S. ruminantium* phytase closely resembles these of related cysteine phosphatases such as phosphoinositide phosphatase PTEN, KAPt and LAR (Chu *et al.*, 2004; Bruder *et al.*, 2017).

1.4.8 Purple acid phosphatases

Purple acid phosphatases (PAP) are otherwise known as tartrate-resistant acid phosphatases. They can be found in plants such as wheat, barley, maize and rice as well as potentially in algae (Dionisio *et al.*, 2011; Rivera-Solís *et al.*, 2014). Their pH optima are around pH 4.5-5.0, temperature optima between 58-65 °C and molecular weights are around the range of 37-72 kDa. They are resistant to tartrate and their function relies on metal ions bound at the active site (Wynne *et al.*, 1995; Hegeman and Grabau, 2001; Dionisio, Holm and Brinch-Pedersen, 2007; Kong *et al.*, 2014). Some PAP enzymes display high activity against phytate, such as the *Arabidopsis* PAP phytase AtPAP15. It is one of 29 PAP enzymes in *Arabidopsis*, and like other PAPs contains a dinuclear metal centre at the active site, which classifies them as metallophosphoesteraes (Zhang *et al.*, 2007). The two metal ions in the PAP metalloenzymes' active sites are usually a combination of Fe^{3+}, Fe^{2+}, zinc or manganese and are what gives the enzymes its purple coloration (Dionisio *et al.*, 2011).

PAP phytases are considered a major contributor to the mature grain phytase activities of barley and rye, where they are measured as ~650 FTU/kg (10.8 µkat/kg) and 6000 FTU/kg (100 µkat/kg) respectively (Madsen *et al.*, 2013). Together with the MINPP subgroup of HAP phytases, PAP phytases make up the complement of cereal phytases (Dionisio, Holm and Brinch-Pedersen, 2007). Furthermore, the single cell green alga *Chlamydomonas reinhardtii* was shown to express six PAP enzymes with potential phytase activities (Rivera-Solís *et al.*, 2014). To date, no structure of a purple acid phytase is available.

1.5 *In vivo* function of phytase

Numerous bacterial strains have been shown to produce phytate-degrading enzymes, most of which are intracellular. The exceptions are *Bacillus* and *Enterobacter* bacteria which produce extracellular phytases; *E. coli* produces periplasmatic phytases and *S. ruminantium* and *M. multiacidus* produce phytases associated with the outer membrane (Konietzny and Greiner, 2004).

The collective ability to dephosphorylate phytate *in vitro* gave the phytases their name. Historically because the *in vivo* function of phytases was largely unknown, this classification was only a placeholder (Konietzny and Greiner, 2002). It has been suggested that the bacterial phytase is produced in response to nutrient and energy limitation. Hence it would not be required in nutrient-rich environments, in which lactic acid bacteria evolved to thrive. Lactic acid bacteria show no significant extracellular phytase activity (Zamudio, González and Medina, 2001; Reale *et al.*, 2007). An exception to these are sourdough bacteria *Lactobacillus amylovorus* (Sreeramulu *et al.*, 1996) and *Lactobacillus plantarum* (Zamudio, González and Medina, 2001), which do exhibit high extracellular phytase activity.

1.5.1 *In vivo* function of phytase in fungi

Organic phosphate is present in soil more abundantly than free inorganic phosphate. In particular, phytate is the predominant form of phosphate. This bound phosphate is likely inaccessible to plants, therefore it must be released by enzymes before becoming available to the plant (Tang *et al.*, 2006; Turner, Richardson and Mullaney, 2007, p. 221). Most fungal phytases are extracellular, such as the yeast *Schwanniomyces castellii* , *Arxula adeninivorans*, *Pichia spartinae* and *P. rhodanensis* (Vohra and Satyanarayana, 2002; Konietzny and Greiner, 2004). Exceptions are *Saccharomyces cerevisiae* and *Pichia anomala,* which produce intracellular phytases (Vohra and Satyanarayana, 2002).

Fungal extracellular phytases have been shown to be a major contributor to phytate degradation during composting. It can be inferred that plants in general benefit from

phytase activity provided by fungi present in soil. However, difficulties in isolating and assessing phytate degrading organisms *in vivo* has been a bottleneck in the research of the natural function of fungal phytases (Turner, Richardson and Mullaney, 2007, p. 61).

Several fungal species have been isolated from the environment that were found to exhibit phytate-degrading activity. For example, phytases were found in isolates of *Penicillium simplicissimum* isolated from soil (Tseng, Fang and Tseng, 2000), in *Pichia anomala* isolated from flower buds of *Woodfordia fruticosa* (Vohra and Satyanarayana, 2002), *Rhizopus oligosporus* isolated from fermented soybean (Sutardi and Buckle, 1988). Furthermore, numerous *Aspergillus* subspecies express one or more phytase enzymes (Fujita *et al.*, 2003; Turner, Richardson and Mullaney, 2007, p. 66).

Fathallh Eida *et al.* (2013) studied microbes responsible for phytate degradation in compost. In the study, fungal and bacterial isolates were obtained from saw dust and coffee residue composts. The organisms were screened for their phytate degrading capability by observing their growth first on phytase screening medium (PSM) plates, and then the most effective isolates were examined in liquid PSM medium.
Phytase screening medium (PSM) is an agar-based solid growth medium containing sodium phytate or calcium phytate. Phytate-degrading microbes growing on PSM will create a clear zone around their colonies, where the precipitated phytate was degraded (Bae *et al.*, 1999). Fathallh Eida et al. (Fathallh Eida *et al.*, 2013) proceeded to select the most effective fungal and bacterial isolates that were subsequently incubated in phytate-containing organic materials (mushroom media residue and rice bran) to closely reflect the natural environment from where they came from. Consequently, only the fungal isolates displayed phytate degrading activity in the organic material (Fathallh Eida *et al.*, 2013).

Singh et al. (Singh and Satyanarayana, 2010) characterised the phytase from the thermophilic mould *Sporotrichum thermophile*. This mould is known for its important role in soils by producing several cell wall degrading enzymes. It produces a glycoprotein HAP phytase with broad substrate specificity. It was demonstrated that the phytase can successfully liberate inorganic phosphate from natural phytate salts with Ca^{+2}, Mg^{+2}, and Co^{+2} and to a lesser extent those with Al^{3+}, Fe^{2+}, Fe^{3+} and Zn^{2+}. The addition of the mould

to the roots of growing *Triticum aestivum* L. wheat promoted the growth and the biomass of the plant as well as the inorganic phosphate content (Singh and Satyanarayana, 2010).

Tarafdar et al. (Tarafdar and Marschner, 1995) showed that utilisation of organic phosphorus from phytate was enhanced in sterilised wheat *Triticum aestivum* L. var. Star, when the plant was grown in the presence of the mycorrhizhal fungus *Glomus mosseae* and *Aspergillus fumigatus*, both prominent phytase producers.

1.5.2 *In vivo* function of phytase in bacteria

Phytases have been detected in various bacterial species, including *Bacillus, Bifidobacterium, Citrobacter braakii*, *Enterobacter, E. coli, Klebsiella, Lactobacillus, Megasphaera elsdenii, Prevotella, Mitsuokella, Pseudomonas* and *Selenomonas ruminantium*. Most of them produce intracellular phytase, with the exception of *Bacillus subtilis* and *B. subtilis* var. natto (Jain, Sapna and Singh, 2016). Lactic acid bacteria have not been found to produce phytases, instead they rely on non-specific acid phosphatases to liberate phosphorus from phosphorus compounds (Zamudio, González and Medina, 2001). An exception to the lack of lactic acid bacteria phytases are sourdough bacteria *Lactobacillus amylovorus* (Sreeramulu *et al.*, 1996) and *Lactobacillus plantarum* (Zamudio, González and Medina, 2001), which exhibit high extracellular phytase activity.

Bacterial phytase production is inducible in nature and is under complex regulatory control. Conditions such as carbon limitation, presence of phytate or Ca^{2+} ions induce phytase production. Moreover, phytase synthesis appears to be carried out only in the stationary phase of bacterial culture growth. The late stationary phase and anaerobic conditions were found to significantly increase activity of two intracellular phytases in *E.coli* (Greiner, Konietzny and Jany, 1993). Inorganic phosphate starvation appeared to trigger *E.coli* phytase synthesis (Konietzny and Greiner, 2004). A *Raoultella terrigena* phytase activity was very low in the exponential growth phase and grew significantly in the stationary phase of a culture grown in non-limiting media containing phytate. Here, introduction of carbon deficient conditions induced an immediate phytase synthesis, but not phosphate deficiency (Greiner, Haller and Konietzny, 1997).

In general, the tight regulatory control of phytase induction brought about by inorganic phosphate limitation is a common trend across most of observed bacterial (and fungal) phytases, except *Raoultella terrigena* and *Selenomonas ruminantium* (Yanke *et al.*, 1998). Because of these observations, it has been postulated that phytase is not necessary for stable growth in bacteria. Instead, its synthesis becomes induced in response to nutrient or energy limitation, which occur during the stationary phase of bacterial growth. Furthermore, lactic acid bacteria that mostly do not produce phytases are known to have evolved to live in nutrient-rich conditions. Hence this species never had the evolutionary pressure to produce phytases (Konietzny and Greiner, 2004).

Most bacteria are not able to grow on phytate as the sole source of carbon and phosphorus. However, *Klebsiella aerogenes* was reported to be able to do that (Tambe *et al.*, 1994), as well as certain strains of *Pseudomonas* (Cosgrove, Irving and Bromfield, 1970). Furthermore, a study by Richardson *et al.* (Richardson and Hadobas, 1997) analysed 200 randomly selected bacterial isolates obtained from soil and studied their capacity to utilise phytate as their sole carbon and phosphorus sources. The vast majority of isolates (over 99.5%) were unable to do this. However, the *Pseudomonas* strains CCAR53 and CCAR59 were found to be able to utilise IP_6 as the sole carbon source in solid and liquid media, as indicated by depletion of IP_6 and accumulation of inorganic phosphate in the absence of other carbon sources (Richardson and Hadobas, 1997).

General characteristics of some notable bacterial phytases are outlined in Table 1.2 below.

Species	Molecular weight (kDa)	Optimal temperature (°C)	Optimal pH	localisation
Bacillus subtilis	36–38	60, 70	6.0–8.0	extracellular
Escherichia coli	42-45	55	4.5	periplasmic
Enterobacter		50, 70	6.0-8.0	extracellular
Klebsiella	10–13, 40, 700	60-70	4.5 - 5.2	extracellular
Serratia		50	6.0-8.0	extracellular

Table 1.2 General characteristics of a representative selection of bacterial phytases (Greiner, Konietzny and Jany, 1993; Tambe *et al.*, 1994; Greiner, Haller and Konietzny, 1997; Kim, Kim, *et al.*, 1998; Liu *et al.*, 1998; Idriss *et al.*, 2002; Konietzny and Greiner, 2004; Turner, Richardson and Mullaney, 2007; Kalsi *et al.*, 2016).

Typical bacterial phytases are extracellular, while the *E.coli* phytase exhibits periplasmic localisation. Typical pH optima for acidic bacterial phytases are in the range of pH 4.5-5 and for the alkaline phytases the optima are in the range of pH 6.0-8.0. Their temperature optima are typically around 60 °C, with the *Serratia* phytases having the optimum of 50 °C.

Interestingly, an unusually large phytase protein (700 kDa) and an unusual small peptide phytase (10-13 kDa) were seemingly isolated from *Klebsiella aerogenes*, as evidenced by gel filtration chromatography. The two differed in their biochemical and kinetic characteristics. The high molecular weight enzyme retained activity after incubation at high temperatures, while the peptide lost 70 % of its activity. The enzymes had significantly different pH optima, at 5.2 and 4.5 for the peptide and large protein respectively. Despite these interesting findings, the authors expressed uncertainties about the true identity of the 700 kDa protein – there was a possibility that it was in fact the small peptide associated with another larger protein (Tambe *et al.*, 1994).

In general, most bacterial phytases tend to span molecular weights of about 35-45 kDa, with some exceptions e.g. the *Klebsiella aerogenes* phytases (Tambe *et al.*, 1994). They have a broad range of pH optima, ranging from pH 4.5 to pH 8. Their optimum temperatures for activity are typically in the range of around 55-70 °C (Lei *et al.*, 2013).

Bacterial phytases can belong to histidine acid phosphatases, beta propeller phytases or cysteine phytases. No bacterial purple acid phytases have been confirmed. However some homologous sequences in bacteria have been found (Schenk *et al.*, 2000). *Bacillus subtilis* was found to produce an extra-cytoplasmic phosphodiesterase enzyme very closely related to PAPs (Rodriguez *et al.*, 2014). Multiple inositol phosphate phosphatases (MINPP) are phytases that can occur in human commensal gut bacteria, such *as Bacteroides thetaiotaomicron, Bifidobacterium, Prevotella* and *Alistipes* (Stentz *et al.*, 2014). Certain pathogenic bacteria such as *Bdellovibrio bacteriovorus* are thought to express cysteine phytases as part of their mechanism of phosphate acquisition from prey (Gruninger *et al.*, 2014).

HAP phytases include phytases with the catalytic motif HD or HAE, subdividing them into the HD and HAE subclasses of the HAP phytases. Sequence alignments of a representative group of bacterial HAP phytases including both subclasses are presented in the Appendix 2. Bacterial species analysed include *Klebsiella* sp ASR1, *E.coli, C.braakii*, *H.alvei,* Y.*kristensenii, B.thetaiotaomicron,* B.*pseudocatenulatum* and *B.longum.* The phylogenetic tree based on the alignments is presented below:

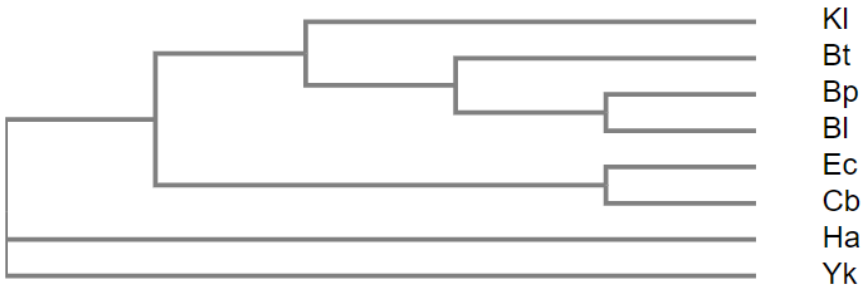

Figure 1.13 Phylogenetic tree of a representative group of HAP phytases.
Kl: *Klebsiella* sp ASR1; Ec: *E.coli*; Cb: *C.braakii*; Ha: *H.alvei*; Yk: Y.*kristensenii*; Bt: *B.thetaiotaomicron*; Bp: B.*pseudocatenulatum*; Bl: *B.longum*. Created using the online tool Clustal Omega.

1.5.3 *In vivo* function of phytase in plants

Phytate and its mineral salts are the predominant form of phosphorus in soil. Plants are generally regarded as unable to utilise phytate or other organic phosphorus compounds directly (Perez Corona, van der Klundert and Verhoeven, 1996). Instead, they secrete enzymes or more often rely on microbial phosphohydrolases to mineralise the phosphorus compounds to orthophosphate anions such as $H_2PO^-_4$ and HPO^{2-}_4 (Li *et al.*, 1997). Therefore enzymatic dephosphorylation has to take place for the phosphorus to be taken up as phosphate, $H_2PO^-_4$ and HPO^{2-}_4 .

In addition to phytate-degrading symbiotic fungi inhabiting the rhizosphere, various plant species were found to secrete phytase from their roots in phosphorus-deficient conditions independently from microbiological contributions (Li *et al.*, 1997; Secco *et al.*, 2017). Li et al. (1997) found phytase activity in root secretions of sixteen plant species spanning upland rice, tomato, lupin, timothy, grass, clovers, legumes and alfalfa. In particular, it was found that grass *Brachiaria decumbens* CIAT 606 and legume *Stylosanthes guianensis* CIAT 184 showed the highest phytase activity. These species are tropical forage crops and are especially well evolved to thrive in phosphorus-deficient conditions. It can be posited that the secretion of phytases in these plants is the result of adaptation to the low phosphorus availability in acidic soils (Li *et al.*, 1997).

Hayes et al. (Hayes, Richardson and Simpson, 1999) grew five pasture species: *Trifolium subterraneum, Trifolium repens, Medicago polymorpha, Phalaris aquatica* and *Danthonia richardsonii* under supplied or deficient phosphorus conditions. They extracted the phytase and acid phosphatases under sterile conditions from roots and assessed the enzyme activity. In general, phytase activity was only around 5% of the phosphatase activity. Interestingly, in four of the five tested plants except *Trifolium repens*, phytase extracted activity was significantly higher when grown under the P-deficient conditions (Richardson, Hadobas and Hayes, 2000).

Again, Richardson et al. (Richardson, Hadobas and Hayes, 2000) grew wheat *Triticum aestivum* L. under adequate and deficient phosphorus supply in sterile conditions, before examining root phytase activity. No secreted phytase activity was detected in assays

utilising intact roots. However upon extraction from crude root extracts, phytase activity was detected at 4 mU/g (66.7 µkat/g) root fresh weight for the plants grown in adequate phosphorus conditions, and 24 mU/g (400 µkat/g) root fresh weight for plants grown in phosphorus-deficient conditions (Richardson, Hadobas and Hayes, 2000).

In addition to certain plants producing phytases in their roots, phytases occur in grains, seeds and pollen of higher plants (Reddy *et al.*, 1989). During the germination phase of growth, phytases allow the growing plant to utilise the phosphate, minerals and the *myo*-inositol that were stored in the form of phytate (Reddy, Kim and Kaul, 2017). Phytate is the major storage form of phosphorus in virtually all cereal grains and seeds, accounting for about 60-90 % of their total phosphorus content (Wu *et al.*, 2009).

Differences in extraction methods and analytical procedures could lead to disagreements between published data on phytase activity and phosphorus content in seeds. As shown by Greiner and Egli (Greiner and Egli, 2003), aqueous extraction yielded different apparent phytase activities than direct incubation of dry-milled grains in phytate containing buffer. Surfactant and protease inhibitor use increased the success of phytase extraction, hinting at association of phytases with membrane structures and a degree of proteolysis during extraction otherwise. Furthermore, despite the possibility of phosphate liberation from sources other than phytate, phosphate quantification as opposed to residual phytate quantification proved to be a relatively accurate measure of phytase activity (Greiner and Egli, 2003).

Azeke et al. (Azeke *et al.*, 2011) examined the sterilised seeds of rice *Oryza sativa*, maize *Zea mays*, millet *Panicum miliaceum*, sorghum *Sorghum bicolor* and wheat *Triticum aestivum* to determine their phytate and phosphorus contents as well as their intrinsic phytase activities. It was found that all extracted phytases had high activities, ranging from 0.21 – 0.67 U/g (1 unit = 1 µmol of phosphate liberated per minute), equivalent to 3.5 – 11.2 nkat/g. However, other authors have reported significantly different values of phytase activity (as reviewed in Azeke *et al.*, 2011). This could be attributed to the differences in the exact analytical methods between the research groups.

Lazali et al. (Lazali *et al.*, 2014) used *in situ* RT-PCR to pin point the location of phytase transcripts in germinating seeds and root nodules in bean *Phaseolus vulgaris* L. After 72

hrs of germination, the seeds showed the presence of phytase transcripts in all germinating organs. With fluorescent imaging, the embryo showed the greatest phytase transcription signal, followed by the radicle and the cotyledon.
Because the cotyledon is the most abundant organ in plant seeds, its phytase activity was chosen to be assessed and compared to the activity in nodules. Cotyledon phytase was found to be around 22 times higher than nodule phytase (43 nmol/min/g vs 2nmol/min/g).

A summary of general characteristics of plant phytases is shown in Table 1.3 below.

Source		Molecular weight (kDa)	Optimal temperature (°C)	Optimal pH
maize	Zea mays	76, 80 (dimers)	55	4.8
rockcress	Arabidopsis thaliana	60.4		4.5
wheat bran	Triticum	47	45, 55	5-7.2
soybean	Glycine max	59-60	55-60	4.5-5
squash	Cucurbita maxima	66.5 +/-4	48	4.8
mung beans	Vigna radiata	~160	57	7.5

Table 1.3 General characteristics of selected plant phytases
(Peers, 1953; Nagai and Funahashi, 1962; Mandal, Burman and Biswas, 1972; Lim and Tate, 1973; Goel and Sharma, 1979; Buckle, 1986; Gibson and Ullah, 1988; Laboure, Gagnon and Lescure, 1993; Maugenest, Martinez and Lescure, 1997; Liu *et al.*, 1998; Hegeman and Grabau, 2001; Rasmussen, Sorensen and Johansen, 2007; Zhang and Lei, 2008; Lei *et al.*, 2013).

In summary, certain plants have been proven to exude phytase enzymes from their root. Mostly, these phytases become synthesised in significantly larger amounts when growing in phosphorus-deficient conditions and are an especially useful trait for tropical plants growing on notoriously P-deficient soil. However, in general plant root phytases were found to have low activity in comparison to acid phosphatases or to microbial phytases found in the rhizosphere. On the other hand, microbial phytases in the rhizosphere have been shown to be major source of phytate-degrading enzymes in many cases.

Plants show high phytase activity in germinating seeds in comparison to root nodules. In particular, the embryonal zone of the seed showed the highest activity, followed by cotyledon and radicle. This activity is crucial to mobilise and hydrolyse phytate stored in seeds, to enable the phosphate, *myo*-inositol and minerals to be utilised. As shown in Table 1.3, plant phytases typically show the optimal temperatures in the range of 45-60 °C, pH optima around pH 4.8-5 with some exceptions (e.g. soybean). Their molecular weights tend to differ between 47-66.5 kDa, with exceptions reaching 80 or 160 kDa – probably depending on the number of subunits.

1.5.4 *In vivo* function of phytase in animals

Phytases produced by animal tissues have not been researched as extensively as microbial phytases. Certain reports showed phytate-degrading activity in animals to be located in the blood and liver, as well as the intestinal mucosa of rats, rabbits, guinea pigs, chicken, calves and humans. However, further research contradicted these findings to some extent, arguing that the phytate degrading activity originated in gut bacteria or in non-specific phosphatases (reviewed in Konietzny and Greiner, 2002).

Ellestad et al. (Ellestad, Angel and Soares, 2002) found phytase activity in fish. Fish cannot be strictly categorised as carnivores, omnivores or herbivores, as they change their dietary habits throughout the year, depending on food availability. Fish that are mostly omnivores or herbivores and have a particular preference for plant material could exhibit phytase activity. The omnivorous tilapia hybrid *Oreochromis niloticus × O. aureus* was found to be capable of digesting 50% of its dietary phytate phosphorus (Ellestad, Angel and Soares, 2002).

All in all, the intestinal phytase activity in animals provides little contribution towards dietary phytate degradation (Iqbal, Lewis and Cooper, 1994), providing a niche for the commercial phytases to play an important role in animal diet.

1.6 Phytases in the Industry of Animal Feed

During the last thirty years, there has been a pronounced interest in phytases from scientists and entrepreneurs in the aspects of nutrition, environmental protection and biotechnology (Konietzny and Greiner, 2004). Phytase addition to animal feed is of utmost importance in the industry of monogastric animals, in particular swine and poultry, as well as aquaculture farming. The industry of feed supplements constantly strives to optimise the existing commercial enzymes as well as discover new candidates for development. As such, it is important to conduct basic characterisations and catalytic parameters of the candidate enzymes and compare them to those of the commercially used ones. Among the several phytase manufacturers the assay techniques may differ, making it impossible to reliably compare their enzymes based on the manufacturer's specifications. However, Menezes-Blackburn et. al (Menezes-Blackburn, Gabler and Greiner, 2015) conducted detailed side-by-side comparisons of seven currently used commercial phytases from several different manufacturers and microbial sources. Table 1.4 below outlines the manufacturer, the source organisms and expression organisms.

trademark	supplier	donor organism	production organism
Quantum	AB Vista	*Escherichia coli*	Trichoderma resei
Quantum Blue	AB Vista	*Escherichia coli*	Trichoderma resei
PhyzymeXP	Danisco	*Escherichia coli*	Schizosaccharomyces pombe
AxtraPHY	Danisco	*Buttiauxella* spp	Trichoderma resei
Ronozyme Hiphos	Novozymes/DSM	*Citrobacter braakii*	Aspergillus oryzae
Ronozyme NP	Novozymes/DSM	*Peniophora lycii*	Aspergillus oryzae
Natuphos	BASF	*Aspergillus niger*	Aspergillus niger

Table 1.4 General information on a selection of commercially used phytases (Menezes-Blackburn, Gabler and Greiner, 2015).

Table 1.5 below shows the results of the detailed characterisations of these commercial phytases. It can be seen that their optimum pH of activity falls mostly within the range of pH 3.5-4.5 with the exception of AxtraPHY, which has a narrow pH optimum of pH 3.0. Comparisons of their activity at pH of 3.0 and pH 7.0 were designed to reflect the physiological pH of the animal's stomach and intestines, respectively. Those experiments revealed the commercial phytases to be vastly more active at the lower pH of 3.0 than the pH of 7.0, making them ideal for phytate dephosphorylation in the stomach. The K_M values for phytate assays showed differences between the enzymes, but showed similar values between pH 3.0 and 5.0 for each enzyme.

trademark	Quantum	Quantum Blue	PhyzymeXP	AxtraPHY	Ronozyme Hiphos	Ronozyme NP	Natuphos
optimum pH range at 80% of activity	4.0–5.0	3.5–5.0	3.0–5.0	3	3.0–4.5	4.5–5.5	4.5–5.5
phytase activity at pH 3.0 in relation to pH 5.5 (%)	92.5	101.3	82.8	235.1	145.7	12.5	64.2
phytase activity at pH 7.0 in relation to pH 5.5 (%)	0.8	2.2	1.7	0.5	0.6	7.8	7
K_M for phytate at pH 5.0 and 37 °C (µM)	228	142	285	272	364	75	35
K_{cat} for phytate at pH 5.0 and 37 °C (s^{-1})	1545	1821	1327	1054	1478	1532	318
K_M for phytate at pH 3.0 and 37 °C (µM)	257	178	302	311	427	98	142
K_{cat} for phytate at pH 3.0 and 37 °C (s^{-1})	1012	1274	984	768	1061	824	170

Table 1.5 Table of general characteristics of a selection of commercially used phytases

(Menezes-Blackburn, Gabler and Greiner, 2015).

The above commercial phytases were modified by selective molecular modifications to suit the digestive tract of the target farm animals. They need to achieve high activity in the target parts of the digestive system, where the pH varies from pH 2-5 in the gizzard to pH 4-5 in the crop, and less so at pH 6.5 – 7.5 in the poultry small intestine. While six of

the commercial phytase products are used as liquid supplements, the Natuphos *A.niger* phytase comes in a solid formulation. This discrepancy in formulation was introduced as postprocessing to achieve optimal activity, which along with the selected expression system and product formulation affect the final efficacy of the phytase (Menezes-Blackburn, Gabler and Greiner, 2015).

Overall, commercial phytases have been successfully introduced into mainstream farming to improve yield of food production, address environmental issues with phosphorus pollution of groundwaters and provide economical advantage over using phosphorus supplements (Lei *et al.*, 2013).

1.7 Aims and plans

The mainstay of the Ph.D. project revolves around enzymatic characterisations of wild-type MINPPs and comparing their enzymatic properties to the commercial phytase Quantum Blue. The project will investigate the basic enzymatic characteristics as well as binding assays and product profiles using HPLC analysis. Further on, mutagenesis will be employed to elucidate roles of potentially key residues involved in the enzymatic catalysis and structure and the resulting mutant enzymes will be examined for their thermostability. The long-term aim is to introduce new phytases to the animal feed industry, with optimised dephosphorylation abilities, increased thermostability and tolerance to a wider pH range.

2 General Characterisations of HAE phytases.

2.1 Introduction

Phytases for use in animal feed are developed with a range of characteristics in mind. Some such qualities are designed to help the enzyme survive and retain its activity for long enough, so that a significant amount of phytate can be degraded. A look at the anatomy of animal gut can give an idea of the vast differences in pH that the enzyme will have to withstand. Achieving a high level of activity of the phytase in the pH of the particular regions in the animal gut is one of the main goals in phytase engineering.
In the case of intermittent feeding in broilers, the feed is stored in the crop (Svihus *et al.*, 2013). There, the feed material undergoes fermentation, bringing the pH to the range of about 5.5 (Svihus *et al.*, 2013; Zeller *et al.*, 2016). In regular feeding regimens, feed can pass straight past the crop and into the proventriculus and the gizzard (Svihus, 2014). Those organs are considered the true stomach of the bird, as they produce hydrochloric acid and pepsinogen at pH 2, creating a strongly acidic environment. In practice, presence of feed along with environmental factors bring the pH into the average range of 3.5 in these organs.

Currently, all commercial phytases belong to the histidine acid phosphatase (HAP) class of phytases (Menezes-Blackburn, Gabler and Greiner, 2015). In particular, they fall into the HD subdivision, named after the aspartate residue in their proton donor sequence. The recently discovered HAE subclass of HAP phytases, named after the putative glutamate proton donor, has sparked interest due to its broad substrate specificity and therefore possible use in optimisations (Stentz *et al.*, 2014).

The aims of the experiments described in this chapter were to conduct basic characterisations of wild type HAE phytases, to lay foundations for the search of a viable candidate phytase for future, more detailed characterisations and potential optimisations with the commercial use for the industry of the animal feed in mind.

For the experiments, it was decided to characterise three wild-type HAP phytases

originating from human enteric bacteria *Bacteroides thetaiotaomicron* (Bt), *Bifidobacterium pseudocatenulatum* (Bp) and *Bifidobacterium longum* subsp. infantis ATCC 15697 (Bl) to look for viable candidates for enzyme engineering. The investigations included the commercial Quantum® Blue (QB) enzyme (AB Vista) as comparison. Using the molybdate blue method described below, the phytases were tested for their activity at a range of pH from pH 2 to pH 9; their retained activity after incubation at a range of temperatures from 30 °C to 95 °C; and their kinetic activity at pH 5. Using differential scanning fluorimetry, the phytases' thermostability was tested at pH 3.5 and 7 at a range of substrate concentrations, from 0 mM to 2 mM; and in oxidising and reducing conditions.

Phytase activity is traditionally assayed by measuring phosphate release (Eeckhout and De Paepe, 1994). The inorganic phosphate (Pi) in the solution is reacted with a colourimetric reagent, which gives rise to changes in absorbance at various wavelengths which can be followed using a spectrophotometer. These colour changes stem from the reaction of molybdenum Mo^{VI} with phosphate, whereby ammonium molybdate becomes reduced and produces the compound molybdenum blue, giving rise to the blue appearance of the solution (Miller and Taylor, 1914).

The molybdenum blue method has been the key method for the spectrophotometric detection of orthophosphate in water for many years. In particular, it detects the 'molybdate reactive phosphorus' (MRP) fraction of the sample, which in addition to orthophosphate, can contain some proportion of inorganic polyphosphates, labile organic P compounds and colloidal P species. As numerous species interact with ammonium molybdate to various degrees depending on their nature and the conditions of the experiment, the exact methods diverged over the years, leading to a variety of different wavelengths monitored for changes (as reviewed in Nagul *et al.*, 2015). Over the years, the molybdenum blue method has been widely adapted as a phosphate release assay to measure phytase activity. Often the wavelength of 700 nm is monitored for the changes in absorbance, yielding successful assays of phytase activity among several different research groups and phytase classes (Shimizu, 1992; Eeckhout and De Paepe, 1994; Bae *et al.*, 1999; De Angelis, 2003; Chu *et al.*, 2004; Huang *et al.*, 2009; Fu *et al.*, 2011; Reddy *et al.*, 2015; Niu *et al.*, 2016). A less often used wavelength of monitoring the molybdenum

blue formation is 882 nm, (Hayes, Richardson and Simpson, 1999; Richardson, Hadobas and Hayes, 2001) with equally successful results. However, following from the wider range of available literature and industry standards (Qvirist, Carlsson and Andlid, 2015), this thesis describes research using the 700 nm method.

2.2 Methods

2.2.1 Colourimetric assay

Fresh colour reagent was prepared before each experiment by mixing four parts of Solution A with one part of Solution B. Solution A consisted of 15 g of ammonium heptamolybdate·$4H_2O$, 55 ml of concentrated sulphuric acid, topped up to 1 L with ddH_2O. Solution B consisted of 27 g of $FeSO_4 \cdot 7H_2O$, 200 µl of concentrated sulphuric acid, topped up to 1 L with ddH_2O.

Enzymatic reactions were diluted at the ratio of 1:2 with ddH_2O. 100 µl of the dilution was added to 100 µl of the colour reagent in a flat-bottomed Nunc MicroWell 96-well microplate (ThermoFisher Scientific). The colourimetric reaction was allowed to progress for 30 min at room temperature, before placing the microplate in the plate reader and measuring the absorbance at 700 nm. At the same time, buffer controls with no added enzyme were allowed to react with the colour reagent. The resulting values were subtracted from the sample measurements.

2.2.2 pH profiles

pH profile experiments were used to measure the activity of the enzymes at each consecutive pH in 0.5 intervals, from pH 2.0 to pH 9.0 using a range of buffers as follows. The buffers were all at concentration of 0.1 M. Glycine-HCl was used for pH 2.0 – 3.5, sodium acetate was used for pH 4.0 – 5.5, HEPES-NaOH was used for pH 6.0-8.5 and glycine-NaOH for pH 9.0. The *B.thetaiotaomicron* phytase (Bt) was at a starting

concentration of 171 nM, the *B.pseudocatenulatum* phytase (Bp) was at 1.3 µM, the *B.longum* phytase (Bl) was at about 1.7 µM and Quantum Blue (QB) was at 17.5 µg/ml (molar concentration unknown).

For a single reaction, 10 µl of an enzyme (typically 0.1-2 mg/ml) was added to 90 µl of 1mM IP_6 (Sigma) dissolved in the pH buffers. Each reaction was carried out as a quadruplicate. The reactions were allowed to proceed in 200 µl PCR tubes at 37 °C in an incubator for 60 min (in case of Bt, Bp and Bl) or 30 min (for Quantum Blue). The reactions were diluted, added to the colour reagent and the absorbance was measured.

2.2.3 Temperature profiles

To determine the temperature profiles of reaction, phosphate release was measured after allowing the enzymatic reaction to proceed while incubating at certain temperatures. Enzymes were used at the following starting concentrations: Bt was at a starting concentration of 12.3 µM, Bp was at 29.7 µM, Bl was at 52.6 µM and Quantum Blue was at 17.5 µg/ml. For each reaction, 90 µl of 1mM IP_6 (Sigma) in a 200 µl PCR tube was preheated in a PCR thermocycler for about 10 min. Next, 10 µl of the enzyme was added and the reactions were incubated for 30 min. The samples were cooled in a room temperature water bath, diluted with 100 µl of ddH_2O and then 100 µl of the dilution was added to 100 µl of the colour reagent. After 30 min absorbance measurements were taken.

2.2.4 Kinetics

To determine the Km and Vmax values of QB, Bt and Bp the enzymes were diluted with 0.2 mM NaAc buffer at pH 5.0 and added to 1 mM IP_6. The following final concentrations of enzymes were used: QB: 3.5 µg/ml (molar concentration of QB is unknown), Bt: 12.2

pM and Bp: 67 pM. Reactions were carried out for 30 min at room temperature. Phosphate release was measured using the colourimetric reagent described in section 2.2.1.

2.2.5 Thermostability using DSF

Differential scanning fluorimetry (DSF) was used to determine the temperature of unfolding, as a measure of thermostability, in the presence or absence of substrate. Enzyme concentrations were as described before. Fluorescent dye SYPRO Orange (Life Technologies) was used as a marker of unfolding. The amounts of reagents for one set of triplicates determinations were:

10 µl	enzyme
50 µl	0, 1 or 2 mM IP_6 in 0.1 M glycine pH 3.5 or 0.1 M HEPES pH 7.0
5 µl	SYPRO 1:100 dilution
35 µl	ddH_2O

20 µl of the above master mix was used for each triplicate and added to a 96-well plate in the RT-PCR machine. Another 20 µl was used as a background measurement with no enzyme. The machine ran a temperature gradient in the range of 25 – 95 °C with intervals of 0.5 °C every 20 sec, measuring fluorescence at 470/570 nm. The resulting data was processed in Excel. First, the background signal from the dye-only measurement was subtracted. Next, the first derivative was calculated by dividing the change in the relative fluorescence by the change of the temperature.

DFS experiments in oxidising and reducing conditions were performed as described, with the addition of 10 mM 1,4-Dithiothreitol (DTT, Sigma-Aldrich) or 10 mM trans-4,5-Dihydroxy-1,2-dithiane (Sigma-Aldrich).

2.2.6 Protein expression and purification

Expression vector pOPINF (Berrow *et al.*, 2007) was used to clone the Bp, Bt and Bl genes along with an N-terminal His-tag. The original constructs were provided by Arthur Li (Li, 2014). The pOPINF constructs were transformed into Rosetta (DE3) (Novagen) *E.coli* cells for protein expression. The transformants were grown on ampicillin-containing LB agar (100 μg/ml ampicillin) overnight. A single colony was used to inoculate 10 ml of ampicillin-containing LB medium and allowed to grow at 37 °C on a 200 rpm shaker.

For a 1 L protein purification procedure, 1 ml of the overnight culture was used to inoculate 100 ml of fresh media and allowed to grow overnight; the next day, 20 ml of the second overnight culture was used to inoculate 1 L of media. The culture was allowed to grow until its OD600 reached 0.6. Then, the cultures were transferred to a 30 °C shaking incubator. Protein expression was induced by adding isopropyl β-D-1-thiogalactopyranoside (IPTG) to a final concentration of 0.1 mM (for Bp and Bl) or 0.5 mM (for Bt). The culture was allowed to grow overnight and the cells were then harvested by centrifugation at 6000 rpm for 1 hr at 4 °C. The cell pellet was frozen in liquid nitrogen and transferred to -80 °C storage before protein purification.

The cell pellet was added to lysis buffer (50 mM Tris-HCl pH 8, 300 mM NaCl, 10 mM imidazole) to make up the volume of 30 ml. RNAse and DNAse were added to the buffer. The pellet was left on a magnetic stirrer at 4 °C until fully resuspended. The suspension was placed into a pre-chilled French press at 4 °C and lysed twice in a row at 1,200 psi. Cell debris was removed by centrifugation at 15,000 g at 4 °C.

A metal ion affinity chromatography column HisTrap HP containing 5ml of Ni-NTA resin (GE Healthcare) was equilibrated with wash buffer (50 mM Tris-HCl pH 8, 300 mM NaCl, 20 mM imidazole). The supernatant containing the soluble cell lysis fraction was loaded onto the column using a peristaltic pump P-1 (GE Healthcare). The column was then washed and eluted (elution buffer: 50 mM Tris-HCl pH 8, 300 mM NaCl, 250 mM imidazole) using the ÄKTAprime plus (GE Healthcare) chromatography system. Protein

fractions suitable for further purification were identified using the chromatogram and SDS-PAGE and concentrated to a volume of 2.2 ml using a Vivaspin centrifugal concentrator (10,000 MWCO, GE Healthcare).

A HiLoad 16/600 Superdex 75 pg gel filtration column (GE Healthcare) was equilibrated with gel purification buffer (10 mM Tris-HCl pH 7.4, 150 mM NaCl) using ÄKTAprime plus. The concentrated protein was loaded onto a 2ml loop and then purified using the column. The eluted fractions were analysed using the chromatogram and SDS-PAGE for the presence of protein.

Images of protein purification including chromatograms and SDS-PAGE pictures are included in Appendix 3.

2.3 Results and Discussion

2.3.1 pH profiles

The first experiment that was performed was an investigation of the relative enzyme activities at a range of pH from pH 2.0 to 9.0 to gain an idea of the enzymes' pH optima and how they relate to the pH present in animal gut.

Enzymes were tested at a range of pH with IP_6 substrate. The buffers chosen were: glycine-HCl for pH 2.0-3.5, sodium acetate for pH 4.0-5.5, HEPES-NaOH for pH 6.0-8.5 and glycine-NaOH for pH 9.0. At 30 min or 60 min timepoints, the reactions were stopped by the addition of the colour reagent. After 30 minutes the absorbance was measured at 700nm. Triplicate determinations were made. Mean and standard deviations are plotted in the figures.

Calibration curve was obtained with a range of inorganic phosphate concentrations

ranging from 0-2 mM. As can be seen in the figure below, absorbance at 700 nm is proportional to phosphate concentration. The signal is linear throughout the whole data, which is until the absorbance of at least 1.4.

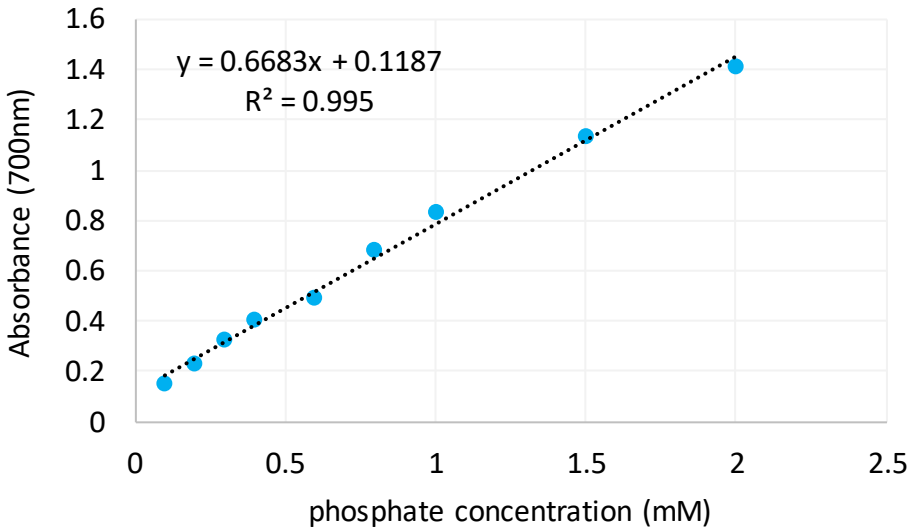

Figure 2.1 Phosphate calibration curve.
A range phosphate concentrations in a colourimetric reaction with ammonium molybdate. Increasing phosphate concentrations yielded increased signal at 700 nm due to formation of molybdenum blue in a linear fashion. Trendline was fitted with the R2 value of 0.995 using Microsoft Office Excel.

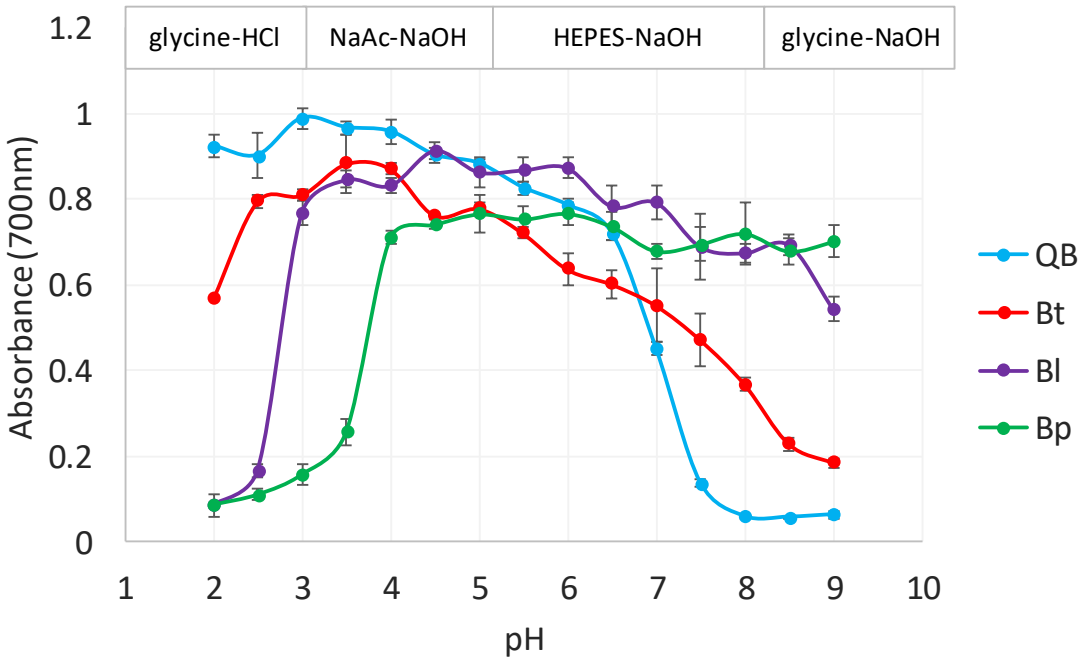

Figure 2.2 pH profiles of catalytic activity against IP_6 of four phytases (Bt, Bl, Bp, QB) Buffers used were as follows: glycine-HCl for pH 2-3, NaAc-NaOH for pH 3.5-5, HEPES-NaOH for pH 5.5-8, glycine-NaOH for pH 8.5-9. Activity of four phytases: *Bt, Bl, Bp* and QB, at concentrations of 50 µg/ml, 74 µg/ml, 48 µg/ml and 2 µg/ml, respectively, was measured at these different pH values using the phosphate release assay. The reactions proceeded for 60 min for *Bt, Bl* and *Bp* and for 30 min for QB. Means of triplicate measurements are presented along with standard deviation error bars.

As seen in Figure 2.2 above, Quantum Blue has the highest activity at pH 3.0 with a steady decrease until pH 6.5, where it reaches ~75% of its activity. After this there is a rapid drop in activity with negligible activity above pH 8.0.

The *B.thetaiotaomicron* phytase has low activity at pH 2.0 with an increase in activity between 2.5 and 3.5, where the activity peaks. This is followed by an almost linear decrease in activity with the higher pH and a small second optimum at pH 5, where the activity is at ~90% of maximum. At pH 9.0 there is still ~25% of activity left.

The *B.longum* phytase shows negligible activity levels at pH 2.0 and 2.5, after which the activity rapidly increases at pH 3.0 to ~90% of maximum, and rises until a peak at pH 4.5. From there the activity shows a general gentle downward trend, with small additional

optima at pH 6.0, 7.0 and 8.5 until pH 9.0 where it is at ~55%. The activity at the final measured pH of 9.0 is significantly higher than that of QB and Bt.

Lastly, Bp shows negligible activity starting from pH 2.0 with slow increase until pH 3.5. At pH 4.0 the activity is relatively high and stays at a similar level until pH 9.0. The last measured pH 9.0 shows the highest activity in Bp compared to the other enzymes, at ~95% of maximum activity. Interestingly, both Bl and Bp show a 50% drop in activity at pH 7.

Feed material has been shown to remain in the broiler proventriculus/gizzard for 25-30 minutes (Jackson and Duke, 1995; Svihus *et al.*, 2002). This provides a short window of opportunity for the enzyme to dephosphorylate phytate. Therefore, a commercially viable phytase product would have to be highly active for at least 30 minutes at pH of around 3.5 after being ingested. Indeed, commercially available phytase tend to be most active at the pH range of 4.0 – 6.0 (Menezes-Blackburn, Gabler and Greiner, 2015).

A study by Tamayo-Ramos et al. (Tamayo-Ramos *et al.*, 2012) investigated the pH profile of Bp and Bl recombinant and purified phytases, albeit in different buffers. The recombinant His-tagged proteins were purified from *E.coli*. They found that for both enzymes, the activity becomes significant only from pH 4.5. Below that, it was shown to be negligible. Variation in enzyme preparation and overall conditions may have contributed to the differences in the results. Additionally, Tamayo-Ramos used sodium citrate buffer for pH 3.0 and citrate is a phytase inhibitor, which may have contributed to the negligible apparent activity.

The results from the study show a clear peak in activity for both enzymes at pH 5.5. The study was conducted in sodium acetate buffer, same as in my experiment, however my results show a more rapid increase in activity with increasing pH and thereafter a plateau. For measurements in the range of 6.0 to 7.2 the study used a bis-Tris buffer, where I used HEPES – a buffer more suitable for the maintenance of enzyme activity

(Taha *et al.*, 2014). This may explain the higher activity in my results in that range, and seemingly a formation of a pH optimum peak in the study.

Quantum Blue enzyme shows a significantly higher activity at low pH. This is consistent with its use as a commercial phytase. It is intended to work quickly in the stomach and is optimised to be effective in the low pH of proventriculus and gizzard (Abvista.com). Its activity falls off substantially after pH 7, making it largely inactive after passage through gizzard and upon entering the small intestine. On the other hand, its activity at pH 2-3 was significantly higher than that the other three enzymes.

Zeller et al. (Zeller *et al.*, 2016) conducted a study looking at the effects of QB phytase supplementation in feed in broilers. The wheat-soybean based feed was subjected to microwave treatment before feeding to inactivate most of the intrinsic phytase present in the grain to allow to discriminate between the effects of the intrinsic and the adjunct dietary phytase. The microwave-treated wheat then showed 19% of the phytase activity present in the non-treated wheat. Furthermore, synergistic effects were found between the intrinsic phytase in the crop and the supplemented phytase (Zeller *et al.*, 2016).

From the three wild-type phytases, only Bt was somewhat active at pH 2-2.5, albeit less so than QB, which would mean it might be a suitable candidate for low pH environment. However, for it to be an appropriate candidate for commercial enzyme development, it needs to show other qualities, such as a wide optimal temperature of reaction, retaining activity during and after exposure to high temperatures or being resistant to proteases.

2.3.2 Temperature profiles of reaction

After investigating the enzyme activity at a range of pH's and determining their pH optima, I showed that QB is most active at low pH among the four enzymes and that Bt has the highest activity from the three wild-type phytases. This could be of interest to the

industry of animal feed supplements, however more conditions had to be investigated first.

Candidate phytases must show a wide activity spectrum at relevant temperatures to ensure they are most active in the feed environment. In particular, an ideal phytase would be catalytically active, easy to produce, resistant to proteases, thermostable and pH stable – all at the relevant body temperatures for the target animals. Chicken body temperature ranges from 39-41 °C (Bolzani, Ruggeri and Olivo, 1979) and pig body temperature varies from 37 °C to 40 °C (Ingram and Legge, 1970) therefore it is crucial that the supplemental phytase is highly active at this and the surrounding temperatures.

Typically, enzymes showing good tolerance of high temperatures – either before or during the reaction – also display resistance to proteases. Hence, obtaining a highly thermostable engineered enzyme would ensure its increased chance of survival in contact with the digestive enzymes of the animal gut. For example, a luciferase enzyme engineered with protease resistance against trypsin and chymotrypsin in mind, displayed such structural changes as to increase the thermostability by a few degrees (Riahi-Madvar and Hosseinkhani, 2009).

I conducted experiments investigating the temperature profiles of activity of three wild-type HAP phytases and a commercial HD phytase. I wanted to gain understanding of the temperature optima of activity at two different pH's. These pH values were chosen for assays because they reflect the pH present in animal gut at different stages of digestion, most plant and microbial phytases have optima in the range of pH 3.5-7.0 (Turner, Richardson and Mullaney, 2007, p. 232).

The experiments were carried out at pH 3.5 in a glycine-HCl buffer and at pH 7 in a HEPES-NaOH buffer. Enzymes were diluted in the aforementioned buffers to a suitable concentration so that the resulting trace showed a meaningful activity profile. Substrate IP_6 was pre-incubated at each specific temperature ranging from 30 °C to 95 °C before the enzyme was added and the reaction was allowed to continue for 30 min. Phosphate release was measured with the colourimetric assay and observed by measuring the

absorbance at 700 nm. Triplicate determinations were made and the means and standard deviations are shown in the Figure 2.3 below.

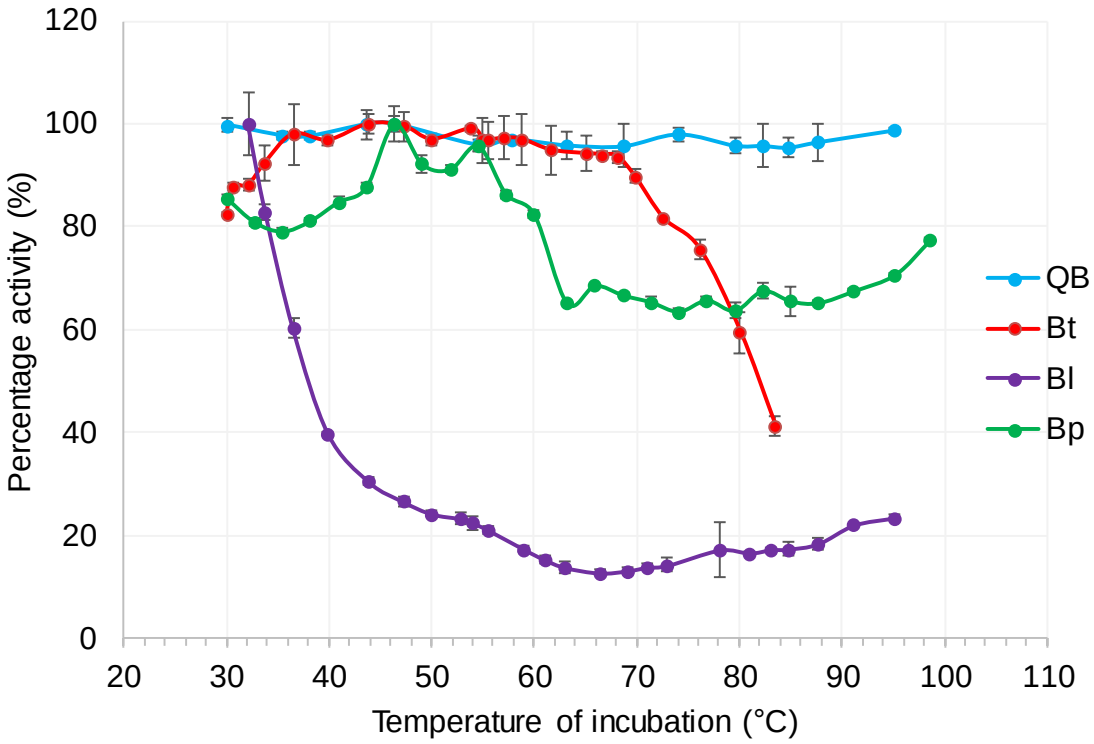

Figure 2.3 Temperature stability profiles of phytases (Bt, Bl, Bp, QB) at pH 3.5. Enzymes *Bt, Bl, Bp* and QB, at concentrations of 50 µg/ml, 74 µg/ml, 48 µg/ml and 2 µg/ml, respectively, were incubated for 10 min at a range of temperatures from 30 °C to 95 °C in 0.1 M glycine-HCl buffer. Post-incubation activity was measured using the molybdenum phosphate release assay, shown as percentage of maximum phosphate release as assayed with IP_6. Phytase reactions with IP_6 were carried out for 30 min.

Figure 2.3 shows the phosphate release representing phytase activity at a range of temperatures at pH 3.5 of three bacterial phytases in comparison to the commercial phytase Quantum Blue. The activity of Bt started at ~90% of its maximum activity at 30 °C with maximum activity in the range 36- 69 °C after which activity declined to 40% of maximum activity at 83 °C , the final temperature of measurement. Bt thus appears to have a broad temperature optimum.

Bl activity started at 100% of its activity at 30 °C, followed by a steep downwards slope. The trace forms a gentle shoulder at ~54 °C at 22% of activity, while still following a gentle downwards trend until 67 °C followed by a negligible upwards trend.

Quantum Blue displayed a stable level of activity throughout the experiment, as expected of a highly engineered enzyme for non-ruminant feed applications. Bp showed a low activity throughout with a slight plateau in the range of 45-55 °C.

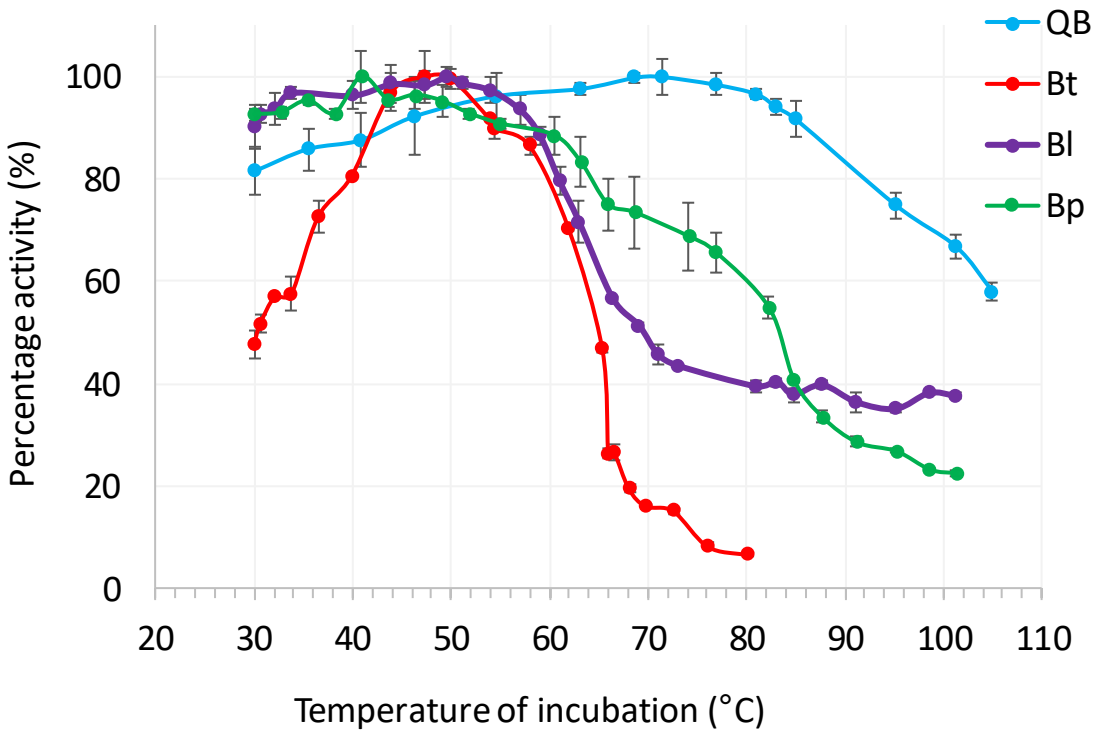

Figure 2.4 Temperature stability profiles of phytases (Bt, Bl, Bp, QB) at pH 7.0. Enzymes *Bt, Bl, Bp* and QB, at concentrations of 50 µg/ml, 74 µg/ml, 48 µg/ml and 2 µg/ml, respectively, were incubated at a range of temperatures from 30 °C to 95 °C in 0.1 M HEPES-NaOH buffer. Post-incubation activity was measured using the molybdenum phosphate release assay, shown as percentage of maximum phosphate release as assayed with IP_6. Phytase reactions with IP_6 were carried out for 30 min.

As seen in Figure 2.4 above, at pH 7 the QB activity starts at 82 % at 30 °C and follows a gentle upwards trend until reaching a wide peak at 69-71 °C. A slightly sharper decline in the trend follows, until the final measurement at 105 °C where the activity reached 58 %. Bt starts at a lower activity than the other three enzymes: at 30 °C it is at 48 %, followed by a sharp increase until a well-defined peak at 47 °C. The activity then drops sharply until

66 °C where it is at 26 % and gently slopes down until the final measurement at 83.5 °C where activity was at 7 %.

At pH 7, Bl and Bp show similar traces from the lowest temperature of 30 °C until they diverge at 60 °C. Until then, both enzymes show traces of activity rising from 30 °C where their activities are at 90% and 92 % respectively. Bl shows a gentle peak with the maximum activity at 49.6 °C. At 60 °C, having reached 80% activity, the signal falls off rapidly until 71 °C where activity is at 46 % and the signal only decreases very slowly. At the final measured temperature of 103.2 °C the activity is at 43% maximum.
Bp appears to peak at 41 °C, however that data point seems anomalous and doesn't follow the trend seen by looking at the surrounding data points. Its standard deviation is 0.062, which is over twice as high as the average standard deviation for the data set for Bp (0.030). As such, I would disregard the peak at 41 °C and accept the data point at 46 °C (96 % of maximum activity measured) as the true peak of activity. Its standard deviation is at 0.032 which falls very close to the average standard deviation. After the Bp peak the signal of activity slowly drops until 77 °C at 66 % activity. Then, it rapidly decreases until 85 °C (41 % activity). The trend then slowly falls until the final measurement of 23 % activity at 101 °C.

The three wild-type enzymes Bt, Bl and Bp clearly show a lower optimal temperature of activity than QB at pH 7. Their peaks were at 47.3 °C, 49.6 °C and 46 °C respectively, which places their optima in a similar range, perhaps reflecting the close similarity of their structures. *Bt*Minpp, *Bl*Minpp and *Bt*Minpp share a catalytic pocket lined with basic residues, substitution of which with acidic residues reduces activity in *Bt*Minpp (Li, 2014). While it is difficult, here, to separate pH influences on enzyme activity from thermal stability, increase of pH from 3.5 to 7 seemed to sharpen the thermal stability profile of Bt in particular. Above the temperature optima the individual activities declined rapidly after the peaks. QB shows its peak activity at a higher temperature of 69-71 °C, the peak is very wide compared to the other three enzymes and does not precede such a rapid decline in signal.

Arguably, temperature profiles of activity at pH 5-5.5 could have been performed instead. The reason being, Bl and Bp showed pH optima at pH 4.5 and as a plateau at the range of pH 4-9, respectively, therefore it could be argued that the temperature assay should be

conducted to include these pH's. However, I chose the assay to be carried out at pH 3.5 and 7.0 to have a larger range of investigation as well as to reflect the conditions in the animal gut.

Tamayo-Ramos et al. (Tamayo-Ramos *et al.*, 2012) investigated the optimal temperatures of reaction of Bl and Bp at pH 5.5 in sodium acetate buffer. The enzymes used were purified recombinant protein. They showed that both enzymes reach 100% of their activity at 50 °C, which is very close to my result of 49.6 °C for Bl and similar to the value 46 °C observed here for Bp, both at pH 7. The temperature profile at pH 5.5 that they reported for both Bl and Bt was quite sharp either side of the optima and quite similar to that reported here for Bt (Figure 2.4). Thus, the activity trace for Bp shows a sharp peak with activity falling off at temperatures lower and higher than 50 °C. However, Bl shows a wider range of activity, displaying a plateau from 50 °C to 55 °C, followed by a sharp decrease to ~35% of its activity at 60 °C. The differences between the above results and those acquired by me could stem from the subtle variations in purification and storage procedures, as well as addition of 1 mM EDTA by Tamayo-Ramos et al. into the dialysis buffer. EDTA and other additives such as bovine serum albumin are sometimes added to protein preparations to increase their stability (Bisswanger, 2014). EDTA was shown in the above study to inhibit the activity of Bp down to 85 % and Bl to 69 % at pH 5.5 at 50 °C.

A study by Lan et al. (Lan *et al.*, 2011) investigated a HAP phytase from *Mitsuokella jalaludinii*, a bovine rumen bacterium. The enzyme was purified and allowed to react with substrate IP_6 at a range of temperatures. It was shown that the optimum temperature for the phytase activity was 55-60 °C. Similarly, Yanke et al. (Yanke, Selinger and Cheng, 1999) showed that the phytase from *Selenomonas ruminantium*, another ruminal bacterium phytase, has a similar temperature optimum of 50-55 °C with the activity rapidly dropping off after 60 °C. HAP phytases from *Hafnia alvei* and *Yersinia kristensenii* were shown to have the temperature optima at 65 °C and 55 °C (Ariza *et al.*, 2013). In fact, most phytase-producing micro-organisms show the phytase optimum of wild type enzyme to lie in the range of 50-70 °C (Lan *et al.*, 2011).

2.3.3 Determination of kinetic parameters

To be able to use enzymes most effectively, it is important to know their performance characteristics as thoroughly as possible. While the substrate concentrations obtained in the digestive tract of the chicken are undefined, as is the interfacial chemistry of phytase action on phytate contained in the aleurone grains of cereal components of animal feedstuffs, an important initial characterization of any enzyme is its fit to the Michaelis-Menten model and derivation of Km and Vmax parameters. Of necessity, for phytases these analyses are most commonly performed on wholly soluble substrate, IP_6. It is worth remembering however that theoretical calculations of the solubility of $InsP_6$ in intracellular physiological media, place the upper limit of solubility of IP_6 at approximately 50µM in the presence of physiological (1mM) Mg^{2+} It is, of course, common for the feedstuff industry to add divalent metals, particularly Ca^{2+}, as monocalcium phosphate or limestone to animal feedstuff (Veiga *et al.*, 2014).

Here, enzyme activity was investigated by measuring the phosphate release using the colourimetric assay, which is proportional to the enzyme activity. Various concentrations of IP_6 from 0 µM to 2500 µM were added to the enzyme diluted with 0.2 M NaAc buffer at pH 5.0. The concentrations of enzymes used were 67 pM (Bp), 12.2 pM (Bt) and 3.5 µg/ml (QB, molar concentration unknown).

The reaction was carried out at 25 °C for 30 min, followed by the addition of the colourimetric reagent and subsequent incubation for 30 min before measuring the absorbance at 700 nm. The data was collected in triplicate measurements and the averages were used for the analysis.

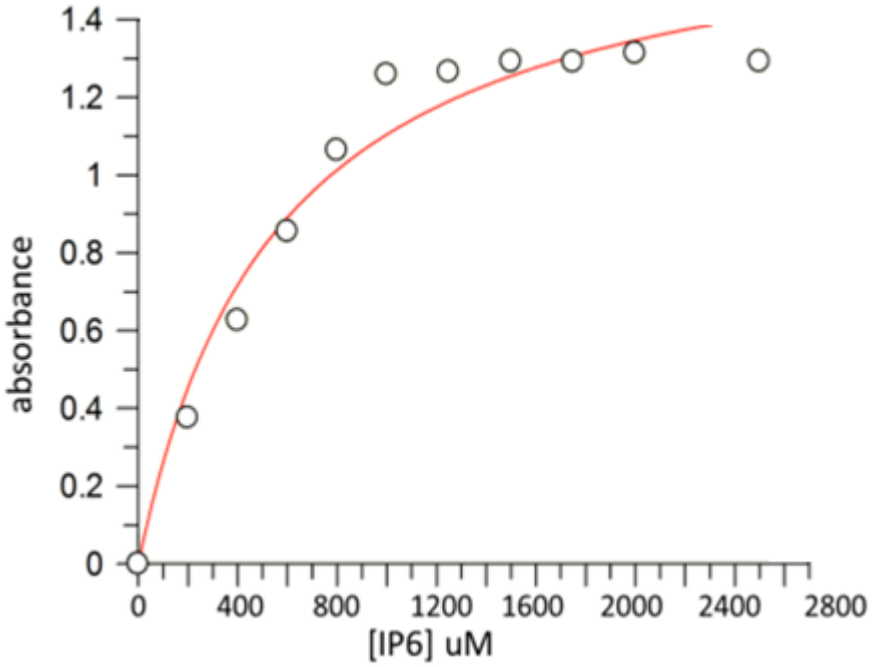

Figure 2.5 Activity of Quantum Blue phytase vs range of concentrations of substrate IP_6 at pH 5.
Buffer used was 0.2 M NaAc. QB concentration was 3.5 µg/ml (molar concentration of QB unknown). Reactions were carried out for 30 min and assayed using the molybdenum blue method at 700 nm. Curve was fitted to Michaelis-Menten equation using the non-linear least squares regression. Vmax was calculated as 1.7249 AU/min and Km as 561.9 µM.

As seen in Figure 2.5, the reaction with QB was carried out at a range of substrate concentration high enough to see substrate saturation, which means at this specific conditions the Vmax was reached and no more phosphate was released despite addition of more concentrated IP_6. The value of Km was 561.9 µM.

A study involving measuring the phytase activity of Quantum Blue at pH 5.0 and at the temperature of 37 °C revealed the Km value of 142 µM (Menezes-Blackburn, Gabler and Greiner, 2015). The discrepancy in the experimental values from this work and the literature may stem from differences in assay conditions, such as the nature and

concentration of the buffer used, storage conditions of the enzymes prior to the experiment, the method of phosphate detection or intrinsic variations of the detector.

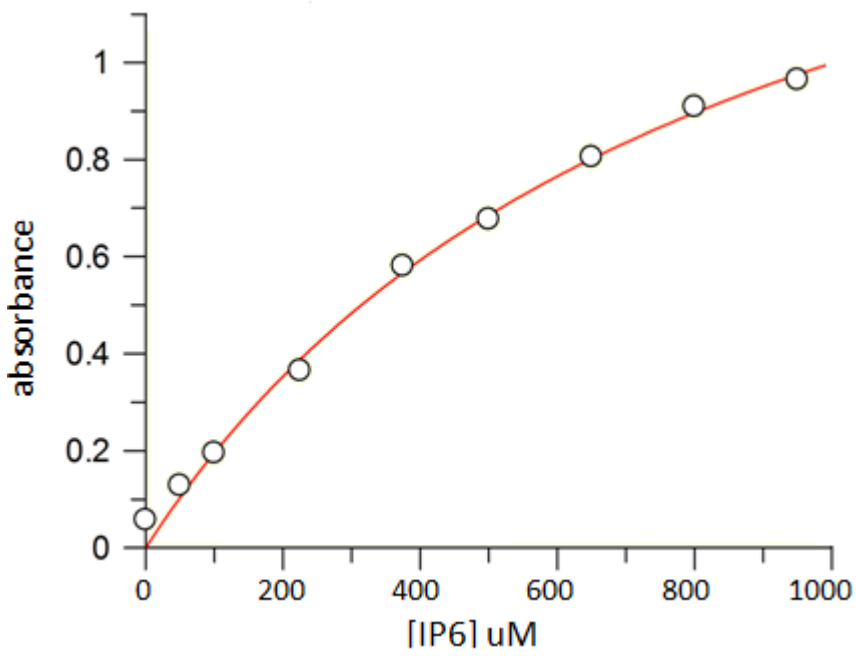

Figure 2.6 Activity of *B. pseudocatenulatum* Minpp vs range of concentrations of substrate IP_6 at pH 5.
Buffer used was 0.2 M NaAc. *Bp* concentration was 67 pm. Reactions were carried out for 30 min and assayed using the molybdenum blue method at 700 nm. Curve fitted to Michaelis-Menten equation using the non-linear least squares regression. Vmax was calculated as 1.84 AU/min and Km as 841.1 µM.

Figure 2.6 above shows the plot of activity of the Bp phytase against a range of substrate concentrations. The experiment was conducted using triplicate measurements. The average standard deviation was 0.016.

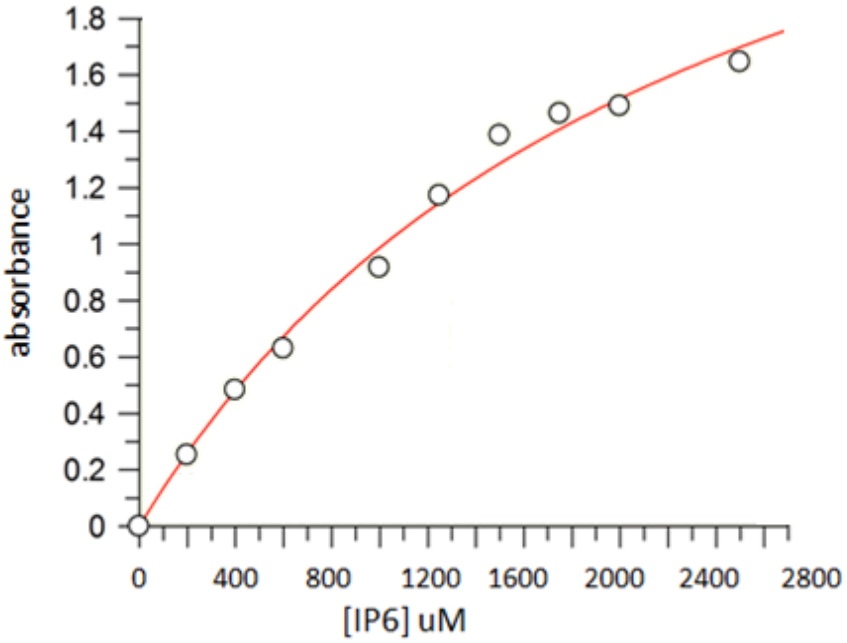

Figure 2.7 Activity of *B. thetaiotaomicron* Minpp vs range of concentrations of substrate IP_6 at pH 5.
Buffer used was 0.2 M NaAc. *Bt* concentration was 12.2 pm. Reactions were carried out for 30 min and assayed using the molybdenum blue method at 700 nm. Curve was fitted to Michaelis-Menten equation using the non-linear least squares regression. Vmax was calculated as 3.27 AU/min and Km as 2311.5 µM.

The reaction with Bt wasn't carried out until full completion; however I used the Graphit software to fit a suitable curve and calculated the estimated Vmax and Km. The Lineweaver-Burk plot shows a straight trace – a sign of a data set that fits the Michaelis-Menten kinetic model, adding validity to my experiment. The value of Vmax given was 3.27 with the standard error of 0.33. Km was given as 2311.5 with the standard error of 394.3.

One assumption behind the Michaelis-Menten mechanics is that no reverse reaction takes place, however in reality under certain circumstances it is possible for some product to be transformed back into substrate. Conventionally, the experiments to determine Vmax and Km are performed by obtaining the initial velocity V_0 of each reaction at each substrate concentration. This would be done by monitoring the reaction progression in real time by recording the change in absorbance with substrate accumulation. V_0 would then be obtained from the ratio of the change in absorbance over time. In certain

circumstances a second enzyme can be used that will rapidly transform the product into another species that cannot react with the enzyme under investigation.

This method was not possible however because a real time assay for phosphate release or IP_6 consumption is not available. The colourimetric reagent provides an end-point reaction that stops the enzyme reaction. Furthermore, phytases are not known to catalyse the reverse reaction to any significant degree. Hence I used the change in absorbance after 30 min for each substrate concentration as the rate of reaction.

2.3.4 Differential Scanning Fluorimetry to investigate thermostability and the effect of substrate IP_6.

Having determined the basic properties of the phytase enzymes such as their pH profiles, incubation temperature tolerance and kinetic parameters, I obtained a general portrayal of the enzymes' characteristics. While the incubation temperature experiments gave me an idea of the enzymes' activity after being subjected to a range of temperatures, a more detailed experiment was desired to determine the melting temperature of the proteins. The enzymes industry and especially animal feed industry are interested in the melting temperatures of enzymes to consider the optimal conditions for the pelleting processes in addition to considerations for processing, transportation, storage and application. Furthermore, thermostability is often correlated with protease resistance, another desirable characteristic in industrial enzymes (Yao *et al.*, 2012; Niu *et al.*, 2017).

Differential Scanning Fluorimetry (DSF) is a method that monitors unfolding of proteins in real time and is performed in a thermocycler with an addition of a fluorescent dye, typically SYPRO Orange (Invitrogen). The fluorescent dye is highly fluorescent in the non-polar environment around the hydrophobic sites in the interior of proteins in their native state. Fluorescence is quenched in the aqueous environment, but when the protein unfolds exposing hydrophobic sites probe fluorescence increases. The reaction mixture is incubated at an increasing temperature and the change in fluorescence signal allows for

following the changes in the protein conformation. The method requires relatively low amounts of proteins and tolerates impurities up to a point. In the industry it is often used to screen for stabilising conditions (Niesen, 2007).

Here, I used DSF to determine the melting temperature of my enzymes in various conditions. In the first experiment I wanted to see what the melting temperatures are at pH 3.5 and 7 – first without any substrate, and also with a range of substrate IP_6 concentrations to see what effect the IP_6 has on the protein unfolding. Upon binding to their ligand while in their native state, proteins are known to often undergo conformational changes that confer increased tolerance to heat, proteolysis resistance and photooxidation among other characteristics (Citri and Garber, 1963; Griessler *et al.*, 2000; Lejeune *et al.*, 2001).

Figure 2.8 below shows the results of a DSF experiment with the Bt phytase. The graphs show averages of triplicate measurements for each of the four IP_6 concentrations: 0 mM, 0.5 mM, 1.0 mM and 2.0 mM conducted at pH 3.5 and 7.0. Background values of measurements involving a 'no-enzyme' control were subtracted from the experimental values. Next, the first derivative was calculated to help visualise the progressive changes in fluorescence between the temperature increments. Finally, data was normalised to show percentage of the maximum fluorescence for each trace.

Without any substrate at both pH 3.5 and 7.0, the Bt enzyme shows transition points at 38 °C, indicating mid-points of protein unfolding. Addition of higher increasing substrate IP_6 increases the unfolding temperature from 38 °C to 49 °C at pH 3.5 and to 52 °C at pH 7.0. It is perhaps consistent that the kinetic analysis (Figure 2.7) yielded a Km of approx. 2.3 mM, a concentration around which increasing substrate concentration yields thermal stabilization of the protein (Figure 2.8).

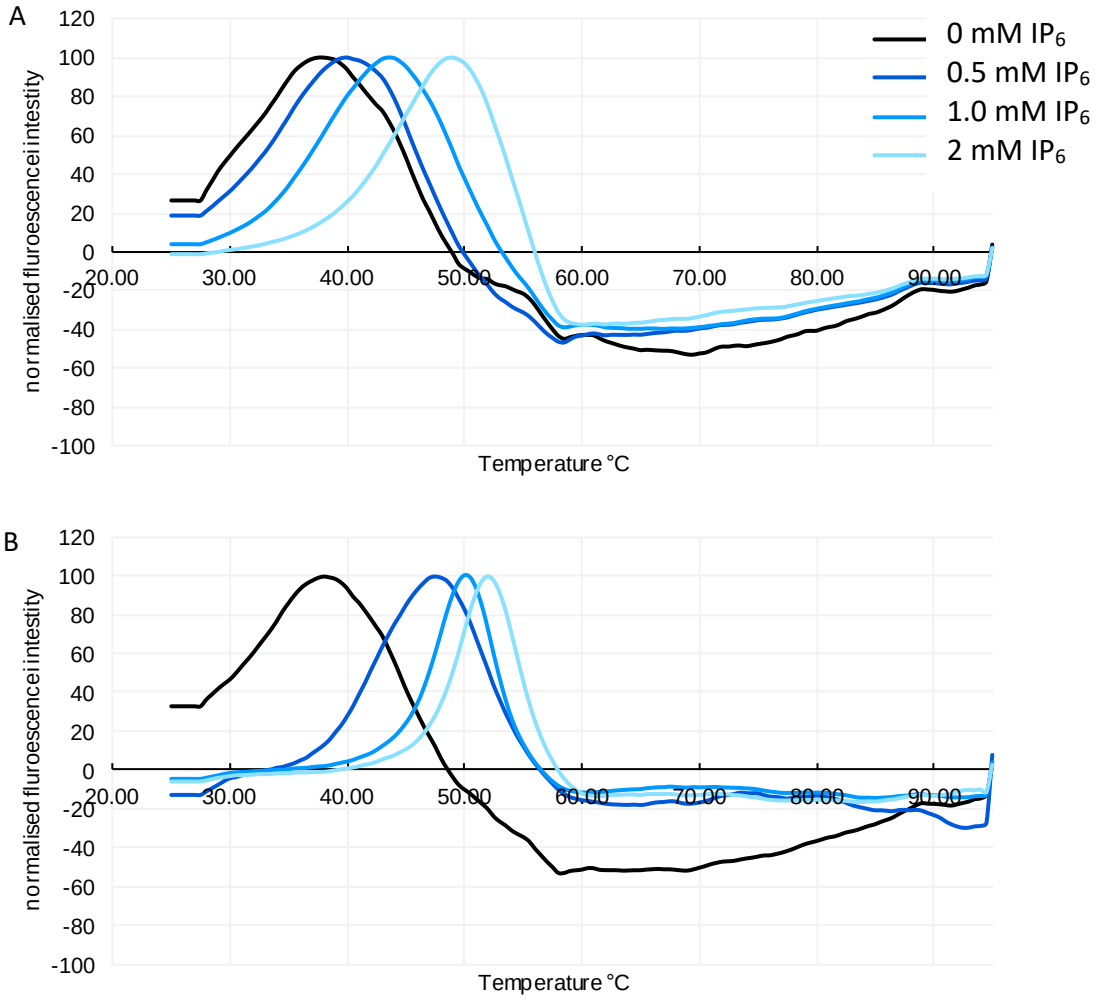

Figure 2.8 Differential Scanning Fluorimetry of *B. thetaiotaomicron* Minpp. Thermostability vs substrate concentration. Enzyme concentration was 1 mg/ml. The experiment was conducted in a PCR machine with a temperature gradient in the range of 25 – 95 °C with intervals of 0.5 °C every 20 sec, measuring fluorescence of the hydrophobic fluorescent probe SYPRO at 470/570 nm. Data analysis was conducted to calculate the first order derivative of the raw data, and to normalise the trendlines to 100% the maximum signal for each data set. Averages of triplicates measurements are shown for each trace. A: pH 3.5 in 0.1 M glycine-HCl; B: pH 7 in 0.1 M HEPES-NaOH.

Figure 2.9 below shows the results of the DSF experiment with the *Bl*Minpp. It can be seen that at both pH 3.5 and 7.0 addition of even a small concentration of substrate increases the thermostability significantly. Without substrate, the temperatures of unfolding are 31 °C and 31.5 °C for pH 3.5 and 7.0 respectively. The addition of 2mM substrate IP_6 increases the thermostability to 40.5 °C and 43.50 respectively. Interestingly, in addition to the main peak, a shoulder is visible at 0 mM IP_6 concentration at the temperature of around 38 °C at pH 3.5 and 7.0. This may stem from a dual process of unfolding of the enzyme. The shoulder is absent from traces with 2 mM substrate.

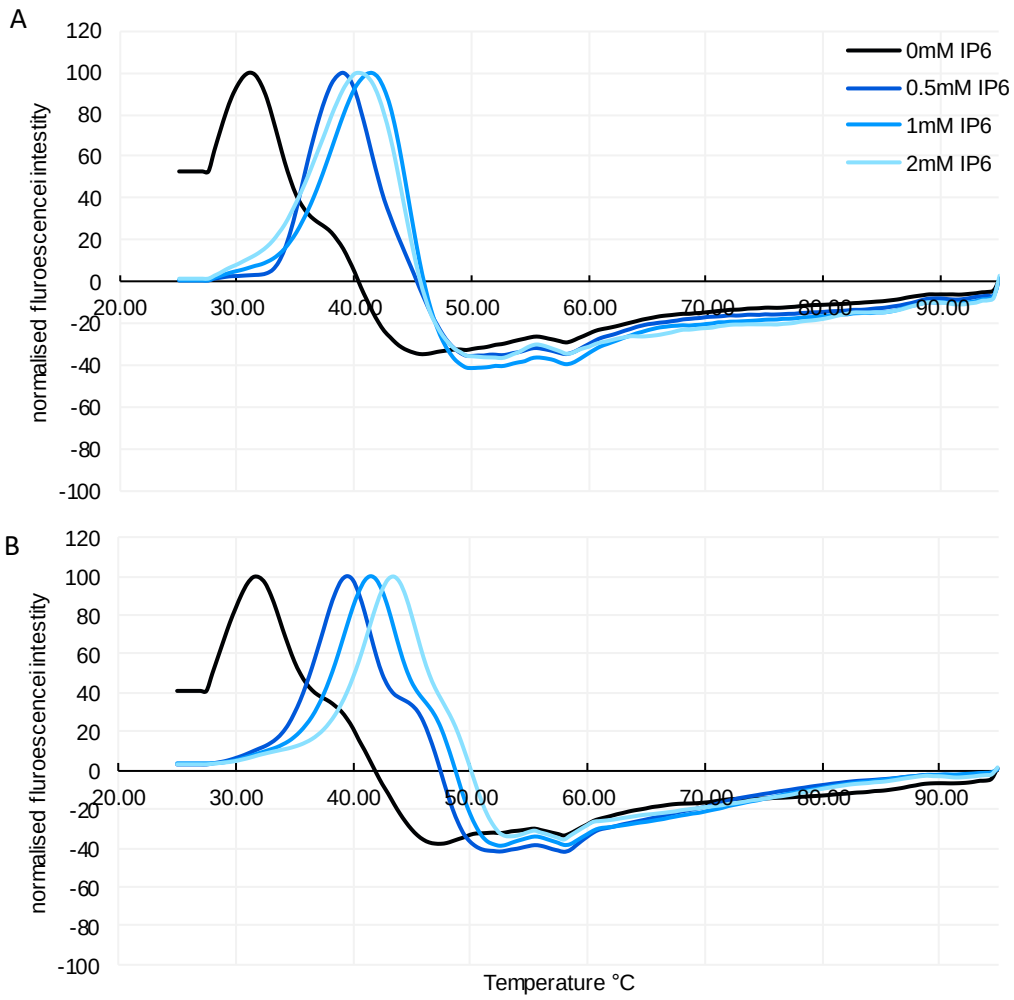

Figure 2.9 Differential Scanning Fluorimetry of *B. longum* Minpp.
Thermostability vs substrate concentration. Enzyme concentration was 3.8 mg/ml. The experiment was conducted in a PCR machine with a temperature gradient in the range of 25 – 95 °C with intervals of 0.5 °C every 20 sec, measuring fluorescence of the hydrophobic fluorescent probe SYPRO at 470/570 nm. Data analysis was conducted to calculate the first order derivative of the raw data, and to normalise the trendlines to 100% the maximum signal for each data set. Averages of triplicates measurements are shown for each trace. A: pH 3.5; B: pH 7.

Figure 2.10 below shows the DSF experiment for the *Bp*Minpp. Immediately, it is apparent that at pH 3.5 and 0 mM substrate, the phytase shows two main peaks of unfolding at the same intensity, hinting at a dual process of unfolding such as the two distinct domains α and αβ unfolding separately. The peaks are at 35 °C and 41 °C. Interestingly, the high temperature shoulder is evident, albeit less prominently, in the traces for *Bl*Minpp (Figure 2.9), but not for the *Bacteroides Bt*Minpp enzyme (Figure 2.8). At 0.5 mM substrate concentration, there is a main peak at 39 °C and a shoulder at around 45 °C, likely corresponding to the second peak from the first trace. The shoulders

are absent from traces with higher substrate concentrations. At pH 7, the main peak is at 46 °C while a small second peak is visible at 50.5 °C with 75.5% of the fluorescence signal of the main peak. The shoulder disappears at substrate concentrations over 1 mM. Here, again, the initial sharp increase in temperature of unfolding with incremental additional substrate is consistent with the lower Km (0.84 mM) of *Bp*Minp for substrate and saturation at supra-mM concentrations.

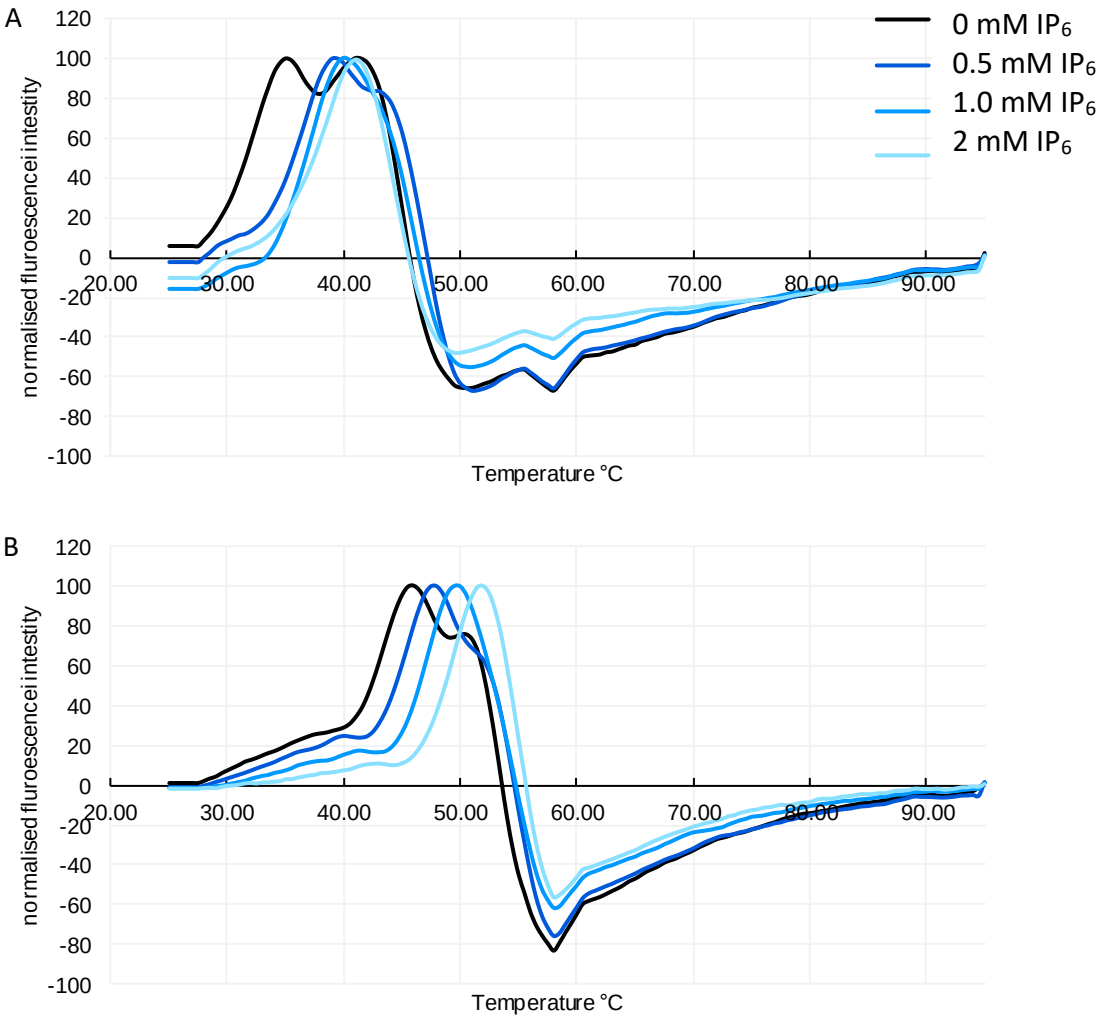

Figure 2.10 Differential Scanning Fluorimetry of *B. pseudocatenulatum* Minpp vs substrate IP_6 concentration.
Averages of triplicates measurements are shown for each trace. Enzyme concentration was 2.5 mg/ml. The experiment was conducted in a PCR machine with a temperature gradient in the range of 25 – 95 °C with intervals of 0.5 °C every 20 sec, measuring fluorescence of the hydrophobic fluorescent probe SYPRO at 470/570 nm. Data analysis was conducted to calculate the first order derivative of the raw data, and to normalise the trendlines to 100% the maximum signal for each data set. A: pH 3.5; B: pH 7.

Figure 2.11 below shows the results of the DSF experiment with the commercial Quantum Blue phytase. Here, the temperatures of unfolding are significantly higher than those of the bacterial phytases described earlier. Interestingly, the main peaks of unfolding remain at similar temperatures despite the range of substrate concentrations. The main peaks are at 81.0-81.5 °C and 83.5-84.0 °C at pH 3.5 and 7.0 respectively. Additional peaks are visible at 58-60 °C and around 74 °C. The Quantum Blue was supplied in its commercial form with possible additional proteins added for increased stability, which may be the sources of some of the additional peaks of unfolding. The main peak most likely originates from the Quantum Blue phytase itself, as it likely has been engineered to withstand high temperatures of industrial processing, with added proteolysis resistance.

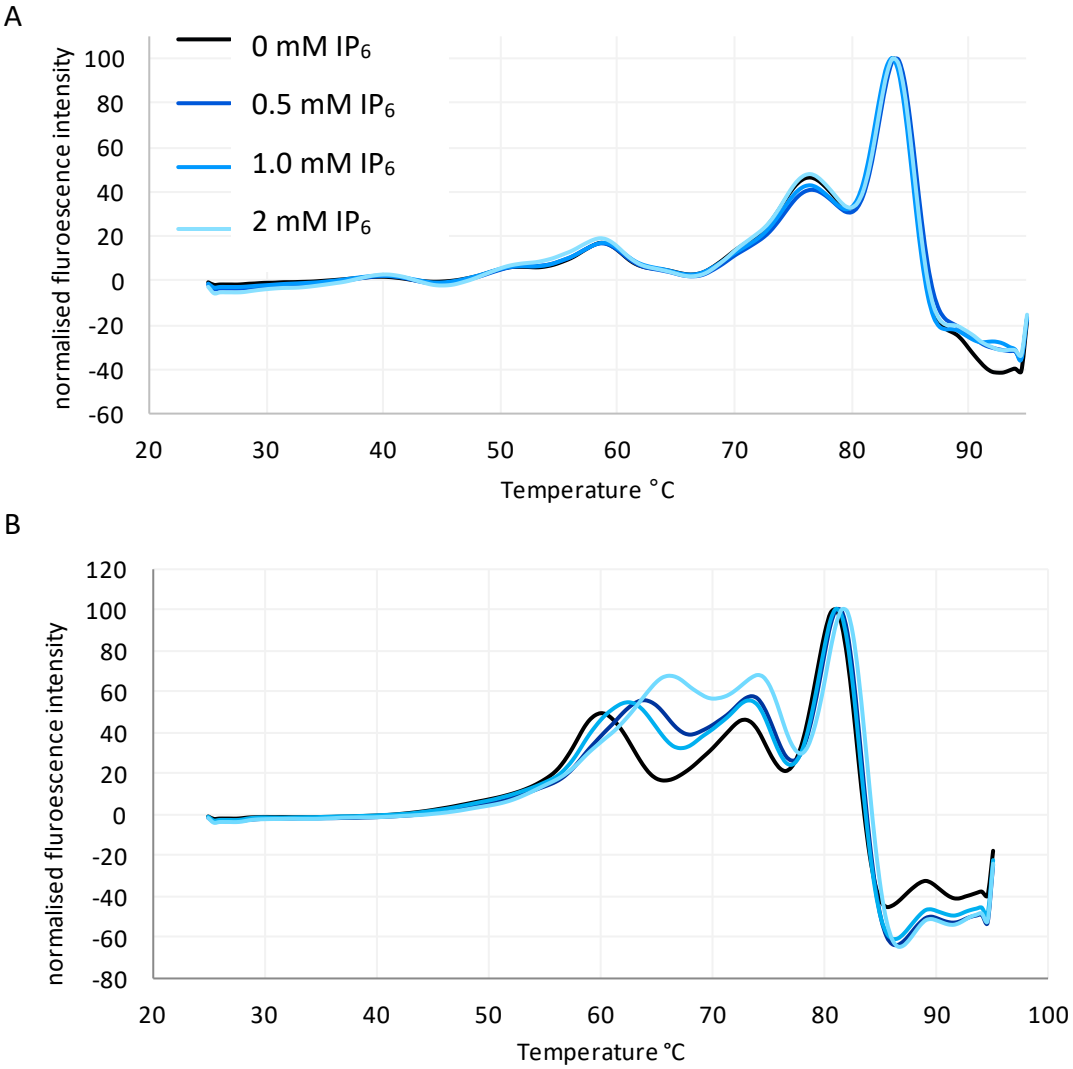

Figure 2.11 Differential Scanning Fluorimetry of QB phytase vs substrate IP_6 concentration at pH 3.5 (A) and 7 (B).
Averages of triplicates measurements are shown for each trace. Enzyme concentration was 7.9 mg/ml. The experiment was conducted in a PCR machine with a temperature gradient in the range of 25 – 95 °C with intervals of 0.5 °C every 20 sec, measuring fluorescence of the hydrophobic fluorescent probe SYPRO at 470/570 nm. Data analysis was conducted to calculate the first order derivative of the raw data, and to normalise the trendlines to 100% the maximum signal for each data set. A: pH 3.5; B: pH 7

Figure 2.12 below shows a summary of the main peaks of unfolding of the four enzymes characterized in this chapter. In case of two peaks appearing, the first one in case of Bp or the more prominent one in case of QB was selected for display.

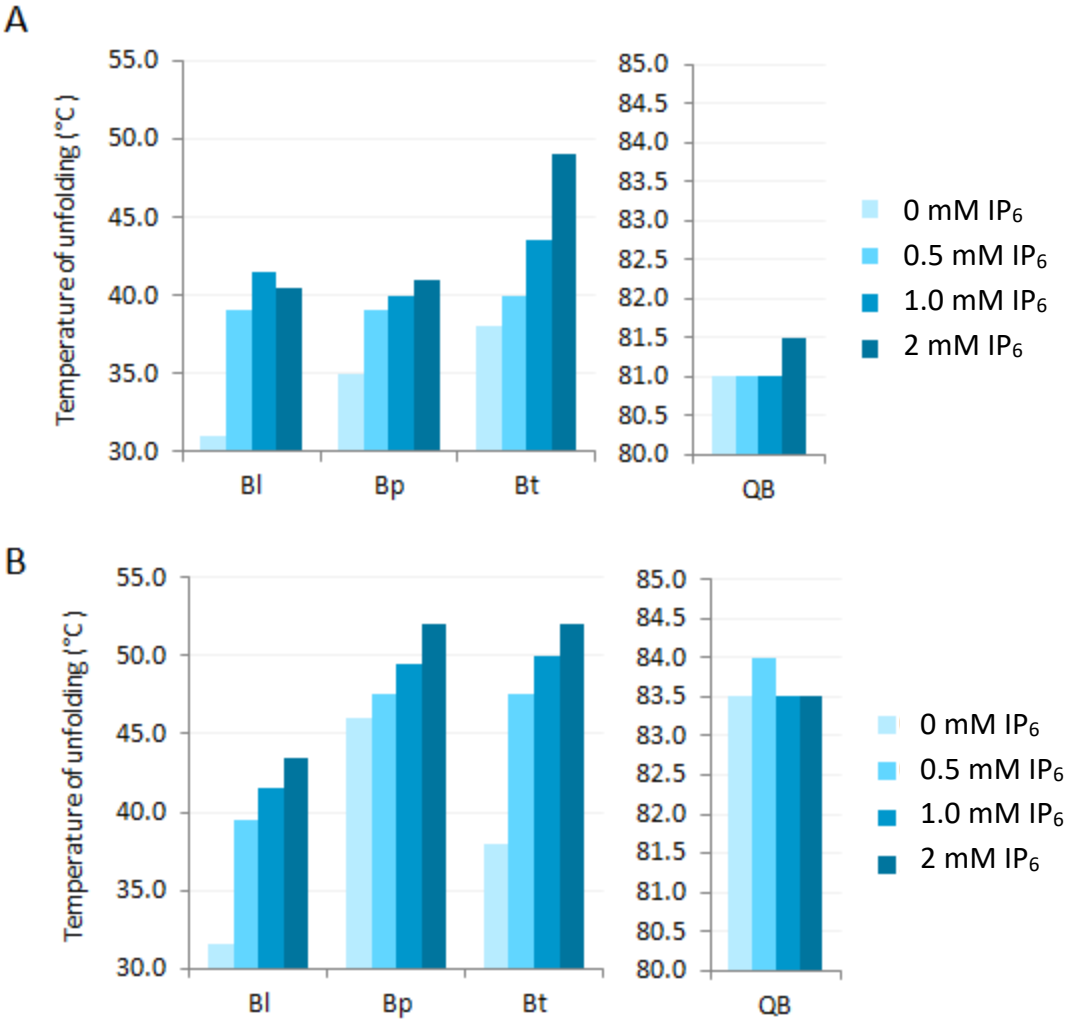

Figure 2.12 Summary graphs of DSF experiments with Bt, Bl, Bp and QB phytases at pH 3.5 and 7.0 at a range of substrate concentrations.
Showing average temperatures of unfolding of the main peaks. No error bars due to standard deviations being negligible. A: pH 3.5. B: pH 7.0.

In general, it is apparent that presence of substrate increases thermostability of the bacterial (HAE) Minpp enzymes as shown by the DSF experiment, however it has little effect on the thermostability of Quantum Blue, an *E.coli* HD phytase. While the Minpps and *E.coli* enzymes are HAP phytases (Rigden, 2008; Stentz *et al.*, 2014) and share a common α + αβ fold structure, it is possible that the substrate-induced stabilization of the Minpp proteins observed here is unique to the HAE (Minpp) sub-class of HAPs. It is also possible that the engineering of the commercial *E.coli* enzyme for thermal stability has masked, or obviated, folding motions associated with the binding and or catalysis of substrate. Hence yielding a lack of effects whether substrate is present or not. The

methodology used to create the Quantum Blue enzyme is patented, however the implications from the above thermostability measurements may hint at the utility of site-directed mutagenesis designed to stabilise the intramolecular forces within the active site of *apo* enzyme so as to stimulate presence of substrate and therefore increase the stability at higher temperatures.

What is clear is that for Minpps pH 7 yielded higher temperatures of unfolding, while the effect was minimal for the highly engineered *E.coli* enzyme (QB). For the Minpp enzymes, the thermostability increased with the increase in substrate concentration.

It is important to note that all the enzymes under investigation are active and capable of substrate turnover. While care was taken to start the experiment as soon as the substrate was added to the reaction, it is unknown how quickly it was dephosphorylated.

2.3.5 DSF to investigate the effect of reducing and oxidising conditions on thermostability of phytases.

Thermostability of proteins is often conferred by formation of disulphide bonds between the sulphur atoms in thiol groups of cysteine residues (Dombkowski, Sultana and Craig, 2014). In the following DSF experiment I used reducing and oxidising conditions to verify potential existence of disulphide bridges in my proteins. Using the reducing agent dithiothreitol (DTT) and its oxidised form trans-4,5-Dihydroxy-1,2-dithiane, I aimed to reduce any potential disulphides and as a result see a difference in the thermostability on DSF. Confirmation of existing disulphide bridges is crucial for understanding the behaviour of the protein at high temperatures and may have an impact on the future investigations and protein engineering.

Figure 2.13, Figure 2.14 and Figure 2.15 show results of the DSF experiment on the three bacterial Minpps Bl, Bp and Bt in the presence and absence of oxidising and reducing conditions. The experiment was undertaken using triplicate measurements and the

average values of these are presented. The results were normalised to show percentage values relative to the maximum fluorescence intensity for the given trace.

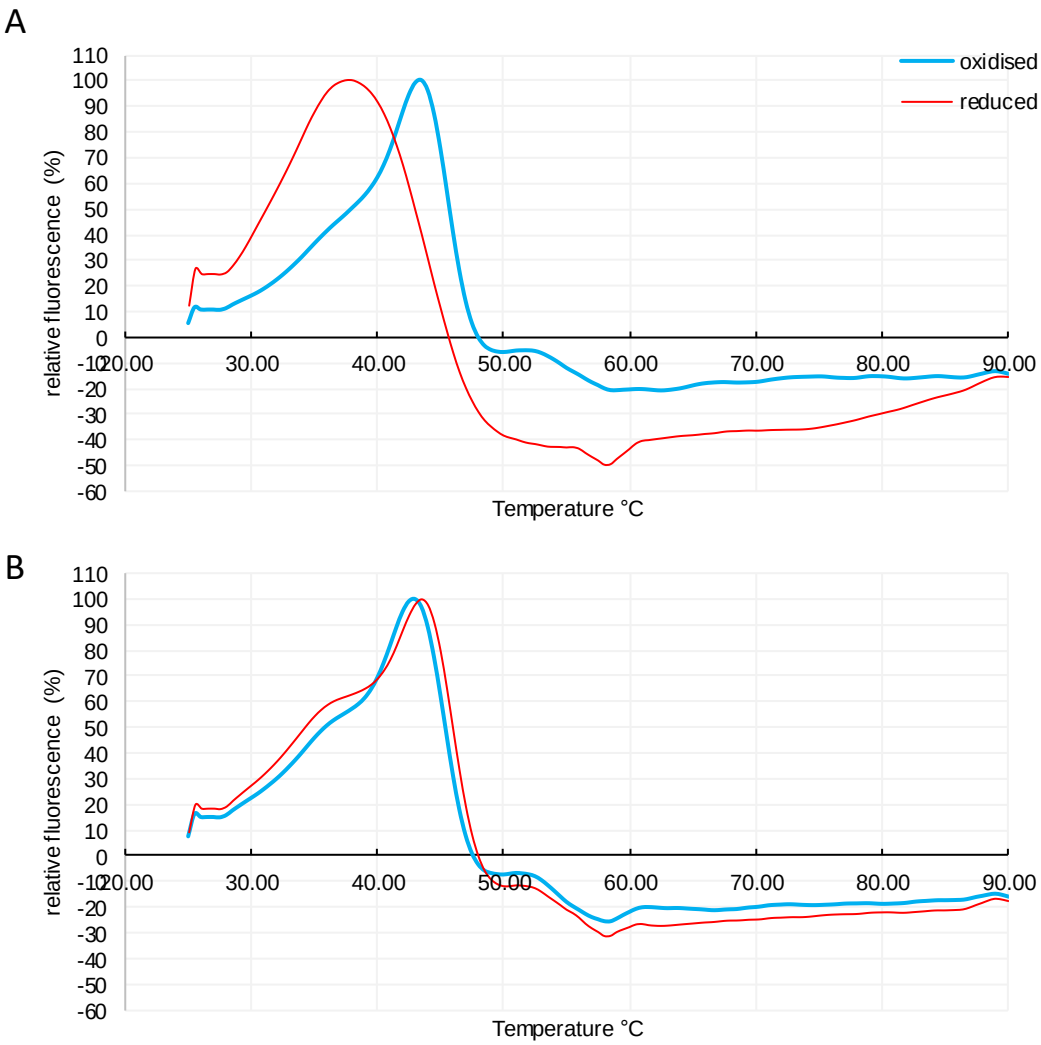

Figure 2.13 Differential Scanning Fluorimetry of *Bt*Minpp in oxidising and reducing conditions.
Comparison between exposure to reducing and oxidising conditions using 10mM oxidising and reducing forms of DTT. Enzyme concentration was 1 mg/ml. The experiment was conducted in a PCR machine with a temperature gradient in the range of 25 – 90 °C with intervals of 0.5 °C every 20 sec, measuring fluorescence of the hydrophobic fluorescent probe SYPRO at 470/570 nm. Data analysis was conducted to calculate the first order derivative of the raw data, and to normalise the trendlines to 100% the maximum signal for each data set. A: pH 3.5, B: pH 7.

Figure 2.13 A shows that the temperature of unfolding for *Bt*Minpp under oxidised conditions occurs at 38 °C. The addition of oxidant markedly increased the unfolding temperature to 42 °C at pH 3.5, but left a slight shoulder at 35 °C. In contrast the

unfolding isotherms were identical for oxidising and reducing conditions at pH 7 matching closely the temperature of unfolding with oxidant at pH 3.5. Again, there was evidence of a more pronounced shoulder at 35 ° C at pH 7. The shoulder and the shift in peak with oxidant at pH 3.5 possibly suggest the presence of a mixed population of protein that is resolved, to some extent, by the inclusion of reductant/oxidant. The prominent effect of oxidant at pH 3.5 may be explained by the lower pH creating an environment with altered redox potential that would shift the equilibrium between reduced and oxidised populations of protein. In this regard, an increase in pH would according to the Nernst equation lower the redox potential favouring oxidation of redox active groups such as thiols and generation of disulphides.

The unfolding isotherms for *Bl*Minpp (Figure 2.14) and *Bp*Minpp (Figure 2.15) are broadly consistent with *Bt*Minpp (Figure 2.13) in that oxidising treatment shifted the temperature of unfolding (maximum fluorescence) to higher temperature (by approximately 3 ° C). In both cases the reduced protein showed a significantly higher temperature shoulder at pH 7.

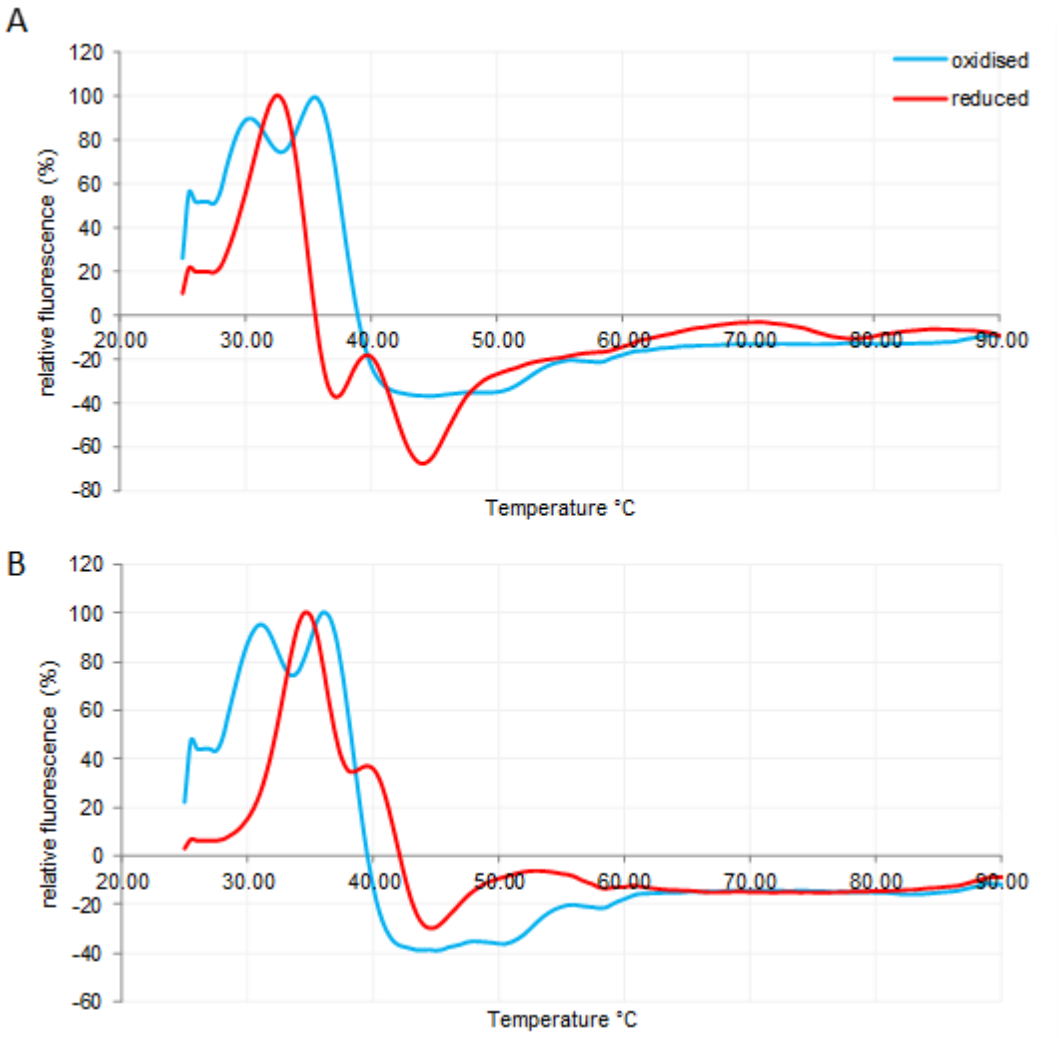

Figure 2.14 Differential Scanning Fluorimetry of *Bl*Minpp in oxidising and reducing conditions.
Comparison between exposure to reducing and oxidising conditions using 10mM oxidising and reducing forms of DTT. Enzyme concentration was 3.8 mg/ml. The experiment was conducted in a PCR machine with a temperature gradient in the range of 25 – 90 °C with intervals of 0.5 °C every 20 sec, measuring fluorescence of the hydrophobic fluorescent probe SYPRO at 470/570 nm. Data analysis was conducted to calculate the first order derivative of the raw data, and to normalise the trendlines to 100% the maximum signal for each data set. A: pH 3.5, B: pH 7.

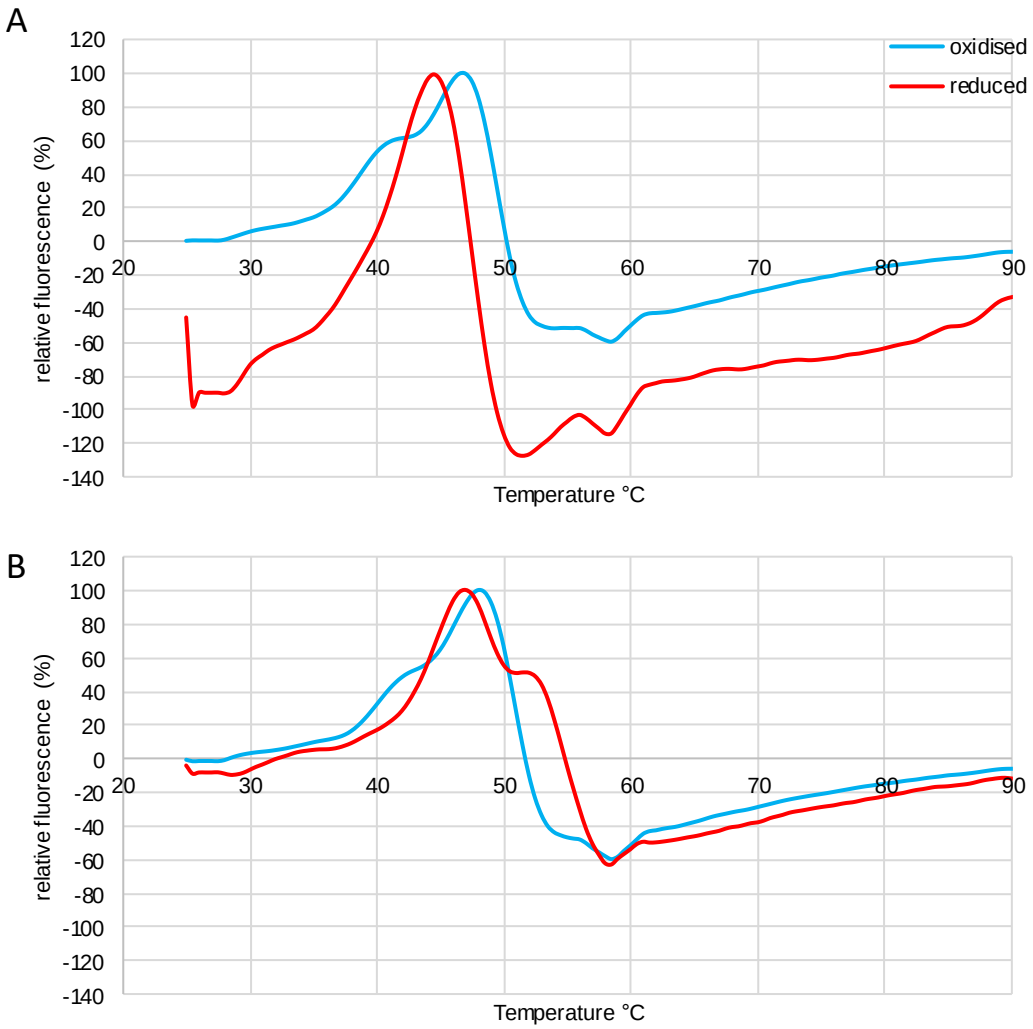

Figure 2.15 Differential Scanning Fluorimetry of *Bp*Minpp in oxidising and reducing conditions.
Comparison between exposure to reducing and oxidising conditions using 10mM oxidising and reducing forms of DTT. Enzyme concentration was 2.5 mg/ml. The experiment was conducted in a PCR machine with a temperature gradient in the range of 25 – 90 °C with intervals of 0.5 °C every 20 sec, measuring fluorescence of the hydrophobic fluorescent probe SYPRO at 470/570 nm. Data analysis was conducted to calculate the first order derivative of the raw data, and to normalise the trendlines to 100% the maximum signal for each data set. A: pH 3.5, B: pH 7.

Redox potential is a measure of the strength of acquisition of electrons by a chemical, in other words how likely it is to become reduced, in comparison to hydrogen. Chemicals that are more electronegative than hydrogen are said to have positive redox potentials and are more capable of oxidising other species and becoming reduced. Substances less electronegative than hydrogen have a negative redox potential and are more capable of reducing other chemicals, thus becoming oxidised (Sun, Ding and Peterson, 2013, p. 184). Anaerobic bacteria, which include *Bifidobacterium longum* (Schell *et al.*, 2002) and

Bacteroides thetaiotaomicron (Xu, 2003), are typically active at negative (low) redox potentials (Sun, Ding and Peterson, 2013, p. 184).

While the reducing agent used in the above experiments is known to undergo oxidation by air (Sigma-Aldrich user manual), which may have impacted the results, it is clear that oxidising conditions increase the unfolding temperature of the HAE phytases (Minpps) studied here. The reducing capacity of DTT increases with pH above pH 7 and is quenched at pH below 3.0 (Lukesh, Palte and Raines, 2012; Wingfield, 2016).

Wang et al. (Wang, Meng and Zhou, 2004) showed that the *Aspergillus niger* phytase lost its thermostability and catalytic activity in the presence of 2 mM DTT. This phytase contains five pairs of disulphide-forming cysteines, strongly suggesting the role of disulphides in the catalytic and structural properties of this phytase.

Singh et al. (Singh and Satyanarayana, 2009) characterised the HAP phytase from Sporotrichum thermophile, a thermophilic fungus. They showed a small effect of DTT on the catalytic activity, which decreased to 97.97 % and 92.89 % with 1 mM and 5 mM DTT, respectively. The authors concluded that the enzyme most likely has no free sulfhydryls, or if any are present, they play a negligible role in the catalysis.

2.4 Conclusions

This chapter describes general characterisations of bacterial Minpps, belonging to the HAE sub-class of HAP phytases (Rigden, 2008; Stentz *et al.*, 2014). The enzymes from *Bacteroides thetaiotaomicron* (Bt), *Bifidobacterium pseudocatenulatum* (Bp) and *Bifidobacterium longum* (Bl) were compared with the commercially engineered *E. coli*–derived HAP phytase Quantum Blue (QB).

Phytase assays based on the colourimetric measurement of the phosphate release revealed that the Bt phytase is most active at pH 3.5-4.0, Bl at pH 4.5-6.0 and Bp plateaus at the range of pH 4.0-6.5. While the bacterial phytases were more active at higher pH than the QB phytase, QB was highly active at pH 2.0-5.0, making it especially suitable for

the use in animal feed supplements, where it needs to be active at the low pH of the stomach. The Minpps displayed Km values in the range 0.56-2.3 mM and, interestingly, for Bt and Bp (Bl was not tested) the Km correlated with substrate- (IP_6) induced increases in thermal stability (unfolding temperature).

Commercial phytases currently in use display lower Km values to reflect their high affinity to phytic acid. One study (Menezes-Blackburn, Gabler and Greiner, 2015) examined the kinetic properties of seven commercial phytases and found the Km values for phytic acid at pH 5 and 37 °C to be 142 μM for Quantum Blue, and varied from 35 μM to 364 μM for the other phytases. Clearly, the commercial phytases displayed higher affinities to phytic acid than the wild-type phytases presented in this work. However the experiments described in this thesis were performed at 25 °C instead of 37 °C, which should be addressed in the future studies.

Assays measuring the recovery after incubation at a range of temperatures at pH 3.5 revealed that QB maintains its activity throughout. The Bl activity was shown to drop after incubation at 32 °C, the Bt activity stayed stable until 70 °C and Bp activity decreased after 60 °C. At pH 7.0, the bacterial phytases showed more similar trends, generally decreasing in activity after 60 °C, while QB was most active at 72 °C.

Perhaps one of the most interesting facets of this work is the possibility raised by DSF experiments (Figs. 2.8 – 2.11) that HAE class HAPs, which share an α + αβ fold structure with the HD phytase from *E.coli,* display substrate stabilization of structure. That the commercial HD class HAP phytase Quantum Blue did not may be a consequence of the extensive engineering of this third generation enzyme. It is interesting that alignments (not shown) of HAE and HD phytases examined here reveal significant insertions in variable loops in the HAE phytases when compared to the HD phytase. It is possible that these and/or the catalytic motions revealed in Chapter 4 for *Bl*Minpp are characteristic of HAE enzymes but not their HD counterparts. One future test would be DSF-based substrate titrations or DSC experiments of the type described here on wild type *E. coli* HD phytase.

3 Comparison of Product Profiles of HAP and Commercial Phytases using IP_6.

3.1 Introduction

Analysing product profiles of phytases can provide insight into the structure of their active sites and into substrate specificity. The presence of a wider variety of each of the IP5, IP4 and IP3 enantiomers at each step of dephosphorylation could be indicative of a larger active site, able to accommodate substrates in several orientations, and allowing the enzyme to accept a wider variety of related substrates. Less variety within each group of enantiomers could indicate higher substrate specificity, which usually brings along higher specific activity and a more compact active site, conducive to only accepting substrates in very specific orientations (Stentz *et al.*, 2014).

Narrow substrate specificity phytases could have implications in transgenic plants, where it would be crucial to control the inositol phosphates involved in the plants' metabolic pathways accurately (Konietzny and Greiner, 2004). Broad substrate specificity phytases would provide an advantage in animal feed additives, which contain a wide variety of inositol phosphates and related substrates (Wyss *et al.*, 1999).

HPLC allows for the separation IP_6 and lower inositol phosphate products of the phytase reaction. The product peaks can be visualised and identified according to a standards chromatogram by comparing the time and order of elution. The particular method of high performance liquid chromatography (HLPC) described in this chapter is suitable for separating and identifying peaks of IP_6, IP_5, IP_4 and IP_3 with high resolution, while peaks of IP_2, IP_1 and Pi have low resolution or coelute with the solvent front (Blaabjerg, Hansen-Møller and Poulsen, 2010). Analyses of the type described in this chapter have been used to characterize the sites in the digestive tract of non-ruminants in which phytate is degraded by adjunct phytases added to feed (Zeller, Schollenberger, Kühn, *et al.*, 2015a; Zeller, Schollenberger, Witzig, *et al.*, 2015; Zeller *et al.*, 2016), and can be compared with phytate degradation by *in vitro* models of intestinal phytate degradation (Briviba *et al.*, 2017), or by recombinant protein.

The aims of this chapter were to gain insight into the nature of the products of dephosphorylation of the wild-type HAE class *Bt, Bl* and *Bt* phytases in comparison to the

commercial QB phytase of the HD class. Each step of dephosphorylation can produce a single or several lower inositol phosphates. The nature and proportions of each product can provide insights into the structure of the enzyme's active site and into its substrate specificity, which carries implications towards its uses in animal nutrition.

In summary, this chapter shows product profiles of reactions of the Gram-negative Minpp phytase from *Bacteroides thetaiotaomicron* and the Gram-positive *Bifidobacteria infantis* and *Bifidobacteria pseudocatenulatum.* Differences are noted between the identities of the products of phytate degradation by the Gram-negative and the Gram-positive bacteria, as different IP_4 products are accumulated to a different extent. At the same time, the commercial phytase Quantum Blue was shown to accumulate predominantly one particular IP_4 (Ins(2,3,4,5)P_4). Hence, the work described here suggests that bacterial Minpp's follow several pathways of phytate degradation, while the Quantum Blue enzyme derived from *E.coli* follows one pathway with a particular preference. The interests in the gut bacterial phytases lie not only with the industry of the animal feed, but also with the potential for human nutrition. Currently, several members of the *Bifidobacterium* genus are commercially used as probiotics to supplement the human diets.

3.2 Methods

3.2.1 Sample preparation

Bacterial phytases from *Bacteroides thetaiotaomicron* (Bt)*, Bifidobacterium longum subsp. infantis ATCC 15697* (Bl), *Bifidobacterium pseudocatenulatum* (Bp) and the commercial Quantum Blue phytase (QB) were typically used at dilutions of 100 ng/ml, 1 µg/ml, 500 ng/ml and 10 ng/ml respectively, unless stated otherwise. 20 µl of the enzyme dilutions was added to 20 µl of 200 µM high purity IP_6 (Merck) dissolved in ddH_2O. Enzymatic reactions were carried out in 0.1 M glycine-HCl buffer at pH 3.5 for a given amount of time at 25 °C before being stopped by boiling the samples in a 100 °C water bath for 10 min. Samples were then cooled to room temperature and centrifuged at 11,000 x*g* to remove debris. Next, 3 µl of sample was added to 97 µl of ddH_2O in a glass

HPLC vial (Thermo Scientific Chromacol Vial 03-FIV (A)) with a perforated cap (11mm autosampler vial crimp caps) on top.

3.2.2 HPLC

Products of the enzymatic reactions were separated by high performance liquid chromatography (HPLC) and detected according to the method of Phillippy and Bland (1988). Here, a 3 mm x 50 mm CarboPac guard column (Dionex) and a 3 mm x 250 mm CarboPac PA200 main column (Dionex) were used for separation and the acid eluent was methanesulfonic acid delivered from solvent reservoirs A and B containing 60 mM and 600 mM methanesulfonic acid respectively. The gradient was delivered at the flow rate of 0.4 ml/min. The gradient percentage concentration varied with time as shown in the table below.

time (min)	% solvent B
0	10
22	60
25	100
38	100

The inert quaternary pump Jasco PU-2089i Plus was used to deliver the solvents. The inert autosampler Jasco AS-2055i Plus was used to inject sample volume of 10 µl at 49 min intervals. The solvent stream eluting from the main column was mixed in a mixing tee and knitted reaction coil (190 µl volume) with a solution of 2 % w/v perchloric acid and 0.1 % w/v ferric nitrate delivered at the flow rate of 0.2 ml/min by a Jasco PU-1585 pump. A Jasco UV-2077 Plus UV detector was used to detect product profile peaks at 290 nm. Chromatographic data was collected and analysed using the ChromNAV software (JASCO). Inositol phosphates were identified by reference to the elution time of the inositol phosphate standards. The standards were prepared by acid hydrolysis (reflux for 24h in 1M HCl) with subsequent rotary evaporation at 35 °C to remove HCl.

3.3 Results and Discussion

The top panel of Figure 3.1 below shows a control run (in red) using IP_6 in 0.1 M glycine buffer at pH 3.5. This shows the elution time of the IP_6 peak as well as the impurities, whose identity can be uncovered by comparing with the elution time of the standards run (in purple). The product profiles of the reaction of the commercial Quantum Blue phytase (QB) with IP_6 carried out for 30 min, 1 hr and 4 hr are shown in blue.

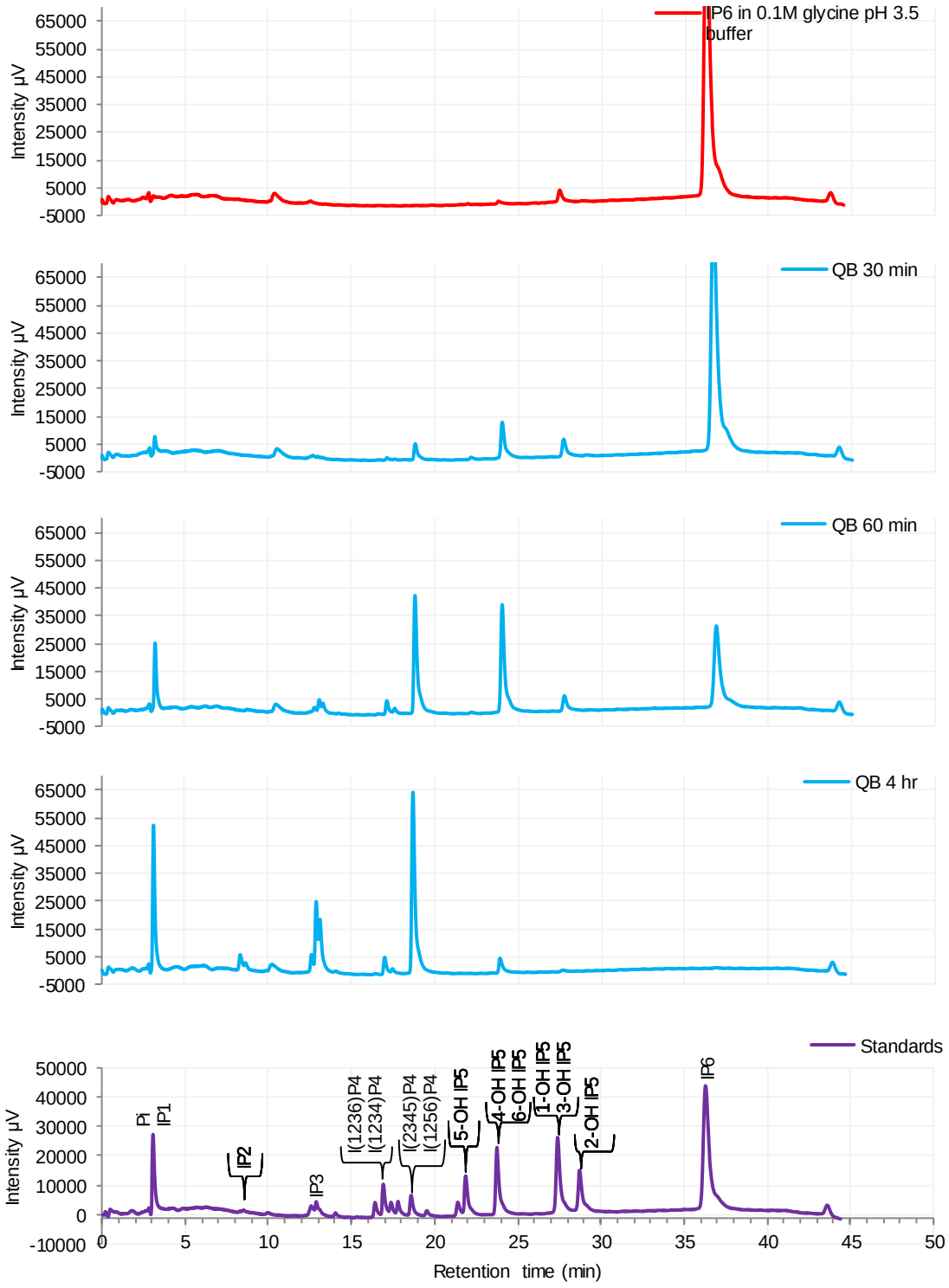

Figure 3.1 Time course of product profiles of QB reaction with IP6.
10 ng/ml QB phytase and 200 µM IP_6 were reacted for 30, 60 and 240 min in 0.1 M glycine-HCl buffer at pH 3.5 at 25 °C. The samples were diluted 1:30 and separated on a 3 mm x 250 mm CarboPac PA200 column (Dionex) using a methanesulfonic acid gradient of 60-600mM, before being mixed with 2 % w/v perchloric acid and 0.1 % w/v ferric nitrate, followed by UV detection of product profile peaks at 290 nm.

The substrate IP_6 peak eluted just after 36 min and is accompanied by a small peak of 1/3-OH-IP_5 [Ins(2,3,4,5,6)P_5 or Ins(1,2,4,5,6)P_5] as signified by the peak at 28 min of elution. Its peak area is 5.8% that of IP_6. These two IP_5 isomers are enantiomers and are not resolvable on non-chiral HPLC such as this.

At limited extents of reaction (30 min) of QB with IP_6 new peaks appear in addition to the 1/3-OH-IP_5 peak which now is at 131% of the peak area in the IP_6 run. The peak at around 24 min of elution is either the 4-OH-IP_5 or the 6-OH-IP_5 enantiomer with the 6-OH-IP_5 likely being the more prevalent one; the *E.coli* phytase Appa from which Quantum Blue is derived attacks the 6-position predominantly, but displays minor activity at the 3-position (Konietzny and Greiner, 2002). The second new peak at about 19 min of elution corresponds to the elution time of Ins(2,3,4,5)P_4 or its enantiomer Ins(1,2,5,6)P_4 with the former being more likely in this case. Again, the *E.coli* phytase has been shown to produce Ins(2,3,4,5)P_4 (Konietzny and Greiner, 2002).

As the reaction progresses to 60 min, the amount of IP_4 and IP_5 increased concomitantly with the substantial disappearance of IP_6. A small cluster of IP_3's becomes visible at ~ 14 min of elution. There are 20 possible stereoisomers of the IP_3's, which are among the least well resolved of IP classes on these columns (Blaabjerg, Hansen-Møller and Poulsen, 2010), so it is not possible to identify individual isomers using this technique. A small peak is visible at 4 min of elution, corresponding to Pi and IP_1 as well as containing the solvent front.

At the extended period of 4 hr the IP_5 has disappeared without any new IP_5's appearing. At the same time the cluster of IP_3's grew significantly larger. Additionally, some IP_2 arising is seen at 9 min of elution the extended period of reaction but it remains unidentified.

In summary, Quantum Blue seems to dephosphorylate the IP_6 into IP_5 and IP_5 into IP_4 fairly easily, and thereafter accumulates Ins(2,3,4,5)P_4 while degrading this more slowly. This pattern of hydrolysis has been observed in feed situations in experiments designed to discriminate between the activity of endogenous feed phytases and adjunct Quantum Blue (Zeller, Schollenberger, Kühn, *et al.*, 2015b; Zeller, Schollenberger, Witzig, *et al.*, 2015; Zeller *et al.*, 2016).

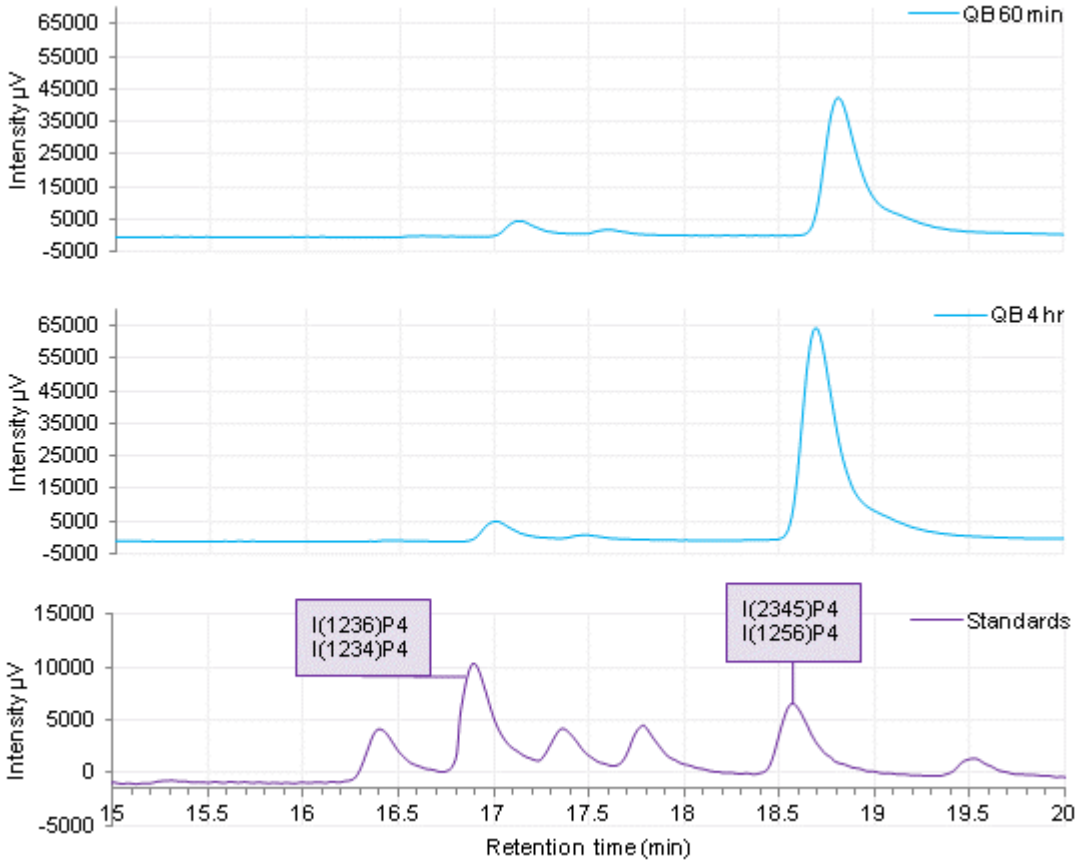

Figure 3.2 Zoomed in fragments of the chromatogram of the time course of product profiles of QB reacting with IP_6.
Zoomed view of the IP_4 cluster from the 60 min and 4 hr reactions of the Quantum Blue phytase with IP_6 and the corresponding standards chromatogram. 10 ng/ml QB phytase and 200 µM IP_6 were reacted for 60 and 240 min in 0.1 M glycine-HCl buffer at pH 3.5 at 25 °C. The samples were diluted 1:30 and separated on a 3 mm x 250 mm CarboPac PA200 column (Dionex) using a methanesulfonic acid gradient of 60-600mM, before being mixed with 2 % w/v perchloric acid and 0.1 % w/v ferric nitrate, followed by UV detection of product profile peaks at 290 nm.

Figure 3.2 above illustrates the chromatograms with a closer view of the IP_4 peaks of the 60 min and 4 h reaction of QB with IP_6 as well as the corresponding standards. A slight shift becomes apparent, as the enzymatic reaction products elute ~10 sec after the corresponding standards run. The figure reveals the production of minor peaks of IP_4 eluting in the position of Ins(1,2,3,4)P_4 or its enantiomer Ins(1,2,3,6)P_4 and another even smaller peak of IP_4 with the retention time of 17.5 min, corresponding to Ins(1,2,4,5)P_4 (Blaabjerg, Hansen-Møller and Poulsen, 2010).

These experiments reveal the complexity of identification of the inositol phosphate products of phytase action, even in defined *in vitro* conditions. It is worth pointing out that one fraction of cereal phytase(s), present in animal feedstuffs, extensively characterized in the early 1960's by Tate and coworkers (Lim and Tate, 1971a, 1973) and reviewed (Konietzny and Greiner, 2002), produced a principal IP_5 [Ins(1,2,3,5,6)P_5 with minor product Ins(1,2,4,5,6)P_5, proceeding to produce a principal IP_4 [Ins(1,2,5,6)P_4 with minor product Ins(1,2,3,6)P_4 (Brearley and Hanke, 1996). Significantly, the IP_4's produced are the enantiomers, in the case of Ins(1,2,5,6)P_4, of the major Quantum Blue IP_4 product, Ins(2,3,4,5)P_4. Similarly, the minor cereal phytase IP_4 product identified by Tate, Ins(1,2,3,6)P_4, is either identical to or the enantiomer of the minor Quantum Blue IP_4 product produced here. These considerations reveal the difficulty even in *in vitro* systems, never mind digestive situations, of wholly rigorous analysis of inositol phosphates without chiral HPLC regimens.

Greiner *et al.* (Greiner, Carlsson and Larsson, 2000) showed that the *E.coli* phytase, whose engineered form became the commercial Quantum Blue enzyme (Menezes-Blackburn, Gabler and Greiner, 2015), degrades IP_6 in a stepwise manner preferentially via D/L-Ins(1,2,3,4,5)P_5, D/L-Ins(2,3,4,5)P_4, D/L-Ins(2,4,5)P_3, Ins(2,5)P_2, to Ins(2)P as the final product, which is in agreement with the data for predominant D/L-Ins(1,2,3,4,5)P_5 and D/L-Ins(2,3,4,5)P_4 accumulation presented in this work.

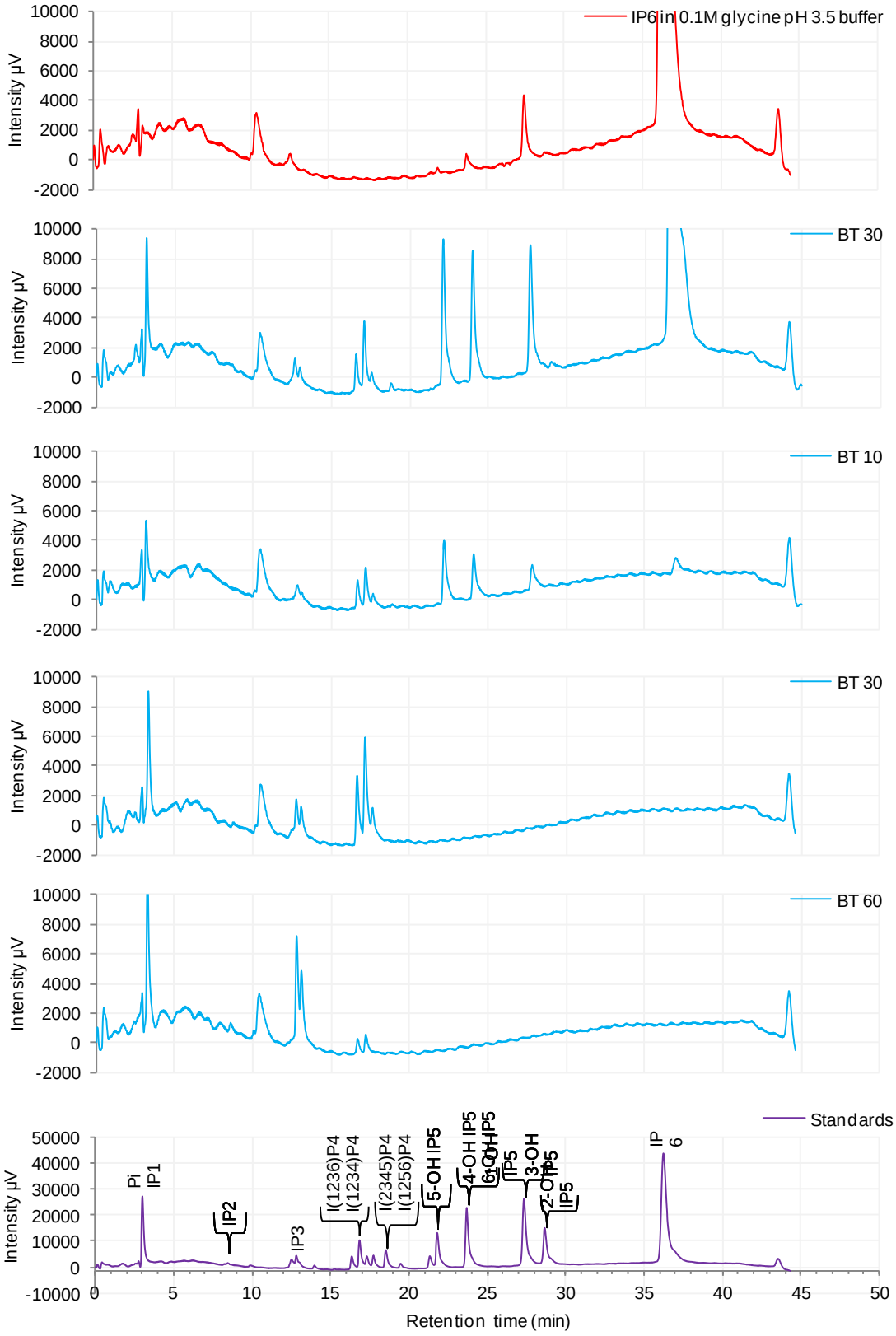

Figure 3.3 Time course of product profiles of *Bt*Minpp reacting with IP_6.
100 ng/ml *B.thetaiotaomicron* phytase and 200 µM IP_6 were reacted for 10, 30 and 60 min in 0.1 M glycine-HCl buffer at pH 3.5 at 25 °C. The samples were diluted 1:30 and separated on a 3 mm x 250 mm CarboPac PA200 column (Dionex) using a methanesulfonic acid gradient of 60-600mM, before being mixed with 2 % w/v perchloric acid and 0.1 % w/v ferric nitrate, followed by UV detection of product profile peaks at 290 nm.

In contrast to the relatively simple product profile produced by Quantum Blue (Figures 3.1, 3.2) confirming published work on *E. coli* phytases (Konietzny and Greiner, 2002), the product profiles of HAE phytase (*Bt*Minpp) acting on IP_6 are more complicated (Li, 2014; Stentz *et al.*, 2014).

Here, at limited extents of reaction (2 min) three distinct IP_5 peaks are visible at 22, 24 and 28 min of elution. According to the standards chromatogram, they are 5-OH-IP_5, 4/6-OH-IP_5 and 1/3-OH-IP_5, respectively. Each contributed to the total IP_5 peak area by 40 %, 29 % and 31 % respectively.

Notably, the peak at 28 min of elution is prominently present in the IP_6 control run as an impurity. There, it constitutes only 1.4 % of the IP_6 peak area. In the enzymatic reaction of the *Bt* phytase with IP_6 for 2 min it constitutes 3.9 % therefore one can be certain that most of the product eluting at 28 min originates from the enzymatic reaction. Although, both bacterial HAP (HD) 6-phytases typified by *E.coli* Appa and fungal HAP (HD) 3-phytases typified by *Aspergillus niger* PhyA produce a single major IP_5 and single minor IP_5 product (reviewed in Konietzny & Greiner, 2002), the near equivalence of at least two different IP_5 peaks, 5-OH-IP_5 and 4/6-OH-IP_5 , and the still substantial production of 1/3-OH-IP_5 for *Bt*Minpp, a HAP (HAE) phytase is unprecedented among phytases (Li, 2014; Stentz *et al.*, 2014).

At 10 min of enzymatic reaction the product profile shows a significant increase in the amount of IP_5 products as they accumulate. Here, they constitute 42 %, 36 % and 22 % of the total IP_5 peak area, respectively for 5-OH-IP_5, 4/6-OH-IP_5 and 1/3-OH-IP_5. It appears that the 1/3-OH-IP_5 product is dephosphorylated faster than the other IP_5's.

A significant cluster of IP_4 peaks becomes visible between 16 and 18 minutes of elution. Figure 3.4 A below illustrates a zoomed in view onto the IP_4 cluster for 10, 30 and 60 min of reaction. Again, the generation of multiple IP_4 products is atypical of phytases. Both *E.coli* Appa and fungal PhyA which produce principal IP_4 peaks of Ins(2,3,4,5)P_4 and Ins(1,2,5,6)P_4 respectively, produce only minor secondary IP_4 products. Some caution is

required here, as the analyses performed cannot distinguish whether particular IP_4's are better substrates in their own right, and therefore persist in the product profiles because, unlike better substrates, are not readily degraded.

Nevertheless, the data shown in Figure 3.4 show at least 4 distinct IP_4 peaks that could additionally hide pairs of enantiomers.

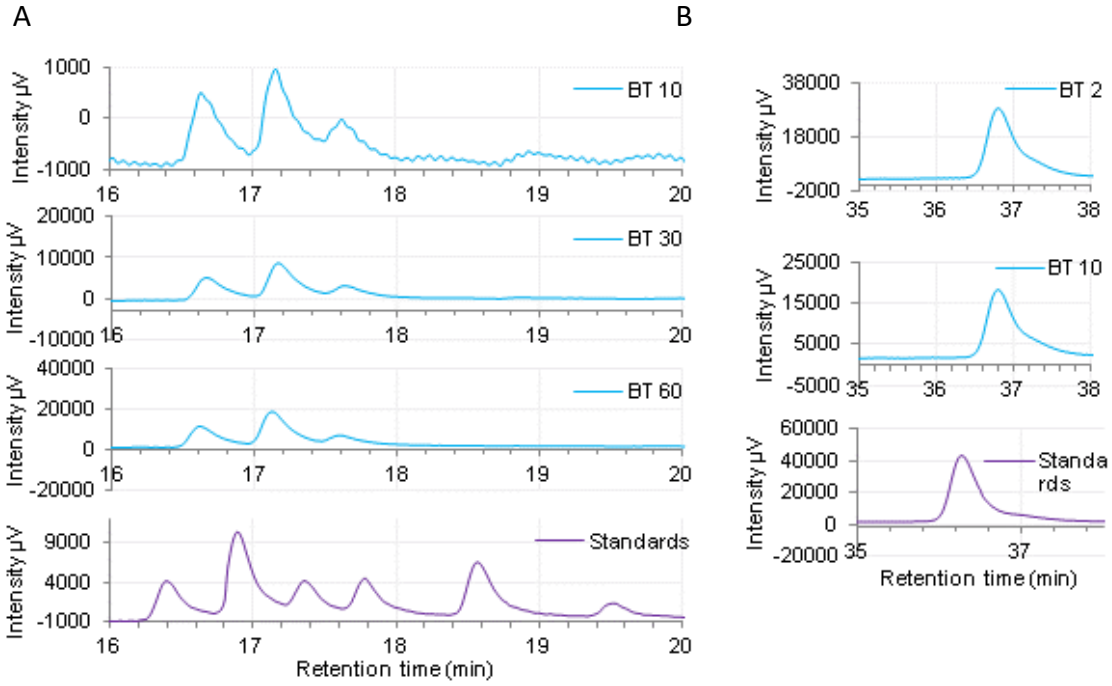

Figure 3.4 Zoomed in fragments of the chromatogram of the time course of product profiles of *Bt*Minpp reaction with IP_6.
100 ng/ml *B.thetaiotaomicron* phytase and 200 µM IP_6 were reacted for 2, 10, 30 and 60 min in 0.1 M glycine-HCl buffer at pH 3.5 at 25 °C. The samples were diluted 1:30 and separated on a 3 mm x 250 mm CarboPac PA200 column (Dionex) using a methanesulfonic acid gradient of 60-600mM, before being mixed with 2 % w/v perchloric acid and 0.1 % w/v ferric nitrate, followed by UV detection of product profile peaks at 290 nm. A: Zoomed view of the IP_4 clusters for 2, 10, 30 and 60 min reaction of *B. thetaiotaomicron* Minpp with IP_6 and the corresponding standards chromatogram. B: Zoomed view of the IP_6 peaks for 2 and 10 min of reaction with the standards peak.

The zoomed view in Figure 3.4 A allows for better examination of the IP_4 peaks present in the 10, 30 and 60 min reaction chromatograms and compare them to the standards chromatogram. Identification of the peaks is hindered by the slight misalignment of the enzymatic sample peaks in relation to the standards peaks. To identify the direction and the degree of the shift, I examined the zoomed in view of the IP_6 peaks in 2 min and 10 min reaction chromatograms and compared them to the standards in Figure 3.4 B. Here, it became apparent that the enzymatic reaction peaks are shifted by about 40 seconds later

than the corresponding standards peaks. By that logic, the principal IP_4 peak on the BT 10, 30 and 60 chromatogram can be identified as being either or both of the enantiomeric pair Ins(1,2,3,6)P_4 or Ins(1,2,3,4)P_4.

The inorganic phosphate (Pi) peak at 3 min of elution appeared, representing a small amount of phosphate liberated from the inositol ring. It constituted 19% of the maximum Pi peak achieved at 1440.

It is clear that even at extended periods of reaction, the relative proportions of IP4 peaks are largely similar. Thus, it seems likely that the different IP4s are produced/degraded at broadly similar rates. By 30 min, two faint peaks are visible at 12-14 min of elution, representing IP_3's but were unable to be resolved using the available standards and this chromatography technique. The inorganic phosphate peak grew further as the phosphate is liberated from the inositol ring, constituting 39% of the maximum reached after 1440 min of reaction.

In summary, under conditions of this assay, *Bt*Minpp generates multiple peaks of inositol phosphate at each level of dephosphorylation, IP_5, IP_4 and IP_3. Even at extended periods of incubation (24 hr, shown in Figure 3.9) only limited accumulation of IP_2 was observed. Among phytases, lily pollen alkaline phytase was reported to hydrolyse IP_6 as far as IP_3, only, proceeding uniquely through 5-OH-IP_5 and Ins(1,2,3,4)P_4 and/or its enantiomer (Ins(1,2,3,6)P_4 to Ins(1,2,3)P_3 (Barrientos, Scott and Murthy, 1994).

Of individual purified phytases characterized thus far only lily pollen alkaline phytase and the Minpps have been shown to show substantial preference for attack at the 5-position, that is with the exception of the F2 fraction of wheat bran phytase(s) characterized by Lim and Tate (Lim and Tate, 1971b). Both the lily pollen and wheat bran F2 fraction yielded Ins(1,2,3)P_3, the latter proceeding to IP_2 and ultimately Ins2P. It is perhaps significant that the Murthy group have since indicated that lily pollen alkaline phosphatase belongs to the HAE (Minpp) subclass of HAP phytases (Jog *et al.*, 2005; Mehta *et al.*, 2006). It is possible that a component of the F2 fraction of wheat bran phytase is one of the Minpps described in cereals by Brinch-Pederson and coworkers (Dionisio, Holm and Brinch-Pedersen, 2007) or one of the Purple Acid Phytases identified in cereals by the same group (Dionisio *et al.*,

2011). Unfortunately, the product profiles of these two classes of cereal enzyme are not described in these works.

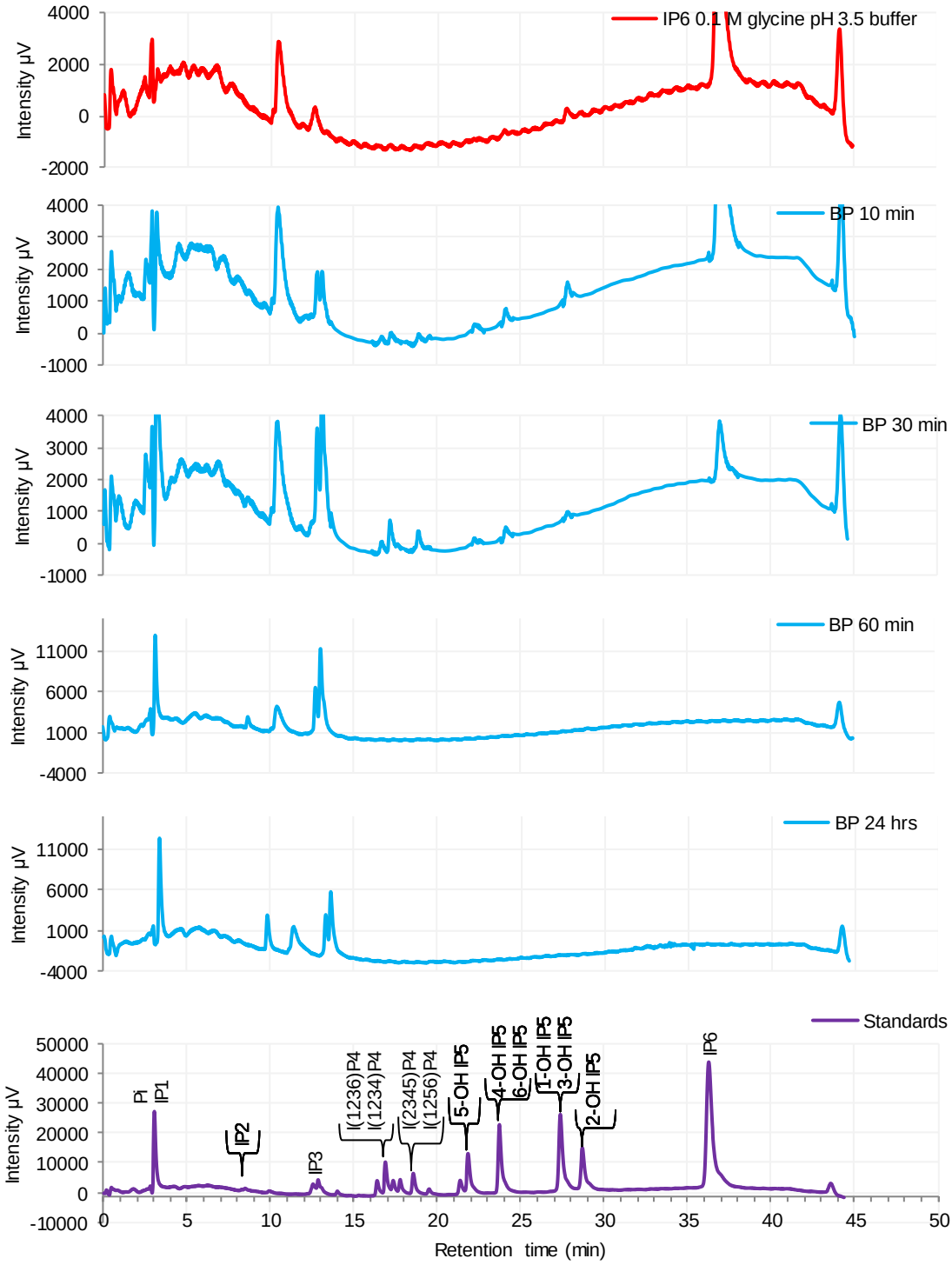

Figure 3.5 Time course of product profiles of *Bp*Minpp reacting with IP_6.
500 ng/ml *B. pseudocatenulatum* phytase and 250 µM IP_6 were reacted for 10, 30, 60 min and 24 hrs in 0.1 M glycine-HCl buffer at pH 3.5 at 25 °C. The samples were diluted 1:30 and separated on a 3 mm x 250 mm CarboPac PA200 column (Dionex) using a methanesulfonic acid gradient of 60-600mM, before being mixed with 2 % w/v perchloric acid and 0.1 % w/v ferric nitrate, followed by UV detection of product profile peaks at 290 nm.

The work described in the foregoing highlights the distinct properties (positional promiscuity) of *Bt*Minpp, the first bacterial HAE subclass HAP phytase characterized. Analysis of its crystal structure reveals the relatively large volume of its active site, accommodating IP_6 substrate in different poses (Stentz *et al.*, 2014). Given the precedence of gut commensal HAE subclass HAP phytases (Minpp) in the Gram-negative bacterium *Bacteroides thetaiotaomicron*, we sought to inquire of the product profiles of HAE HAP phytases (Minpps) from other gut symbionts belonging to the probiotic *Bifidobacteria*. Whereas *Bacteroides thetaiotaomicron* is an obligate anaerobe, these Gram-positive bacteria are microaerotolerant anaerobes and are considered to be early colonizers of the infant gut (Schell *et al.*, 2002).

After a limited time of reaction (10 min) the *Bp*Minpp chromatogram shows significant development as compared to the standards run. The IP_6 peak area decreased by 36% with all the aforementioned IP_5 peaks observed with *Bt*Minpp present, albeit here the 1/-3-OH peak is predominant among IP5's. In this case, the cluster of IP_4 peaks were fractional components with appreciable conversion to IP3's. In this respect, the lack of significant accumulation of IP5's and IP4's seems to distinguish *Bp*Minpp from *Bt*Minpp. However, in common with *Bt*Minpp, *Bp*Minpp seems to produce, at this level of analysis, a similar profile of IP3's to BtMinpp. .

To take a closer look at the IP_4 peaks and to help obtain their identity, the figure below illustrates a zoomed in view of the peaks for the 30 min reaction and for the standards run.

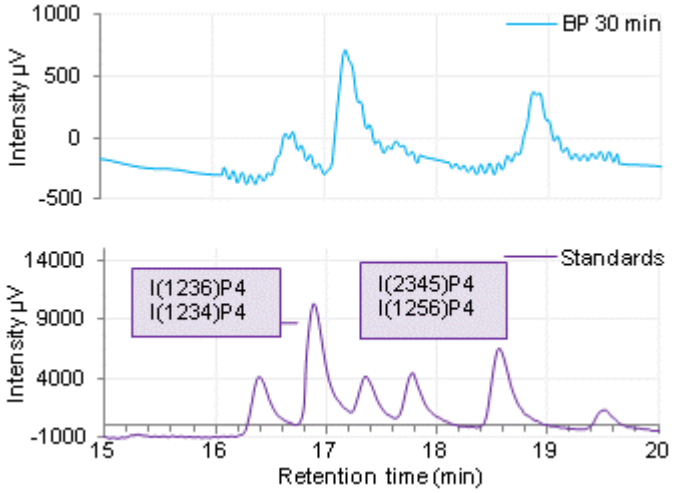

Figure 3.6 Zoomed in fragments of the chromatogram of the time course of product profiles of *Bp*Minpp reacting with IP_6.
Zoomed view of the IP_4 cluster from the 30 min reaction of *B. pseudocatenulatum* phytase with IP_6 and the corresponding standards chromatogram. 500 ng/ml *B. pseudocatenulatum* phytase and 250 µM IP_6 were reacted for 30 min in 0.1 M glycine-HCl buffer at pH 3.5 at 25 °C. The samples were diluted 1:30 and separated on a 3 mm x 250 mm CarboPac PA200 column (Dionex) using a methanesulfonic acid gradient of 60-600mM, before being mixed with 2 % w/v perchloric acid and 0.1 % w/v ferric nitrate, followed by UV detection of product profile peaks at 290 nm.

As seen in the Figure 3.6 above, there is a slight shift of the enzymatic reaction peaks – they elute about 10 sec later. The two most prominent peaks, at 17.2 min and 18.8 min of elution can be identified as Ins(1,2,3,6)P4/Ins(1,2,3,4)P4 and Ins(2,3,4,5)P4/Ins(1,2,5,6)P4. The latter peak was absent from the *Bt*Minpp chromatogram which can be because the corresponding product was not generated during the Bt reaction, or being generated and dephosphorylated further at a rate fast enough to not be detected. I suggest the former explanation is more likely, given the scope of the investigation and the range of reaction times examined (some results not shown). The four remaining smaller IP_4 peaks were unable to be identified due to the nature of the standards available. One further notable departure is the apparent accumulation of a peak of IP_2 for *Bp*Minpp, no such peak accumulated with *Bt*Minpp.

Bifidobacterium pseudocatenulatum strains have been isolated from the stools of breast-milk fed infants, but currently receive much attention as human adult symbionts in context of models of obesity (Benítez-Páez *et al.*, 2016). I also characterized the product

profiles of Minpp from the closely related *Bifidobacterium longum* which is a dominant symbiont in the infant gut.

In broad terms the product profiles of inositol phosphates generated from IP_6 by recombinant *Bl*Minpp (Figure 3.7) were more similar to those generated by *Bp*Minpp (Figure 3.5) than to those generated by *Bt*Minpp (Figure 3.3). Thus, three peaks of IP_5 were generated, with 4/6-OH-IP_5 the predominant species. Again multiple peaks of IP_4 were produced, and these were produced in the same relative proportions to each other as was the case for *Bp*Minpp. For all bacterial Minpps the predominant IP_4 produced was Ins(1,2,3,4)P_4/Ins(1,2,3,6)P_4, though the analysis cannot discriminate between different proportions of the two enantiomers. Similarly, the different Minpps seem to share a common profile of IP_3 products. These are among the most difficult IPs to identify with rigour, an issue compounded by poorer separations of this class of IP than other classes, the greater abundance of stereoisomers, of which there are 20, and the lack of commercially available standards for many individual species.

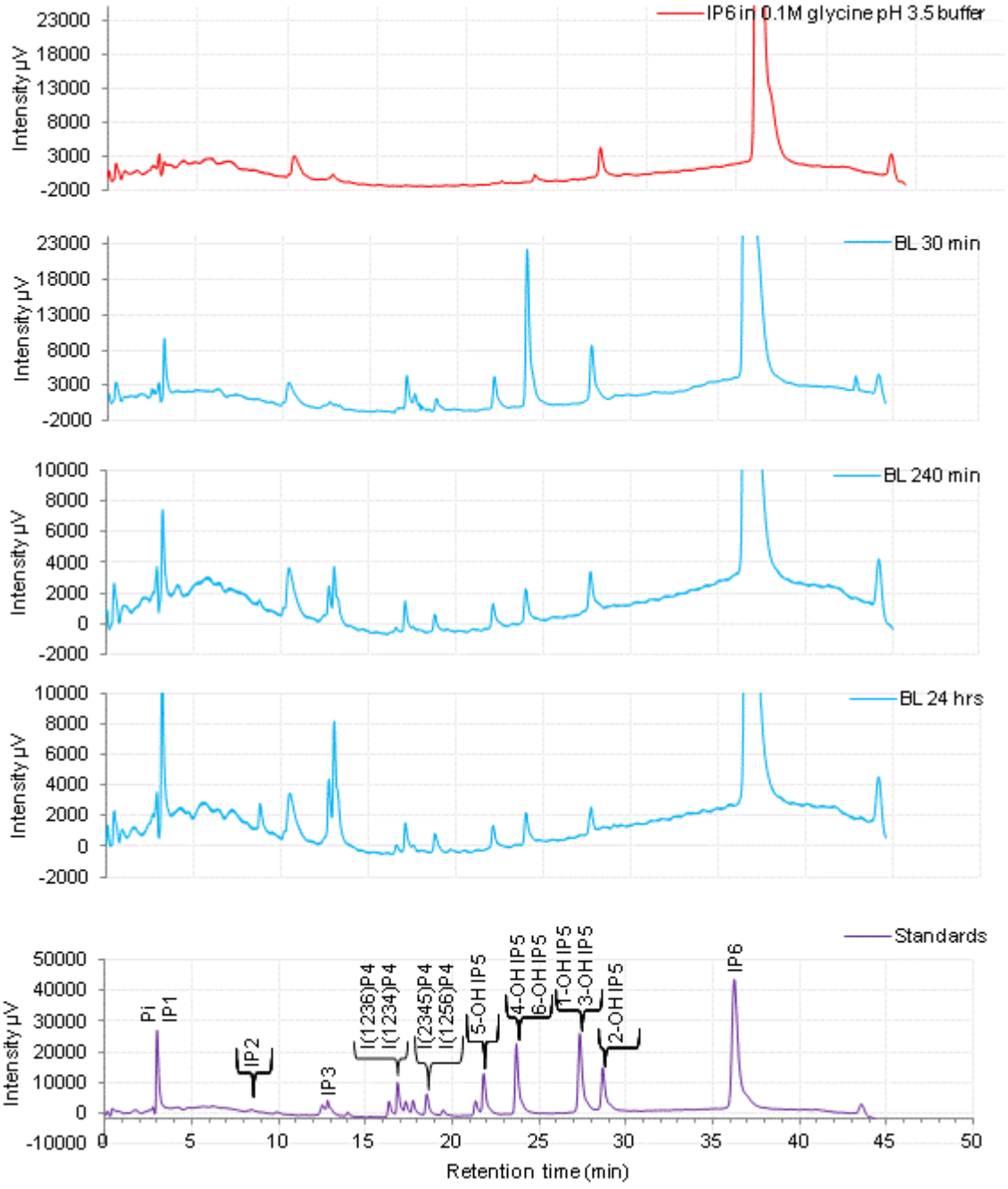

Figure 3.7 Time course of product profiles of *Bl*Minpp reaction with IP_6.
1 µ g/ml *B. longum* phytase and 250 µM IP_6 were reacted for 30, 240 min and 24 hrs in 0.1 M glycine-HCl buffer at pH 3.5 at 25 °C. The samples were diluted 1:30 and separated on a 3 mm x 250 mm CarboPac PA200 column (Dionex) using a methanesulfonic acid gradient of 60-600mM, before being mixed with 2 % w/v perchloric acid and 0.1 % w/v ferric nitrate, followed by UV detection of product profile peaks at 290 nm.

Closer inspection of the IP_4 region of the chromatogram reveals (Figure 3.8) four discrete peaks of IP_4 in order of increasing retention time Ins(1,2,4,6)P_4/Ins(2,3,4,6)P_4, Ins(1,2,3,4)P_4/Ins(1,2,3,6)P_4, Ins(1,2,4,5)P_4/Ins(2,3,5,6)P_4, Ins(1,3,4,5)P_4/Ins(1,3,5,6)P_4 and

Ins(1,2,5,6)P_4/Ins(2,3,4,5)P_4 (these peaks are identifiable in the profiles of IP_6 degradation by culture supernatants *of B. pseudocatenulatum*, Haros et al., 2009) and are the reported order of elution of IP_4 standards on CarboPac columns (Blaabjerg, Hansen-Møller and Poulsen, 2010).

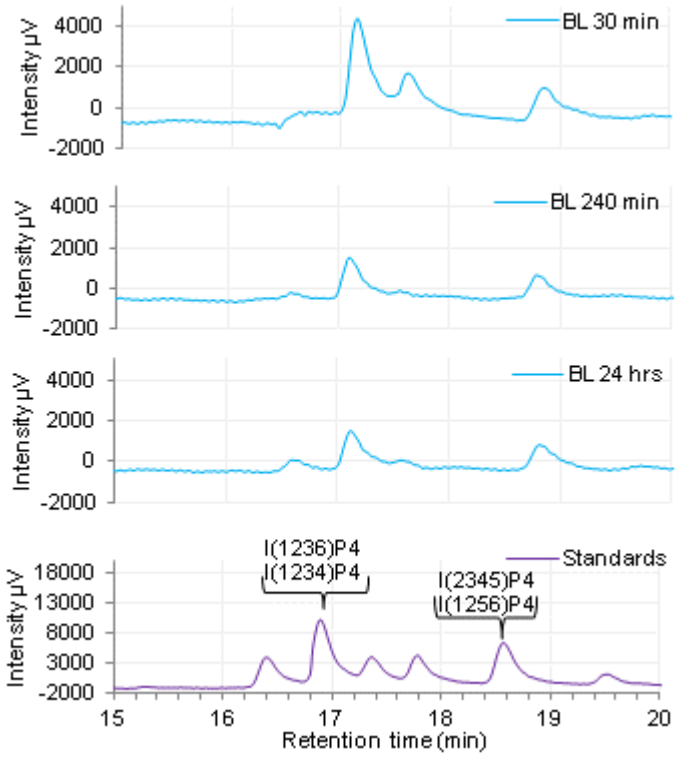

Figure 3.8 Zoomed in fragments of the chromatogram of the time course of product profiles of *Bl*Minpp reaction with IP_6.
Zoomed view of the IP_4 clusters for 30 min, 4 hr and 24 hr reactions of *B. longum* phytase with IP_6 and the corresponding standards chromatogram. 1 µ g/ml *B. longum* phytase and 250 µM IP_6 were reacted for 30, 240 min and 24 hrs in 0.1 M glycine-HCl buffer at pH 3.5 at 25 °C. The samples were diluted 1:30 and separated on a 3 mm x 250 mm CarboPac PA200 column (Dionex) using a methanesulfonic acid gradient of 60-600mM, before being mixed with 2 % w/v perchloric acid and 0.1 % w/v ferric nitrate, followed by UV detection of product profile peaks at 290 nm.

While CarboPac columns, like many anion exchange columns, offer limited resolution of IP_3 and IP_2 species (Haros *et al.*, 2009; Blaabjerg, Hansen-Møller and Poulsen, 2010), analysis of reactions of recombinant Minpps allowed to proceed to complete disappearance of IP_6, IP_5 and IP_4, indicate the likely production of identical IP_2 peaks/species for the three Minpps tested here. Thus a single sharp peak of IP_2 with retention time of 8.3 min was observed concomitant with a substantial peak of what we assume to be IP_1 and inorganic phosphate that elutes in the solvent front at 3.2 min.

While others have discriminated IP_1 species by chromatography on silica-based anion exchange columns in concert with enzymic approaches (Brearley and Hanke, 1996), the columns are not compatible with the acid gradients and UV detection method applied here. We are left with the speculation that the IP_2 products of the Minpp enzymes tested here retain the axial 2-phosphate as is the case for most phytases characterized to date (Konietzny and Greiner, 2002).

Figure 3.9 below shows the product profiles of reactions allowed to proceed to completion of *Bt, Bp, Bl* and QB with phytic acid. The reactions were carried out in room temperature for 24 hours before being analysed on HPLC.

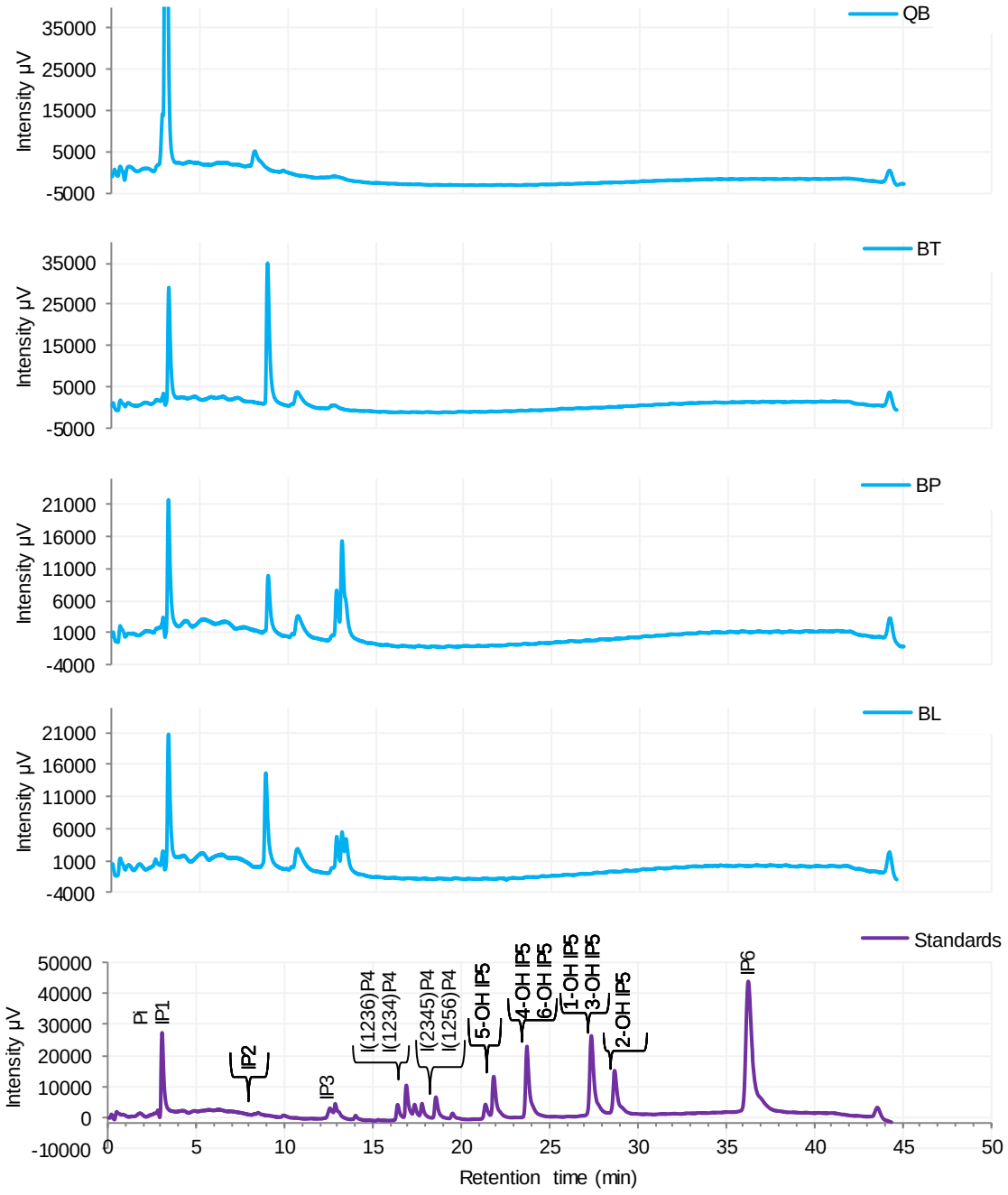

Figure 3.9 Time course of product profiles of QB, *Bt*Minpp, *Bp*Minpp and *Bl*Minpp reacting with IP_6 until completion.

3.2 µg/ml QB, 16 µg/ml *Bt*, 28 µg/ml *Bp* and 38 µg/ml *Bl* phytases and 500 µM IP_6 were reacted for 24 hrs in 0.1 M glycine-HCl buffer at pH 3.5 at 25 °C. The samples were diluted 1:30 and separated on a 3 mm x 250 mm CarboPac PA200 column (Dionex) using a methanesulfonic acid gradient of 60-600mM, before being mixed with 2 % w/v perchloric acid and 0.1 % w/v ferric nitrate, followed by UV detection of product profile peaks at 290 nm.

Immediately, it is visible that the QB phytase, as a representative of the HD phytases with high affinity to phytic acid (Menezes-Blackburn, Gabler and Greiner, 2015), successfully dephosphorylates virtually all IP6, IP5, IP4 and IP3, leaving only low quantities of IP2 and presumably high amounts of IP1 (which elutes in the solvent front and therefore would not be resolved on the chromatogram). This is in contrast to the three wild-type HAE phytases, which are shown to dephosphorylate the IP6 to leave behind significant amounts of a variety of IP3's (in the case of *Bl* and *Bp*) or IP2.

Since different classes of phytase dephosphorylate the substrates starting at different positions of the inositol ring, the pathways of degradation and ultimately the final products of dephosphorylation widely vary. As such, the microbial 6-phytases (which begin dephosphorylation at position 6 of the inositol ring) such as *B.subtilis* produce a varied set of intermediates during the sequential reaction. Acidic phytases from a range of species including *Pseudomonas, Pantoea agglomerans, Escherichia coli* and *Enterobacter cloacae* on the other hand are 3-phytases, beginning the dephosphorylation on the 3 position and carrying on to produce more specific intermediate products, namely D_In(1,2,4,5,6)P_5, D_In(1,2,5,6)P_4, D_In(1,2,6)P_3 and D_In(1,2)P_2 (Mukhametzyanova, Akhmetova and Sharipova, 2012).

4 X-ray structural studies of *Bifidobacterium longum* phytase

4.1 Introduction

The previous chapters revealed some interesting differences in enzyme characteristics between the Bl, Bp and Bt phytases. To further elucidate the characteristics of the HAE group of phytases, I chose to focus my efforts on the phytase from *B. longum* as an exemplar enzyme from the *Bifidobacteria*.

4.1.1 *Bifidobacterium longum* in probiotics

Previously separate species, now *Bifidobacterium infantis* and *Bifidobacterium suis* are categorised under the same species as *Bifidobacterium longum* (Mattarelli *et al.*, 2008). They are a gram positive, obligate anaerobe species belonging to the *Actinomycetales* branch. In 2002, there were about 32 species of *Bifidobacteria* identified, with the vast majority isolated from the human gastro-intestinal tract (GIT). Together with *Bacteroides, Enterococci, Clostridia* and others, the *Bifidobacteria* create a complex microflora that is essential for healthy digestion and homeostasis of the human digestive system (reviewed in Schell *et al.*, 2002).

Species such as *Bifidobacterium breve*, *B. bifidum*, *B. longum* ssp. *longum*, and *B. longum* spp. *infantis* have been found in the microflora of infants. Here, the *Bifidobacteria* have been shown to utilize human milk oligosaccharides, aiding digestion. With progressing age, the proportion of these *Bifidobacteria* decreases in relation to *B. adolescentis* and *B. catenulatum.* With age, the population of *Bifidobacteria* as well as their species diversity naturally decreases together with their reduced ability to adhere to the intestinal mucosa. In addition, antimicrobial therapies are known to negatively affect the GIT microflora, leading to medical disorders, which highlight the importance of maintenance of a healthy microbial flora (reviewed in Arboleya *et al.*, 2016).

Decreased levels of *B. longum* have been shown in individuals suffering from a broad variety of illnesses such as the hepatitis B virus-related cirrhosis, cystic fibrosis and

allergies (reviewed in Arboleya *et al.*, 2016). Drastic depletion of *B. longum* levels accompanies the first stages of the severe acute malnutrition (Million, Diallo and Raoult, 2017). The species' anti-inflammatory properties caused it to be highly successful in preventative probiotics and acute treatments of conditions such as ulcerative colitis and Crohn's disease (Plaza-Díaz *et al.*, 2017). Probiotic preparations including *B. longum* were shown to improve the central nervous system functions in humans. Improvements included decreased symptoms of depression and anxiety, improved problem solving abilities, improved mood (Wang *et al.*, 2016). After a 10 week course of *Bifidobacterium longum* NCC3001 subspecies *longum* strain, a pilot study of patients suffering from the irritable bowel syndrome (IBS) showed a reduction in depression, decreased responses to fearful brain stimuli and a general improvement of the IBS symptoms (Pinto-Sanchez *et al.*, 2017).

Many commercial probiotics contain the *B. longum* spp infantis strain, either in a single-strain formulation or in a product containing several probiotic strains. One such product is marketed in the UK by the trade name Alflorex and it contains a single patented strain, Bifantis, in a capsule. It was shown to be highly effective in treatment of global individual IBS symptoms without adverse effects in two randomised, controlled studies (Brenner and Chey, 2009) . In addition, there are several commercially available probiotic products in the UK that contain a variety of probiotic strains. Bio-kult is available as a capsule containing a mixture of several *Bacillus, Lactobacillus* and *Bifidobacterium* species including *longum* spp infantis. VSL#3 is sold as a sachet containing *Streptococcus, Lactobacillus* and *Bifidobacterium,* including *longum* and *longum* spp infantis. Probio 7 is a capsule product containing *Lactobacillus, Streptococcus* and *Bifidobacterium* including *longum* (Fredua-Agyeman and Gaisford, 2015).

Probiotic species benefit the host through several proposed mechanisms. For example, by increasing the microbial diversity and lowering the pH, the probiotic species help protect against a pathogenic invasion (Islam, 2016). A less known benefit of probiotics is that the bacteria potentially help digest otherwise indigestible food components, increasing the levels of minerals, vitamins and essential amino acids available for the host (O'Sullivan *et al.*, 1992).

As phytic acid is present in plant-based food in high quantities, it confers its antinutritive effects in human diet by chelating minerals and proteins (Kennefick and Cashman, 2000). Phytate degrading activity stemming from human commensal gut bacteria would abolish this problem, as well as confer benefits in the form of providing lower inositol phosphates that are vital for cellular regulation (Sandberg, Rossander and Turk, 1996; Sandberg and Andlid, 2002; reviewed in Shamsuddin, 2002; Bohn, Meyer and Rasmussen, 2008). For these reasons, it is worth investigating the phytate degrading abilities of probiotic bacteria as an additional benefit to adding probiotic products to human diets.

A study by Sharma et al. (Sharma and Trivedi, 2015) identified five phytase producing probiotic bacterial strains by screening sixty-three strains from natural sources. From among several *Bacillus* and two *Pseudomonas* species, the *B. subtilis* P6 strain showed the highest phytase activity of 2.74 EU/ml (where one unit of phytase activity is defined as the amount of enzyme that releases 1 µM of Pi/min under standard assay conditions). Additionally it had a more than 70 % survivability at the stomach-simulating pH of 2.0 and a 2.0 % bile salt tolerance, reflecting highly suitable adaptations for potential human and animal consumption. The authors suggest that a development of a probiotic product containing the *B. subtilis* P6 strain could have a vast potential in food and animal feed industries. It would replace the commercial phytase, which are extensively costly to manufacture. Such a product would increase the nutrient digestibility exponentially and in addition to improved immunity, would benefit consumers and animal product manufacturers (Sharma and Trivedi, 2015).

4.1.2 *Bifidobacterium longum* subsp. *infantis* ATCC 15697 phytase

Haros *et al.* (Haros, Bielecka and Sanz, 2005) tested nine *Bifidobacterium* strains for extracellular phytase and phosphatase activities at 50 °C. Phytase activity was determined on the basis of the degree of dephosphorylation of phytate, by measuring the release of inorganic phosphate using the ammonium molybdate method. General phosphatase activity was based on *p*-nitrophenylphosphate (pNPP) degradation by measuring the release of *p*-nitrophenol as conferred by the increase in absorbance at 405 nm. It is a common assay for phosphatase activity (Lorenz, 2011). Eight strains showed higher

specificity for phytate, suggesting they produced true phytases: *B. adolescentis* ATCC 15703, *B. angulatum* ATCC 27535, *B. animalis* DSM, *B. animalis* DSM 20104*, B. catenulatum* ATCC 27539, *B. globosum* DSMZ 20092, *B. longum* ATCC 15707, *B. pseudocatenulatum* ATCC 27919. The strains that showed the highest percentage of IP_6 dephosphorylation were *B. pseudocatenulatum* (100 % IP_6 degradation) and *B. longum* (12.8 % IP_6 degradation). The strain *B. breve* ATCC 15700 showed a higher specificity for pNPP and a negligible activity against phytate, therefore it was deemed as not showing phytase activity (Haros, Bielecka and Sanz, 2005).

Specific phytase activity in cell suspension of the *B. longum* ATCC 15707 and *B. longum* subsp. infantis ATCC 15697 phytases was determined to be between 0.21-0.26 U/mg protein and 1.011 U/mg of protein. A unit of phytase activity U was defined as 1.0 µmol of Pi liberated per hour at 50 °C (Haros, Bielecka and Sanz, 2005; Haros *et al.*, 2007). The ability of the phytase to generate lower inositol phosphate products during growth was measured through HPLC analysis of the supernatants of cultures grown till stationary phase. After degrading 12.8 % of the initial IP_6, the detected products of the *B. longum* ATCC 15707 phytase constituted of IP_5 (0.41 % of initial IP_6), IP_4 (2.02 %) and IP_3 (1.08 %) (Haros, Bielecka and Sanz, 2005; Haros *et al.*, 2007), indicating that in the above conditions, the phytase accumulates IP_4 products.

Remarkably, the *B. longum* subsp. infantis phytase hydrolysed 100 % of the initial IP_6 as well as 100 % of the subsequently generated IP_5. It generated 2.31 % of the initial IP_6 in the form of IP4 and 97.78 % IP_3. Furthermore, the phytase was shown possess a pH optimum of 6.0-6.5 and a temperature optimum of 50 °C. It retained 51.2 % of its maximum activity level at 37 °C, which is the physiological temperature in the human gut (Haros *et al.*, 2007).

4.1.3 Mutagenesis to elucidate the catalytic mechanism of *Bifidobacterium longum* subsp. *infantis* phytase

The HAP phytase from *Bifidobacterium longum* subsp. infantis ATCC 15697 (hereby referred to as *B. longum* phytase or Bl phytase) was chosen for experiments involving

active site residue mutagenesis that would lead to elucidation of the structure of the enzyme bound to its IP_6 substrate. For this purpose, the enzyme needed to be mutated to prevent substrate turnover, so that structure reflecting the substrate-bound conformation could be obtained.

Like other members of the histidine acid phosphatase phytase group, the Bl phytase displays a two-step catalytic mechanism when dephosphorylating the substrate IP_6 (see Figure 1.5). The conserved N-terminal consensus sequence motif RHGXRXP contains the catalytic histidine (Ostanin *et al.*, 1992) and the downstream HAE motif provides the presumed proton donor glutamate (Stentz *et al.*, 2014). In the first step, the lone electron pair on the ε2 nitrogen of the catalytic histidine carries out a nucleophilic attack on the phosphorus atom of the IP_6 phosphate. While the substrate transfers a phospho group to the enzyme, at the same time the glutamate donates a proton to the leaving group, forming a phosphohistidine intermediate (Ostanin and Van Etten, 1993). In the other branch of HAP phytases, the HD motif provides an aspartate residue to act as the general acid in this reaction (Liu *et al.*, 2004). In the second step, the deprotonated glutamate residue acts as a general base, attacking a water molecule that in turn attacks the phosphamide bond of phosphohistidine, releasing the free inorganic phosphate as product (Ostanin and Van Etten, 1993).

I decided to mutagenise the proton donor glutamate in order to create an inactive form of the enzyme. The premise was that such mutation could stop the turnover, and solving the crystal structure of any complex thus created could shed light on aspects of the catalytic mechanism of the enzyme. Alanine is commonly used in substitution mutations to abolish the function of a protein. However, I chose to substitute the glutamate with a glutamine residue. Glutamine bears closer resemblance in size and shape to glutamate than alanine, as it involves replacing the glutamate sidechain carboxyl group with the glutamine amide group. I hoped to preserve the general shape and conformation of the active site in order to provide a more accurate picture of the wild-type enzyme's behaviour in conjunction with substrate.

4.2 Methods

4.2.1 pET28a

The wild-type Bl phytase construct in a pOPINF vector was provided by Arthur Li (UEA). Mutagenesis attempts on this construct were unsuccessful, therefore as the next step I cloned the gene into a pET28a vector as described below, to pursue mutagenesis in this vector.

pET is the most powerful system of vectors developed for the most successful cloning and expression of recombinant proteins in *E.coli.* The inserted genes of interest are under the control of a strong T7 promoter. Upon induction of expression by a T7 RNA polymerase, the target protein can constitute over 50% of the total cell protein content after a few hours. The pET28a vector contains an N-terminal His-tag (to be cleaved by thrombin) to facilitate protein purification and a kanamycin-resistance gene to confer an antibiotic selection advantage (pET System Manual 11th Edition, Novagen). Figure 1 below illustrates the vector map of pET28a, demonstrating the locations of the multiple cloning site, the kanamycin resistance gene and other points of interest.

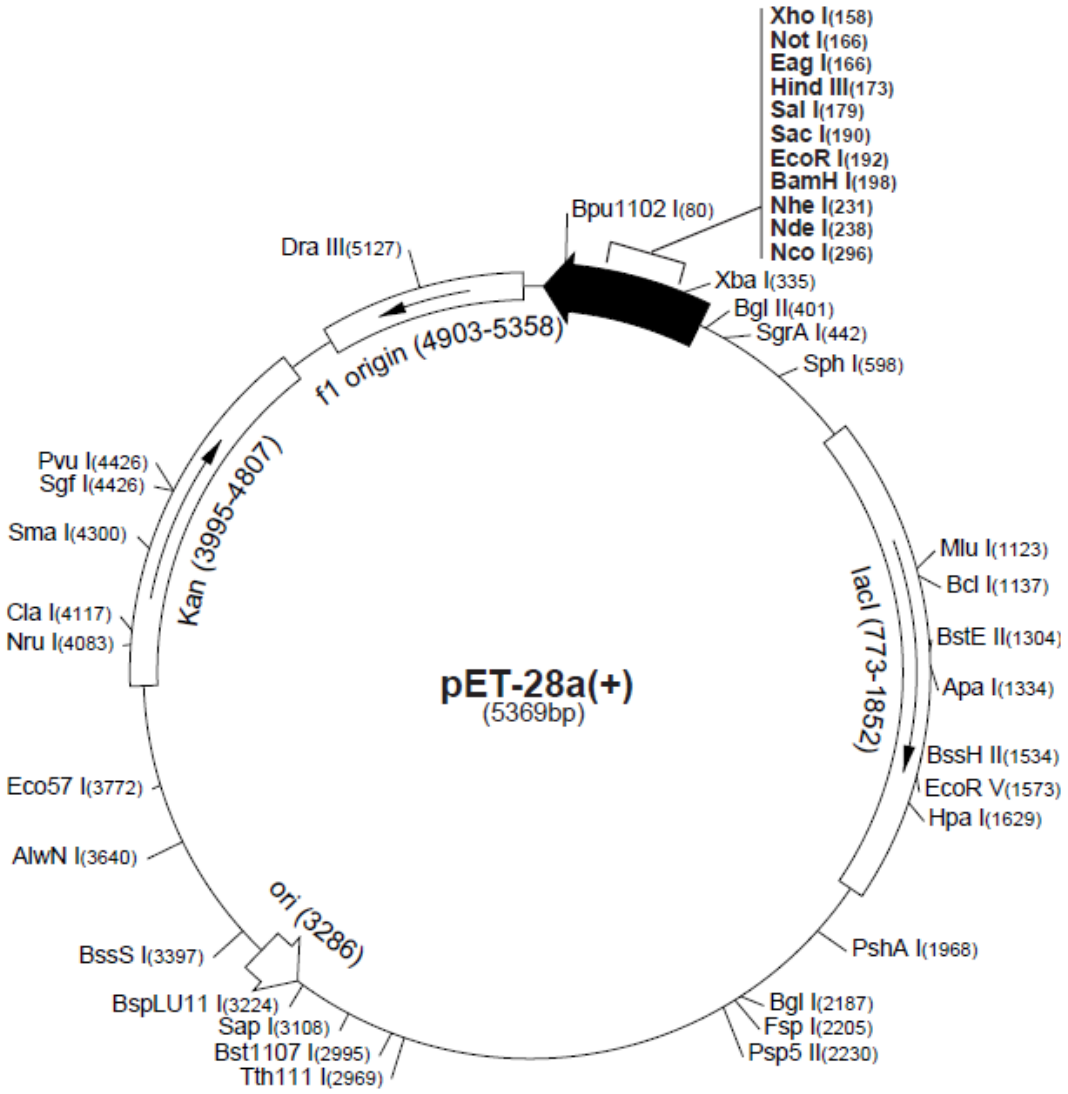

Figure 4.1 Vector map of pET28a.
Locations of interest are as follows: T7 terminator 26-72, His•Tag coding sequence 140-157, cloning site HindIII - NheI: 173-231, T7 promoter: 370-386, lacI coding sequence: 773-1852, pBR322 origin: 3286, Kan coding sequence: 3995-4807, f1 origin: 4903-5358 (image from: pET System Manual 11th Edition, Novagen).

The exact location of the restriction sites is illustrated in the Figure 4.2 below. It outlines the position of the T7 promoter and terminator, His-Tag and the thrombin cleavage site.

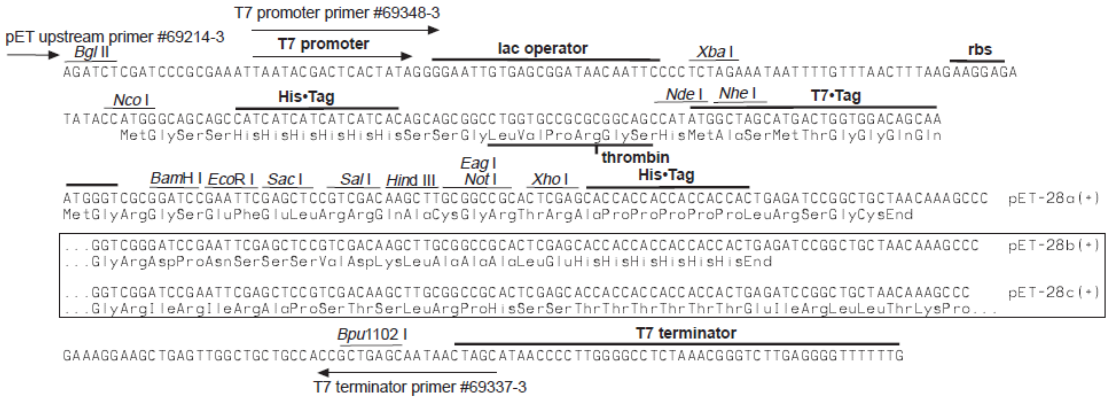

Figure 4.2 pET28a cloning/expression region.
Genetic and amino acid sequence of the cloning and expression region of pET28a, showing the location of the multiple cloning site in relation to the His-Tag and the thrombin cleavage site (image from: pET System Manual 11th Edition, Novagen).

4.2.2 PCR to add restriction sites to the Bl gene

In order to be able to insert the Bl gene into the pET28a vector, I used the purified plasmid containing the Bl gene in the pOPinF vector as template. I carried out a PCR reaction with primers designed to add restriction sites flanking the gene. In order for the restriction enzymes to successfully attach to their restriction sites, an extra sequence of randomly chosen nucleotides was added preceding the restriction site. The primers were constructed as shown below.

Forward primer: 5' – GATATATATAG^CTAGCATGGAGGCCGACGGCC – 3'

Reverse primer: 5' – CATATATATA^AGCTTTTAGATGCGGGCATCCTGACC – 3'

The first sequence (pink) is the random sequence of nucleotides to aid restriction enzyme binding. The middle sequence (yellow) is the restriction site for NheI (on forward primer) and HindIII (on reverse primer), with the caret symbol showing the cutting site of the enzyme. The last sequence (blue) is the sequence of the Bl gene.

The PCR was carried out using the Phusion® High-Fidelity DNA Polymerase (New England Biolabs). Positive and negative controls were employed in order to control for contamination with outside DNA as well as to ascertain the success of the PCR reaction. The ingredients for the reaction were as follows for one reaction:

	Volume per reaction (µl)
Phusion® HF Buffer	10
Deoxyribonucleotide mix 10mM	1
Forward and reverse primer mix 10 µM	5
Phusion polymerase	0.5
Bl-pOPinF plasmid 30ng/ul	4
ddH20	29.5

The conditions for the PCR reaction were as follows:

duration	Temperature °C	
3 min	98	
30 sec	98	x 25
1 min	68	
1 min	72	
10 min	72	
hold	4	

4.2.3 PCR purification

Polymerase chain reaction (PCR) gel purification was carried out to isolate the DNA product and to eliminate the PCR constituents. The kit used was NucleoSpin® Gel and PCR Clean-up (Macherey-Nagel). The PCR products were separated using a 1% agarose gel electrophoresis and visualised under UV light. The Bl gene is 1539 bp long and after identifying the product band on the gel, it was excised and purified using the kit.

4.2.4 Restriction digest of PCR product and pET28a plasmid

The 50 µl restriction digest reactions were carried out overnight at 37 °C using the following ingredients:

	plasmid digest	gene insert digest
NheI (Roche)	1 µl	1 µl
HindIII (Roche)	1 µl	1 µl
Buffer M x10 (Roche)	5 µl	5 µl
Bl-pOPINF 52ng/ µl	40 µl	-
purified gene insert	-	9 µl
ddH20	3 µl	34 µl

4.2.5 Ligation

The restriction digest products were purified using the QIAquick Gel Extraction Kit (Qiagen) according to the manufacturer's instructions, and eluted into 30 µl EB buffer (Qiagen). The DNA concentration was quantified using NanoDrop One (Thermo Scientific). Ligation between the plasmid and the gene insert was carried out and a negative control with plasmid only was used. Using the T4 ligase (Invitrogen) and the manufacturer's protocol, the vector:insert ratio used was 5:1. The following table shows the reaction constituents.

	volume (µl)
Digested plasmid 13 ng/ µl	5 µl
Digested insert 5 ng/ µl	1 µl
T4 DNA ligase buffer x10 (Invitrogen)	1 µl
T4 DNA ligase (Invitrogen)	1 µl
ddH20	2 µl

The reaction was carried out overnight at 16 °C. The ligation product was transformed into competent *E.coli* Stellar cells via heat shock for cloning. Ten colonies were chosen to inoculate ten cultures that were grown in 10 ml LB medium with kanamycin. Plasmid purification was carried out using the QIAprep Spin Miniprep Kit (Qiagen) according to the manufacturer's instructions.

4.2.6 Analytical restriction digest

Analytical restriction digest was performed on the ten purified plasmids to test for the presence of the gene insert. The following were the reaction constituents:

	volume (µl)
plasmid DNA	13
HindIII (Roche)	0.5
NheI (Roche)	0.5
Buffer M x 10 (Roche)	3
ddH20	13

Empty pET28a plasmid was digested as a negative control to be visualised on an agarose gel. The reaction products were separated on a 1 % agarose gel by electrophoresis. Circular pET28a was included as a negative control to test the digestion success.

The successfully ligated plasmids were tested by sequencing for the correct DNA sequence using the services of Eurofins Genomics.

4.2.7 Mutagenesis

Mutagenesis PCR was carried out in 25 µl reactions with the Q5® Site-Directed Mutagenesis Kit (New England Biolabs) using ingredients per reaction outlined in Table 1 below. Positive and negative controls were used to ascertain success of amplification, success of mutagenesis and lack of contamination with external DNA. The Q5 Master Mix precipitates in temperatures lower than room temperature, therefore care had to be taken to warm it up to dissolve all the components. Upon mixing the Master Mix with the other PCR ingredients, the mixture was warmed in hand and thoroughly but gently mixed.

	Volume per reaction (µl)
Q5® Hot Start High-Fidelity 2X Master Mix	12.5
Forward and reverse primer mix 10uM	2.5
Wild-type Bl-pET28a 30g/ µl	1
ddH20	9

The sequence of the mutagenesis primers was as follows:

Sense	5'-CGCCCATGCGcAAACCATGATG-3'
Antisense	5'-AACCGGAACGTCGCCACA-3'

To verify the success of the PCR reaction, the products were transformed into competent cloning *E.coli* strain Stellar by heat shock. 10ml overnight Lysogeny Broth (LB) cultures were purified to extract the plasmid using the QIAprep Spin Miniprep Kit (Qiagen) according to the manufacturer's instructions.
The purified plasmid was sequenced using the sequences services of Eurofins Genomics to confirm the successful mutation. The plasmids were sent in 10 µl aliquots of ~150 ng/ µl. Sequencing was performed using T7 forward and reverse sequencing primers to encompass the gene insert.

4.2.8 Protein expression

The successful plasmid was transformed via heat shock into the competent expression *E.coli* strain Rosetta2 (DE3) pLysS. The cells were grown in LB medium with 50 µg/ml kanamycin, until an OD_{600} of ~0.6 was reached at 37 °C and then cooled to 30 °C. Over-expression of the protein was then induced by adding isopropyl β-D-1-thiogalactopyranoside (IPTG) to the final concentration of 100 µM. Expression took place overnight at 30 °C in a shaking incubator at 180 rpm. Cells were harvested by centrifugation at 6,000 g. The cell pellet was snap-frozen with liquid nitrogen to aid cell lysis and for storage.

4.2.9 Protein purification

The following buffers were used for protein purification:
Lysis buffer: 50 mM Tris-HCl pH 8, 300 mM NaCl, 10 mM imidazole. Wash buffer: 50 mM Tris-HCl pH 8, 300 mM NaCl, 20 mM imidazole. Elution buffer: 50 mM Tris-HCl pH 8, 300 mM NaCl, 300 mM imidazole. Gel filtration buffer: 10 mM Tris-HCl pH 7.4, 150 mM NaCl. The cells were resuspended in lysis buffer and lysed using French Press. From now on, the extracts were kept at 4 °C or on ice throughout the purification procedures and before use. The resulting suspension was centrifuged at 15,000 g for 20 min to remove cell debris. The extract was then purified by loading onto an immobilised metal ion affinity chromatography (IMAC) column Ni-NTA Superflow Cartridge (QIAGEN) at 1 ml/min. The protein fractions were eluted at the flow rate of 3 ml/min by increasing the gradient of elution:wash buffer and were verified by SDS-PAGE. The fractions containing the protein of interest at sufficient quantities were pooled and concentrated using a centrifugal spin concentrator Vivaspin 500 Protein Concentrator (GE Healthcare Life Sciences) with the molecular weight cut off of 10,000 Da until the volume reached ~1.5 ml.
A HiLoad 16/60 Superdex 75 gel filtration column (GE Healthcare Life Sciences) was equilibrated with the gel filtration buffer. Using a 2 ml loop, the protein was loaded onto the column. Using an ÄKTA pure™ liquid chromatography system (GE Healthcare), protein fractions were eluted at the flow rate of 1 ml/min. The fractions were assessed using SDS-PAGE and those containing the pure protein at sufficient quantities were pooled and concentrated to 10 mg/ml.

Images of protein purification including chromatograms and SDS-PAGE pictures are included in Appendix 3.

4.2.10 Crystallisation and X-ray crystal diffraction

Previous work by Dr Arthur Li (UEA) showed that wild-type Bl crystallised in 0.1 M MES pH 6.5, 0.01 M zinc chloride, 18% PEG 6000 at a protein concentration of 9mg/ml. Here, a broader range of conditions was tested producing a PEG 6000 gradient of 14-20% in 2%

increments and a second gradient of pH 6.0, 6.25 and 6.5 of MES and maintaining 0.01 M zinc chloride concentration throughout.

Two sets of identical crystallisation screens were used. Each well contained 200 µl of the crystallisation solution. Protein was concentrated to 7, 8, 9 and 10 mg/ml as determined spectroscopically, and centrifuged at 5,000 g to remove particulate matter. The crystallisations experiments were dispensed manually in droplets of 1 µl protein and 1 µl screening solution. The crystallisation plates were sealed with a clear film and set in 16°C. Crystals grew in both plates under the same conditions: 0.1M MES pH 6.5, 0.01 M zinc chloride, 16% PEG 6000, 9mg/ml protein. Crystals were harvested using a litho loop (Molecular Dimensions) at 16 °C. Crystals were soaked in solutions containing the mother liquor and PEG 400 with and without 10 mM IP_6 before being vitrified and stored in liquid nitrogen.

X-ray diffraction data collection was conducted at the Diamond Light Source (Didcot, Oxfordshire), on beamline I03 using a Pilatus3 6M detector and BART sample charger. The beam operated at energy 12.699 keV and wavelength 0.9763 Å.

Molecular replacement was carried out using Phaser (McCoy *et al.*, 2007) using the structure of *holo* Bl phytase with *myo*-inositol hexasulphate (IS_6) (Isabella Acquistapace, UEA, personal communication) as a model. Next, structure refinement was conducted using cycles of manual remodelling by reference to Fourier difference maps using Coot (Emsley et al., 2010) and automated refinement using PHENIX Refine (Adams *et al.*, 2010).

4.2.11 Domain movement analysis

Pairs of Bl phytase conformers were analysed using DynDom software to test for the presence of dynamic domains, visualise their superimposition and obtain information about the domain movements, in particular the nature of the domain motion, the hinge axes and the identity of the hinge bending residues (Hayward and H. J. C. Berendsen, 1998).

4.3 Results and Discussion

4.3.1 Previous mutagenesis attempts

Mutagenesis of the Bl gene to introduce an active site mutation was first carried out on a Bl-pOPinF construct, as this was the plasmid the construct was supplied in. First attempts at mutagenesis were carried out using the Q5® Site-Directed Mutagenesis Kit and primers specifically designed according to the manufacturer's instructions.

Q5 mutagenesis relies on linear amplification, therefore the specific Q5 primers were non-overlapping. The substitution mutation was introduced by incorporating the desired nucleotide changes in the center of the forward primer, flanked by 11 complementary nucleotides on the 3' side of the mutation. The 5' end of the forward and reverse primers anneals back-to-back. The diagram below shows the amino acid sequence of the area surrounding the active site, with the mutation in place (HAE to HAQ). The nucleotide sequences below show the corresponding forward primer sequences (red) and the reverse primer (blue). The substitution mutation is denoted by a lower-case letter *c*.

TGTGGCGCGTTCCGGTTCGCCcTGCGCAAACCATGATG

ACACCGCTGCAAGGCCAAGCGGGTACGCGTTTGGTACTAC

Extensive attempts on the Bl-pOPinF construct using the Q5 mutagenesis primers and kit proved unsuccessful. Reasons for failure included no product visible on gel electrophoresis, no bacterial colonies after transformation of the products, or the products did not contain the target mutation. Eventually I obtained the correct mutation, however I was unable to overexpress the protein in sufficient quantities.

The next attempt involved using the QuikChange II XL Site-Directed Mutagenesis Kit (Agilent), with PfuUltra HF DNA polymerase and specially designed primers as specified by the manufacturer. The QuickChange II XL primers both contained the mutation and were each complementary to opposite strands of the vector, as the kit polymerase was designed to work with highest fidelity on both plasmid strands at the same time. The forward (red) and reverse (blue) primers used with this technique are shown in the diagram below. The substitution mutation site is denoted by the lower-case letter *c* and *g*.

GGTTCGCCCATGCGcAAACCATGATGCCG

CCAAGCGGGTACGCgTTTGGTACTACGGC

Using this technique, no quantifiable PCR product was detected, and upon bacterial transformation no colonies grew.
The next attempt involved creating a new set of primers that contained both overlapping and non-overlapping regions. The forward (red) and reverse (blue) primers are shown below, embedded in the Bl gene sequence (black), with the substitution site denoted by the lower-case letter *c* and *g.* The polymerase used was Phusion® High-Fidelity DNA Polymerase (New England Biolabs).

TTCCGGTTCGCCCATGCGCcAAACCATGATGCCGTTTGCCGC

CAAGGCCAAGCGGGTACGCgTTTGGTACTACGGCAAACGGCG

This technique yielded wrong size products when visualised via gel electrophoresis. After these multiple attempts testing an extensive range of primers and different PCR conditions, I decided to reclone the Bl gene into a pET28a vector.

4.3.2 Cloning

To clone the Bl gene into the pET28a vector, I used PCR to amplify the gene. By using specially designed primers, I attached restriction sites flanking the gene to enable digestion with restriction enzymes compatible with the pET28a vector.
In the PCR reaction I used negative controls to account for extraneous contamination (omitting template). The reaction products were separated on a 1% agarose gel. The band of around 1540 bp was excised under a UV light. The DNA was extracted using a PCR gel clean-up kit. No picture of the gel was taken, as to not expose the DNA to extra UV radiation and to prevent mutations.
Restriction digestion was carried out on pET28a plasmid on the Bl gene amplified with the restriction sites. Restriction enzymes used were NheI and HindIII. The reaction was carried out overnight at 37 °C. The digestion products were separated on a 1% agarose gel and purified. Another analytical electrophoresis run was carried out on a 1% agarose gel with a small amount to visualise the product for reference.

4.3.3 Ligation

Ligation of the purified gene insert and the linearised vector was set up overnight at 16 °C using T4 ligase using a 1:3 vector:insert ratio. The product was transformed into competent Stellar cells with heat shock, however it did not yield any bacterial colonies. Another attempt at ligation was performed, screening a range of vector:ratios: 3:1, 5:1, 1:1 and 3:1. Negative control was included that contained so insert, to ascertain the success of the restriction digest. The ligation was carried out overnight at 16 °C and the reactions were transformed into Stellar cells. Additionally I used a positive control to check transformation success. After overnight incubation, all ligations yielded colonies with the most successful being the 5:1 vector:insert ratio.

4.3.4 Testing the success of the ligations

To test the success of the ligations, ten colonies numbered 1-10 were used to inoculate 10 ml LB media with kanamycin and cultured overnight. Plasmids were extracted and small amounts were subjected to analytical restriction digestion. The products were separated on 1% agarose gel and visualised under UV light.

The UV gel image showed that plasmids 3, 6, 7 and 10 yielded a fragment corresponding to the size of the empty linearised pET28a plasmid (5583 bp) and a fragment reflecting the size of the gene insert (1539 bp). No additional bands reflecting incomplete digestion of the construct (7122) were seen in these lanes. From these, plasmids 3, 7 and 10 were chosen to be sequenced. The sequencing results showed successful insertion of the gene into the plasmid with no mutations.

4.3.5 Mutagenesis

The first attempt at mutagenesis using the Q5 kit and primers proved successful and generated multiple plasmids containing the target mutation of the active site, as confirmed by sequencing performed by Eurofins Genomics.

4.3.6 Protein expression and purification

The plasmid was transformed by heat shock into the expression strain Rosetta 2 pLysS (Novagen). Protein expression was induced at OD_{600} 0.6 with 100 µM IPTG at 30 °C overnight. Cells were lysed by French Press and the lysate was centrifuged to remove the cell debris.

The clear lysate was purified by His-tag purification on a Ni-NTA Superflow Cartridge (QIAGEN) and the protein fractions were eluted with a buffered imidazole gradient using the ÄKTA pure™ liquid chromatography system (GE Healthcare). The sample was subjected to an SDS-PAGE separation, which showed that the protein purified as a single band as shown in the figure below. The same sample preparation was crystallised and lead to obtaining the crystal structures.

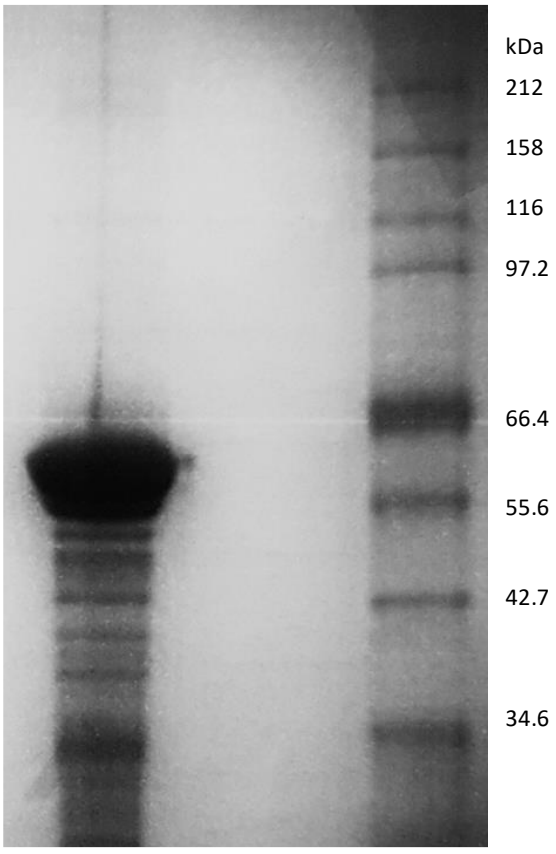

Figure 4.3 10% acrylamide SDS-PAGE gel image of the purified active site mutant E401Q of the Bifidobacterium longum phytase.
Lane 1: 150 µg of the purified and concentrated protein. Lade 2: Molecular weight ladder used was NEB Broad Range Protein Ladder.

4.3.7 Crystallisation

Crystal clusters grew after two weeks at 16 °C in 0.1 M MES pH 6.5, 0.01 M zinc chloride, 16% (w/v) PEG 6000 using 9mg/ml protein.

Figure 4.4 Clusters of protein crystals of the E401Q Bl phytase.
Both crystals grew in 0.1 M MES pH 6.5, 0.01 M zinc chloride, 16% PEG 6000 using 9mg/ml protein after two weeks.

The crystal clusters shown in Figure 4.4 above were separated into single entities. Four crystals were selected for x-ray diffraction and were soaked in mother liquor containing PEG 400 as cryoprotectant with and without the addition of IP_6. Crystals were then flash-frozen in liquid nitrogen and the X-ray diffraction data collection was carried out at the Diamond Light Source (Didcot, Oxfordshire).

4.3.8 X-ray crystal structure solving

From the four crystals, two showed successful diffraction. One crystal that was not soaked in IP_6 diffracted to 1.71 Å resolution, a representative diffraction pattern is shown in the Figure 4.5 below. The crystal that was soaked in IP_6 diffracted to only 2.7 Å resolution and did not appear to have substrate bound in the active site, therefore it is not analysed in this work. Both crystals grew in space group P1, according to autoindexing as part of the Xia2 autoprocessing pipeline. The structure of the E401Q Bl phytase mutant was solved using molecular replacement with a homology model based on the crystal structure of the *apo* form of the wild-type Bl phytase. The final model of the E401Q Bl

phytase X-ray crystal structure was refined at 1.71 Å resolution. The final structure has R_{work} and R_{free} values of 14.7 % and 19.4 %, respectively.

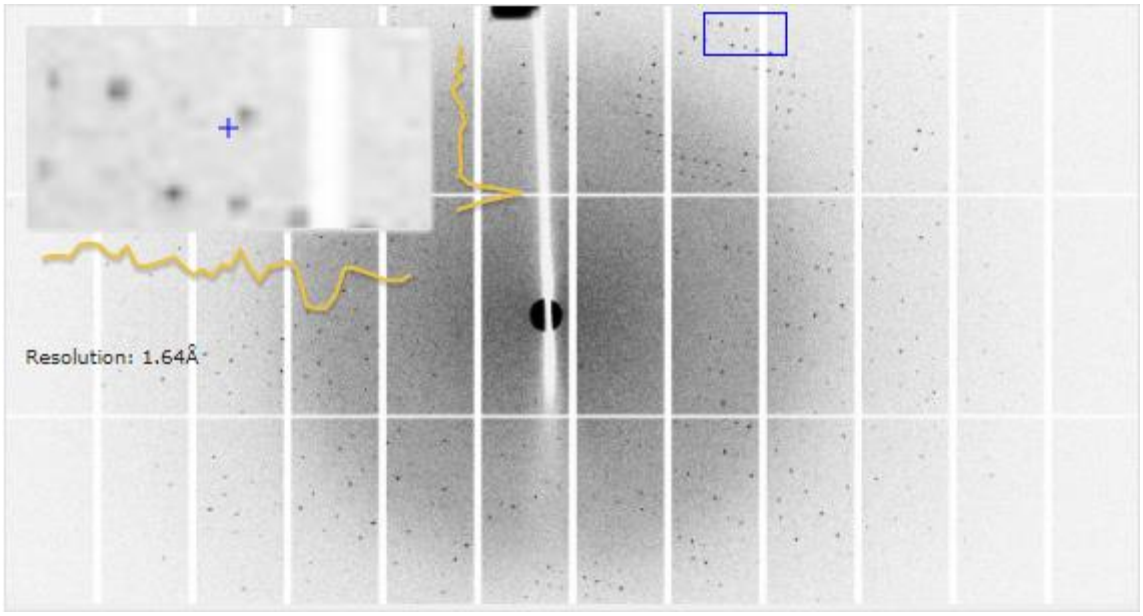

Figure 4.5 Diffraction pattern for x-ray crystallography of E401Q Bl phytase.
The insert shows the resolution at the maximum zoom.

Bl phytase	
Data collection	
Wavelength (Å)	0.97623
Space group	P1
Cell parameters	
a, b, c (Å)	54.6, 72.8, 87.3
α, β, γ (°)	71.4, 72.2, 76.8
Resolution limit (Å)	68.23-1.71 (1.75-1.71)
R_{merge}	0.063 (0.525)
(I)/sd(I)	7.5 (1.4)
Completeness (%)	95.5 (95.0)
Multiplicity	1.9 (1.9)
Overall temperature factor ($Å^2$)	17.3
Refinement statistics	
Protein monomers per asymmetric unit	2
Total atoms	15951
Water molecules	805
R_{work}/%	14.7 (24.3)
R_{free}/%	19.4 (27.9)
Ramachandran analysis (%)	
Most favoured	97.7%
Outliers	0.3%
RMS deviations	
Bonds (Å)	0.009
Angles (°)	0.927
Mean Atomic B-value ($Å^2$)	
Protein	27.3
Water	38.8
Overall	27.9

Table 4.1 Data collection and refinement statistics for E401Q Bl phytase.

Brackets show the statistics for data in the high resolution bin.

4.3.9 Overall X-ray crystal structure analysis

The crystallographic asymmetric unit consisted of two protein monomers with subtle but important differences. Subunit A was found to bind an inorganic phosphate molecule at the active site, while subunit B contained a phosphohistidine intermediate. While it is unknown where the phosphate originated from, it can be speculated that it was picked up during bacterial growth or from an impurity in the purification buffers. It either originated from inorganic phosphate as an impurity in the solutions used during purification, or from any organic phosphate compound from the expression bacteria that served as a substrate for the enzyme. For example, phosphate compounds from the Krebs cycle such as glucose-6-phosphate, phosphoenolpyruvate, glyceraldehyde 3-phosphate as well as ATP and AMP that are present at around 1mM concentrations could be the source of the bound phosphate (Oh *et al.*, 2004; Glick, Pasternak and Patten, 2010, p. 700).

DynDom is a program that allows a user to conduct protein domain motion analysis (Hayward and H. J. Berendsen, 1998). In particular, it can analyse two similar structures to identify the specific residues that change their position between the two protein conformers, and determine the nature and the degree of the shift in the three dimensional space. Figure 4.6 below illustrates a stereo view of the superposition of the structures of the two subunits, with subunit A shown in purple and subunit B shown in blue.

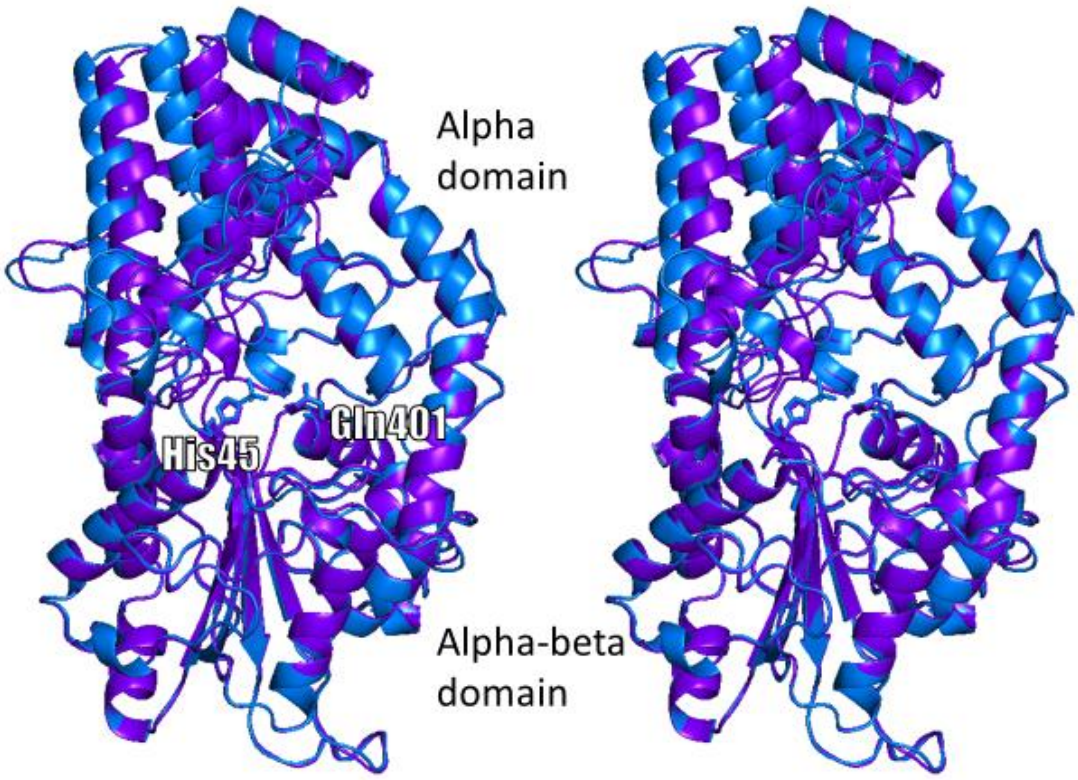

Figure 4.6 Superimposed cartoon representations of the structures of the crystal subunits A and B of the E401Q Bl phytase.
A stereo view of the superimposed x-ray crystal structures of the two crystal subunits of the E401Q Bl phytase. Shown in blue is the structure of the subunit B, with the phosphohistidine intermediate. Shown in purple is the structure of the subunit A, with phosphate bound to the active site. The catalytic histidine and the mutated proton donor residue are labelled His45 and Gln401, respectively. Structures were superimposed with DynDom. The image was created with Pymol and modified.

When the α/β domain was treated as a rigid body, the α domain showed a rotational movement between the two subunits. DynDom analysis of the structures revealed that the structure of the α/β domain is highly similar between the two subunits, but the α domain shows a small translational shift of 1 Å and a 10.6 ° rotation between the two subunits. The image below highlights the motion of the domains.

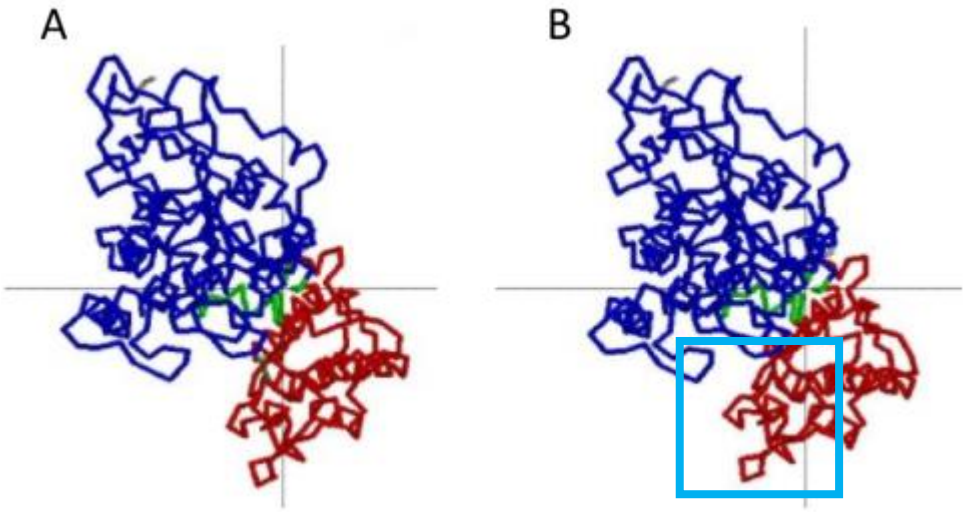

Figure 4.7 Protein domain motion analysis of the two crystal subunits of Bl phytase. A: subunit B, phosphohistidine form; B: subunit A, phosphate-bound form. Blue: the fixed domain; red: the moving domain; green: hinge residues. The grey lines cross at the centre of rotation. Analysis was conducted using DynDom software. The blue square highlights the region undergoing rotation.

The structures of subunits A and B can be treated as snapshots along the reaction coordinate of the Bl phytase. It can be assumed that the subunit A with free inorganic phosphate reflects the final stage of substrate dephosphorylation and represent the enzyme conformation with product bound. Likewise, the subunit B with the phosphohistidine shows the intermediate moment of substrate catalysis.

4.3.10 Domain motion analysis

The structures of the *apo* and *holo* (with IS_6) forms of the enzyme were previously obtained by the members of the Hemmings Lab (Li and Acquistapace, respectively). The Figure 4.8 below highlights the overall structural conformational differences between four structures, showing the overlapping *apo* (red), *holo* (lime), intermediate (blue) and product (purple) forms of the Bl enzyme. The IS_6 and phosphate molecule structures were omitted for clarity.

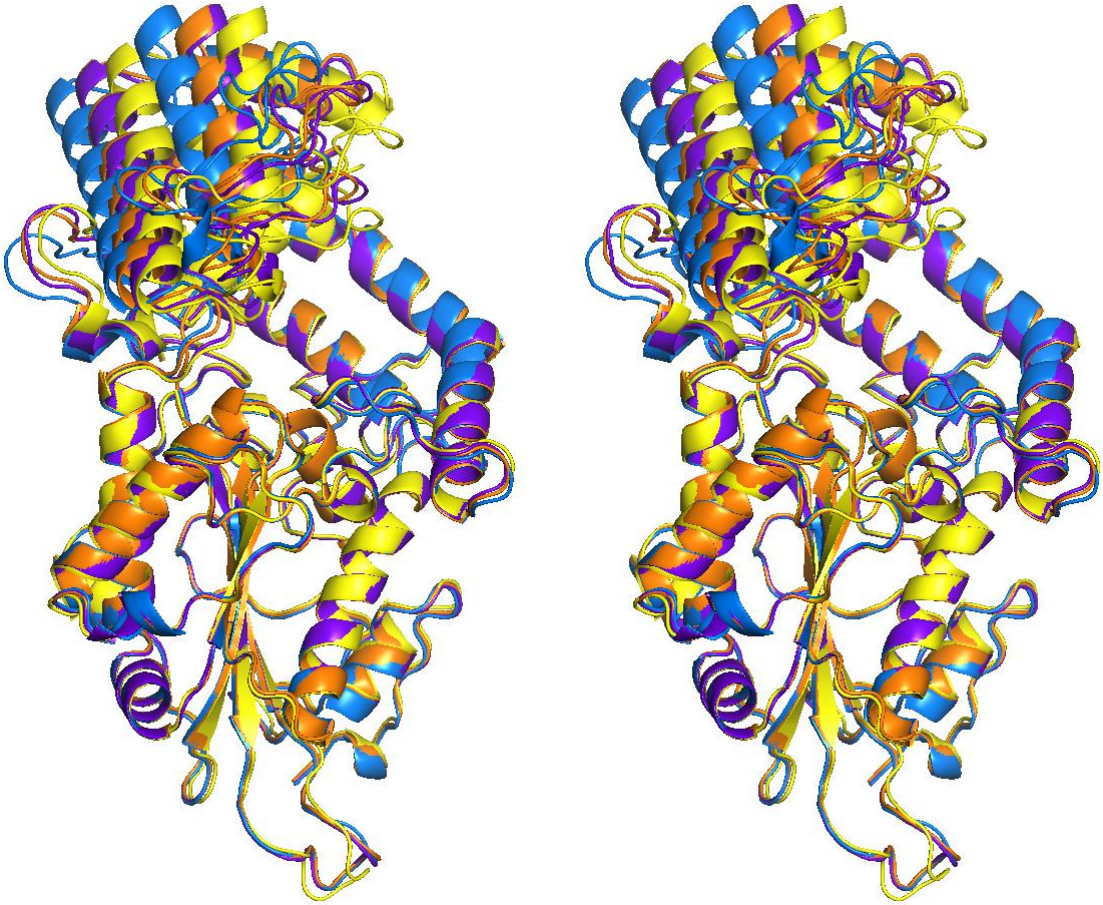

Figure 4.8 Superimposed cartoon representations of the structures of the Bl phytase representing snapshots along the reaction coordinate.
A stereo view of the superimposed x-ray crystal structures of the Bl phytase. Shown in orange: *apo* form; yellow: *holo* form; blue: intermediate form; purple: product-bound form. The image was created with Pymol.

As shown in Figure 4.8, the alpha-beta domain (bottom) maintains a stable conformation between the different conformations of the enzyme, while the alpha domain (top) appears to undergo a shift resembling opening and closing of a lid. The alpha domain of the *apo* form (orange) appears in a midway position between opening and closing. The alpha domain in the *holo* form (yellow) appears to undergo an inwards motion, similar to a closing lid, decreasing the space around the active site region at the interface of the two domains. The alpha domain in the intermediate form undergoes and 'outwards' motion where it shifts past the *apo* form's position. Finally, the product-bound form appears to return to a conformation closely resembling that of the *apo* form.

The *holo* and intermediate conformations appear to assume extreme conformations. DynDom analysis of them identified fixed and moving domains as shown in Figure 4.9 below.

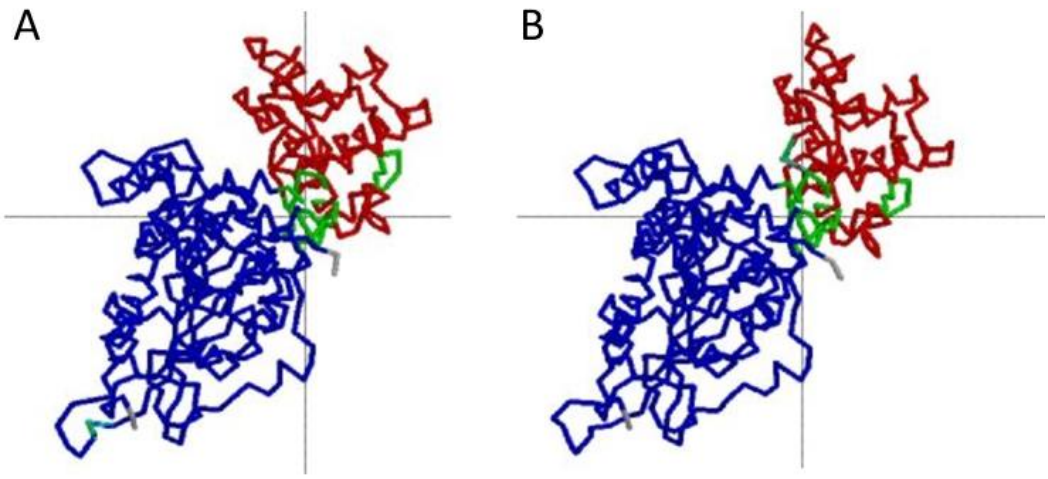

Figure 4.9 Protein domain motion analysis of the *holo* and intermediate forms of Bl phytase.
A: substrate form; B: intermediate form. Blue: the fixed domain; red: the moving domain; green: hinge residues. The grey lines cross at the centre of rotation. Analysis was conducted using DynDom software.

The fixed and moving domains identified by DynDom coincide exactly with the alpha and alpha-beta domains of the Bl phytase. Furthermore, it revealed a rotation angle of 18.4 ° between the two conformers. Analysis of this pair of conformers as well as *holo*-*apo* and *holo*-product-bound forms is shown in the Table 4.2 below.

	holo-apo	*holo*-intermediate	*holo*-product
Rotation angle	10°	18.4°	9.6°
Translation	0.0 Å	- 0.1 Å	0.0 Å
Closure	87.1 %	91.4 %	100 %
Bending residues	47 - 48	47 - 48	48 - 49
	104 - 105	100 - 105	92 - 93
	232 - 234	235 - 240	233 - 240
	314 - 317	314 - 317	282 - 283
	322 - 324	323 - 329	287 - 288
	328 - 329	341 - 344	312 - 313
	347 - 348		317 - 321
			341 - 345

Table 4.2 Domain motion analysis of the alpha domain of the Bl phytase.
Protein domain motion analysis using DynDom. Comparisons of the *apo,* intermediate and product-bound conformations were made in relation to the *holo* conformation. Residues identified as involved in forming the molecular hinge are listed.

Table 4.2 shows the DynDom analyses between the conformations of the *apo,* intermediate and product-bound forms of the enzyme as compared to the *holo* structure. The hinge residues on the connecting region between the two rotating domains were identified and the rotational transition was calculated. Thus, the rotation angle between *holo* and *apo* forms is similar to that between *holo* and product-bound forms, namely 10° and 9.6° respectively, indicating the angle of the difference in the two conformations. The rotational angle between the *holo* and intermediate forms is the highest, at 18.4°. The translation along the rotation vector in all conformers is negligible, –between zero and 0.1 Å, signifying no rigid shift in three dimensional space – the motion of the domain is fully rotational in nature. Translational domain motions are a rare occurrence in proteins (Taylor, Cawley and Hayward, 2014).

Twist and closure motions are on two opposite ends of the possible types of protein domain motions. They can be defined by referring to the line joining the centres of mass of a pair of domains. The twist motion occurs in parallel to that line, while the closure motion occurs perpendicularly. Closure may refer to simple open and closed ‘lid’

movement, but also includes more complex motions, where the two domains remain in close proximity throughout the shift (Shamsuddin *et al.*, 2014; Taylor, Cawley and Hayward, 2014). DynDom assigns a percentage value to the domain motions based on the extent of its closure movement as opposed to its twist. The domain motions in the Bl phytase are particularly closure-oriented, with the *holo* form displaying closure values of 87.1%, 91.4% and 100% against the *apo,* intermediate and product-bound forms respectively.

Analysis of the bending residues reveals overlapping groups of residues undergoing rotations between the pairs of the analysed conformers. Two residues change conformation in all three analysed pairs: Arg 48 and Asp 317. Arg 48 follows the catalytic nucleophilic histidine in the consensus amino acid signature RHGxRxP motif of the enzyme family. Asp 317 is located in the vicinity of the active site, only 7.6 Å from Arg 48.

4.3.11 Analysis of the active site architecture of Bl phytase

A closer look at the active site architecture of the Bl E401Q phytase in the intermediate and product-bound forms with and without electron densities is shown in Figure 4.10 and Figure 4.11 below. The critical hydrogen bond interactions are marked by dotted lines and their distances are shown (Å).

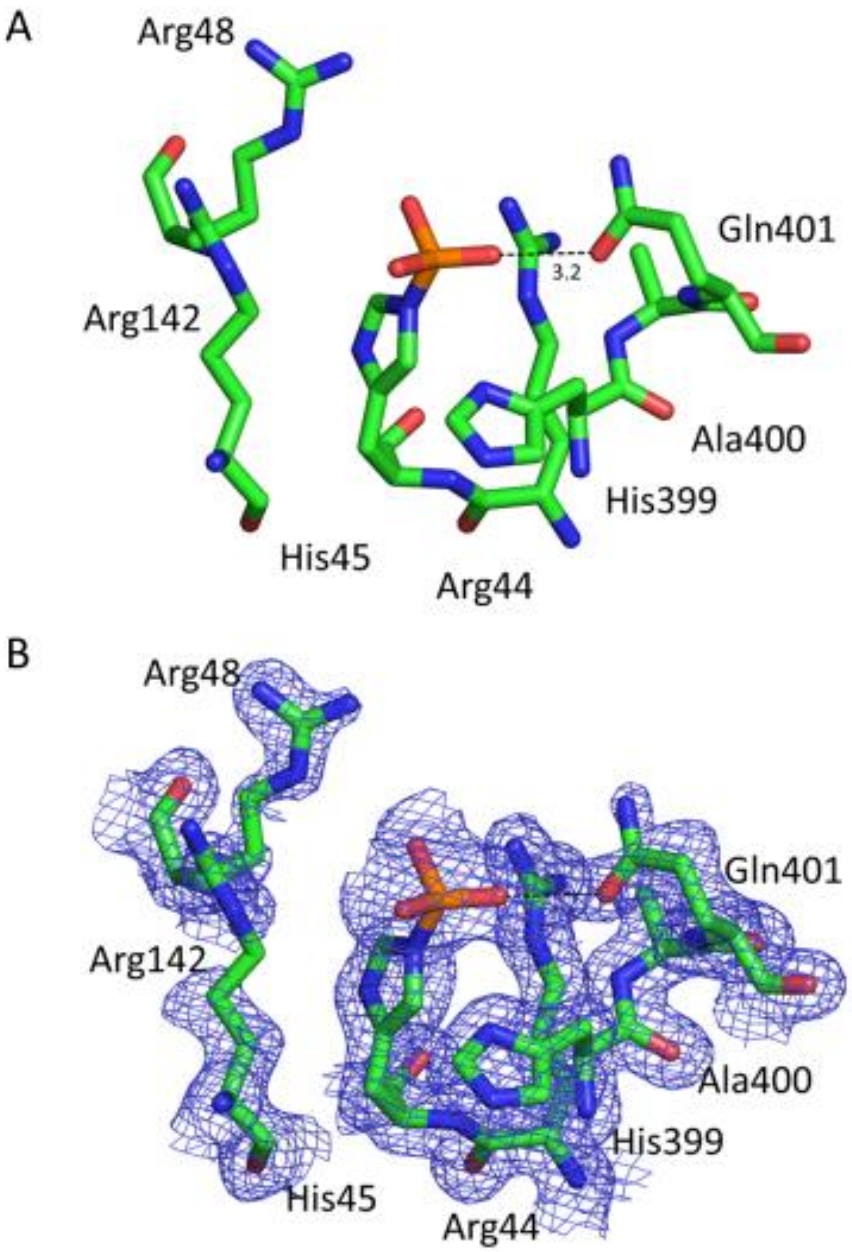

Figure 4.10 Structure of the active site of the E401Q Bl phytase in the intermediate conformation.

Structure of the Bl phytase crystal subunit B with the phosphohistidine intermediate in the active site. A: Key residues in the active site region, showing the hydrogen bond interaction and distance in Å. B: 2mFo-DFc double difference density electron map of the key residues in the active site region, showing the hydrogen bond interaction.

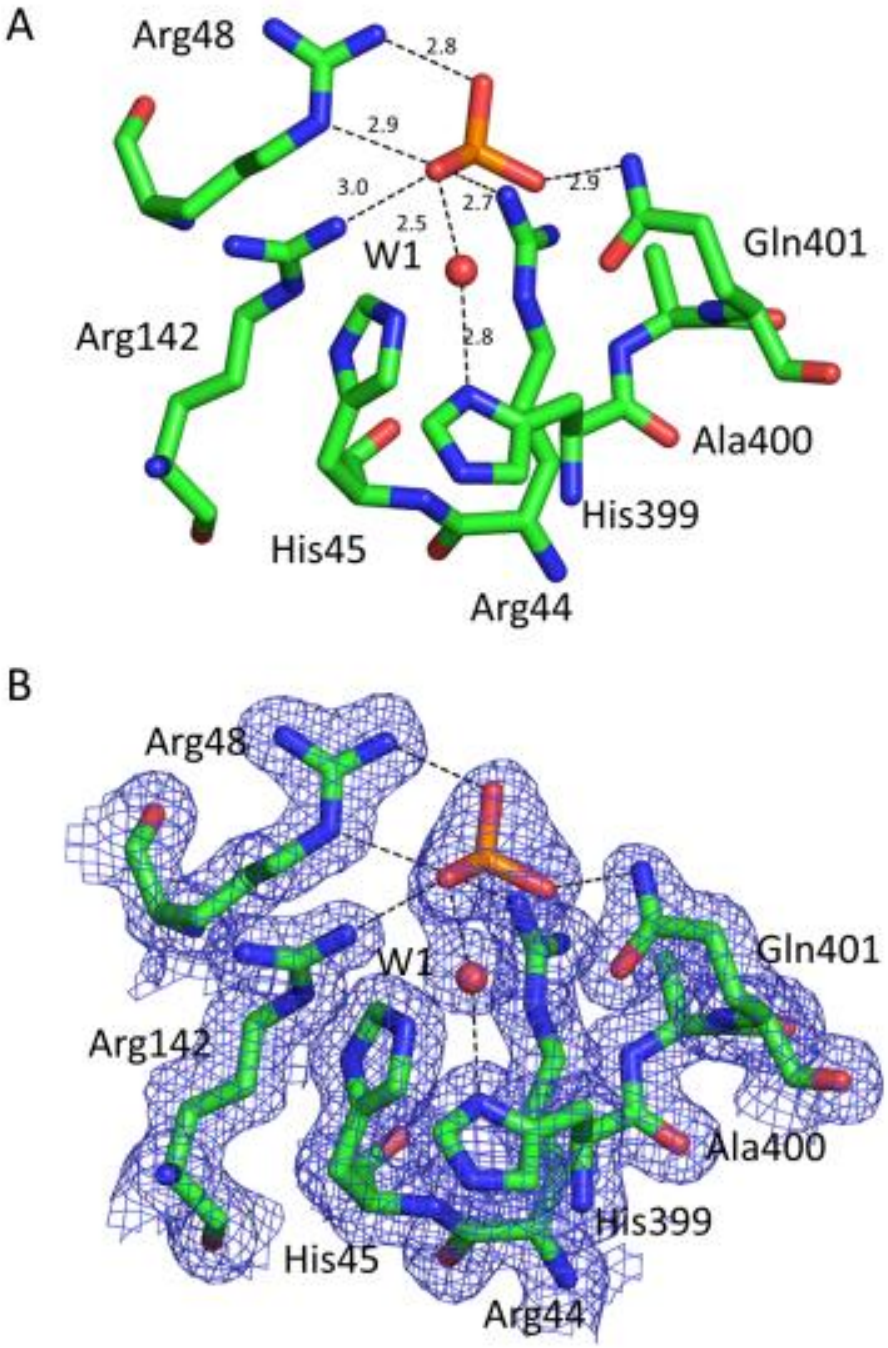

Figure 4.11 Structure of the active site of the E401Q Bl phytase in product-bound conformation.
Structure of the Bl phytase crystal subunit A with phosphate bound in the active site. A: Key residues in the active site region, showing the hydrogen bond interactions and distances in Å. B: 2mFo-DFc double density electron map of the key residues in the active site region, showing the hydrogen bond interactions. W1: a water molecule bound in the active site within hydrogen bonding distance of the phosphate ion.

The double difference 2mFo-DFc density maps show the degree of overlap between the calculated model and the observed electron densities. The blue coloration of the mesh

indicates perfect overlap in this particular region, while red and green coloration would indicate positive and negative densities which should be addressed in the refinement.

The intermediate conformation of enzyme shows only one, albeit weak, interaction in the active site: a weak hydrogen bond between the phosphohistidine oxygen and the Gln 401 ε2 nitrogen. This paucity of hydrogen bonding in the active site of the intermediate conformation may result from the domain motion (and consequent residue shifts) leading to the open conformation of the enzyme. A summary of the active site interactions and their distances in Å are shown in
Table 4.3 below.

		Distance between the atoms in the interaction (Å)	
Interacting atoms		Intermediate conformation	Product-bound conformation
Arg 44 ηN	PO^{3-}_4		2.7
Arg 48 ηN	PO^{3-}_4		2.8
Arg 48 εN	PO^{3-}_4		2.9
Arg 142 ηN	PO^{3-}_4		3.0
His 399 δ1N	H_2O		2.8
H_2O	PO^{3-}_4		2.5
Gln 401 ε2N	PO^{3-}_4	3.2	2.9

Table 4.3 Table of critical interactions between the key residues in the active site of Bl phytase in the intermediate and product-bound conformations.

Moderately strong hydrogen bonds are in the range of 2.7-3.0 Å in length and weak hydrogen bonds reach up to 3.2 Å in length (Minch, 1999). The product-bound conformation appears to contain seven moderately strong hydrogen bonds in the active site, between the 401 ε2 nitrogen atom of Gln 401 and the phosphate oxygen, trapping the phosphate molecule and possibly contributing to the closing domain motion in relation to the phosphohistidine conformation.

A closer look at the active site of the conformers is shown in the Figure 4.12 below, illustrating the profound changes in the tertiary structure of the protein throughout the catalytic cycle. While the α/β-domain (bottom of the figure) has conserved conformation between the different conditions, the alpha domain (top of the figure) displays interesting changes in the residues taking part in ligand binding in catalysis. Together, these structures can illustrate the mechanism of substrate binding and product release.

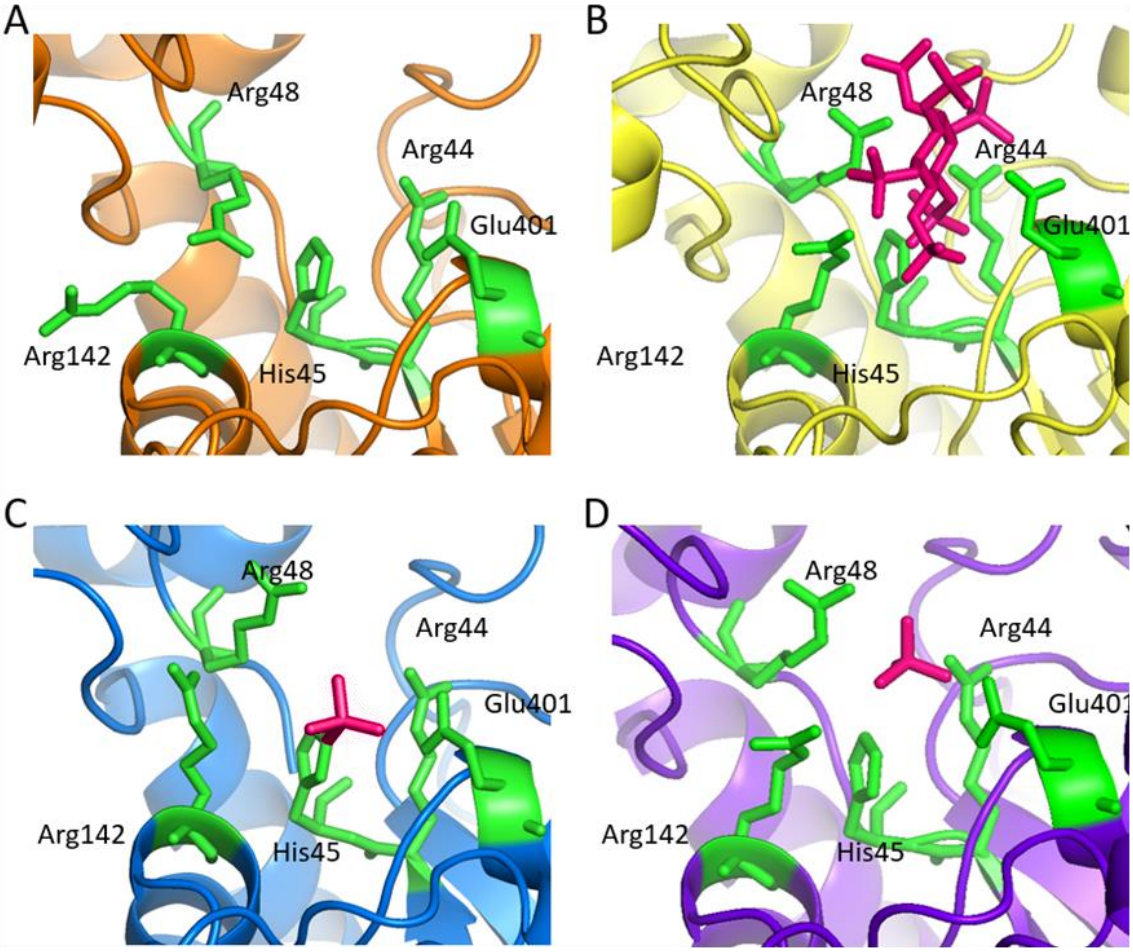

Figure 4.12 Structures of the active site of the Bl phytase as snapshots along the reaction coordinate.
Selected active site residues shown as green sticks and labelled. Atoms of the substrate analogue (*myo*-inositol hexasulphate, IS_6) and those derived from it (phosphate product and phospho-group of the catalytic intermediate are shown as magenta sticks). A: structure of *apo* wild-type Bl phytase; B: structure of *holo* enzyme with IS_6; C: E401Q mutant enzyme form from the A crystal subunit, with the intermediate phosphohistidine 45 in the binding site; D: E401Q mutant enzyme from the B crystal subunit, with phosphate bound in the active site.

Figure 4.12 shows the view of the active site in four conformations, reflecting the steps in the catalytic cycle. Figure 4.12 B shows the ligand-bound conformation, there the Glu 401

side chain is rotated away from the active site. This residue is the proton donor glutamic acid E401. It is likely that this position is assumed due to the negative charges on the IS_6 repelling the carboxylic group of E401. In Figure 4.12 C and Figure 4.12 D the residue is substituted with glutamine. In the structures in conjunction with the intermediate and the product the residue E401Q now appears to have the side chain pointing towards the center of the active site. This change in conformation could be due to the mutation from the negatively charged glutamate residue to the neutral, polar glutamine, allowing the glutamine to hydrogen bond to the neighbouring phosphate.

The distance between the guanidino nitrogen atoms of the arginine residues was measured. R44 and R48 are closest to the centre of the catalytic site when in the substrate-bound conformation and the furthest when in intermediate conformation. When aligned, the distance between the substrate and intermediate forms in R44 is 1.7 Å and in R48 it is only 0.7 Å. R48 is halfway between these positions in the product conformation, with the distance between substrate bound and product bound forms being 0.9 Å and 1.1 Å. R44 is in the same position distant from the active site in both product and intermediate positions.

Similarly, R142 appears in a nearly identical position in the substrate bound and product bound conformations. It undergoes a marked shift (3.2 Å) away from the catalytic center in the intermediate bound conformation. The conformational change in the α-domain in one of the enzyme monomers in the crystallographic asymmetric unit appears to preferentially stabilise the phosphohistidine intermediate under the crystallisation conditions employed.

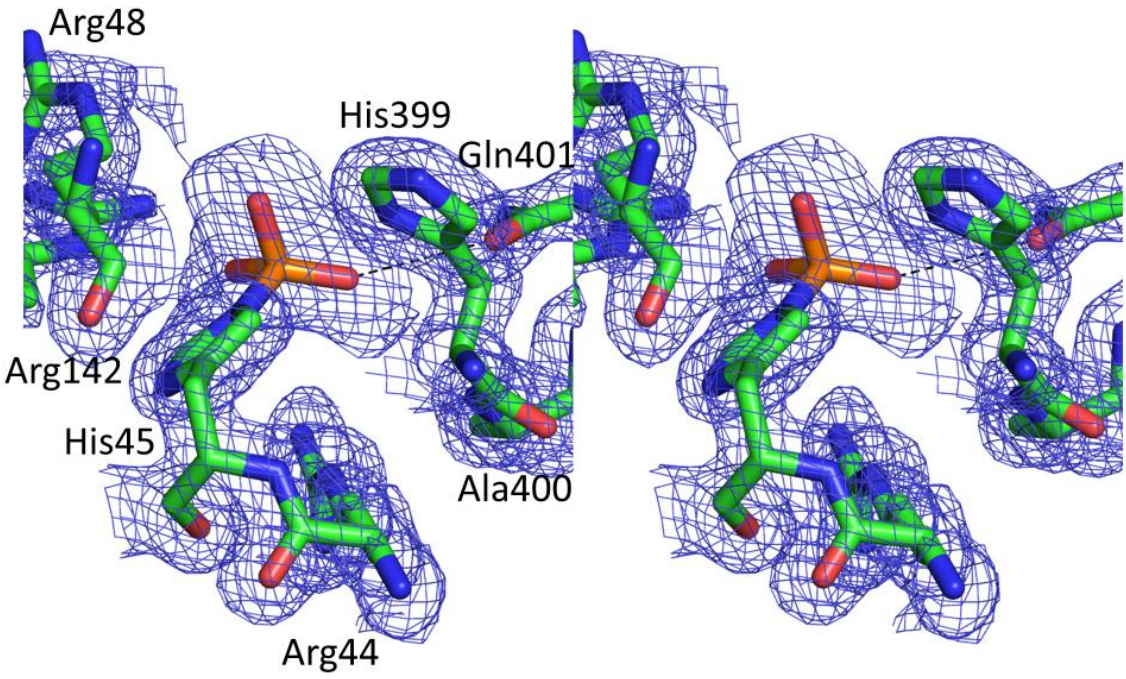

Figure 4.13 Double difference electron density map of the active site of the Bl phytase focused on the continuous bridge of density between the phosphohistidine and Gln 401.
2mFo-DFc difference map contoured at 1.0 σ displayed as blue hatching. Residues of the active site shown as sticks and labelled. A hydrogen bond between an oxygen atom of the phosphohistidine intermediate and Gln401 is indicated by a black dashed line. Absence of red and green densities indicates perfect overlap between the calculated model and the observed data in this snapshot.

Double difference density maps are one of the three types of Fourier maps, which are *calculated, observed* and *difference* maps. The difference maps display the difference between in the spatial distribution of the electron density explained by the molecular model (calculated) and the measured electron density (observed), to visualise the quality of the model and the collected crystallographic data. Here, errors such as positional error and occupational error can become obvious, where atoms can seemingly be wrongly positioned or created within the model. A continuous blue electron density map in the difference map indicates a perfect alignment between the model and the observed densities.

Figure 4.13 shows a stereo view of the double difference electron density map of the intermediate enzyme conformation. Interestingly, a bridge of continuous density can be seen joining the phosphohistidine and Gln 401. This electron density is unexplained, however a few reasons can be speculated. It is possible that the bridge reflects the

conformation of a more advanced stage in the catalytic cycle; a moiety bound between the phosphohistidine and Gln 401, such as a metal ion or (more likely) a water molecule.

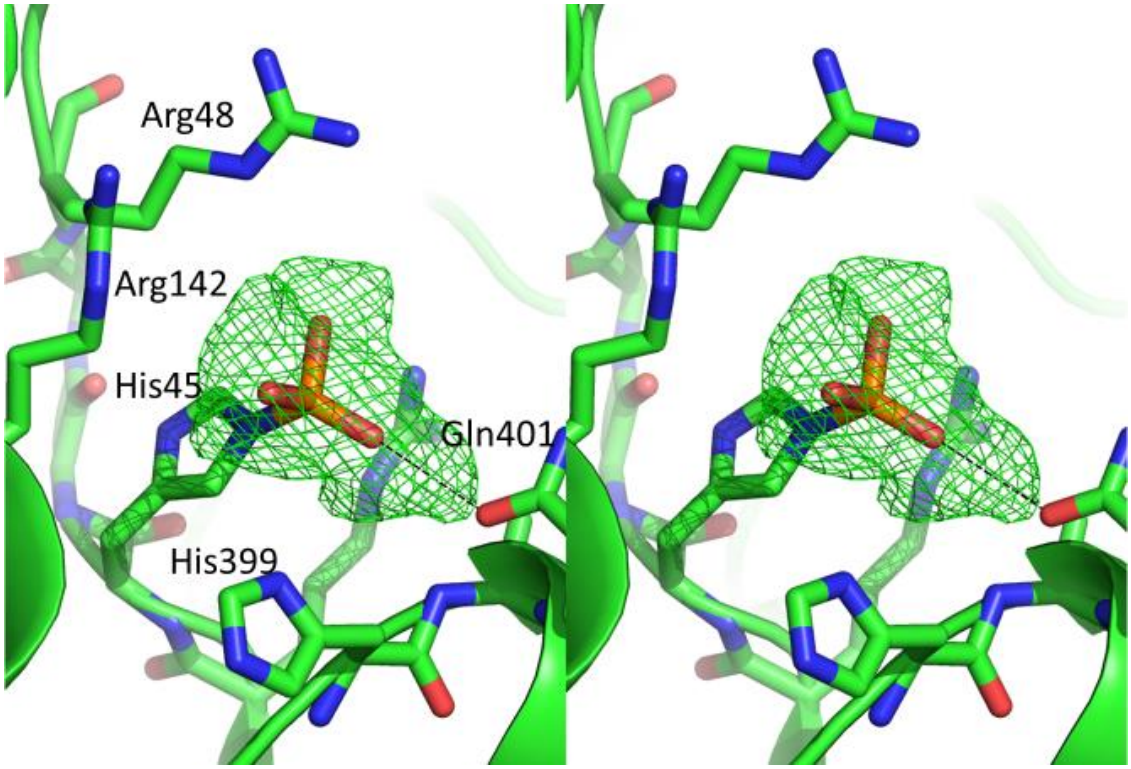

Figure 4.14 Stereo view of Fo-Fc omit map calculated in the vicinity of residue His399 of subunit B in the crystallographic asymmetric unit of the E401Q Bl phytase.
Green hatching shows the mFo-DFc omit map contoured at 3σ. Selected active site residues are shown in stick format. A weak hydrogen bond between the presumed phosphointermediate oxygen atom and Gln401 is indicated by a dashed black line.

Figure 4.14 shows the F_o-F_c omit map of the phosphohistidine at the active site of the mutant enzyme. Omit maps are maps generated after the first stages of refinement, where the newest iteration of the model excludes atoms that were removed from the initial model. While the modelled phospho group fits fairly well into the density adjoining His45, it is apparent that there is a bridge of density connecting the phospho group and Gln401. Further mutagenesis experiments should be undertaken to elucidate the nature of this density. For now, as mentioned above, it can be speculated to originate from additional water molecules or from metal ions. Furthermore, these molecules may be only present in a fraction of the molecules within the crystal, adding more complexity to this puzzle.

4.3.12 Conformational changes in phosphatases and phytases

The particular conformational changes of the active site during substrate catalysis in the Bl phytase do not appear to be prevalent in other phytases. The structure of the related Minpp from *Bacteroides thetaiotaomicron* (Bt phytase) was previously obtained by Arthur Li (UEA, Dr Hemmings Lab) in the product bound and *holo* conformations. After conducting DynDom analysis on these two conformers Figure 4.15, it becomes apparent that they undergo only a small domain motion at rotation angle of only 2.3 °, negligible translation of 0.2 Å and closure of 62.1 %.

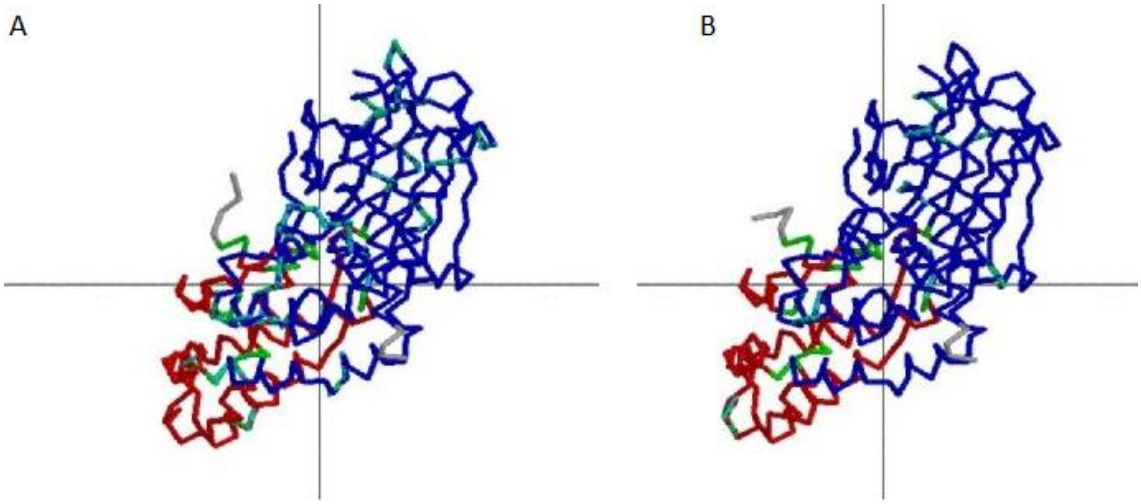

Figure 4.15 Protein domain motion analysis of the product bound and *holo* conformations of a Bt phytase.
A: product bound form; B: *holo* form. Blue: the fixed domain; red: the moving domain; green: hinge residues. The grey lines cross at the centre of rotation. Analysis was conducted using DynDom software.

Lim et al. (Lim *et al.*, 2000) solved the structure of an *E.coli* HAP phytase, which uses aspartate D304 as its proton donor. In the *apo* enzyme, a glutamine E219 interacts with D304 through hydrogen bonding via a water molecule. Upon substrate binding in the catalytically inactive mutant, E219's side chain is repelled away by the negative charges on the phosphate.

Lee et al. (Lee *et al.*, 2003) solved the structure of the *E.coli* glucose-1-phosphatase, an enzyme with a significant similarity to the *E.coli* phytase and with high specificity for phytate. This enzyme belongs to the group of histidine acid phosphatases and therefore

contains the conserved RH(G/N)xRxP motif. It was shown to exhibit no conformational change related to substrate binding in the active site pockets.
Chu et al. (Chu *et al.*, 2004) solved the structure of a cysteine phosphatase, which uses aspartate D212 as the proton donor. It was shown that upon inhibitor ligand binding, the side chain of D212 moves into position as facilitated by the histidine H213.

4.3.13 Conformational changes coupled to the mechanisms of ligand binding

The occurrence of an open and close lid motion accompanying catalysis has been well documented in many enzymes and forms the basis of the theory of induced fit (Koshland, 1963; reviewed in Gutteridge and Thornton, 2004). This theory builds upon Fisher's key and lock theory, which assumes a rigid enzyme form, whose conformation reflects the substrate's shape perfectly at all times, therefore always occurring in the active form. In the induced fit model, the ligand weakly binds to the active site, which triggers a conformational change that creates a stronger bond between the ligand and the active site, thus activating the enzyme. The theory behind it takes into account the flexibility of the enzyme which explains regulation and specificity of catalysis. In particular, its basis is that the alignment of the catalytic and binding residues has to be optimised for the transition state – and the binding of the substrate supplies the energy needed for the enzyme to attain the necessary conformation (Koshland, 1963, 1995). A related theory describes the conformational selection model, whereby the active and inactive enzyme forms exist in solution in equilibrium, with the inactive form being prevalent. The ligand will selectively bind to the active form, shifting the equilibrium towards the active conformation.

Two main types of conformational changes are distinguished. These two types of motion may exist to support substrate binding and catalysis, orientate the catalytic groups, facilitate access of water molecules to the active site and immobilise the intermediates. One of the conformational changes is domain motion, which occurs when two rigid domains move relative to each other, with the motion focused on a flexible hinge joining the two domains. Loop motion occurs with flexible loops on the surface of the protein

shifting between different conformations. Additionally, certain enzymes display side chain rotation that shifts the functional atoms of the residue, and secondary structure changes (Gutteridge and Thornton, 2004).

Dihydrofolate reductase (DHFR) is an example of an enzyme displaying a large scale domain motion during substrate catalysis, that is thoroughly described in literature as a model for domain motions. The enzyme assumes an open conformation in the *apo* form and upon substrate binding, its two domains rotate towards each other by about 1 Å. The degree of the motion is more pronounced between the *apo* and substrate bound conformation, than between the substrate and product bound conformations. It was observed that the product bound conformation shifts closer to the form of the *apo* enzyme (Sawaya and Kraut, 1997; Hammes, 2002; Gutteridge and Thornton, 2004). Hammes *et al.* (Hammes, Chang and Oas, 2009) conducted further research into the conformational changes behind the ligand binding mechanism of DHFR. Using data from dynamic NMR experiments and from detailed kinetic studies, they employed a flux based approach to determine the mechanisms of conformational changes coupled to substrate binding. Their studies revealed two different strategies that occur and overlap depending on the ligand concentration in solution. It was found that at low ligand concentrations the prevailing mechanism followed the conformational selection model, and switches to the induced fit model at high ligand concentrations. At majority of conditions both mechanisms take place and this occurrence likely extends to all enzymes (Hammes, Chang and Oas, 2009). Furthermore, using DHFR as an example, NMR experiments and computer simulations revealed that enzymes cycle through a variety of different conformations in solution. Among these, only a small percentage of occurrences tend to form suitable conformations for substrate binding and catalysis (Agarwal *et al.*, 2016). These reasons may explain the presence of two different subunits in the asymmetrical cell of the protein crystals, one showing an intermediate-bound conformation and the other showing the product bound to the active site.

4.3.14 Conclusions and future plans

Successful substitution mutagenesis of the putative proton donor glutamate to glutamine of the *B. longum* phytase lead to obtaining the crystal structure of two different subunits, one of the intermediate state and one of the phosphate-bound state. The structure was refined to 1.7 A ˚ resolution, with R_{work} and R_{free} values of 14.7 % and 19.4 %, respectively. Putting the work in context of the work performed by other research group members (Li and Acquistapace, unpublished) allowed us to piece together the step-by-step mechanism of action of the *B.longum* MINPP. For further confirmation of the conformations utilised during the catalysis, it would be beneficial to conduct a structural NMR study, which along with crystallographic and computational techniques could validate the proposed mechanism of action (Agarwal *et al.*, 2016).

In a similar experiment, the Sts-2, a member of the phosphatase superfamily of enzymes, was crystallised in the intermediate and product-bound conformations. As in HAP phytases, its active site nucleophilic histidine forms a phosphohistidine intermediate during catalysis. The solved structure of this state allowed to gain insight into the conserved basic residues involved in stabilisation of the intermediate. In the product-bound conformation, vanadium oxide was used in place of phosphate. This structure provided clues into the possible role of Glu476 in activating a uniquely positioned water molecule, crucial for catalysis (Chen *et al.*, 2009).

The structure of an active site mutant of the *B. longum* phytase, together with structures of the wild type enzyme in apo-form and in complex with a non-hydrolyzable substrate analogue, allowed me to determine the conformational changes associated with substrate binding and catalysis. This revealed the ~10 ˚ rotation of the alpha domain between the formation of the phosphohistidine intermediate and the release of the free inorganic phosphate. These changes lead to open and closed conformation depending on the stage of the catalytic cycle, presumably assisting the binding of substrate and intermediate and the release of product.

In the next stages of the project, a mutagenesis experiment could be carried out to substitute arginines 44, 48 and 142 with alanine residues. Enzymatic and X-ray structural

characterization of such mutants would give a fuller elucidation the roles of the arginines in substrate binding and catalysis. Alternatively, wild-type enzyme could be crystallised in solution with tungstate, vanadium or molybdate ions as a substitute for phosphate, which has proven to be a successful way to study structure of phytases and related enzymes in the past (Lindqvist, Schneider and Vihko, 1994; Ishikawa *et al.*, 2000; Davies *et al.*, 2002; Chen *et al.*, 2009).

Further analysis of the hydrogen bond interactions in the active site of the Bl phytase, in particular of the *apo* and *holo* forms could elucidate the potential relationship between the active site interactions and the overall enzyme conformation.
It would be interesting to obtain crystal structures of other related MINPP phytases in various conformations and to conduct the domain motion analysis on them. Primarily, further investigation of the residues involved in Bl and Bt phytase hinge motions could potentially reveal similarities and identify conserved residues involved in domain motions.

5 Binding studies of an HAE phytase

5.1 Introduction

5.1.1 Techniques for experimental determination of binding characteristics

The high catalytic activity of phytases towards IP_6, and the abundance of water as phosphate acceptor has confounded many attempts to solve the structures of substrate-bound phytases by X-ray crystallography. Consequently, it is common to use non-hydrolysable substrate analogs such as inositol hexasulfate (IS_6) to explore the catalytic mechanism of phytases. An alternative approach, as revealed in Chapter 4, is to inactivate the enzyme by site-directed mutagenesis, such that the *bona fide* substrate is not turned over. To check whether the catalytically modified enzyme has retained proper conformation of the active site, its ligand-binding properties, and to gather further evidence of its negligible activity, I investigated the ability of *bona fide* substrates (IP_6, IP_5) to bind to the enzyme. Several techniques are appropriate for experimental determination of the binding constants of ligands and native substrates to enzymes.

One such technique is the radioimmunoassay (RIA), allowing to one to study the concentrations of antigens, hormones and drugs in body fluids. It is a highly sensitive technique that uses gamma-radiating isotopes, such as tyrosine-bound iodine. During the experiment, a known amount of the radioactive antigen is mixed with its antibody, followed by unlabelled antigen of the same type. The unlabelled antigen competes for the binding site. Next, the radioactive complex gets separated from the free radioactive antigen and the ratios of the two are measured using the gamma counter. By comparison to a reference amount assayed at the same time, it becomes possible to quantify the molecule in question with high sensitivity (Goldsmith, 1975). A disadvantage of this technique is the need for specialist training and availability of specific equipment and materials.

A closely related technique is the enzyme-linked immunosorbent assay (ELISA), whereby the antigen is bound to a surface and detected by an antibody. Next, an antibody is added

that is specific to the first one. It carries an enzyme that triggers a colourimetric/fluorescent change upon reaction with substrate. This change is detected by spectrophotometry and provides a measure of the amount of the specific antigen in the solution and follow the antibody-antigen interactions (György *et al.*, 2013). The advantage of ELISA is that it removes the necessity of performing radiolabelling and undergoing specific training and safety regimens, and allows for use of simpler equipment.

A method allowing for a more detailed assessment of protein-ligand interactions is surface plasmon resonance (SPR). It allows the user to analyse structural changes as well as kinetic parameters of protein-ligand complexes at great sensitivity. During the procedure, one of the species is immobilised on a thin layer of gold on the surface of a chip and exposed to a flow of an analyte containing the other species. During the procedure, a polarized light beam irradiates the chip from below and is reflected onto a detector by total internal reflection. The incident light interacts with free electrons on the surface of the metal and excites them, in a manner sensitive to the bound material. This phenomenon is called the surface plasmon resonance. This light will become absorbed, causing a localised drop in intensity as seen by the detector. The value of the intensity shift is directly proportional to the mass of the material bound on the surface.

SPR is a highly sensitive technique yielding a thorough characterisation of the kinetic parameters. Unlike RIA and ELISA, it allows to use unlabelled and unmodified ligands in low quantities. However, the process of immobilisation may interfere with the binding reaction and the fact that the reaction happens on a surface may artificially elevate the binding affinities (Lin *et al.*, 2011; György *et al.*, 2013).

Isothermal titration calorimetry is a non-destructive biophysical technique widely used for single and multiple active binding sites. It is designed to quantify the thermodynamic parameters through studying the strength of formation and dissociation of protein-ligand complexes with great sensitivity. ITC is one of the few techniques which allow the user to characterise several thermodynamic properties directly, unlike the techniques which make use of the spectral differences. Instead, it relies on the measurement of the reaction heat. In particular, the method compares the amount of energy needed to keep a constant temperature between a reference cell and a sample cell containing the experimental

solution. The heat of reaction is directly proportional to the binding that occurs between the molecules in the sample cell.

ITC is a relatively straight-forward and cheap technique, and can be used without any modification or immobilisation of its constituent species. Compared to SPR however, the method requires a higher amount of material and requires establishment of very specific experimental environments (György *et al.*, 2013; Falconer, 2016; Huang and Lau, 2016).

Circular dichroism (CD) is a technique allowing to observe protein folding and unfolding events and to study the effects of binding parameters (e.g. solute concentrations, presence of ions, protein concentration) on the protein's conformational change. It relies on the phenomenon of the same name, whereby circularly polarized light absorbs differently into two forms of chiral species. This is usually conferred by the difference in extinction coefficients of two enantiomers. Performing CD in the UV range allows to examine the proportions of the secondary structures in protein molecules as well as DNA. By comparing the structure spectra of the protein before and after binding, one can obtain detailed information on the conformation of the target protein and to gain insight into the binding mechanism. Furthermore, metal ions show differences in the visible range CD upon binding to proteins, allowing this technique to be used in the study of metalloproteins (Lin *et al.*, 2011; György *et al.*, 2013).

Analytical ultracentrifugation (AU) is a versatile technique allowing to thermodynamically characterise protein complexes in solution, without the need for modification with probes or interaction with extrinsic entities. The technique measures the rate of sedimentation of protein complexes in real-time during an ultracentrifugal run (100,000x*g*) to derive sedimentation coefficients. These in turn allow one to determine molar mass and binding constants and affinity between ligands and proteins (Lebowitz, Lewis and Schuck, 2002). This classical technique played a key role in the development of modern biochemistry and molecular biology, leading to great advances in protein science (Balbo and Schuck, 2005). However, the limitation of the method is the difficulty in sensing the small differences in molecular weight changes upon binding of small ligands to proteins (Arkin and Lear, 2001).

5.1.2 Fluorescence polarisation and anisotropy

Fluorescence polarisation measurements allow one to analyse protein interactions in solution in a simple and straight-forward manner. The molecules under investigation may have fluorophores attached or remain unmodified, in which case the technique can make use of inner fluorophores such as tryptophan, tyrosine, NADH or FAD. Additionally, fluorescent probes bound to target molecules will display fluorescence.

If the molecule is completely immobile and exposed to a polarised beam of light at the excitation wavelength, the emitted light will be nearly 100% be polarised too. However, even a fixed and non-rotating fluorophore will exhibit a small degree of depolarisation due to a difference between the excitation dipole and the emission dipole of the molecule. As it is, the fluorescent polarisation technique relies on the fact that large molecules and complexes will display some degree of movement and rotation in solution, while smaller molecules will move and rotate even more rapidly. During the lifetime of the excited state (10 nanoseconds), the molecule will exhibit rotational diffusion proportional in rate and extent to its size, shape and viscosity of the solution.

In contrast, the process of light absorption in a chromophore takes only around 1 femtosecond, making fluorescence measurements the only possible technique to use depolarisation as a measure of molecule size. Hence, the more motile and diffused the molecule is in solution, the less uniformly polarised light will be emitted. This feature allows to follow the binding behaviours of fluorescent molecules and competitor ligands.

During the experiment, the sample is irradiated with plane-polarised light at the excitation wavelength. Next, the emission light is measured by recording the intensities in the polarization planes parallel and perpendicular to the excitation light. The proportion of the intensities of the parallel and perpendicular constituents of the emitted light is the fluorescence polarisation. It is calculated from the following equation:

$$P = \frac{I \parallel - I \perp}{I \parallel + I \perp}$$

where P is the level of polarisation, expressed in polarisation units; I∥ is intensity of polarised light parallel to the excitation light and I⊥ is the intensity in the perpendicular

direction. However, this technique does not take into account the second dimension parallel to the original plane of the polarized light.

Fluorescence anisotropy is an expression of the same phenomenon as fluorescence polarisation. However, by including the second plane perpendicular to the original excitation light, it takes into account the contribution of all degrees of rotational freedom. This ensures a more accurate representation of the physical phenomena in a three dimensional space. It can be represented by slightly modifying the polarisation formula to represent the total intensity of an emission excited by parallel polarised light as follows:

$$P = \frac{I \parallel - I \perp}{I \parallel + 2I \perp}$$

Fluorescence polarisation and anisotropy is an optimal technique for investigating due to the diversity, readily available commercial probes and instruments equipped with polarisers. The method is simpler than several other techniques by allowing the use of a homogenous assay mixture, as opposed to the need to separate the free and bound ligands. Furthermore, the assay is made safer by abolishing the need to use radioisotopes. Lastly, the speed and simplicity of the technique allows the user to create a high-throughput method with highly reproducible data (Lakowicz, 2006; Mocz, 2006; Jameson, 2011; György *et al.*, 2013).

Due to its suitability, I conducted binding experiments using fluorescence anisotropy. The fluorescent probe used was 2-FAM-IP_5, synthesised from 1,3,4,5,6-*myo*-inositol pentakisphosphate and 5-carboxyfluorescein, shown in the diagram below.

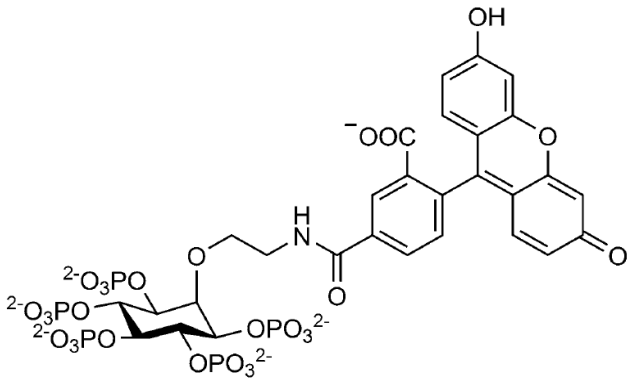

Figure 5.1 Structure of 2-FAM-IP$_5$ fluorescent probe used in displacement assays. Synthesised from a 1,3,4,5,6-*myo*-inositol pentakisphosphate constituent (left) and a 5-carboxyfluorescein constituent (right). The fluorophore is attached to the axial oxygen on carbon on position 2 on the inositol ring (image from Riley, Windhorst, Lin, & Potter, 2014).

2-FAM-IP$_5$ comprises of the fluorophore attached axially to carbon 2 of the inositol ring, with phosphates on the remaining five positions. This makes it a suitable probe to use with phytases, as usually phytase enzymes are unable to remove the axial phosphate (Wyss *et al.*, 1999; Adeola and Cowieson, 2011). This leaves the remaining five phosphates on the probe to be available for co-ordination by active site residues that would ordinarily co-ordinate the IP$_6$ substrate.

2-FAM-IP$_5$ was synthesized by the group of Professor Barry Potter (University of Bath). It was designed for studying cellular internalisation of inositol phosphates into animal cells, as an alternative to radiolabelled IP$_5$ and metal-dye detection HPLC. The fluorescent-labelled inositol phosphate allowed for studying true cellular internalisation (as opposed to cell-surface binding) in real time using confocal microscopy as well as immunofluorescence. The excitation wavelength was 490 nm and emission was 535 nm (Riley *et al.*, 2014).

More recently, Watson et al. (Watson *et al.*, 2016) used 2-FAM-IP$_5$ to elucidate binding of inositol phosphates to an allosteric site of the HDAC3:SMRT complex. It is a large transcriptional repression complex, comprising histone deacetylases (HDAC) and silencing mediator for retinoid and thyroid receptors (SMRT). It was found that the complex becomes activated upon binding to inositol phosphate analogues derivatised on carbons 2 and 3, therefore the 2-FAM-IP$_5$ was deemed a suitable fluorescent probe to study the

molecular details of substrate binding. Binding was investigated using fluorescence anisotropy (Watson *et al.*, 2016). The successful use of 2-FAM-IP_5 as a ligand binding probe in the fluorescence anisotropy experiment is an evidence for the validity of the 2-FAM-IP_5 probe in enzymatic assays using fluorescence anisotropy.

5.1.3 Mutagenesis of the active site Bl mutant E401Q phytase

The *Bifidobacterium longum* subsp*. infantis ATCC 15697* phytase (Bl) was mutated to replace the active site glutamate (residue 401) with a glutamine residue. The goal was to create an inert enzyme to study the binding of substrates without their turnover. Glutamine was chosen as replacement for glutamate, as changing the hydroxyl to an amino group result in a closely resembling residue of the same size. Such a change was expected to result in a decreased substrate turnover while the enzyme conformation would remain constant. The catalytic mechanism of the histidine phosphatase superfamily is shown in Figure 1.5.

HAP phytase belong to the histidine phosphatase superfamily. HAP phytases can be divided into the HD phytases and HAE phytases, named after the active site residues taking part in the catalytic mechanism. During substrate catalysis, the active site histidine conducts a nucleophilic attack on the phospho group of the substrate (e.g. IP_6), forming a phosphohistidine residue. Subsequently, the negatively charged proton donor (suspected glutamic acid residue in the *Bl* phytase and other HAE phytases, and aspartic acid residue in HD phytases) attacks a water molecule. The water molecule in turn attacks the phospho group on the phosphohistidine intermediate, yielding free phosphate (Ostanin *et al.*, 1992; Ostanin and Van Etten, 1993; Rigden, 2008).

A B

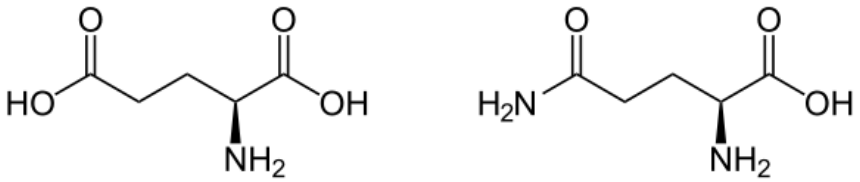

Figure 5.2 Structures of amino acids A: glutamic acid; B: glutamine.
In biological conditions, glutamic acid becomes deprotonated and negatively charged, allowing it to conduct an attack on a water hydrogen. Glutamine is a charge neutral molecule which makes it unable to conduct the attack.

As shown in Figure 5.2 above, glutamic acid contains a carboxyl that does not form a peptide bond. In neutral and alkaline environments the carboxyl will lose a proton to form the negatively charged anion glutamate. In the HAE phytases, the deprotonated proton donor will be able to attack the hydrogen in the water molecule and the activated water molecule will subsequently attack the phosphate on the phosphohistidine intermediate. On the other hand, glutamine contains a side chain amide in place of glutamate's hydroxyl. This renders it a charge neutral, polar amino acid which makes it unable to conduct the attack on the water molecules, thus in theory abolishing the glutamine mutant's ability to catalyse the reaction with IP_6.

5.1.4 Summary and aims

So far fluorescein-modified inositol phosphates have found use as probes of substrate binding to the IP3 receptors (Ding et al., 2010), as probes of inositol phosphate uptake into animal cells (Riley et al., 2014) and as ligands reporting protein : protein interaction (Watson et al., 2016). The use of such molecules has not been considered for enzymes of inositol phosphate metabolism. Here, an assay has been developed that allows simple analysis of ligand/substrate binding to inositol polyphosphate phosphatases. This assay is applicable to the HAP phytases and is likely to be relevant to the cysteine and purple acid phosphatase phytases as well. It may perhaps be unsuitable for assaying members of the beta barrel phytase family, by virtue of the ability of these enzymes to cleave the phosphate on the axial 2-position. In general, the high catalytic activity of phytases and their simple transfer of phosphate to water (solvent) makes it likely that inactivation of the enzyme by active site mutagenesis will be necessary, as demonstrated here for use of the probe with HAP HAE phytases, for other classes of phosphatase. It is also possible to envisage the use of the probe with bi-substrate enzymes, such as inositol phosphate kinases (inositol phosphate : nucleotide phosphotransferases), which transfer phosphate between ATP and a free hydroxyl on an inositol phosphate substrate.

This chapter also reveals the usefulness as posited (Kolozsvari, Parisi and Saiardi, 2014) of DAPI as a real-time assay reagent for phytases. Since, only IP_5 and IP_6 show appreciable shift in the fluorescence of DAPI, this probe can be used for assays of enzymes converting IP_4 to IP_5 and IP_6 and for enzymes that dephosphorylate IP_5 or IP_6. The principal value of this approach is in its ability to offer real-time assay of phosphatase activity with a close to physiological substrate analog.

In summary, this chapter investigated the binding of substrates to the *Bl*Minpp E401Q mutant. By comparison to the wild-type enzyme, it was shown that IP_6 indeed binds to the mutant, and shows negligible turnover. This work validates the use of the E401Q active site mutant as a model for binding studies. Additionally, the mutant was used to study the binding of a range of IP_5 substrates of phytases. These results complement the product profiles obtained with HPLC, presented in Chapter 3, which show snapshots of the products present at different stages of inositol phosphate degradation.

Looking forward, the 2-FAM-IP_5 assay needs to be tested further with a larger selection of phytases at a wider range of pH. In the future of the project, rhodamine could be used as the IP_5-conjugated probe for displacement assays at pH 3.5. Rhodamine is a pH-insensitive versatile fluorescent probe with excitation wavelength of 552 nm and emission of 574 nm. Its use would enable similar experiments to be conducted at pH encountered in the gastro-intestinal tract to gain an insight into the substrate-binding properties of the mutant and by inference feed phytases at lower pH (Sridharan *et al.*, 2014). Rhodamine was not available in the lab during my experiment, however it would be a useful tool for further characterisation of the inert enzyme in the future.

5.2 Materials and Methods

Protein purification was conducted as described in Chapter 2. Images of protein purification including chromatograms and SDS-PAGE pictures are included in Appendix 3.

5.2.1 Fluorescent enzyme assay using DAPI probe

A DAPI-based fluorescent assay was constructed to monitor phytase activity. Saiardi and co-workers noted that DAPI undergoes a bathochromic shift when bound to polyanions (Kolozsvari et al., 2014). They were able to monitor IP_4 conversion to IP_6 catalyzed by inositol phosphate multikinase by virtue of the observation that IP_6 and less so IP_5, but not IP_4, induces a shift of DAPI fluorescence to longer wavelengths. They posited that DAPI could find use in phytase assays.

Using 100 µM DAPI and 10 µM IP_6 in 0.1 M glycine-HCl pH 3.5 buffer, four replicate 20 µl samples were dispensed into a 384-well black fluorescent (Corning Product #3575) assay plate and placed in a HIDEX Sense (Tuurku, Finland) plate reader. Using the native Hidex software, continuous 405/560nm fluorescence measurements were taken over a period of 8 minutes to verify the stability of the fluorescence signal. Subsequently, 1 µl of 10

µg/ml protein (wild-type or mutant) was added and fluorescence of the DAPI/IP_6 complex measured for 5 minutes. Rates of enzyme catalyzed reaction were determined from slopes of the initial rate curves.

5.2.2 Fluorescent polarisation assay using 2-FAM-IP_5 probe

Modified inositol phosphates derivatised with fluorescent groups, commonly fluorescein or BODIPY, have been used to probe binding of inositol phosphates to proteins and enzymes including the IP_3 receptor (Ding *et al.*, 2010). Recently, Ins(1,3,4,5,6)P_5-modifed with a fluorescein group attached by a short spacer to carbon 2 (of the inositol ring) [2-FAM-IP_5] was shown to be taken up by cultured animal cells (Riley *et al.*, 2014). The same compound was shown to bind to an inositol phosphate binding site of histone deacetylase (Watson *et al.*, 2016). Here, I have used the same compound to probe binding of inositol phosphate (substrates) to catalytically silenced *Bl*Minpp. For this purpose, 2µl of 100 nM 2-FAM-IP_5 (provided by Barry Potter, University of Bath) was added to 200 µl of 500 nM purified E401Q protein diluted in 20 mM HEPES pH 7.3, 1 mM $MgCl_2$. Four replicate 20 µl samples were dispensed into a 384-well black fluorescent assay plate. Using a CLARIOstar (BMG LABTECH, Germany) plate reader fitted with a fluorescein polarization filter set (excitation 485nm, 505nm dichroic mirror, emission 515nm), gain adjustment on the horizontal and perpendicular measurement were set to give a polarization value of 35 mP for 2 nM 2FAM-IP_5 probe diluted in the buffer alone. After 30 minute incubation of probe with varying dilutions of protein in buffer, the polarization of the probe was measured. Data were exported with MARS Software (BMG) and fitted to a 4-parameter logistic.

5.3 Results and Discussion

5.3.1 Assay of activity of *Bl*Minpp E401Q

A simple colourimetric phosphate release assay was conducted over a 24 hr period with the E401Q mutant protein at a 1 mg/ml concentration with 10 mM IP_6. No phosphate detection occurred, suggesting the enzyme had no activity or was otherwise misfolded. No data is shown for this assay, however the fluorescent assays that follow in this chapter will provide evidence for the enzyme's negligible substrate turnover while still retaining enough conformation to bind substrates.

The lack of substrate turnover by the E401Q mutant suggests that the enzyme is either inactive or misfolded. To distinguish between these possibilities, an enzyme assay was constructed using DAPI (Kolozsvari, Parisi and Saiardi, 2014). To this end, residual IP_6 in solution is measured by its effect on the fluorescence of 4',6-diamidino-2-phenylindole (DAPI). DAPI is a fluorescent stain, originally used to visualise DNA due to its binding into the minor groove of AT-rich DNA sequences (Kapuscinski, 1995). In recent years DAPI was discovered to show a shift in fluoresce upon forming complexes with IP_6 and IP_5's, but not lower inositol phosphates (Kolozsvari, Parisi and Saiardi, 2014).

Here, the metabolism of IP_6 was followed by monitoring of the fluorescence of IP_6-DAPI complexes at 405/560nm in the presence of the E401Q mutant and the wild-type protein at pH 3.5 in 0.1M glycine-HCl buffer. The assay was conducted using protein concentration of 0.5 µg/ml, 10 µM IP_6 and 100 µM DAPI.

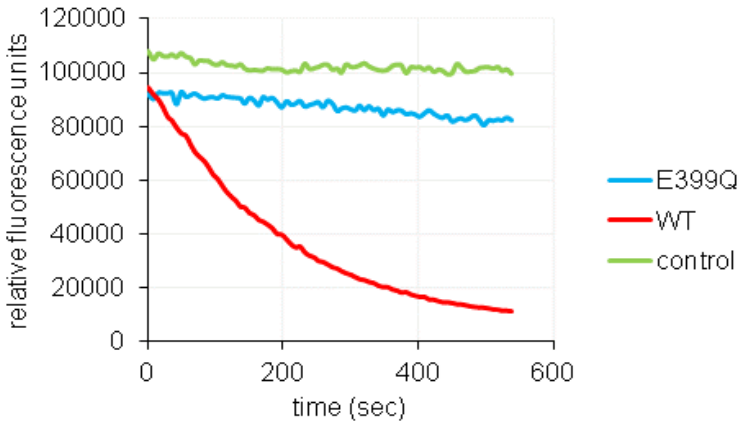

Figure 5.3 IP_6 consumption over time by E401Q mutant and wild-type *B.longum* phytases.
Kinetic fluorescence assay at 405/560nm using 100 µM DAPI fluorescent probe, 10 µM IP_6 and 0.5 µg/ml protein at pH 3.5. Representative single measurements shown.

The experiment was conducted using duplicate measurements for the mutant and wild-type proteins and a quadruplicate measurement for the no enzyme control. The negative control was used to monitor stability of fluorescence over time. Addition of the wild-type enzyme caused a reduction in signal, suggesting consumption of IP_6 and possibly of IP_5, as DAPI becomes fluorescent when forming complexes with both IP_6 and IP_5 (Kolozsvari, Parisi and Saiardi, 2014).

Consumption of IP_6 by the mutant is reflected by the difference in slope between the mutant trace and the control: 19.14 RFU/ sec (SD=4.32). An initial rate calculation for the wild-type enzyme showed a difference in slope of 265.92 (SD=79.56) between the enzyme and control. This experiment showed that the mutant displayed 7.2% of the rate of reaction of the wild-type enzyme. However, the actual values could differ greatly due to the high standard deviations of the results. To test whether the difference in reaction rates was significant, I used the statistical unpaired t test. The two-tailed P value equalled 0.0484, proving that the difference in rates between the two enzymes was statistically significant.

Kolozsvari et al. (Kolozsvari, Parisi and Saiardi, 2014) successfully employed the novel DAPI method to investigate the enzymatic activity of phytase extracted from wheat and to determine the amount of phytic acid in plant seeds. The unique properties of DAPI causing a fluorescent shift from 420 nm to 550 nm upon reaction with IP_6 and IP_5 were

proved to be a successful basis for a phytase assay an were utilised in this thesis to show that the E401Q active site mutant of the *Bl* phytase had negligible catalytic activity. It also helped prove that the glutamate to glutamine substitution mutation of the HAE phytase is a good model to study the binding affinities to the natural substrates IP_6 and IP_5.

5.3.2 Assays of binding of IP_5 and IP_6 to *Bl*Minpp E401Q

A preliminary experiment was set up to establish whether the E401Q mutant binds the 2-FAM-IP_5 probe, to establish the validity of the experiment. A range of nine protein concentrations was used, from 0.001 nM to 2000 nM, with three replicate measurements for each concentration. The experiment was conducted first using 0.1 M glycine-HCl buffer at pH 3.5, however I noted that 2-FAM-IP_5 lost its fluorescence at this pH, presumably due to protonation of its carboxyl functions.

The next experiment was carried out using the PK/10 buffer at pH 7.3. *Bl*Minpp remains active at this pH, as shown in Figure 2.2 in Chapter 2.

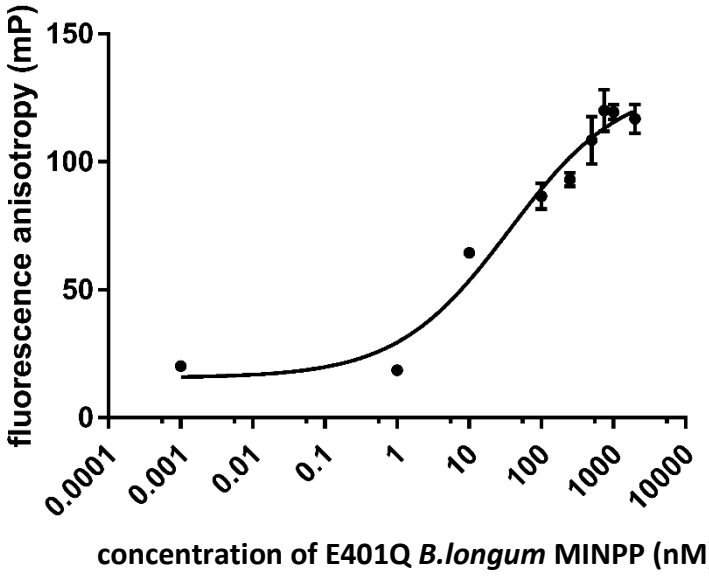

Figure 5.4 Binding curve of E401Q *B.longum* phytase to 2-FAM-IP_5 fluorescent probe using fluorescence anisotropy
The fluorescent polarisation was measured at excitation 485 nm and emission 515 nm using concentrations of 0-2000 nM of protein binding to the fluorescent 2-FAM-IP_5 probe. The error bars reflect the standard error of the mean.

The experiment at pH 7.3 showed progressive binding of 2FAM-IP_5 to increasing concentrations of protein. The results were fitted to a 4-parameter logistic regression fit using the GraphPad Prism software. The following formula was used for the 4-parameter fit:

$$y = \frac{Top - Bottom}{1 + (\frac{EC50}{x})^{slope}}$$

where top and bottom are the maximum and minimum values obtained. Despite several wide error bars, the data shows an acceptable fit (r^2 value = 0.9204). The half maximal effective concentration (EC_{50}) was 36.28 nM.

Once the experimental technique was validated by demonstration of a successful binding curve at pH 7.3, experiments were undertaken to test the ability of IP_6 to displace the fluorescent probe, and hence to measure how strongly the mutant enzyme binds IP_6. For this experiment, the protein concentration held constant at 2000 nM and probe concentration at 2 nM to approximately reflect the EC_{50} value from the binding curve. IP_6 concentrations were increased exponentially : 1 nM, 10 nM, 100 nM, 1 uM and 10 uM. Quadruplicate measurements were made.

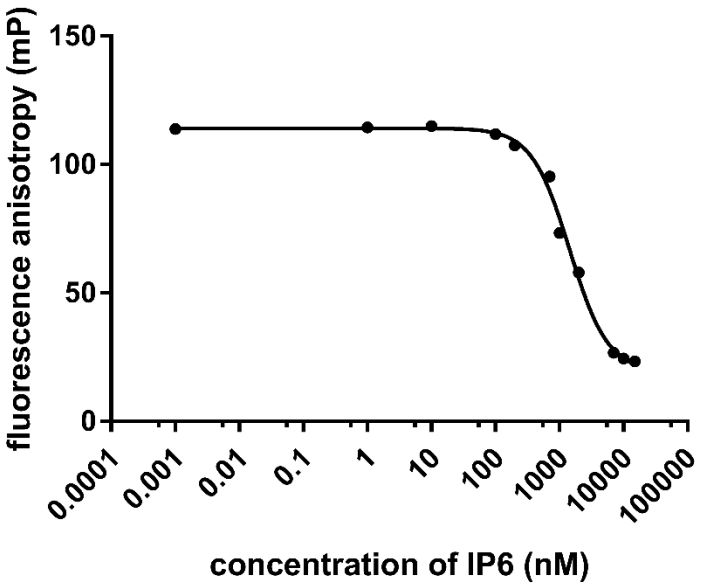

Figure 5.5 Displacement of 2-FAM-IP_5 from the E401Q *B. longum* mutant phytase by IP_6. The fluorescent polarisation was measured at excitation 485 nm and emission 515 nm using concentrations of 0-10000 nM of IP_6 and protein concentration of 2000 nm, binding to the fluorescent 2-FAM-IP_5 probe. Average values from quadruplicate measurements are shown. Standard error of the mean error bars are smaller than the symbols plotted.

The experiment showed good reproducibility between the quadruplicate measurements as several data points fall within the steepest part of the curve. The data conforms well to the 4-parameter logistic regression fit (r value = 0.9975). The mutant enzyme appears to bind IP_6, reflected by the curve fit, with a EC_{50} for displacement of 1491 nM.

Once the IP_6 displacement curve was established, an experiment was set up to investigate displacement by a range of potential IP_5 substrates. Here, protein was set at 1000 nM concentration with probe at 2 nM. The following compounds were tested: 1-OH-IP_5, 2-OH-IP_5, 3-OH-IP_5, 4-OH-IP_5, 5-OH-IP_5 and 6-OH-IP_5, all *myo*- stereoisomers, as well as IP_6 and *scyllo*-IP_5. The *myo*-IP_5's were obtained from Sichem (Germany) as K+ salts and the *scyllo*-isomer was obtained from Professor Barry Potter (University of Bath). There exists only one stereoisomer of *scyllo*-IP_5, as all the phosphates are equatorial. The figure below illustrates the difference between the *scyllo*- and *myo*- stereoisomers.

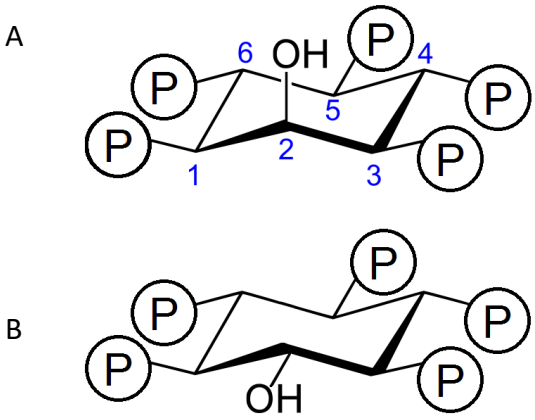

Figure 5.6 Structures of myo-IP_5 and scyllo-IP_5.
A: chair conformation of *myo*-inositol 1,3,4,5,6-pentakisphosphate. B: chair conformation of *scyllo*-inositol pentakisphosphate.

The experiment was conducted at pH 7.3 in 20 mM HEPES pH 7.3, 1 mM $MgCl_2$ and protein concentration at 2000 nM. A positive control was used to ascertain binding of the probe to the enzyme, where only enzyme, buffer and probe was used without competing ligand/substrate. Additionally, a control with probe and buffer only was used to calibrate the instrument. The figure below shows a box plot of the results.

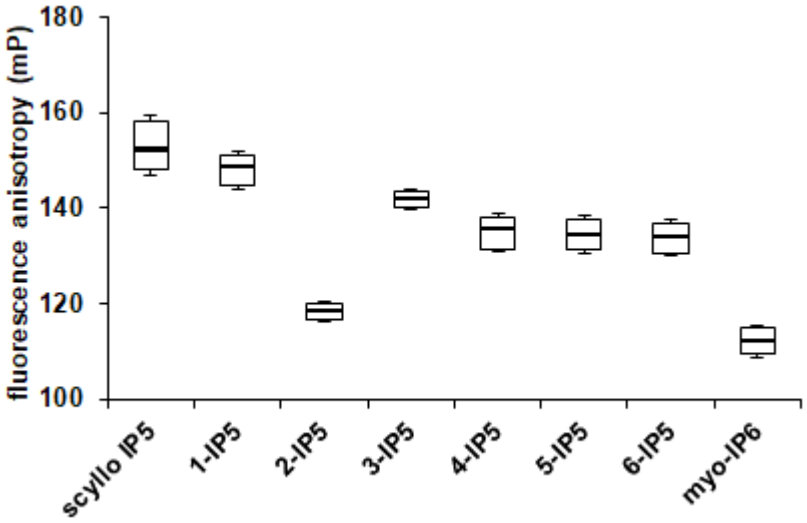

Figure 5.7 Displacement of 2-FAM-IP_5 from the *B. longum* Minpp E401Q mutant with IP_5 and IP_6 ligand/substrates.
Single concentrations of 1000 nM substrate and 2000 nM protein concentration were used in the presence of 2nM 2-FAM-IP_5. The experiment was conducted at pH 7.3. The boxes represent the range of the quadruplicate values. The horizontal lines represent the mean values and the error bars show standard error of the mean.

The displacement experiment shown in Figure 5.8 reveals differences in the strength of binding of different inositol phosphates to the *Bl*Minpp E401Q mutant. *Myo*-IP_6 substrate yielded the lowest value for polarization of the probe, reflecting the strongest binding to the enzyme 2-OH-IP_5 was the second strongest-binding substrate, with polarization similar to that obtained with IP_6. 4-OH-IP_5, 5-OH IP_5 and 6-OH-IP_5 were weaker displacers of probe, while 1-OH-IP_5 was the weakest binding of all the *myo*-IP_5 isomers. *Scyllo*-IP_5 was the weakest binding substrate. The experiment demonstrates how fluorescence polarization is an appropriate technique to report binding of different IP_5 substrates to inert phytase mutants.

Cho et al. (Cho *et al.*, 2006) studied the chicken MINPP phytase to investigate its usefulness as an alternative to the phytases in the animal feed industry. Assays of activity and structural studies revealed the *scyllo*-IP_6 to be a poor substrate for the chicken MINPP. Indeed, they found the MINPP to show the Km value for *scyllo*-IP_6 to be around 1740 µM, a 12-fold lower affinity that what was shown for *myo*-IP_6. These results are in agreement to the results presented above in terms of low affinity to *scyllo*-IP6 of the Minpp phytase. An explanation to this phenomenon could be that *scyllo*-IP_6 lacks the axially positioned phospho group present in the *myo*-IP_6, which prevents the ligand from effectively binding to the active site.

Before examination of the binding of IP_5 substrates in detail, the selection of substrates to investigate was limited to the most relevant ones. To date, there have been no 1-phytases described in the literature, therefore 1-OH-IP_5 was omitted from the experiment. The HPLC analysis of the product profiles of wild-type *Bl*Minpp enzyme (Chapter 3) showed a prominent peak of 1/3-OH-IP_5. Because no 1-phytases have been reported, it might be assumed that the peak is given rise to by 3-OH-IP_5, hence this particular IP_5 was chosen to be included in the test. The second most prominent IP5's were 4OH-IP_5 and 6-OH-IP_5. Both have been shown to be products of discrete phytases (Konietzny and Greiner, 2002). Without identification of enantiomeric products of Minpp action, we must assume that both are equally likely products of Minpp activity. Therefore both were tested for in this experiment. The third most prominent IP_5 present in BlMinpp products (Chapter 3) was 5-OH-IP_5, therefore it was tested as well.

The experiment was set up using final concentration of 2000 nM of the *Bl*Minpp E401Q mutant e, 2 nM 2-FAM-IP_5 fluorescent probe, and substrate concentrations of 1 nM, 10 nM, 100 nM, 200 nM, 500 nM, 1 µM, 2 µM, 5 µM and 10 µM in 20 mM HEPES pH 7.3, 1 mM $MgCl_2$. The assay mixtures were incubated for 30 min before measurement in the plate reader.

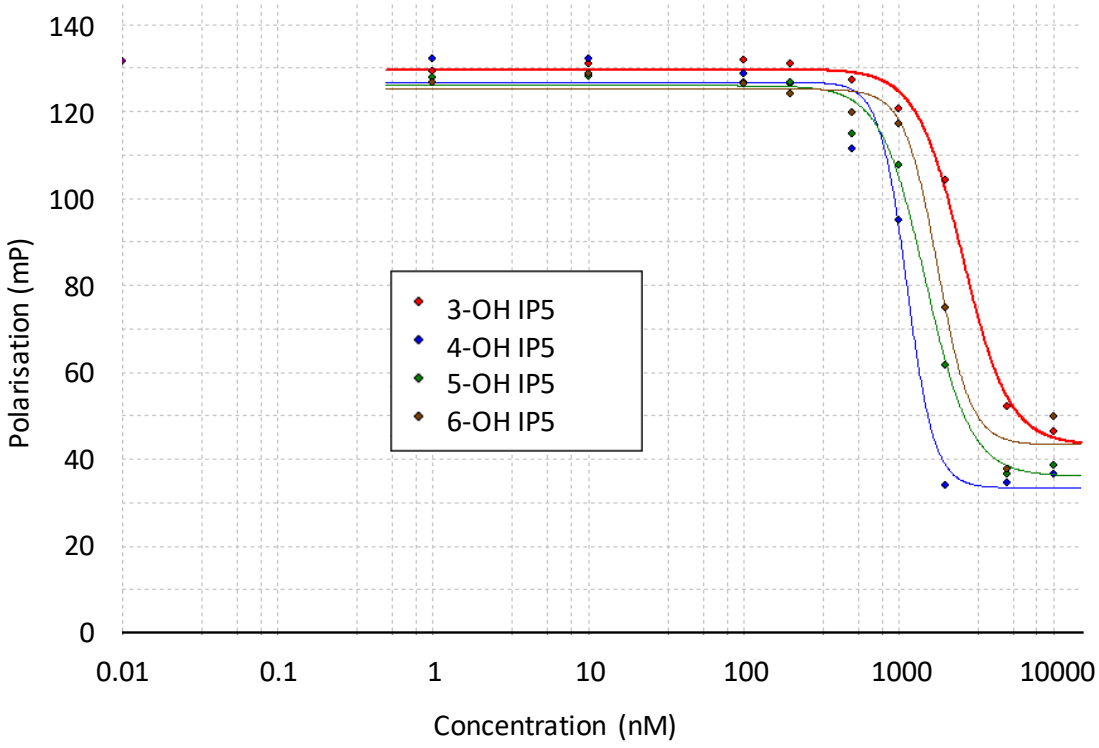

Figure 5.8 Displacement of 2-FAM-IP_5 from BlMinpp E401Q mutant by IP5.
The experiment was conducted at pH 7.3, with quadruplicate replicates.

During the experiment quadruplicate measurements were taken and for clarity only averages were plotted on the figure above. 4-OH-IP_5 showed strongest binding to the enzyme, with the lowest EC50 value of 1122.7 nM. The data shows a good approximation to the 4-parameter fit, with r value of 0.991188. 5-OH-IP_5 yielded an EC50 value of 1485 nM. 6-OH-IP_5 was the second-weakest ligand with the EC50 value of 1770 nM, while 3-OH-IP_5 was the weakest ligand with EC50 of 2591 nM. All r values were over 0.99.

While no studies have been found in the literature to date about displacement of specific lower inositol phosphates by HAP phytases, studies have been carried out into the

chelating capacities of different IPs to calcium and zinc. This is especially relevant in animal nutrition, where zinc and calcium supplements can be added to the feed or the elements could be present in the plant based animal feed already, as well as considerations for human nutrition. In one study (Simpson and Wise, 1990), inositol compounds (IP_3 – IP_6) were investigated for their solubility and binding affinities to zinc and calcium, minerals commonly chelated by IPs, which contributes to the antinutritive properties of IP_6 and related compounds. Zinc was found to be virtually insoluble at the concentrations of Zn and Ca designed to mimic those present in human nutrition. Less zinc was found to be bound to Ca-IP_6 complexes than to Ca-IP_5 complexes. Interestingly, in general the IP_3 and IP_4 were shown to be more easily hydrolysed by phytase when bound to a zinc or calcium ion than IP_5 and IP_6. Synergistic effects were observed, whereby if the two cations are present at the same time, the proportion of insoluble IP6 increases.

In another study (S. Yu *et al.*, 2012), the specific IP_5 positional isomers as well as a range of IP_{1-6} inositol phosphates were investigated for their effect on protein aggregation , pepsin activity and interactions with Fe^{3+}. Here, Fe^{3+} was found to bind mostly to IP_6, followed by IP_5(1,3,4,5,6), IP_5(1,2,3,4,5) and IP_5(1,2,4,5,6), which showed 66.4%, 65.7% and 58.4% of the affinity to IP6 respectively. IP_4(1,2,4,5) and IP_3(1,4,5) showed 24.1% and 16.2% of the affinity to IP6, respectively. IP_2(1,4) and IP_1(2) showed negligible binding to Fe^{3+}.

The results and the literature discussed in this chapter draw attention to the need for the phytases to conduct as thorough and swift hydrolysis of substrates as possible in the early stages of the digestive tract to obtain efficient release of phosphorus and minerals. They highlight the importance of considering the product profiles of degradation of phytate in more detail, i.e. defining the characteristics of the specific isomers, in order to maximise phytase efficiency in any given scenario.

6 Disulphide mutagenesis and characterisation of mutant Bl phytase

6.1 Introduction

Differential scanning calorimetry (DSC) was developed to address the need for an information-rich technique measuring the stability, folding and binding interactions of proteins. Increase in temperature lead to changes, or 'transitions' in the protein structure, leading to what can be referred to as 'thermal melting'. Most molecules of biological origin such as lipids and nucleic acids, in addition to proteins, succumb to these processes, which can be investigated using DSC (Johnson, 2013) .

The DSC instrument consists of two cells – a reference and a sample cell, as shown in Figure 6.1 below. The cells are filled with a buffer solution and a protein dissolved in the same buffer, respectively. In the conventional DSC mode, the instrument will slightly increase the temperature of the cells and measure the subtle difference in temperatures between the cells stemming from the differential heat absorptions. As the instrument raises the cell temperature incrementally, thermally induced processes will begin to take place in the sample cell, causing more heat to be absorbed initially (Johnson, 2013).

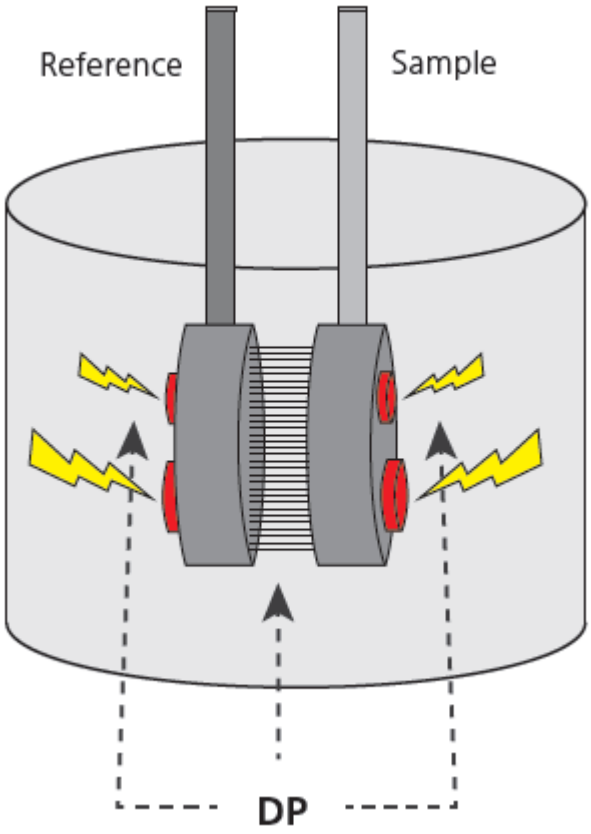

Figure 6.1 The thermal core of a DSC instrument.
DSC measures the differential power (DP) needed to maintain the sample and reference cells at the same temperature during the ramping of temperature that comprises the experiment (image adapted from Malvern manual).

Sensitive temperature sensors on the surface of the cells will reroute the electrical power to or from the sample cell, depending on the change in heat absorption. This additional thermal energy is directly proportional to the excess heat capacity of the thermally induced processes. This differential thermal energy is displayed as a thermogram as shown in Figure 6.8. Data can be transformed to take into account the baseline, or subtract the trace from a buffer/buffer run (where buffer is used in both cells as a preliminary measurement). The DSC technique is reliable for as long as the protein sample is of high purity, with negligible precipitate or unfolded protein molecules. While the DSC measures heat capacity changes with incrementally increasing temperature, isothermal titration calorimetry (ITC) is a related technique that measures interactions at a fixed temperature (Johnson, 2013).

6.1.1 Sources of heat capacity changes during a DSC experiment

Several processes contribute to the change in heat capacity seen during the incremental rise in temperature during a DSC experiment. For example, the 'hydrophobic effect' is a term used for the thermodynamic consequences of exposure of the intrinsic hydrophobic residues to the solvent environment in the denatured state of the protein. It is the major contributor to the changes in heat capacity seen during a DSC experiment (Spolar, Ha and Record, 1989).

Intramolecular vibrations are another source of heat capacity changes, although to a lesser extent than the hydrophobic effect. The protein's internal degrees of freedom are characterised by weak forces that are easily affected by unfolding. Their numbers increase as the unfolding progresses, leading to changes in heat capacity (Sturtevant, 1977).

Electrostatic charges are potentially another source of heat capacity changes. As charged residues create pairs of negative and positive charges, a negative change in heat capacity occurs. However, charged groups exhibit strong tendencies to maintain contact with the solvent environment throughout the majority of macromolecular processes, therefore the contribution of the electrostatic charges to heat capacity changes is small (Sturtevant, 1977).

In water and simple molecules in solution, the breaking of hydrogen bonds with increasing temperature is a major source of heat capacity. This occurs in proteins to a lesser extent, as proteins must be able to preserve maximal hydrogen bonding to be structurally and functionally sound (Sturtevant, 1977).

Furthermore, different residues contribute to the heat capacity changes to a variable extent depending on their structure. Aromatic groups of the amino acid residues were found to have some significant effects, while the hydroxyl, amine and amide groups were found to have minuscule contributions that largely cancel each other out (Ooi *et al.*, 1987). On the other hand, changes in the exposure of polar and uncharged residues were found to not affect the heat capacity at all (Spolar, Ha and Record, 1989).

6.1.2 Summary and aims

This chapter focused on thermostability of a *Bifidobacterium longum* phytase and its cysteine mutants, to confirm the presence of the disulphide bridges and elucidate their role in the structure and activity of the enzyme. I described the process of site-directed mutagenesis to substitute cysteine residues with alanine residues and the reasoning behind introducing the specific mutations. In particular, three mutants were created: one double mutant for each of the two disulphides (mutants D1 and D2) and one quadruple mutant for both disulphides (mutant D1D2).

I carried out thermostability measurements, where I assayed phytase activity after incubation at a range of temperatures. Despite some variance between the triplicate measurements as reflected by the size of the standard deviation error bars, the activity of the four Bl variants generally shows a downward trend with the increase in incubation temperature at the pH 3.5. At pH 5.5 the activity profiles reached a peak at 50-55 °C for the wild-type and the D2 mutant, while the D1 and D1D2 mutants peaked at 37 °C. Data for pH 7.4 shows large error bars, which would need to be addressed in the future. Here, the activity appears to peak at around 30-37 °C.

The double mutant D1D2 shows the lowest activity profile after incubation at a range of temperatures. Its protein expression yield was the lowest of the four Bl variants, which may be correlated with low overall stability. The disparity between the two single disulphide mutants may be related to each disulphide residing in different folds of the protein – disulphide D1 is located in the alpha domain, while disulphide D2 is located in the alpha/beta domain.

Differential scanning calorimetry (DSC) was conducted to examine the melting temperature (Tm) that reflects the thermally induced structural transitions of proteins in solution. It is a powerful technique, used in the industry to predict shelf lives of products, develop purification strategies and characterise and evaluate proteins, lipids and pharmaceuticals. Most of all, it enables the study of folding and unfolding without the need to label the proteins. Thus, this technique allows proteins to be examined in as close

to their natural state as possible, giving a reliable estimate of its temperature of unfolding (Morar-Mitrica, Nesta and Crotts, 2013).

Furthermore, molecular dynamics simulations were performed to elucidate the flexible regions of the protein as it unfolds with the increasing temperature, to complement the experimental data resulting from the DSC experiments.

6.2 Methods

6.2.1 Site-directed mutagenesis of cysteines

To introduce cysteine mutations to the *Bifidobacterium longum* phytase (Bl), mutagenesis was conducted using the Q5 Hot Start High-Fidelity DNA Polymerase (New England Biolabs) with primers designed according to the manufacturer's protocol. Q5 mutagenesis relies on linear amplification, therefore the specific Q5 primers were non-overlapping.

Primers for disulphide D1 were named D1C1 and D1C2 for cysteines C278 and C291 respectively. Primers for disulphide D2 were named D2C1 and D2C2 for C483 and C501. Below are the sequences for the primer sets, with the forward primer shown in yellow, reverse primer in blue and the mutation site shown in pink. PCR reactions performed with the first set of D2C2 primers shown below was unsuccessful as it repeatedly resulted in products with the wild-type sequence. The experimental conditions for the mutagenesis PCR are shown below.

5' - CATGGTACAAGCTGACCGAACTGAAAAGCTGCCTGGCCG - 3'

Primers were manufactured by Eurofins Genomics. Successful sets of primer sequences are shown below.

D1C1:

5' – cggcaccaagaaaggcggcaagaacgccgcgccaggtg – 3'

D1C2:

5’ - gtgccgatgcgtccaaagatcccgacgcagccggcgaagtct – 3’

D2C1:

5’ – caacgagaacgaggttccgttccgttccgaagccacgccggtc – 3’

D2C2:

5’ – catggtacaagctgaccgaactgaaaagcgccctggcc – 3’

	Volume per reaction (µl)
Q5® Hot Start High-Fidelity 2X Master Mix	12.5
Forward and reverse primer mix 10 µM	2.5
template (wild-type or mutant) Bl-pET28a 30 mg/µl	1
ddH_2O	9

The durations and temperatures for the mutagenesis PCR for each cysteine mutant are outlined in the table below.

		Temperature °C				
step	step duration	D1C1	D1C2	D2C1	D2C2	
initial denaturation	3 min	98				
denaturation	30 sec	98				x 25
annealing	1 min	67	60	58	55	
extension	1 min	72				
final extension	10 min	72				
hold	infinite	4				

PCR products were separated using DNA gel electrophoresis on 1% agarose gel and visualised under UV light. The successful constructs were transformed into chemically competent *E.coli* Stellar cells via heat shock. Plasmids were purified from liquid culture

using the QIAprep Spin Miniprep Kit (Qiagen) according to the manufacturer's instructions. The success of mutagenesis was confirmed by sequencing, using the services of Eurofins Genomics.

6.2.2 Protein expression

The successful constructs were transformed into chemically competent *E.coli* Rosetta2 (DE3) pLysS cells. Cells were grown at 37 °C in liquid culture containing LB medium with 50 µg/ml kanamycin until an OD_{600} of ~0.6 was reached and were transferred to 30 °C. Protein over-expression was induced by addition of 100µM IPTG. Cultures were incubated overnight at 180 rpm rotation. Cell pellets were harvested by centrifugation at 6,000g before being flash-frozen in liquid nitrogen to aid cell lysis and stored at -80°C.

6.2.3 Protein purification

Protein purification was conducted as described in Chapter 2. Images of protein purification including chromatograms and SDS-PAGE pictures are included in Appendix 3.

6.2.4 Mass Spectrometry

Intact mass of the protein was measured using the time-of-flight mass spectrometry services of the Proteomics Facility at the John Innes Centre by Dr Gerhard Saalbach.

6.2.5 Phytase Activity Assays

Phytase activity was assessed using a colourimetric assay based on measuring the release of inorganic phosphate (Pi). The use of the colourimetric reagent is a classic method of assaying phytase activity (Eeckhout and De Paepe, 1994). Fresh colourimetric reagent was made up each time before the assay by mixing four parts of solution A with one part of solution B. Solution A consisted of 15 g of ammonium heptamolybdate·$4H_2O$, 55 ml of

concentrated sulphuric acid, topped up to 1 L with ddH_2O. Solution B consisted of 27 g of $FeSO_4 \cdot 7H_2O$, 200 µl of concentrated sulphuric acid, topped up to 1 L with ddH_2O. 100 µl of the colourimetric reagent was added to 100 µl of the reaction and incubated at room temperature for 30 min before measuring the absorbance at 700 nm.

In this chapter, the reactions were prepared by incubating protein (at concentrations of 1.7-7.0 mg/ml) at the range of temperatures in a PCR thermocycler for 30 min. After the incubation, the proteins were cooled to room temperature and mixed with 1 mM IP_6 at pH 3.5, 5.5 and 7.4. Buffers used were 100 mM glycine-HCl at pH 3.5, 100 mM NaAc-NaOH at pH 5.5 and 10 mM Tris-HCl with 150 mM NaCl at pH 7.4. The reactions were allowed to proceed for 30 min at room temperature before using the colourimetric reagent to measure phosphate release.

6.2.6 Differential Scanning Calorimetry

The DSC experiments were conducted using the MicroCal VP-Capillary DSC machine (Malvern Instruments) with manual loading. The active cell volume was 130 µl. 300 µl of sample was used for loading. Before the main experiment, several buffer/buffer runs were conducted, using buffer in both reference and sample cells for proper equilibration of the machine. Protein samples were centrifuged at 5,000x*g* to remove particulate matter. Protein concentrations of 0.2-1 mg/ml were tested and the reference buffer used alongside was the same buffer the protein was dissolved in. Scan rates of 60 °C/h and 200 °C/hr were tested. The temperature range was 10-100 °C. Data was collected and analysed using the MicroCal VP-Capillary DSC software.

6.2.7 Molecular Dynamics Simulations

Gromacs v4.6.5 was used to perform molecular dynamics (MD) simulations (Pronk *et al.*, 2013). The GROMOS96 54a7 force field was employed. Simulations were performed at 298 K in aqueous solution for a total of 1 nanosecond using 1 fs timesteps. A monomer

taken from the crystal structure of *Bl*Minpp containing two disulphide bridges (Arthur Li, UEA, personal communication) was used to represent the oxidised enzyme. A second model in which the cysteines were replaced with alanines by deleting the relevant atoms from the cysteine sidechains was created to represent the D1D2 double mutant. The simulations were performed in a cubic box with sides extending at least 10 Å from any atom of the molecule. The box was solvated with water molecules, with chloride counter ions added at random positions to ensure charge neutrality. Prior to the unrestrained MD simulations, energy minimization for 10,000 steps followed by 20 ps of position-restrained MD was performed to equilibrate the protein molecule and water molecules in the simulation boxes. Root mean square fluctuations (rmsf) of the Cα atoms were calculated for each simulation over the complete 1 ns unrestrained MD trajectory.

6.3 Results and Discussion

6.3.1 Site directed mutagenesis of cysteines

Bioinformatics analysis revealed four cysteines in the Bl gene: C278, C291, C483 and C501. Amino acid sequences are shown in Appendix 1. Structure of the Bl phytase E401Q revealed the pairing to be 278-291 (hereby referred to as disulphide 1 or D1) and 483-501 (disulphide 2, D2) as visible in the Figure 6.2 below.

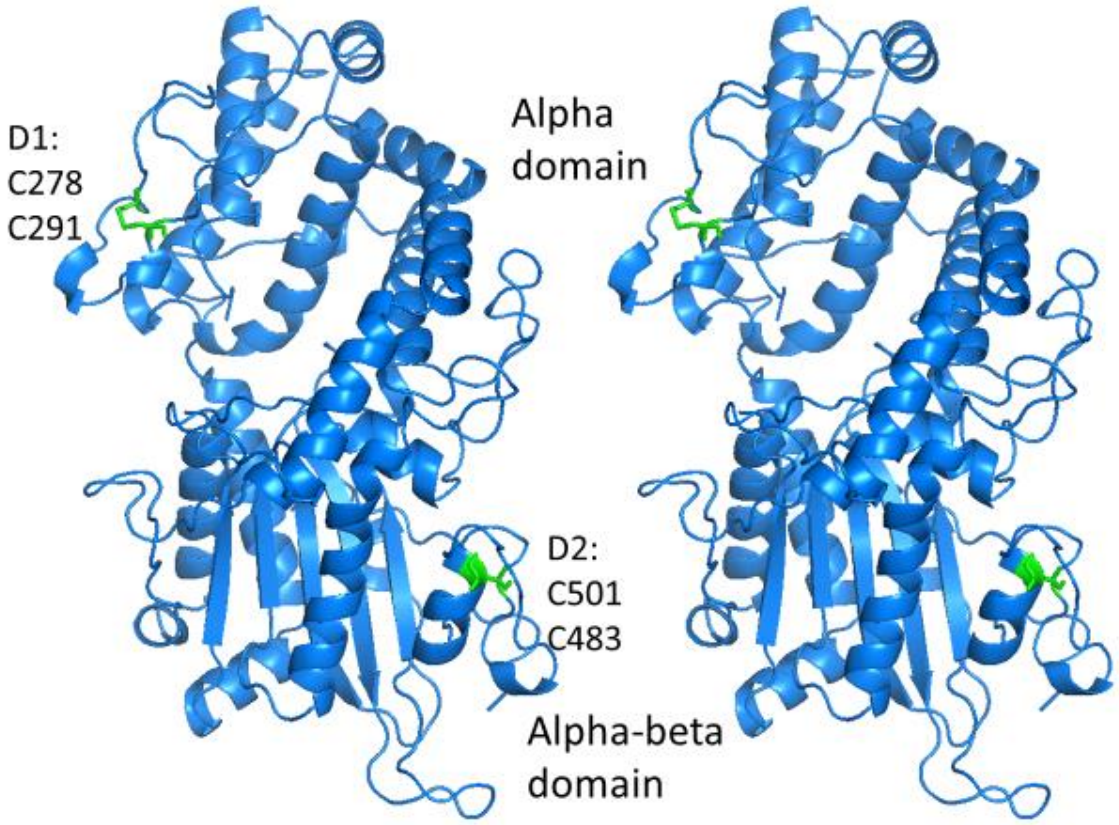

Figure 6.2 Location of disulphide bridges in Bl phytase.
Stereo view of crystal subunit B of Bl phytase E401Q. Shown in green are cysteines 278 and 291 forming disulphide D1 and cysteines 483 and 501 forming disulphide D2.

The cysteine pairs form a disulphide bridge in the crystal form and it can be assumed the same happens in solution. So far, all structurally characterised HAP phytases were shown to have every cysteine participating in disulphide pairings, with no single unpaired cysteines, that contributed to structural and catalytic activities of the enzymes (Ullah and Mullaney, 1996; Lee *et al.*, 2003; Wang, Meng and Zhou, 2004; Mullaney and Ullah, 2005; Böhm *et al.*, 2010)

To investigate the effect of disulphides D1 and D2, site-directed mutagenesis was carried out to substitute the cysteines and prevent disulphide bridge formation. Because free cysteines can contribute to irreversible aggregation and lead to unfolding of the protein structure (Xia, Longo and Blaber, 2015), both cysteines were substituted in the given disulphide. Serine and alanine were considered for the candidate amino acid to substitute the cysteines with. Their structures (shown in Figure 6.3 below), sizes, hydrophobicity and possible interactions with the surrounding residues were taken into account.

Cysteine: 121.15 g·mol−1 Alanine: 89.09 g·mol−1 Serine: 105.09 g·mol−1

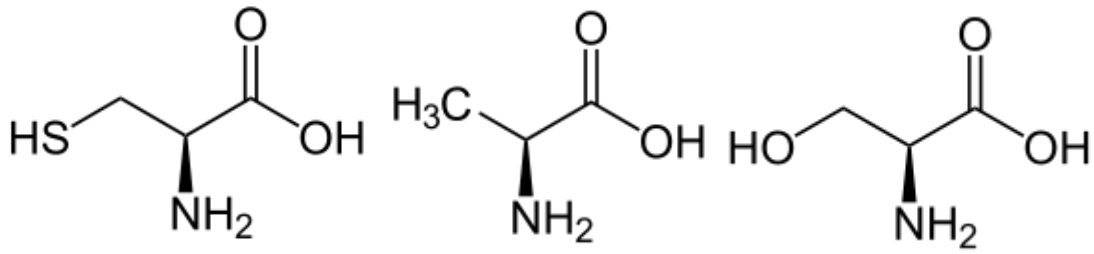

Figure 6.3 Comparison of the structure of cysteine to candidate substitution mutagenesis residues.

Serine is an amino acid that is isosteric to cysteine, with a closely related structure – cysteine's γ S atom is substituted with serine's γ oxygen. The similarity in sizes could be an advantage in ensuring no cavity is introduced in the protein's structure when substituting the cysteine. However, serine is less hydrophobic than cysteine and can introduce new hydrogen or salt bridges, potentially inducing significant and unwanted structural changes.

Alanine has the same hydrophobicity as cysteine. It is commonly used for cysteine substitution mutations to prevent disulphide bridge formation,

The smaller size of alanine could introduce a cavity in the structure, which usually traps a water molecule, making up for the difference in size as compared to cysteine and serine. In certain cases the alanine mutation has been shown to maintain the same extent of hydrogen bond interactions as the cysteine wild-type.

Extensive analysis of different cysteine substitution mutations by Xia et al. (Xia, Longo and Blaber, 2015) led to the conclusion that alanine is the optimum candidate for substitution of cysteine. As such, both cysteines in the putative disulphide were substituted with alanine residues. Three mutants were created – one removing each of the two disulphides and one double mutant removing both disulphides.

Mutant C278A/C291A was designated the name D1, removing the disulphide from the alpha domain. Mutant C483A/C501A was designated D2, removing the disulphide from

the alpha/beta domain. The double mutant C278A/C291A/ C483A/C501A was named D1D2, removing both disulphides. PCR mutagenesis was conducted using the Q5 ® Site-Directed Mutagenesis Kit (New England Biolabs). Separate sets of primers were designed for each cysteine. Success of introduction of the correct mutations was confirmed using the sequencing service of Eurofins Genomics.

6.3.2 Protein expression and purification

Bl variant proteins were purified by metal affinity chromatography, followed by size exclusion chromatography. The proteins expressed as monomers. Images from protein purification chromatography and SDS-PAGE gel images are available in Appendix 3.

6.3.3 Mass Spectrometry

Intact mass spectrometry of mutants D1, D2 and D1D2 as well as the wild-type protein was carried out using the services of the Proteomics Facility at the John Innes Centre by Dr Gerhard Saalbach in order to confirm the success of the mutagenesis. The experimentally determined intact protein mass was close to the theoretical molecular weight, as outlined in Table 6.1 below.

	expected molecular weight (Da)	intact mass spectrometry molecular weight (Da)
WT	58188.81	58184.56
D1	58124.69	58122.43
D2	58124.69	58122.20
D1D2	58060.57	58060.18

Table 6.1 Intact mass spectrometry of the wild-type and mutant Bl phytase.

6.3.4 Retention of activity after pretreatment at different temperatures

Phytase activity of the four Bl variants was assessed and compared with activity of Quantum Blue after 30 min incubation at a range of temperatures. After incubations, the proteins were cooled to room temperature and mixed with 1 mM IP_6 at pH 3.5, 5.5 and 7.4. The reactions were allowed to proceed for 30 min at room temperature. pH 3.5 and 7.4 were chosen to reflect the pH close to that of the stomach and intestine, while pH 5.5 is the standard pH of phytase assays. The results are presented by taking into account the phosphate calibration curve of the assay and the mass concentration of protein and are displayed as nanokatals (nkat) per mg of protein.

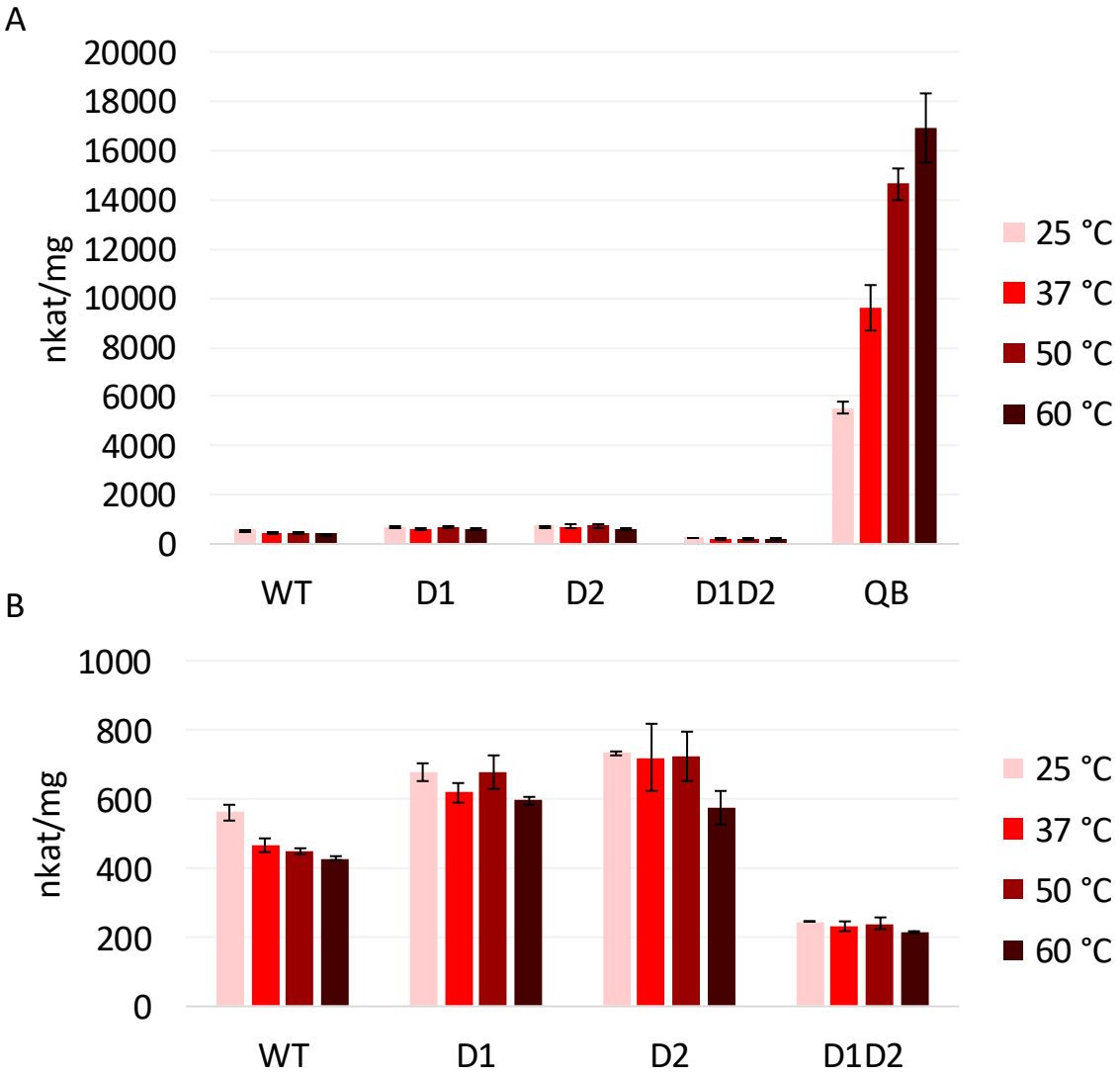

Figure 6.4 Phytase activity assay of Bl phytase variants WT, D1, D2 and D1D2 in comparison with commercial Quantum Blue phytase at pH 3.5.
Showing nanokatals per mg of protein. Error bars show standard deviation of triplicate measurements. A: The overall view of the assay results of the five enzymes. B: a zoomed-in view of the four Bl variants.

Figure 6.4 above shows the activity of the phytases assayed at room temperature at pH 3.5 after pre-incubation at a range of temperatures. Interestingly, Quantum Blue is seen to increase in activity with the increase in incubation temperature, although the actual reaction with IP6 was carried out at room temperature for all data points.

Figure 6.4 B shows a closer look at the four Bl variant phytases. Here, the two mutants D1 and D2 appear to have a slightly higher activity than the wild-type, although the values' error bars overlap at certain points. The double mutant D1D2 shows the lowest activity in general. Despite some variance between the triplicate measurements as reflected by the

size of the standard deviation error bars, the activity of the four Bl variants generally shows a downward trend with the increase in incubation temperature at the pH 3.5.

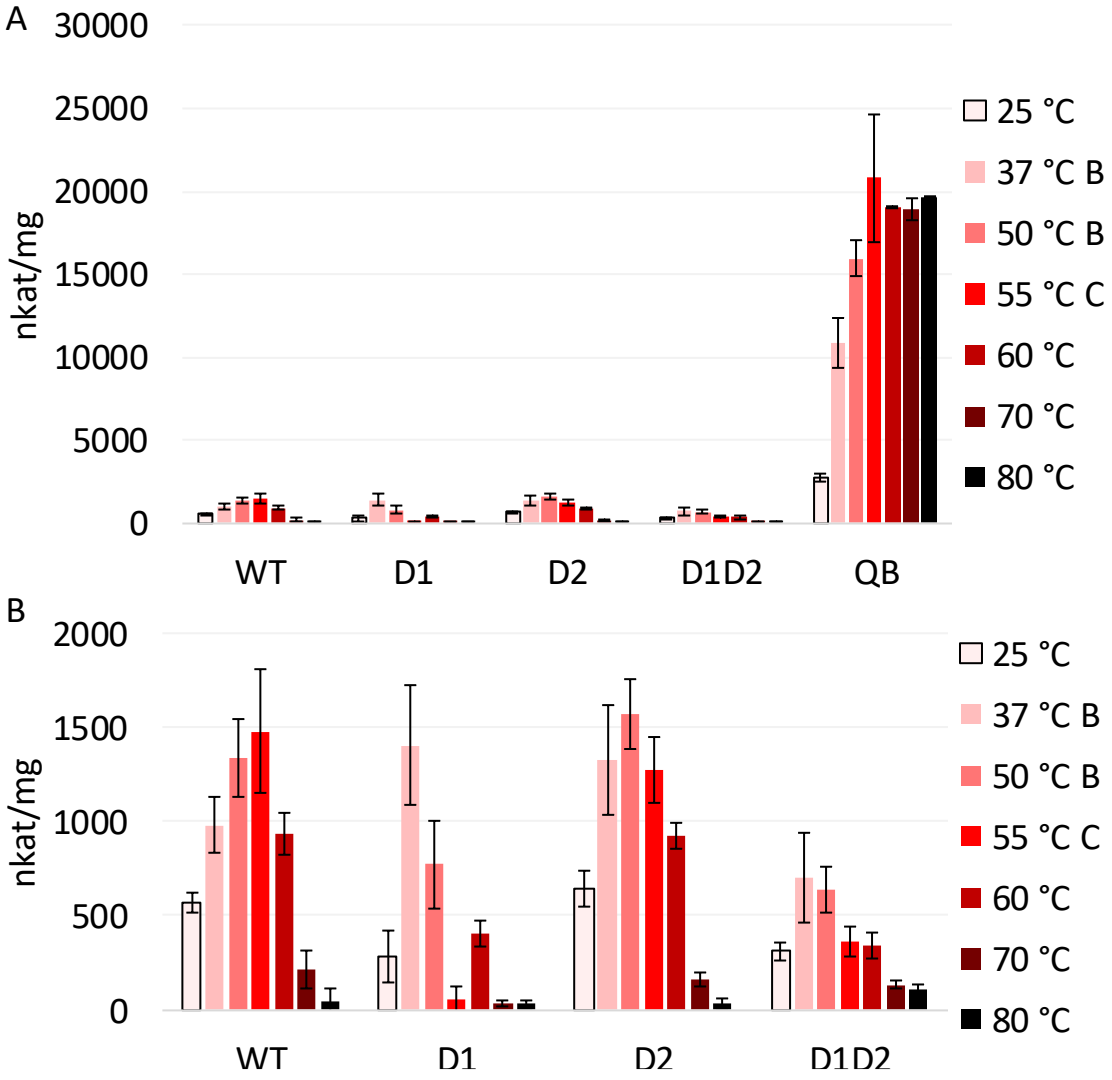

Figure 6.5 Phytase activity assay of Bl phytase variants WT, D1, D2 and D1D2 in comparison with commercial Quantum Blue phytase at pH 5.5.
Showing nanokatals per mg of protein. Error bars show standard deviation of triplicate measurements. A: The overall view of the assay results of the five enzymes. B: a zoomed-in view of the four Bl variants.

Figure 6.5 above shows the activity of the phytases assayed at room temperature at pH 5.5 after pre-incubation at a range of temperatures. Quantum Blue shows the highest activity at 55 °C, although the error bar overlaps the following data. Rather, it can be assumed that activity plateaus after incubation at the range of 55-80 °C. A closer look at the Bl variants in Figure 6.5 B reveals that in general, the double mutant D1D2 once again shows the lowest activity. The wild-type and D2 variants show very similar levels of activity.

The D1 mutant, although it appears to reach a similar level of maximum activity as the wild-type and D2 variants, generally shows the second lowest overall activity across the range of temperatures. Here, the data for 55 °C and 60 °C doesn't follow the expected trend of decreasing activity after incubation at higher temperatures. Despite the low error bars, it can be assumed that some of the data is erroneous. Overall, the Bl variants all appear to lose their activity after incubations at temperatures higher than 70 °C at pH 5.5.

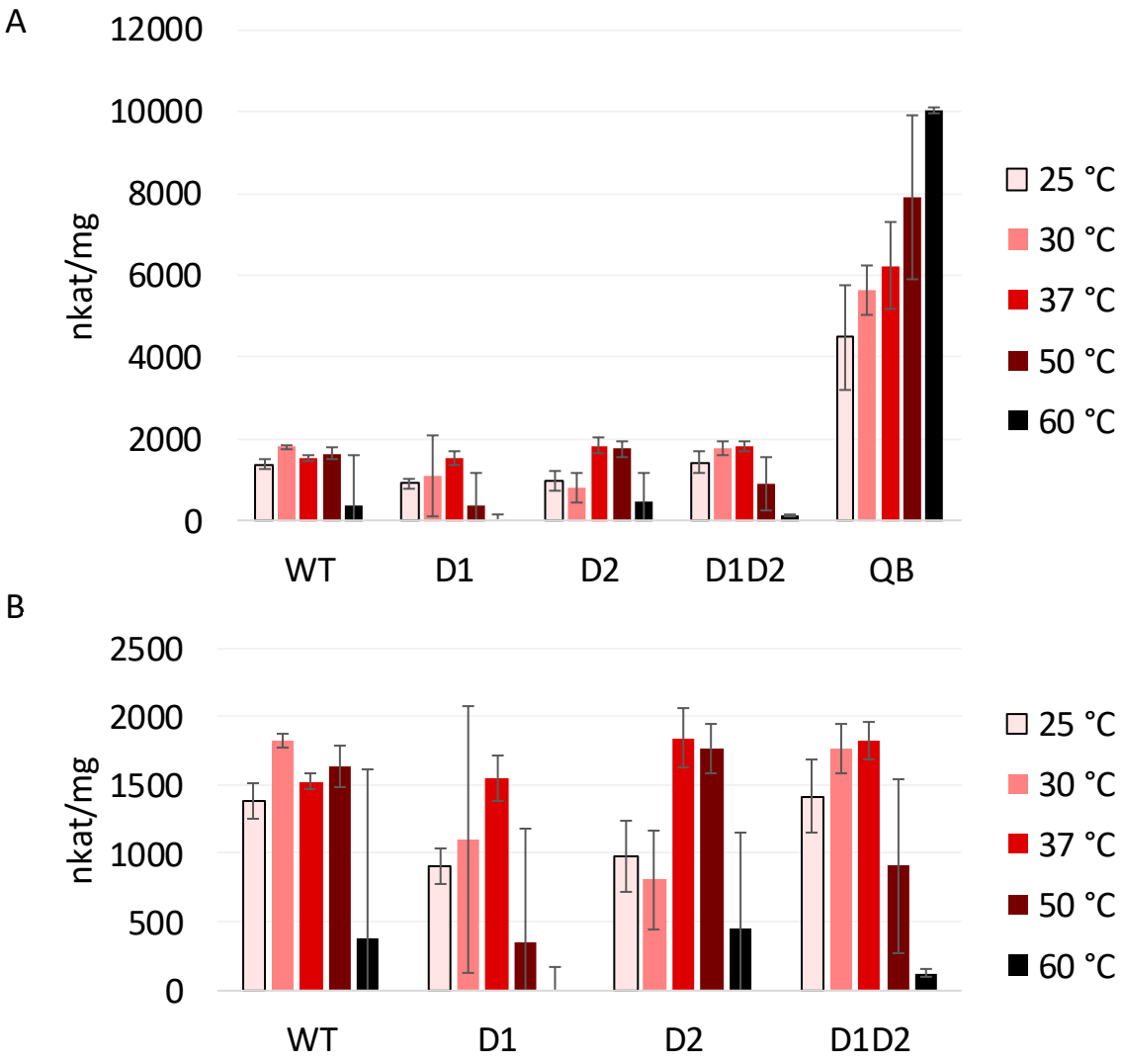

Figure 6.6 Phytase activity assay of Bl phytase variants WT, D1, D2 and D1D2 in comparison with commercial Quantum Blue phytase at pH 7.4
Showing nanokatals per mg of protein. Error bars show standard deviation of triplicate measurements. A: The overall view of the assay results of the five enzymes. B: a zoomed-in view of the four Bl variants.

Figure 6.6 above shows the activity of the phytases assayed at room temperature at pH 7.4 after pre-incubation at a range of. Quantum Blue is seen to increase in activity after incubation at increasing temperatures, as with assays at pH 3.5 and 5.5. In this case however, the Bl variants D2 and D1D2 as well as the wild-type show similar levels of activity. The D1 mutant shows arguably the lowest activity of the five enzymes, although some of the error bars are rather wide.

Overall, this experiment showed Quantum Blue to reach the highest levels of activity at pH 5.5 where the phosphate release reached around 1150 µmol/min/mg after incubation at temperatures above 55 °C. Reactions at pH 7.4 yielded the lowest activity (around 600 µmol/min/mg at 60 °C).

On the other hand, after incubations at a range of temperatures, the Bl variants showed highest overall activity after at pH 7.4, reaching around 120 µmol/min/mg at 30-37 °C. At pH 5.5 the wild-type, D1 and D2 variants reached maximum activities of around 90 µmol/min/mg at the range of 37-55 °C, while the D1D2 mutant reached the maximum of around 42 µmol/min/mg at 37 °C. At pH 3.5 the four Bl variants showed lowest activities, reaching the maxima of 35-45 µmol/min/mg at 25 °C.

Overall, these results confirm the greater catalytic activity of Quantum Blue compared to *Bifidobacterium longum* Minpp (*Bl*Minpp) at pH in the range 3.5 – 7.4, with *Bl*Minpp, irrespective of mutation, increasing in absolute activity and activity relative to Quantum Blue from pH 3.5 to pH 7.4. At pH 7.4, the activity of 25 °C – pre-treated protein reached approximately 30% of that of Quantum Blue, while at higher temperatures that of *Bl*Minpp was significantly reduced by comparison. These results likely reflect the optimisation, by unpublished modifications, of the temperature stability of the commercial product Quantum Blue.

Of the single cysteine pair mutations of *Bl*Minpp, D1, C278A/C291, was the most compromised in terms of its stability to temperature pre-treatment at pH 5.5 and 7.4, but

not at pH 3.5. In contrast, in combination with the D2, C483A/C501A mutation it activity was most compromised at pH 3.5 and 5.5.

The double mutant D1D2 shows the lowest activity profile after incubation at a range of temperatures. Its protein expression yield was the lowest of the four Bl variants, which may be correlated with low overall stability. The disparity between the two single disulphide mutants may be related to each disulphide residing in different folds of the protein – disulphide D1 is located in the alpha domain, while disulphide D2 is located in the alpha/beta domain.

6.3.5 Differential Scanning Calorimetry

Differential scanning calorimetry (DSC) was conducted to examine the melting temperature (Tm) that reflects the thermally induced structural transitions of proteins in solution. It is a powerful technique, used in the industry to predict shelf lives of products, develop purification strategies and characterise and evaluate proteins, lipids and pharmaceuticals. Most of all, it enables the study of folding and unfolding without the need to label the proteins. Thus, this technique allows proteins to be examined in as close to their natural state as possible, giving a reliable estimate of its temperature of unfolding (Morar-Mitrica, Nesta and Crotts, 2013).

All enzymes investigated in this chapter were tested for their refolding abilities by using the same sample of protein for several consecutive DSC measurements. Experiments were conducted at pH 3.5 and 7.4 to reflect the pH of the stomach and the intestine, as well as pH 5.5 which is a pH of standard phytase assays.

At pH 3.5 and 5.5 the wild-type Bl phytase showed no recovery, the protein did not refold after return to starting temperature from the first temperature ramp. Instead, the traces showed single peaks of melting temperature of 42.3 °C and 52.04 °C and Tm onset of 28.12 °C and 41.45 °C, respectively, as seen in Figure 6.7 below.

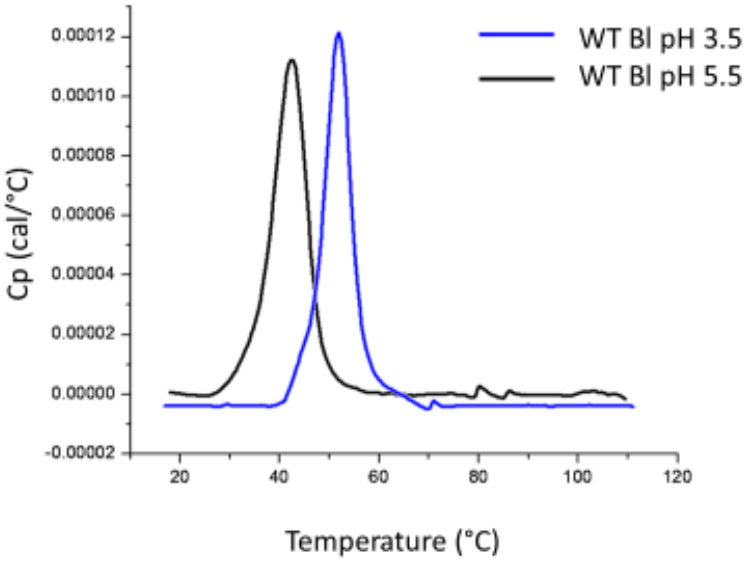

Figure 6.7 Differential scanning calorimetry of the wild-type Bl phytase at pH 3.5 and pH 5.5.
Wild-type *B. longum* phytase was tested in terms of its temperature of unfolding at pH 3.5 and 5.5. Protein concentration was 1 mg/ml. The experiment was run with a temperature ramp at 200 °C/hr.

The thermograms of the wild-type Bl phytase at pH 3.5 and 5.5 showed clear single peaks without apparent shoulders. Small anomalies were seen at 80 °C and 70 °C, possibly originating from an instrument artifact.

In contrast, as shown in Figure 6.8 below, the wild-type Bl phytase at pH 7.4 showed some degree of recovery after the first three runs, displaying progressively smaller folding isotherms in subsequent runs. At pH 3.5 and 5.5 this was not observed as the protein appeared to unfold irreversibly, therefore the subsequent traces are not shown for these pH values.

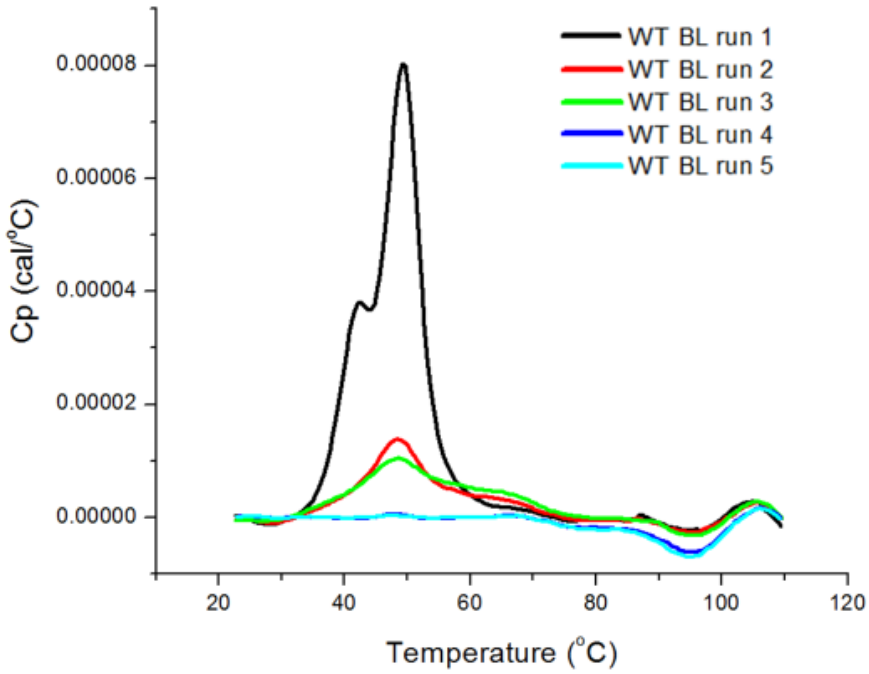

Figure 6.8 Differential scanning calorimetry of the wild-type Bl phytase at pH 7.4. Wild-type *B. longum* phytase was tested in terms of its temperature of unfolding at various pH. Protein concentration was 1 mg/ml. The experiment was run with a temperature ramp at 200 °C/hr. The same protein sample was used for five consecutive experimental runs.

Even so, the melting temperature was broadly consistent in the range of 47.8-49.2 °C between runs, dropping by 0.3-0.6 °C at each iteration as outlined in Table 6.2 below. The extent of the thermal denaturation reversibility is a significant finding of this experiment, as, even though the melting temperature of *Bl*Minpp is quite unremarkable compared to other engineered phytases, proteins in general typically exhibit aggregation and irreversible denaturation at the temperatures high enough to induce unfolding (Johnson, 2013).

Interestingly, a small lower temperature unfolding peak is visible at around 42 °C in run 1. Without any evidence of impurity in the protein preparation, the presence of this peak could hint at a two-stage unfolding event, albeit one specific to this pH. The absence of a similar shoulder in the pH 3.5 and pH 5.5 experiments argues that the shoulder does not arise from an impurity in the protein preparation.

	Tm Onset (°C)	Tm (°C)
WT Bl run 1	33.68	49.18
WT Bl run 2	32.63	48.59
WT Bl run 3	31.48	48.33
WT Bl run 4	44.25	47.79

Table 6.2 Melting temperatures and their onsets of several consecutive exposures to high temperatures of the wild-type Bl phytase at pH 7.4.

While *Bl*Minpp has not undergone systematic or iterative engineering of its protein stability, it is still informative to compare *Bl*Minpp with a highly engineered commercial phytase. For this purpose Quantum Blue (QB) was subjected to DSC. Interestingly, at pH 3.5 QB showed extensive recovery across nine temperature cycles, with the peak shifting by only 7 °C towards lower temperatures, as seen in Figure 6.9 and the data table below.

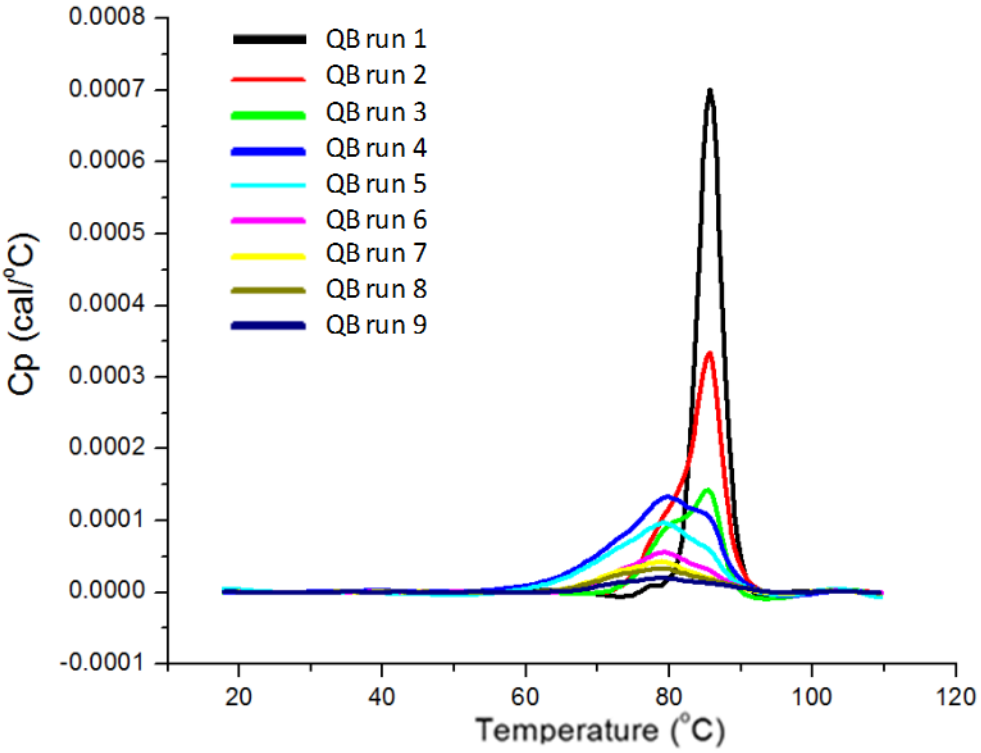

Figure 6.9 Differential scanning calorimetry of the commercial QB phytase at pH 3.5. Commercial phytase Quantum Blue was tested in terms of its temperature of unfolding at pH 3.5. Protein concentration was 1 mg/ml. The experiment was run with a temperature ramp at 200 °C/hr.

	Tm Onset (°C)	Tm (°C)
QB run 1	79.45	85.64
QB run 2	72.78	85.60
QB run 3	71.40	85.56
QB run 4	54.70	79.93
QB run 5	57.71	79.40
QB run 6	65.35	79.07
QB run 7	62.48	78.86
QB run 8	61.92	78.75
QB run 9	65.12	78.83

Table 6.3 Melting temperatures and their onsets of several runs of the commercial Quantum Blue phytase at pH 3.5.
Quantum Blue phytase was shown to have a high degree of structural recovery after numerous consecutive exposures to high temperatures at pH 3.5. The same recovery was not observed at pH 5.5 or 7.4.

The Quantum Blue phytase shows a single initial peak of unfolding, however runs 2 and 3 begin to show a slight shoulder at around 78 °C. This becomes more apparent in run 4. In run 5 the peak is now where the shoulder was, with the shoulder now positioned at around 85 °C. Interestingly, the peaks in runs 3 and 4 are at the same heat capacity height, at the different temperatures of 85 °C and 78 °C. All in all, QB has a high melting temperature of 85.64 °C at the first run, reflecting its suitability for use as a commercial phytase, allowing it to withstand the high temperatures of pelleting and likely adding protease resistance capabilities.

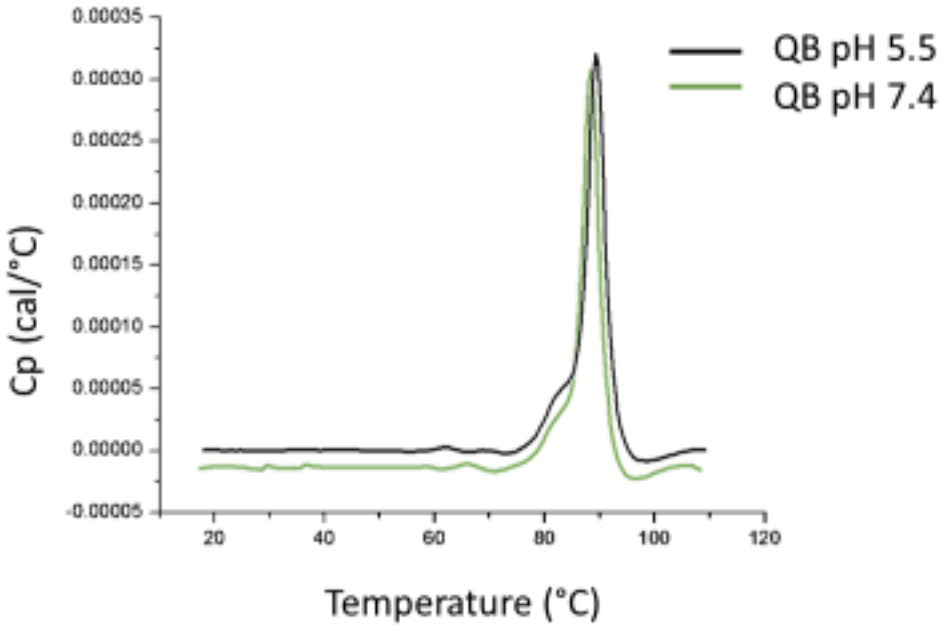

Figure 6.10 Differential scanning calorimetry of the commercial QB phytase at pH 5.5 and pH 7.4.
Commercial phytase Quantum Blue was tested in terms of its temperature of unfolding at various pH. Protein concentration was 1 mg/ml. The experiment was run with a temperature ramp at 200 °C/hr.

A number of studies including Zeller *et al.* (Zeller *et al.*, 2016) have shown the efficacy of QB, a histidine acid phytase (HAP), in mobilizing phosphate from phytate during passage of feed through the digestive tract of chickens. This enzyme can even encounter pH <1 in the gizzard (Lee *et al.*, 2017). Here, QB showed no recovery at pH 5.5, nor 7.4. At both pH 5.5 and 7.4, the QB showed single thermogram peaks with a shoulder preceding the peak at around 82 °C. The melting temperatures were 89.43 °C and 89.26 °C, with the Tm onsets of 77.48 °C and 76.86 °C, respectively. The heat capacity peak is smaller in Figure 6.10 than in Figure 6.9, possibly stemming from a lower amount of protein loaded into the instrument cell. While the thermostability of QB appears higher by about 4 °C at pH 5.5 and 7.4, the difference could stem from the use of different buffers for each pH. Additionally, the thermogram for QB at pH 5.5 shows a small peak at around 67 °C. While it can be attributed to an instrument error, it could also stem from possible protein impurities.

To create the D1 Bl phytase mutant, cysteines C278 and C291 were substituted with alanine residues in order to remove the disulphide bridge formed by them. To test the hypothesis that this action would decrease the thermostability of the enzyme, a DSC experiment was undertaken.

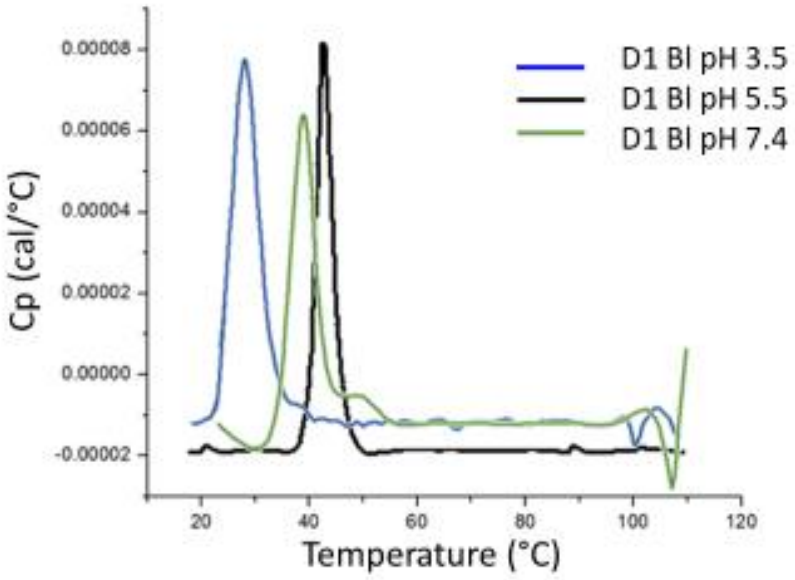

Figure 6.11 Differential scanning calorimetry of the D1 mutant Bl phytase at pH 3.5, 5.5 and 7.4.
Disulphide knockout mutant D1 of *B. longum* was tested in terms of its temperature of unfolding at various pH. Replicate data not available due to low levels of protein expression for mutant phytases. Protein concentration was 1 mg/ml. The experiment was run with a temperature ramp at 200 °C/hr.

As seen in Figure 6.11, at pH 3.5 the D1 mutant showed a single thermogram peak. The melting temperature was 27.78 °C with the Tm onset of 22.91 °C. This is in stark contrast to the wild-type Bl phytase which showed a melting temperature peak at 42.3 °C. The thermogram shows a slight shoulder following the main peak, at around 38 °C. The same shoulder is prominently visible at pH 7.4, but not at pH 5.5. The thermogram for the D1 mutant at pH 5.5 shows a single main peak at 42.69 °C and the Tm onset at 38.27 °C. Small peaks are visible at 22 °C and 90 °C, possibly due to anomalies. The difference in peak height of the trace at pH 7.4 could be due to overall broadening of the peak at this pH, or due to a lower amount of protein loaded into the instrument. Furthermore, the

mutant Bl enzymes expressed less efficiently than the wild-type, further decreasing the amount of available sample for the DSC runs, which contributes to the different peak heights between the Bl variants.

At pH 7.4, the main peak of melting temperature is at 38.39 °C and the Tm onset is at 33.07 °C. The shoulder at around 48 °C is more prominent than at pH 3.5. The peak and trough after 100 °C is likely a result of drastic heat capacity changes accompanying protein aggregation at high pressure and temperature (Durowoju *et al.*, 2017). Overall, the thermostability of the D1 mutant increased at pH 7.4 by around 10 °C.

In wider context, the observations of 'shoulders' on the thermograms at pH 3.5 and 5.5 may hint at different domains of the proteins unfolding at different temperatures, which does not seem to happen at pH 7.4. Because the DSC is a technique that utilised a large amount of protein for each experiment (about 300 µg) and the mutant phytases expressed in low concentrations, I was unable to obtain sufficient numbers of replicate measurements. It would be useful in the future of the project to optimise the expression conditions to obtain higher amounts of protein. Alternatively, differential scanning fluorimetry (DSF) could be carried out on the disulphide mutants to further examine the potential of various protein domains displaying different levels of thermostability.

To create the D2 Bl mutant, cysteines C483 and C501 were substituted with alanine residues to remove the disulphide D2 in order to examine the role of disulphide D2 in thermostability using DSC experiments.

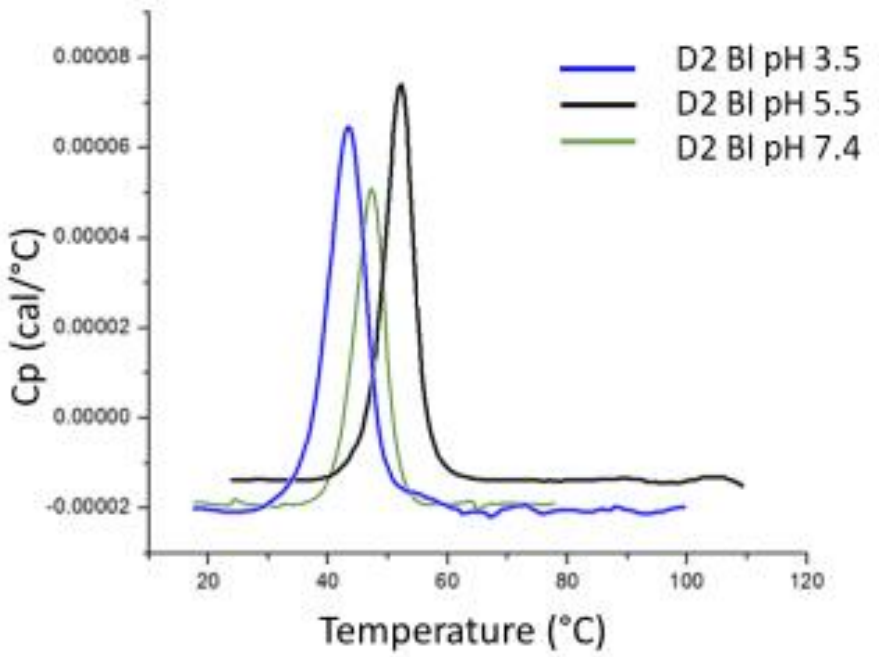

Figure 6.12 Differential scanning calorimetry of the D2 mutant Bl phytase at pH 3.5, 5.5 and 7.4.
Disulphide knockout mutant D2 of *B. longum* was tested in terms of its temperature of unfolding at various pH. Replicate data not available due to low levels of protein expression for mutant phytases. Protein concentration was 1 mg/ml. The experiment was run with a temperature ramp at 200 °C/hr.

The D2 mutant at pH 3.5, 5.5 and 7.4 showed single peaks with no shoulders or anomalous traces. The Tm onset was at 30.08 °C, 39.87 °C and 38.03 °C respectively. Like D1, the D2 mutant showed the highest melting temperature at pH 5.5, the values were 43.36 °C, pH 3.5; 51.37 °C, pH 5.5 and 47.34 °C, pH 7.4.. The melting temperatures of the D2 phytase were similar to the wild-type enzyme, suggesting no contribution of the D2 disulphide to the thermostability in this case.

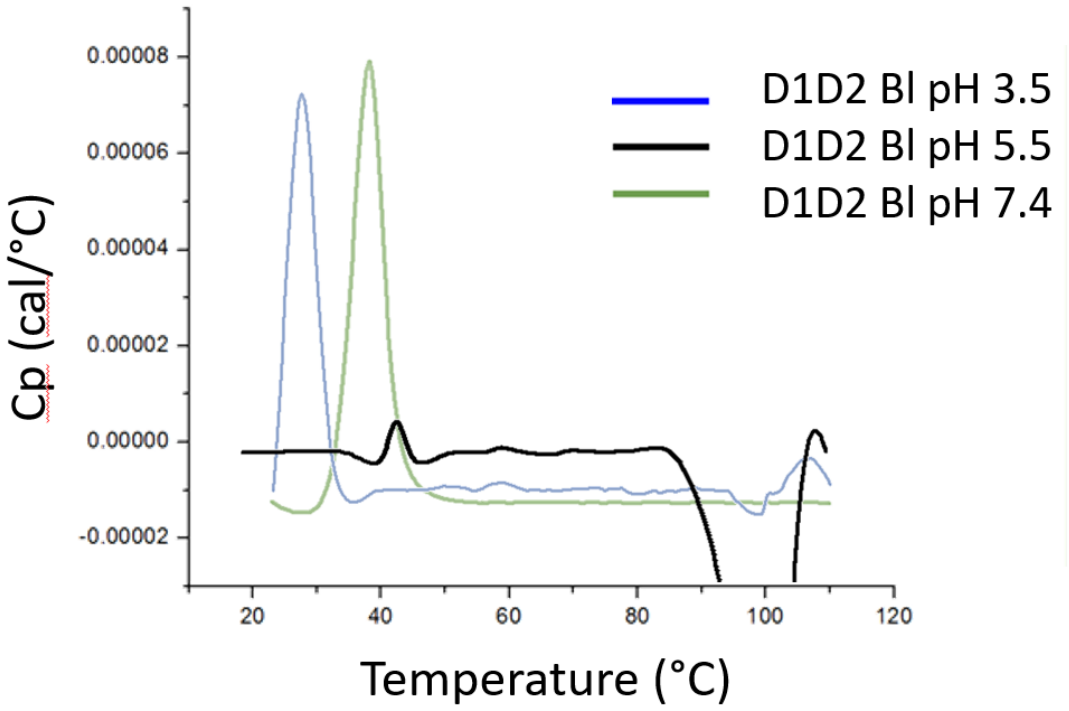

Figure 6.13 Differential scanning calorimetry of the D1D2 mutant Bl phytase at pH 3.5, 5.5 and 7.4.
Double disulphide knockout mutant D1D2 of *B. longum* was tested in terms of its temperature of unfolding at various pH. Replicate data not available due to low levels of protein expression for mutant phytases. Protein concentration was 1 mg/ml. The experiment was run with a temperature ramp at 200 °C/hr.

To investigate any potential additive effects of disulphides D1 and D2, a double mutant was created with all four cysteines substituted with alanine residues.

The D1D2 mutant showed clear thermogram peaks at pH 3.5 and 7.4, with peaks at 27.40 °C and 37.80 °C. The thermogram of the enzyme at pH 5.5 shows a small but clear peak at 42.25 °C and an intense negative peak at around 100 °C. Given the low general stability of the mutant Bl enzymes in this series of experiments, one explanation may be that the protein precipitated out of solution during the temperature ramp and the aggregate dissolved again due to high pressure and temperature at ~100 °C. Ideally, the experiment should be repeated to not only gain at least three replicates of each data point, but to ascertain the nature of the small peak at pH 5.5. Like the D1 and D2 mutants, the D1D2 mutant displayed maximal melting temperature at pH 5.5.
All in all, the double disulphide knock-out D1D2 showed the lowest temperature of unfolding, on par with the single D1 mutant, across the different pH conditions. On the

other hand, the wild-type and the single D2 mutant showed highly similar temperatures of unfolding throughout the pH conditions. These points are better visualised in Figure 6.15.

In contrast to Quantum Blue, the *Bl*Minpp phytase enzymes rarely showed recovery in the DSC runs and none of the purified cysteine mutant enzymes showed refolding. However, these enzyme samples were purified using the metal affinity purification, followed by size exclusion chromatography. Together with time taken to concentrate the samples to a desired volume, time taken between the initial cell lysis to the DSC experiment was between 2 to 3 days. While the fully purified D1 phytase showed no recovery, a preliminary experiment performed on the D1 mutant lysed on the same day as the experiment showed a certain, albeit limited, degree of recovery, shown in the figure below.

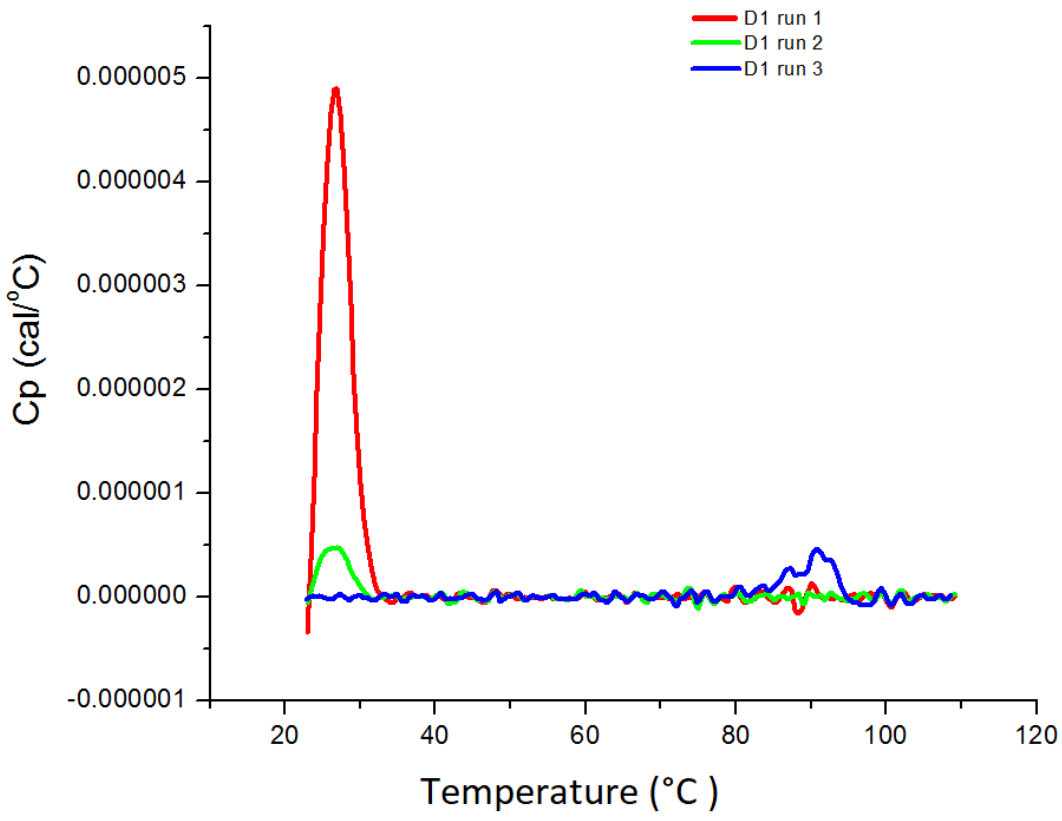

Figure 6.14 Differential scanning calorimetry of the D1 mutant Bl phytase at pH 8.0. Disulphide knockout mutant D1 of *B. longum* was tested in terms of its temperature of unfolding during three consecutive experiments on the same sample at pH 8, to examine its recovery after unfolding. Protein concentration was 0.2 mg/ml. The experiment was run with a temperature ramp at 200 °C/hr.

The above experiment was conducted using a 0.2 mg/ml protein sample at pH 8.0 in the lysis buffer (50 mM Tris-HCl pH 8, 300 mM NaCl, 10 mM imidazole), on the same day as cell lysis and following metal affinity purification. The sample was subjected to limited centrifugal concentration. The peak heat capacity is reduced one order of magnitude from that Figure 6.11, likely stemming from the lower protein concentration. The background noise is highly visible at this scale. Despite this, a small peak of refolding is visible in the second DSC run of the sample. The melting temperatures were 26.94 °C and 26.92 °C for runs 1 and 2, respectively, while the Tm onsets were 22.93 °C and 22.91 °C. In this regard, the melting temperature is much reduced from that recorded at pH 7.4 (Figure 6.11), but perhaps indicates a progressive decrease in Tm above pH 7. Run 3 showed no significant peak in the 23 °C region, but showed an anomalous peak at around 90 °C, possibly as a result of heat capacity changes due to fully unfolded protein with hydrophobic residues exposed. The experiment was repeated with the same qualitative result, namely the limited recovery of protein after a single cycle of DSC.

Figure 6.15 below shows a summary of the melting temperatures of the phytases examined in this chapter, at pH 3.5, 5.5 and 7.4. It can be immediately seen that each Bl phytase variant was most stable at pH 5.5 and least stable at pH 3.5. pH 3.5 is close to the physiological pH of the stomach and the target location for the commercial phytase activity. While the QB phytase is also least stable at pH 3.5, its overall stability is significantly higher than the Bl phytase.

On average, the D1 mutant showed a 25% decrease in melting temperature when compared to the wild-type Bl phytase. The D2 mutant appears to have a negligible effect on thermostability, showing on average 99% of the thermostability of the wild-type. The double mutant D1D2 appears to have the same effect as the D1 mutant, as its thermostability was at 74% of the wild-type. Considering melting temperature alone, the thermostability of Quantum Blue was on average 184% of that of the Bl phytase.

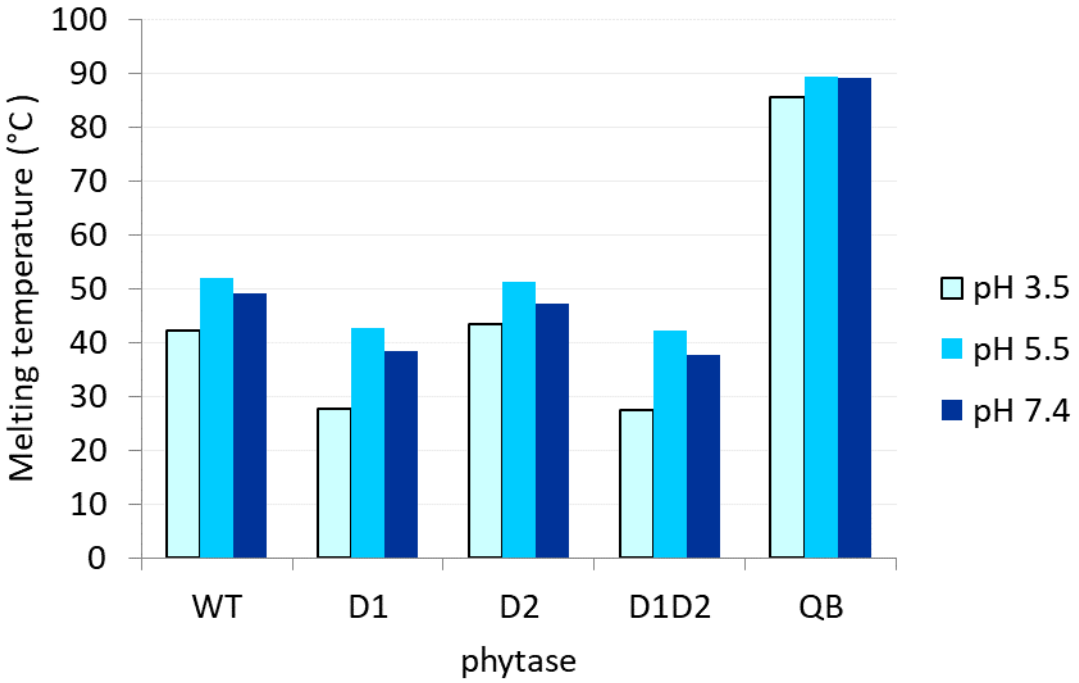

Figure 6.15 Summary of the melting temperature values of a range of phytases using differential scanning calorimetry.
Wild-type (WT) and disulphide knockout mutants (D1, D2, D1D2) of *B. longum* phytase were compared to the commercial Quantum Blue (QB) phytase in terms of their temperatures of unfolding at various pH. Bars represent single measurements of protein concentrations from 0.2 mg/ml to 1.0 mg/ml. Replicate data not available due to low levels of protein expression for mutant phytases.

Considering the much greater catalytic activity of Quantum Blue revealed in Figures 6.4 – 6.6, particularly at pH 3.5 and pH 5.5, the comparison of Quantum Blue and *Bl*Minpp makes obvious the considerable challenge in engineering novel classes of phytase to match the overall performance of a 3rd generation commercial histidine acid (HD) phytase.

A few studies have reported success in engineering improved thermal stability of HAP phytases, we may assume that there are as many, or more, unsuccessful attempts not reported. Nevertheless, in a study of the HAP phytase from *Citrobacter braakii*, Sanchez-Romero et al. (Sanchez-Romero *et al.*, 2013) engineered three variants of the phytase, each with two or three new disulphides. The residues for mutagenesis were selected on the basis of molecular dynamics simulations, which pinpointed the regions of the protein with the highest propensity to unfold at higher temperatures, with the aid of the structural examination. The premise of this experiment was that the newly introduced

disulphides would be positioned as to not modify the overall structure of the protein to a significant level, but to increase the thermostability of the enzyme as well as its kinetic properties.

An approach by Yu et al. (X.-W. Yu *et al.*, 2012) achieved a 7 °C increase in thermostability of a lipase enzyme by introducing novel disulphides into the hinge regions of the protein. Lipases, like phytases, are ester hydrolases and display a domain motion resembling the closing and opening of a lid, depending on the stage in the catalytic cycle. Yu et al. used rational disulphide engineering based on computational prediction and analysis of the hinge residues involved in domain motions. The two new disulphides were introduced in such a way as to stabilise the protein structure at the hinge, while allowing the conformational changes crucial to catalysis to take place. By decreasing the protein flexibility and lowering the entropy of unfolded protein, the resulting enzyme displayed a higher tolerance to low pH and increased half-life at 60 °C in addition to increased thermostability, while maintaining the same catalytic properties.

In a study of the beta-propeller *B. subtilis* phytase 168phyA, Cheng et al. (Cheng, Wong and Lim, 2007) substituted the Ser-161 and Leu-212 residues for cysteines in order to stimulate disulphide bond formation. The locations for the substitutions were chosen based on sequence alignment with related phytases that contain disulphide bonds and confirmed by molecular modelling. Upon investigation, the mutant and wild-type phytases showed similar melting temperatures and mid-points of transitions as well as identical activity with sodium phytate at pH 6.0 at 37°C.

Interestingly, the mutant protein showed unexpected improvements in other areas. Its activity with the alternative substrate guanosine triphosphate (GTP) was the same as its activity with IP_6, and 1.7 times higher than that of the wild-type phytase; activity with adenosine triphosphate and adenosine diphosphate was 1.35 and 2.19 times higher than that of the wild-type enzyme. Furthermore, the mutant enzyme's yield from *B.subtilis* was 3.5 times higher than that of the wild-type.

However, it exhibited poor refolding capabilities after exposure to temperatures of over 80°C for 10 minutes and significantly lower phytase activity. This hints at the possibility that the introduction of extra disulphide bonds may negatively affect the enzyme's

recovery after thermal unfolding and its maintenance of activity. This may be due to possible protein aggregation or alternatively due to the sensitivity of the SH group of cysteine to oxidation at high temperatures, leading to increased destabilisation of the protein structure at higher temperatures (Mozhaev *et al.*, 1988).

In another study, Mullaney et al. (Mullaney *et al.*, 2012) created disulphide deletion mutants in the HAP *A.niger* PhyA phytase. As a result, the optimum temperature of activity of the mutant phytases was lowered from 60 °C to as low as 42 °C, closer to the body temperature of target animals in the animal feed industry. Certain processing methods for production of phytase-supplemented feed use temperatures of up to 70 °C for manufacture. The disulphide knockout phytases in this case showed a higher percentage of retained activity after being subjected to 70 °C for 5 minutes than the wild-type phytase. Additionally, double cysteine mutants retained a higher percentage of activity than the single cysteine mutants, hinting at a direct effect of the presence of cysteines (not necessarily disulphides) on retaining activity.

In the light of the above, it may be useful to consider introducing stabilising substitution mutations to mutant enzymes that show poor expression levels, such as the mutants described in this thesis.

6.3.6 Insights to protein stability from molecular dynamics simulations

Molecular dynamics simulations (MD) were performed to elucidate the flexible regions of the protein as it unfolds with the increasing temperature, to complement the experimental data resulting from the DSC experiments. To demonstrate the validity of the computational protein model, Figure 6.16 below displays the alignment of the active sites of the crystal structure of the *Bl*Minpp with the computational model resulting from energy minimisation.

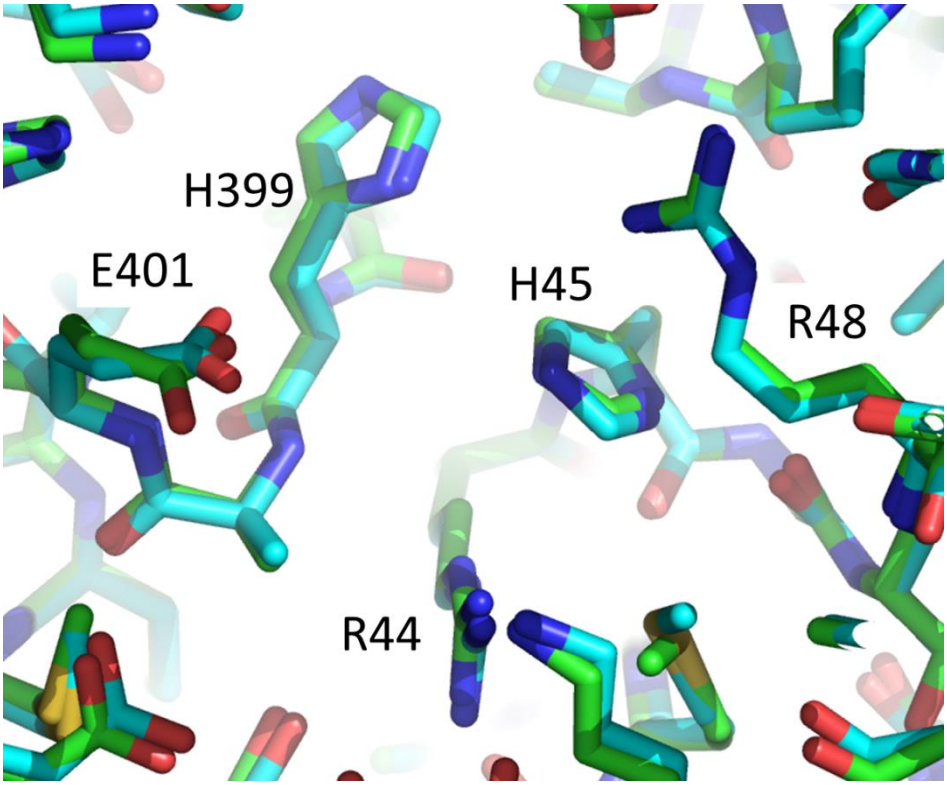

Figure 6.16 Comparison of the active site of *Bl*Minpp with the active site of the structure resulting from energy minimisation.
Selected active site residues are labelled and shown in stick format with carbon atoms coloured (A) in green for the crystal structure and (B) in cyan for the structure resulting from energy minimisation.

Figure 6.17 below presents the Cα trace of the oxidised form of the enzyme (A) with the disulphide-forming cysteines in grey, and the cysteine-free double mutant D1D2 (B). The traces are coloured according to the RMSF, however the values are not normalised between the two structures. The oxidised enzyme shows a particularly flexible region around the disulphide D1, while the reduced form (cysteine-free) shows high flexibility in the region neighbouring D2.

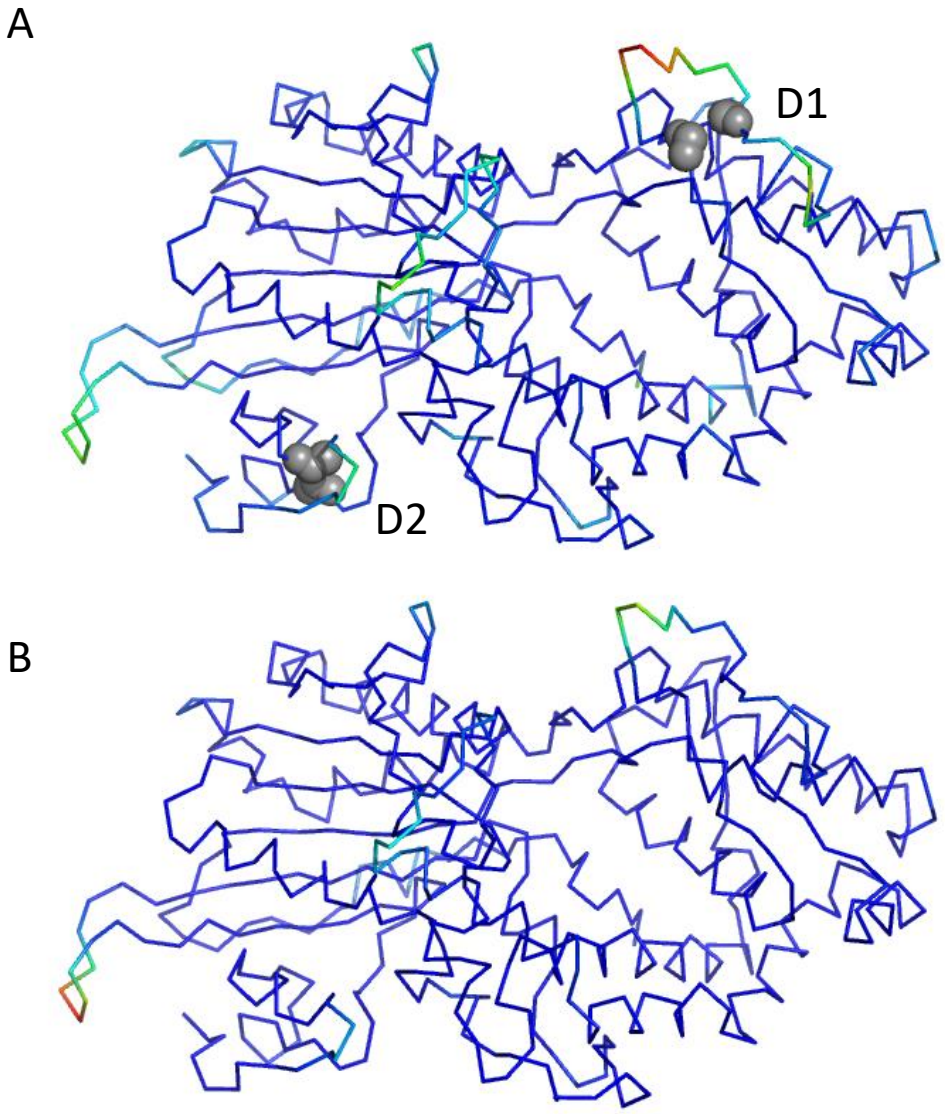

Figure 6.17 Root mean square fluctuations of residues in *Bl*Minpp as calculated from molecular dynamics trajectories at 298K.
(A) the oxidised enzyme (B) the cysteine-free D1D2 double mutant. α-carbon atoms coloured in a spectrum according to RMSF with lowest values (least mobile regions) shown in blue and highest (most mobile regions) in red. Disulphides D1 and D2 are labelled.

Figure 6.18 below shows the root mean square fluctuations (RMSF) at 298 K (25 °C) of each residue. In blue, the data representing the wild-type, or oxidised form with disulphide bridges is shown; in orange, the data for the double mutant D1D2, or the reduced form, is shown. It can be seen that the regions close to the cysteine substitution mutation sites 278/291 and 483/501 display relatively high flexibility in both forms, which adds purchase to the idea that disulphide-forming cysteines act to stabilise the protein structure.

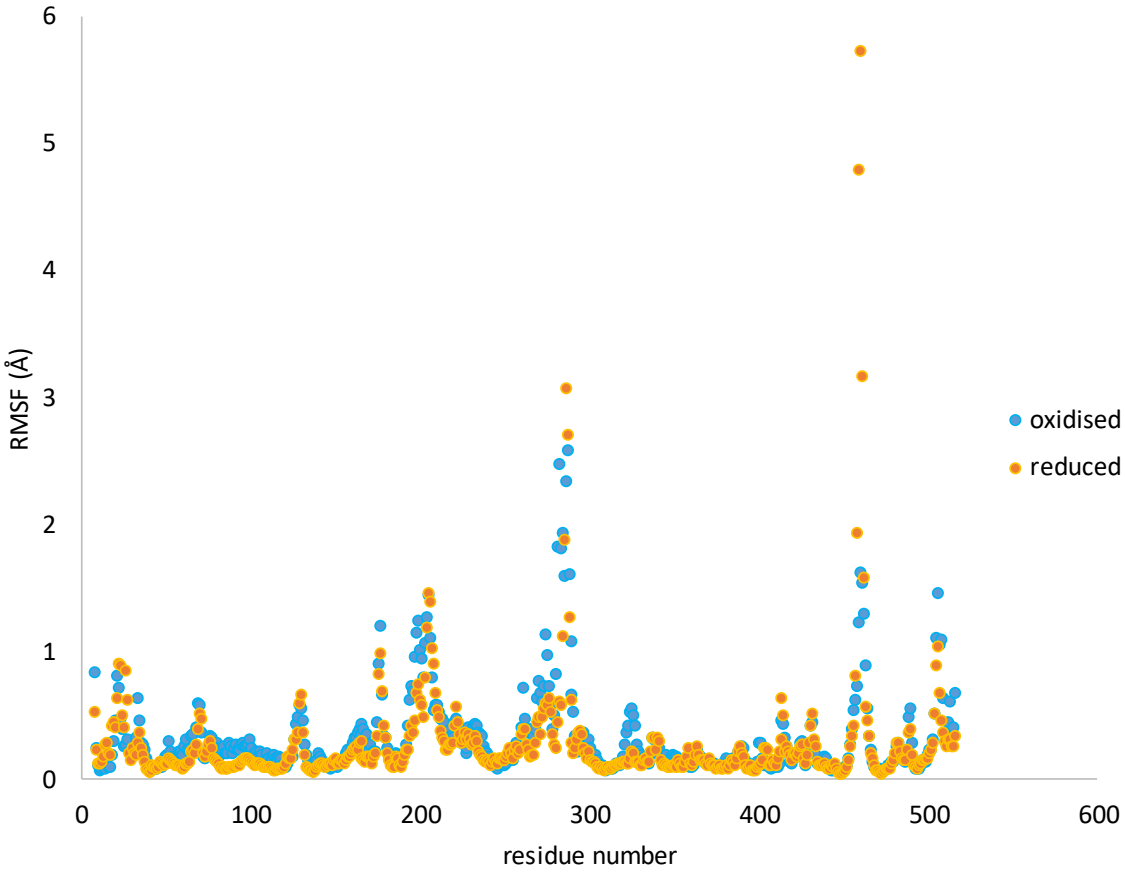

Figure 6.18 Root mean square fluctuations of residues in *Bl*Minpp as calculated from molecular dynamics trajectories at 298K plotted against residue number.
Values for the oxidised enzyme shown as light blue dots while those from the cysteine-free D1D2 double mutant are shown as orange dots.

In Figure 6.18, the molecular dynamics (MD) technique is employed to identify the flexible regions and amino acids in the *Bl* phytase. Root mean square fluctuations (RMSF) show the simulated average mobility of the atoms within each residue over time, where higher values indicate more mobility over time. Lower values are thought to contribute to the structural strength of the protein.

In a similar experiment, Fei et al. (Fei *et al.*, 2013) make note of the fact that more thermostable proteins tend to have higher numbers of salt bridges, which while weaker than disulphide bonds, provide slightly higher flexibility for the protein. In their investigation they conducted molecular dynamics simulations of the HAP *E.coli* AppA phytase. They identified possible residues taking part in salt bridge formation, and performed site-directed mutagenesis E31Q to remove the salt bridge by preventing the

glutamate residue from forming it. Indeed, the thermostability of this mutant phytase decreased by 14% as compared to the wild-type, while the optimum temperature and the pH profile stayed the same. Their molecular dynamics simulations revealed a possible site for introduction of a new salt bridge, where salt bridge addition mutation was performed at Q307D. The salt bridge addition mutant phytase showed a 9% increase in thermostability over the wild-type. These experiments further validate the use of molecular dynamics simulations to assess the sites of existing disulphide and salt bridges as well as to pinpoint the locations of new disulphide or salt bridges to introduce with site-directed mutagenesis.

6.4 Conclusions

This chapter focused on thermostability of a *Bifidobacterium longum* phytase and its cysteine mutants. I described the process of mutagenesis and the reasoning behind introducing the specific mutations. I carried out thermostability measurements, where I assayed the phytase activity after incubation at a range of temperatures. I found that while the Quantum Blue enzyme shows highest activity at pH 5.5 after incubations at a range of 55-80 °C, the Bl variants show the highest activities at pH 7.4. In general, the double mutant D1D2 showed lowest levels of activity of the Bl variants.

The DSC experiments revealed that the D1 disulphide is crucial for thermostability of the enzyme while the D2 disulphide seems to have an insignificant effect on the thermostability of the enzyme, as shown by cysteine knockout mutations. The double mutant D1D2 appeared to have the similar thermostability as the D1 mutant, suggesting no additive effects of the double cysteine knockout. Despite the lack of evidence for altered thermostability in the variants without the D2 disulphide, the phytase activity assays revealed the D1D2 mutant to have lowest activity after incubation at a range of temperatures. This may suggest that the double mutant does play an important role in stabilising the structure of the enzyme enough to carry out catalysis after exposure to higher temperatures.

Furthermore, the purified wild-type Bl phytase showed partial recovery at pH 7.4, while the commercial phytase Quantum Blue showed recovery at pH 3.5. Interestingly, an incomplete purification of the D1 mutant showed a small degree of recovery, hinting at limited shelf-life of the purified Bl phytases. In general, DSC proved a suitable technique for evaluating the thermostability of proteins. Molecular dynamics simulations provided further evidence for the disulphides playing a stabilising role in the protein structure.

In the future of the project, the state of disulphide bridging in proteins could be assayed using the Ellman's reagent, which allows for the free sulfhydryls to be quantified. A possible approach to the project could aim to introduce new disulphide links on the basis of the crystal structure of the protein, e.g. by substituting residues which form salt bridges or strong hydrogen bonds with cysteine pairs. Additionally, the protein domain motion analysis from Chapter 4 could aid in the rational disulphide design to optimise the Bl phytase for potential industrial use.

7 Final Discussion

This thesis provides insights into the enzymes belonging to the HAP class of phytases. Such enzymes are of interest to the industry of the animal feed. Phytases degrade phytate, a substance comprising an inositol ring with six phospho groups. Phytate is highly abundant in plant based animal feed and is indigestible by monogastric animals. Hence, addition of phytases as a supplement to the animal feed allows the animal to access the phosphate stored in the phytate molecule, and brings about several economic and environmental benefits as discussed in Chapter 1, the Introduction.

7.1 Final discussion of Chapter 2

In Chapter 2, experiments were described that were performed to elucidate the general characteristics of the enzymes from the bacteria *Bacteroides thetaiotaomicron (Bt), Bifidobacterium infantis* subsp. longum *(Bl)* and *Bifidobacterium pseudocatenulatum (Bp)* and compare them to the commercial phytase Quantum Blue (QB), to lay foundations for the search of a viable candidate phytase for future, more detailed characterisations and potential optimisations with the commercial use for the industry of the animal feed in mind.

Experiments conducted using the phosphate release assay tested the phytases for their activity at a range of pH from pH 2 to pH 9. They showed the QB enzyme to be most active at pH 3, which reflects the pH present in the first stages of the digestive tract of swine and poultry, which are the target of the commercial phytases. The wild-type enzymes showed peak activity at pH 3.5 for *Bt,* 4.5 for *Bl* and a plateau of pH 5-6 for *Bp.* Of these, only *Bt* would retain 100 % of its activity in the acidic environment of the crop and proventriculus in poultry or stomach of swine. However, for it to be an appropriate candidate for commercial enzyme development, it needs to show other qualities, such as a wide optimal temperature of reaction, retaining activity during and after exposure to high temperatures or being resistant to proteases (Menezes-Blackburn, Gabler and Greiner, 2015).

Resistance to incubation temperatures was tested to investigate thermostability of the phytases, which has implications in the high-temperature pelleting process in manufacturing the phytase supplements. The ideal commercial phytase must retain its ability to reach its full activity after exposure to the pelleting temperatures of over 90°C. Using the phosphate release assay, a range of temperatures from 30 °C to 95 °C was used for incubation for 30 min, before assaying the remaining activity of the enzymes. The three wild-type enzymes Bt, Bl and Bp clearly show a lower optimal temperature of activity than QB at pH 7. Their peaks were at 47.3 °C, 49.6 °C and 46 °C respectively, which places their optima in a similar range, perhaps reflecting the close similarity of their structures. *Bt*Minpp, *Bl*Minpp and *Bt*Minpp share a catalytic pocket lined with basic residues, substitution of which with acidic residues reduces activity in *Bt*Minpp (Li, 2014). While it is difficult, here, to separate pH influences on enzyme activity from thermal stability, increase of pH from 3.5 to 7 seemed to sharpen the thermal stability profile of Bt in particular.

Arguably, temperature profiles of activity at pH 5-5.5 could have been performed instead. The reason being, Bl and Bp showed pH optima at pH 4.5 and as a plateau at the range of pH 4-9, respectively, therefore it could be argued that the temperature assay should be conducted to include these pH's. However, I chose the assay to be carried out at pH 3.5 and 7.0 to have a larger range of investigation as well as to reflect the conditions in the animal gut. However, in the future it would perhaps be beneficial to include the pH 5.5 to reflect the traditional conditions of assaying phytases and to increase the scope of investigation.

Enzyme kinetics experiments were performed to gain an understanding of their performance characteristics *in vitro* and fit the data to the Michaelis-Menten model. Traditionally, such experiments are conducted by monitoring substrate consumption or product accumulation in real-time, however no such assay was available at the time. Instead, the colourimetric phosphate release assay was utilised as the conventional assay for phytase activity, which provides an end-point reaction to the assay. Hence, absorbance changes after a 30 min reaction was used for each concentration of substrate. The limitation of this technique is that *in vitro* the reaction is carried out with very little chemical additions, i.e. only in the presence of a buffering agent and any possible impurities, while it is common that the commercial formulations include additions such as

Ca2+, as monocalcium phosphate or limestone to animal feedstuff, while *in vivo* the presence of physiological (1mM) Mg^{2+} can affect phytate solubility (Veiga et al., 2014). The Km value of QB at pH 5.0 was found to be 561.9 µM in my experiment, however it has been previously published as 142 µM (Menezes-Blackburn, Gabler and Greiner, 2015). The discrepancy in the experimental values from this work and the literature may stem from differences in assay conditions, such as the nature and concentration of the buffer used, storage conditions of the enzymes prior to the experiment, the method of phosphate detection or intrinsic variations of the detector. Furthermore, the Km of *Bp* was found to be 841.1 µM and that of *Bt* was 2311.5 µM, pointing to lower affinity to IP6 as compared to QB. This is consistent with the fact that they are wild-type phytases and that it is likely that QB was engineered and optimised for higher activity against IP6.

The enzymes industry and especially animal feed industry are interested in the melting temperatures of enzymes to consider the optimal conditions for the pelleting processes in addition to considerations for processing, transportation, storage and application. Furthermore, thermostability is often correlated with protease resistance, another desirable characteristic in industrial enzymes (Yao *et al.*, 2012; Niu *et al.*, 2017). Thermostability measurements were performed using differential scanning calorimetry (DSF). This method was chosen due to the low amounts of protein required (about 10 µg of enzyme per reaction) its speed and efficiency, however a downside was that it uses a fluorescent probe that binds to the hydrophobic residues of the protein, possibly altering the protein's unfolding behaviour. However, the same protocol was applied to the three wild type phytases and the Quantum Blue, allowing for an effective comparison tool to investigate the nature of thermal unfolding of these enzymes and is a common tool in the industry (Niesen, 2007). As expected the wild-type enzymes exhibited pointedly lower temperature of unfolding compared to Quantum Blue, which demonstrates significant changes to the original *E.coli* phytase from which QB was derived. In general, the wild-type enzymes unfolded at around 30-45 °C, while QB unfolded at around 81-84 °C. Interestingly, addition of a range of 0.5-2.0 mM substrate IP_6 to the wild-type enzymes produced an almost linear increase in thermostability, the same effect was largely absent from the QB experiment. This suggests active site stabilisation upon substrate binding which translates to an increase in thermostability in the wild-type enzymes, which has been demonstrated in literature before (Citri and Garber, 1963; Griessler *et al.*, 2000;

Lejeune *et al.*, 2001). The same changes were absent from QB, which may suggest that it was subjected to site-directed mutagenesis in order to simulate the intramolecular interactions stabilising the active site to mimic substrate binding. On the other hand, it is possible that the substrate stabilisation demonstrated in this chapter is unique to the HAE phytases, despite them sharing a common α + αβ fold structure with the HD phytases (Rigden, 2008; Stentz *et al.*, 2014). A future direction would be to conduct the same experiment using a wild-type HD phytase to gain insight into the possible forces affecting thermostability in these enzymes.

For further insight into the thermostability of the wild-type phytases described in this thesis, I used reducing and oxidising conditions to verify potential existence of disulphide bridges in my proteins. Using the reducing agent dithiothreitol (DTT) and its oxidised form trans-4,5-Dihydroxy-1,2-dithiane, I aimed to reduce any potential disulphides and as a result see a difference in the thermostability on DSF. Confirmation of existing disulphide bridges is crucial for understanding the behaviour of the protein at high temperatures and may have an impact on the future investigations and protein engineering.

Anaerobic bacteria, which include *Bifidobacterium longum* (Schell *et al.*, 2002) and *Bacteroides thetaiotaomicron* (Xu, 2003), are typically active at negative (low) redox potentials (Sun, Ding and Peterson, 2013, p. 184). While the reducing agent used in the above experiments is known to undergo oxidation by air (Sigma-Aldrich user manual), which may have impacted the results, it is clear that oxidising conditions increase the unfolding temperature of the HAE phytases (Minpps) studied here. The reducing capacity of DTT increases with pH above pH 7 and is quenched at pH below 3.0 (Lukesh, Palte and Raines, 2012; Wingfield, 2016).

Wang et al. (Wang, Meng and Zhou, 2004) showed that the *Aspergillus niger* phytase lost its thermostability and catalytic activity in the presence of 2 mM DTT. This phytase contains five pairs of disulphide-forming cysteines, strongly suggesting the role of disulphides in the catalytic and structural properties of this phytase.

Singh et al. (Singh and Satyanarayana, 2009) characterised the HAP phytase from Sporotrichum thermophile, a thermophilic fungus. They showed a small effect of DTT on the catalytic activity, which decreased to 97.97 % and 92.89 % with 1 mM and 5 mM DTT,

respectively. The authors concluded that the enzyme most likely has no free sulfhydryls, or if any are present, they play a negligible role in the catalysis. Here, the lowered thermostability of the enzymes in reducing conditions suggests presence of disulphide-forming cysteines, which upon reduction break the disulphide bridge, destabilising the enzyme and lowering the temperature of unfolding.

7.2 Final discussion of Chapter 3

Analysing product profiles of phytases can provide insight into the structure of their active sites and into substrate specificity (Stentz *et al.*, 2014). The particular method of high performance liquid chromatography (HLPC) described in this chapter is suitable for separating and identifying peaks of IP6, IP5, IP4 and IP3 with high resolution, while peaks of IP2, IP1 and Pi have low resolution or coelute with the solvent front (Blaabjerg, Hansen-Møller and Poulsen, 2010). Analyses of the type described in this chapter have been used to characterize the sites in the digestive tract of non-ruminants in which phytate is degraded by adjunct phytases added to feed (Zeller, Schollenberger, Kühn, et al., 2015a; Zeller, Schollenberger, Witzig, et al., 2015; Zeller et al., 2016), and can be compared with phytate degradation by *in vitro* models of intestinal phytate degradation (Briviba et al., 2017), or by recombinant protein. In Chapter 3, HPLC was performed to identify and quantify the different products of substrate (phytate) degradation by the phytases with the aims to gain insight into the nature of the products of dephosphorylation of the wild-type HAE class *Bt, Bl* and *Bt* phytases in comparison to the commercial QB phytase of the HD class, which carries implications towards its uses in animal nutrition.

Interesting differences were found between the bacterial phytases. In summary, this chapter shows product profiles of reactions of the Gram-negative Minpp phytase from *Bacteroides thetaiotaomicron* and the Gram-positive *Bifidobacteria infantis* and *Bifidobacteria pseudocatenulatum.* Differences are noted between the identities of the products of phytate degradation by the Gram-negative and the Gram-positive bacteria, as different IP_4 products are accumulated to a different extent. At the same time, the commercial phytase Quantum Blue was shown to accumulate predominantly one particular IP_4 ($Ins(2,3,4,5)P_4$). Hence, the work described here suggests that bacterial Minpp's follow several pathways of phytate degradation, while the Quantum Blue enzyme derived from *E.coli* follows one

pathway with a particular preference. The interests in the gut bacterial phytases lie not only with the industry of the animal feed, but also with the potential for human nutrition. Currently, several members of the *Bifidobacterium* genus are commercially used as probiotics to supplement the human diets.

7.3 Final discussion of Chapter 4

Chapter 4 discusses mutagenesis and structural studies of the *Bifidobacterium infantis* subsp. longum (*Bl)* phytase in order to investigate its mechanism of action, as a representative example of the novel HAE class of phytases. This work shed light on the key residues taking part in substrate binding and catalysis in addition to protein domain motions accompanying the catalysis.

Successful substitution mutagenesis of the putative proton donor glutamate to glutamine of the *B. longum* phytase lead to obtaining the crystal structure of two different subunits, one of the intermediate state and one of the phosphate-bound state. The structure was refined to 1.7 A ˚ resolution, with R_{work} and R_{free} values of 14.7 % and 19.4 %, respectively. Putting the work in context of the work performed by other research group members (Li and Acquistapace, unpublished) allowed us to piece together the step-by-step mechanism of action of the *B.longum* MINPP. For further confirmation of the conformations utilised during the catalysis, it would be beneficial to conduct a structural NMR study, which along with crystallographic and computational techniques could validate the proposed mechanism of action (Agarwal *et al.*, 2016).

The *Bifidobacterium infantis* subsp. longum are a gram positive, obligate anaerobe species belonging to the *Actinomycetales* branch. In 2002, there were about 32 species of *Bifidobacteria* identified, with the vast majority isolated from the human gastro-intestinal tract (GIT). Together with *Bacteroides, Enterococci, Clostridia* and others, the *Bifidobacteria* create a complex microflora that is essential for healthy digestion and homeostasis of the human digestive system (reviewed in Schell *et al.*, 2002).

Decreased levels of *B. longum* have been shown in individuals suffering from a broad variety of illnesses such as the hepatitis B virus-related cirrhosis, cystic fibrosis and allergies (reviewed in Arboleya *et al.*, 2016) as well as malnutrition (Million, Diallo and Raoult, 2017). On the other hand, probiotic supplementations with *B. longum* have proven to be effective against a range of conditions such as ulcerative colitis and Crohn's disease (Plaza-Díaz *et al.*, 2017) and improving the brain function in humans (Pinto-Sanchez *et al.*, 2017; Wang *et al.*, 2016).

Using site-directed mutagenesis, I mutagenised the putative proton donor glutamate in order to create an inactive form of the enzyme. The premise was that such mutation could stop the turnover, and solving the crystal structure of any complex thus created could shed light on aspects of the catalytic mechanism of the enzyme. Alanine is commonly used in substitution mutations to abolish the function of a protein. However, I chose to substitute the glutamate with a glutamine residue. Glutamine bears closer resemblance in size and shape to glutamate than alanine, as it involves replacing the glutamate sidechain carboxyl group with the glutamine amide group. I hoped to preserve the general shape and conformation of the active site in order to provide a more accurate picture of the wild-type enzyme's behaviour in conjunction with substrate.

The structure of an active site mutant of the *B. longum* phytase, together with structures of the wild type enzyme in apo-form and in complex with a non-hydrolyzable substrate analogue, allowed me to determine the conformational changes associated with substrate binding and catalysis. This revealed the ~10 ° rotation of the alpha domain between the formation of the phosphohistidine intermediate and the release of the free inorganic phosphate. These changes lead to open and closed conformation depending on the stage of the catalytic cycle, presumably assisting the binding of substrate and intermediate and the release of product.

In the next stages of the project, a mutagenesis experiment could be carried out to substitute arginines 44, 48 and 142 with alanine residues. Enzymatic and X-ray structural characterization of such mutants would give a fuller elucidation the roles of the arginines in substrate binding and catalysis.

Further analysis of the hydrogen bond interactions in the active site of the Bl phytase, in particular of the *apo* and *holo* forms could elucidate the potential relationship between the active site interactions and the overall enzyme conformation.
It would be interesting to obtain crystal structures of other related MINPP phytases in various conformations and to conduct the domain motion analysis on them. Primarily, further investigation of the residues involved in Bl and Bt phytase hinge motions could potentially reveal similarities and identify conserved residues involved in domain motions.

7.4 Final discussion of Chapter 5

Chapter 5 continues the investigation of the active site mutant phytase, describing binding studies using novel fluorescent probes. Here, an assay has been developed that allows simple analysis of ligand/substrate binding to inositol polyphosphate phosphatases. This assay is applicable to the HAP phytases and is likely to be relevant to the cysteine and purple acid phosphatase phytases as well. It may perhaps be unsuitable for assaying members of the beta barrel phytase family, by virtue of the ability of these enzymes to cleave the phosphate on the axial 2-position. In general, the high catalytic activity of phytases and their simple transfer of phosphate to water (solvent) makes it likely that inactivation of the enzyme by active site mutagenesis will be necessary, as demonstrated here for use of the probe with HAP HAE phytases, for other classes of phosphatase. It is also possible to envisage the use of the probe with bi-substrate enzymes, such as inositol phosphate kinases (inositol phosphate : nucleotide phosphotransferases), which transfer phosphate between ATP and a free hydroxyl on an inositol phosphate substrate.

In summary, this chapter investigated the binding of substrates to the *Bl*Minpp E401Q mutant. By comparison to the wild-type enzyme, it was shown that IP_6 indeed binds to the mutant, and shows negligible turnover. This work validates the use of the E401Q active site mutant as a model for binding studies. Additionally, the mutant was used to study the binding of a range of IP_5 substrates of phytases. These results complement the product profiles obtained with HPLC, presented in Chapter 3, which show snapshots of the products present at different stages of inositol phosphate degradation.

Looking forward, the 2-FAM-IP_5 assay needs to be tested further with a larger selection of phytases at a wider range of pH. In the future of the project, rhodamine could be used as the IP_5-conjugated probe for displacement assays at pH 3.5. Rhodamine is a pH-insensitive versatile fluorescent probe with excitation wavelength of 552 nm and emission of 574 nm. Its use would enable similar experiments to be conducted at pH encountered in the gastro-intestinal tract to gain an insight into the substrate-binding properties of the mutant and by inference feed phytases at lower pH (Sridharan *et al.*, 2014). Rhodamine was not available in the lab during my experiment, however it would be a useful tool for further characterisation of the inert enzyme in the future.

7.5 Final discussion of Chapter 6

Chapter 6 focused on thermostability of a *Bifidobacterium longum* phytase and its cysteine mutants, to confirm the presence of the disulphide bridges and elucidate their role in the structure and activity of the enzyme. I described the process of site-directed mutagenesis to substitute cysteine residues with alanine residues and the reasoning behind introducing the specific mutations. In particular, three mutants were created: one double mutant for each of the two disulphides (mutants D1 and D2) and one quadruple mutant for both disulphides (mutant D1D2).

I carried out thermostability measurements, where I assayed phytase activity after incubation at a range of temperatures. Despite some variance between the triplicate measurements as reflected by the size of the standard deviation error bars, the activity of the four Bl variants generally shows a downward trend with the increase in incubation

temperature at the pH 3.5. At pH 5.5 the activity profiles reached a peak at 50-55 °C for the wild-type and the D2 mutant, while the D1 and D1D2 mutants peaked at 37 °C. Data for pH 7.4 shows large error bars, which would need to be addressed in the future. Here, the activity appears to peak at around 30-37 °C.

The double mutant D1D2 showed the lowest activity profile after incubation at a range of temperatures. Its protein expression yield was the lowest of the four Bl variants, which may be correlated with low overall stability. The disparity between the two single disulphide mutants may be related to each disulphide residing in different folds of the protein – disulphide D1 is located in the alpha domain, while disulphide D2 is located in the alpha/beta domain.

Differential scanning calorimetry (DSC) was conducted to examine the melting temperature (Tm) that reflects the thermally induced structural transitions of proteins in solution. It is a powerful technique, used in the industry to predict shelf lives of products, develop purification strategies and characterise and evaluate proteins, lipids and pharmaceuticals. Most of all, it enables the study of folding and unfolding without the need to label the proteins. Thus, this technique allows proteins to be examined in as close to their natural state as possible, giving a reliable estimate of its temperature of unfolding (Morar-Mitrica, Nesta and Crotts, 2013).

The DSC experiments revealed that the D1 disulphide is crucial for thermostability of the enzyme while the D2 disulphide seems to have an insignificant effect on the thermostability of the enzyme, as shown by cysteine knockout mutations. The double mutant D1D2 appeared to have the similar thermostability as the D1 mutant, suggesting no additive effects of the double cysteine knockout. Despite the lack of evidence for altered thermostability in the variants without the D2 disulphide, the phytase activity assays revealed the D1D2 mutant to have lowest activity after incubation at a range of temperatures. This may suggest that the double mutant does play an important role in stabilising the structure of the enzyme enough to carry out catalysis after exposure to higher temperatures. Future directions would include optimisation of overexpression conditions for the mutant phytases, as the expression levels presented in this thesis were too low to allow sufficient numbers of replicate measurements using the DSC technique.

Furthermore, molecular dynamics simulations were performed to elucidate the flexible regions of the protein as it unfolds with the increasing temperature, and provided further evidence for the disulphides playing a stabilising role in the protein structure.

7.6 Final conclusions

One of the key findings of this thesis is providing more evidence towards the theory that Minpp phytases use glutamate as the proton donor in the catalytic mechanism. This is in contrast to the well-characterised commercial phytases, that instead use an aspartate residue for proton donation. Interesting findings from the enzymatic assays, high performance liquid chromatography and thermostability experiments lay the foundations for potential future optimisation of the phytases for use by the industry of the animal feed.

Bacterial phytases have a promising future in the industry of the animal feed, in general showing affinity for a broader substrate range and showing higher proteolysis resistance (Greiner and Farouk, 2007; Adeola and Cowieson, 2011). Paired with the increased interest from the probiotics industry, bacterial phytases are an interesting target of future research into their use in both animal feed and human nutrition industries.

8 Bibliography

Abelson, P. H. (1999) 'A potential phosphate crisis.', *Science (New York, N.Y.)*, 283(5410), p. 2015. Available at: http://www.ncbi.nlm.nih.gov/pubmed/10206902.

Adams, P. D., Afonine, P. V, Bunkóczi, G., Chen, V. B., Davis, I. W., Echols, N., Headd, J. J., Hung, L.-W., Kapral, G. J., Grosse-Kunstleve, R. W., McCoy, A. J., Moriarty, N. W., Oeffner, R., Read, R. J., Richardson, D. C., Richardson, J. S., Terwilliger, T. C. and Zwart, P. H. (2010) 'PHENIX: a comprehensive Python-based system for macromolecular structure solution', *Acta Crystallographica Section D*, 66(2), pp. 213–221. doi: 10.1107/S0907444909052925.

Adeola, O. and Cowieson, a J. (2011) 'Opportunities and challenges in using exogenous enzymes to improve nonruminant animal production.', *Journal of Animal Science*, 89(10), pp. 3189–218. doi: 10.2527/jas.2010-3715.

Agarwal, P. K., Doucet, N., Chennubhotla, C., Ramanathan, A. and Narayanan, C. (2016) 'Conformational Sub-states and Populations in Enzyme Catalysis', (865), pp. 273–297. doi: 10.1016/bs.mie.2016.05.023.

Agranoff, B. W. (2009) 'Turtles all the way: Reflections on myo-inositol', *Journal of Biological Chemistry*, 284(32), pp. 21121–21126. doi: 10.1074/jbc.X109.004747.

Anderson, R. J. (1915) 'The hydrolysis of phytin by the enzyme phytase contained in wheat bran.', *The Journal of Biological Chemistry*, 20, p. 475.

De Angelis, M. (2003) 'Phytase activity in sourdough lactic acid bacteria: purification and characterization of a phytase from Lactobacillus sanfranciscensis CB1', *International Journal of Food Microbiology*, 87(3), pp. 259–270. doi: 10.1016/S0168-1605(03)00072-2.

Angyal (1989) 'Numbering of atoms in myo-inositol: Recommendations 1988', *European Journal of Biochemistry*, 180(3), pp. 485–486. doi: 10.1111/j.1432-1033.1989.tb14672.x.

Arboleya, S., Stanton, C., Ryan, C. A., Dempsey, E. and Ross, P. R. (2016) 'Bosom Buddies: The Symbiotic Relationship Between Infants and *Bifidobacterium longum* ssp. *longum* and ssp. *infantis* . Genetic and Probiotic Features', *Annual Review of Food Science and Technology*, 7(1), pp. 1–21. doi: 10.1146/annurev-food-041715-033151.

Ariza, A., Moroz, O. V., Blagova, E. V., Turkenburg, J. P., Waterman, J., Roberts, S. M., Vind, J., Sjøholm, C., Lassen, S. F., De Maria, L., Glitsoe, V., Skov, L. K. and Wilson, K. S. (2013) 'Degradation of phytate by the 6-phytase from Hafnia alvei: a combined structural and solution study.', *PLoS ONE*, 8(5), p. e65062. doi: 10.1371/journal.pone.0065062.

Arkin, M. and Lear, J. D. (2001) 'A New Data Analysis Method to Determine Binding Constants of Small Molecules Using Equilibrium Analytical Ultracentrifugation with Absorption Optics', *Anal. Biochem.*, 299, pp. 98–107. doi: 10.1006/abio.2001.5396.

Azeke, M. A., Egielewa, S. J., Eigbogbo, M. U. and Ihimire, I. G. (2011) 'Effect of germination on the phytase activity, phytate and total phosphorus contents of rice (Oryza sativa), maize (Zea mays), millet (Panicum miliaceum), sorghum (Sorghum bicolor) and wheat (Triticum aestivum)', *Journal of Food Science and Technology*, 48(6), pp. 724–729. doi: 10.1007/s13197-010-0186-y.

Bae, H. D., Yanke, L. J., Cheng, K. J. and Selinger, L. B. (1999) 'A novel staining method for detecting phytase

activity', *Journal of Microbiological Methods*, 39(1), pp. 17–22. doi: 10.1016/S0167-7012(99)00096-2.
Balbo, A. and Schuck, P. (2005) 'Analytical ultracentrifugation in the study of protein self-association and heterogeneous protein-protein interactions', *Protein-Protein Interactions(E Golemis and …*, (301), pp. 253–277.
Barrientos, L., Scott, J. J. and Murthy, P. P. (1994) 'Specificity of hydrolysis of phytic acid by alkaline phytase from lily pollen.', *Plant physiology*, 106(4), pp. 1489–1495. doi: 10.1104/pp.106.4.1489.
Benítez-Páez, A., Moreno, F. J., Sanz, M. L. and Sanz, Y. (2016) 'Genome Structure of the Symbiont Bifidobacterium pseudocatenulatum CECT 7765 and Gene Expression Profiling in Response to Lactulose-Derived Oligosaccharides', *Frontiers in Microbiology*, 7. doi: 10.3389/fmicb.2016.00624.
Berrow, N. S., Alderton, D., Sainsbury, S., Nettleship, J., Assenberg, R., Rahman, N., Stuart, D. I. and Owens, R. J. (2007) 'A versatile ligation-independent cloning method suitable for high-throughput expression screening applications', *Nucleic Acids Research*, 35(6). doi: 10.1093/nar/gkm047.
Bisswanger, H. (2014) 'Enzyme assays', *Perspectives in Science*. Elsevier, 1(1–6), pp. 41–55. doi: 10.1016/j.pisc.2014.02.005.
Blaabjerg, K., Hansen-Møller, J. and Poulsen, H. D. (2010) 'High-performance ion chromatography method for separation and quantification of inositol phosphates in diets and digesta', *Journal of Chromatography B: Analytical Technologies in the Biomedical and Life Sciences*, 878(3–4), pp. 347–354. doi: 10.1016/j.jchromb.2009.11.046.
Böhm, K., Herter, T., Müller, J. J., Borriss, R. and Heinemann, U. (2010) 'Crystal structure of Klebsiella sp. ASR1 phytase suggests substrate binding to a preformed active site that meets the requirements of a plant rhizosphere enzyme', *FEBS Journal*, 277(5), pp. 1284–1296. doi: 10.1111/j.1742-4658.2010.07559.x.
Bohn, L., Meyer, A. S. and Rasmussen, S. K. (2008) 'Phytate: impact on environment and human nutrition. A challenge for molecular breeding', *Journal of Zhejiang University SCIENCE B*, 9(3), pp. 165–191. doi: 10.1631/jzus.B0710640.
Bolzani, R., Ruggeri, F. and Olivo, O. M. (1979) 'Average normal temperature of the chicken in the morning and after 1-2 days of fasting.', *Bollettino della Società italiana di biologia sperimentale*, 55(16), pp. 1618–22. Available at: http://www.ncbi.nlm.nih.gov/pubmed/576010.
Brearley, C. a and Hanke, D. E. (1996) 'Metabolic evidence for the order of addition of individual phosphate esters in the myo-inositol moiety of inositol hexakisphosphate in the duckweed Spirodela polyrhiza L.', *The Biochemical journal*, 314 (Pt 1, pp. 227–233.
BRENDA. The Comprehensive Enzyme Information System (2017) *Phytase*. Available at: https://www.brenda-enzymes.org/search_result.php?quicksearch=1&noOfResults=10&a=9&W[2]=phytase&T[2]=2.
Brenner, D. M. and Chey, W. D. (2009) 'Bifidobacterium infantis 35624: a novel probiotic for the treatment of irritable bowel syndrome.', *Reviews in gastroenterological disorders*, 9(1), pp. 7–15. Available at: http://www.ncbi.nlm.nih.gov/pubmed/19367213.
Briviba, K., Schollenberger, M., Rodehutscord, M. and Greiner, R. (2017) 'Dephosphorylation of myo -inositol phosphates in the in vitro intestinal Caco-2 cell model', *International Journal of Food Sciences and Nutrition*. Taylor & Francis, 0(0), pp. 1–6. doi: 10.1080/09637486.2017.1330404.
Bruder, L. M., Gruninger, R. J., Cleland, C. P. and Mosimann, S. C. (2017) 'Bacterial protein tyrosine

phosphatase-like *myo* -inositol phosphatases, PhyA, in complex with the Ins(1,3,4,5)P_4 and Ins(1,4,5)P_3 second messengers', *Journal of Biological Chemistry*, (10), p. jbc.M117.787853. doi: 10.1074/jbc.M117.787853.

Buckle, K. A. (1986) 'The characteristics of soybean phytase', *Journal of Food Biochemistry*, 10(3), pp. 197–216. doi: 10.1111/j.1745-4514.1986.tb00100.x.

Caffrey, J. J., Hidaka, K., Matsuda, M., Hirata, M. and Shears, S. B. (1999) 'The human and rat forms of multiple inositol polyphosphate phosphatase: Functional homology with a histidine acid phosphatase up-regulated during endochondral ossification', *FEBS Letters*, 442(1), pp. 99–104. doi: 10.1016/S0014-5793(98)01636-6.

Chakraborty, S., Ásgeirsson, B. and Rao, B. J. (2012) 'A Measure of the Broad Substrate Specificity of Enzymes Based on "Duplicate" Catalytic Residues', *PLoS ONE*, 7(11), pp. 1–10. doi: 10.1371/journal.pone.0049313.

Chen, Y., Jakoncic, J., Parker, K. A., Carpino, N. and Nassar, N. (2009) 'Structures of the phosphorylated and VO3-bound 2H-phosphatase domain of Sts-2', *Biochemistry*, 48(34), pp. 8129–8135. doi: 10.1021/bi9008648.

Cheng, C., Wong, K.-B. and Lim, B. L. (2007) 'The effect of disulfide bond on the conformational stability and catalytic activity of beta-propeller phytase.', *Protein and peptide letters*, 14(2), pp. 175–83. doi: 10.2174/092986607779816069.

Chi, H., Tiller, G. E., Dasouki, M. J., Romano, P. R., Wang, J., O'keefe, R. J., Puzas, J. E., Rosier, R. N. and Reynolds, P. R. (1999) 'Multiple inositol polyphosphate phosphatase: evolution as a distinct group within the histidine phosphatase family and chromosomal localization of the human and mouse genes to chromosomes 10q23 and 19.', *Genomics*, 56(3), pp. 324–336. doi: 10.1006/geno.1998.5736.

Chi, H., Yang, X., Kingsley, P. D., O'Keefe, R. J., Puzas, J. E., Rosier, R. N., Shears, S. B. and Reynolds, P. R. (2000) 'Targeted Deletion of Minpp1 Provides New Insight into the Activity of Multiple Inositol Polyphosphate Phosphatase In Vivo', *Molecular and Cellular Biology*, 20(17), pp. 6496–507. doi: 10.1128/MCB.20.17.6496-6507.2000.

Cho, J., Choi, K., Darden, T., Reynolds, P. R., Petitte, J. N. and Shears, S. B. (2006) 'Avian multiple inositol polyphosphate phosphatase is an active phytase that can be engineered to help ameliorate the planet's "phosphate crisis"', *Journal of Biotechnology*, 126(2), pp. 248–259. doi: 10.1016/j.jbiotec.2006.04.028.

Cho, J., King, J. S., Qian, X., Harwood, A. J. and Shears, S. B. (2008) 'Dephosphorylation of 2,3-bisphosphoglycerate by MIPP expands the regulatory capacity of the Rapoport-Luebering glycolytic shunt.', *Proceedings of the National Academy of Sciences of the United States of America*, 105(16), pp. 5998–6003. doi: 10.1073/pnas.0710980105.

Chu, H. M., Guo, R. T., Lin, T. W., Chou, C. C., Shr, H. L., Lai, H. L., Tang, T. Y., Cheng, K. J., Selinger, B. L. and Wang, A. H. J. (2004) 'Structures of Selenomonas ruminantium phytase in complex with persulfated phytate: DSP phytase fold and mechanism for sequential substrate hydrolysis', *Structure*, 12(11), pp. 2015–2024. doi: 10.1016/j.str.2004.08.010.

Citri, N. and Garber, N. (1963) 'The interaction of penicillinase with penicillins', *Biochimica et Biophysica Acta (BBA) - Specialized Section on Enzymological Subjects*, 67(19 65), pp. 64–72. doi: 10.1016/0926-6569(63)90208-6.

Cordell, D. and White, S. (2011) 'Peak phosphorus: Clarifying the key issues of a vigorous debate about long-term phosphorus security', *Sustainability*, 3(10), pp. 2027–2049. doi: 10.3390/su3102027.
Cosgrove, D. J., Irving, G. C. J. and Bromfield, S. M. (1970) 'Inositol phosphate phosphatases of microbiological origin. The isolation of soil bacteria having inositol phosphate phosphatase activity', *Australian Journal of Biological Sciences*, 23(2), pp. 339–344. doi: 10.1071/BI9700339.
Davies, D. R., Interthal, H., Champoux, J. J. and Hol, W. G. J. (2002) 'Insights into substrate binding and catalytic mechanism of human tyrosyl-DNA phosphodiesterase (Tdp1) from vanadate and tungstate-inhibited structures.', *Journal of molecular biology*. England, 324(5), pp. 917–932.
Denu, J. M. and Dixon, J. E. (1998) 'Protein tyrosine phosphatases: mechanisms of catalysis and regulation', *Curr Opin Chem Biol*, 2(5), pp. 633–641. doi: 10.1016/S1367-5931(98)80095-1.
Ding, Z., Rossi, A. M., Riley, A. M., Rahman, T., Potter, B. V. L. and Taylor, C. W. (2010) 'Binding of Inositol 1 , 4 , 5-trisphosphate (IP3) and Adenophostin A to the N-Terminal region of the IP 3 Receptor : Thermodynamic Analysis Using Fluorescence Polarization with a Novel IP 3 Receptor Ligand', *Molecular pharmacology*, 77(6), pp. 995–1004. doi: 10.1124/mol.109.062596.
Dionisio, G., Holm, P. B. and Brinch-Pedersen, H. (2007) 'Wheat (Triticum aestivum L.) and barley (Hordeum vulgare L.) multiple inositol polyphosphate phosphatases (MINPPs) are phytases expressed during grain filling and germination', *Plant Biotechnology Journal*, 5(2), pp. 325–338. doi: 10.1111/j.1467-7652.2007.00244.x.
Dionisio, G., Madsen, C. K., Holm, P. B., Welinder, K. G., Jorgensen, M., Stoger, E., Arcalis, E. and Brinch-Pedersen, H. (2011) 'Cloning and Characterization of Purple Acid Phosphatase Phytases from Wheat, Barley, Maize, and Rice', *PLANT PHYSIOLOGY*, 156(3), pp. 1087–1100. doi: 10.1104/pp.110.164756.
Dombkowski, A. A., Sultana, K. Z. and Craig, D. B. (2014) 'Protein disulfide engineering', *FEBS Letters*. Federation of European Biochemical Societies, 588(2), pp. 206–212. doi: 10.1016/j.febslet.2013.11.024.
Durowoju, I. B., Bhandal, K. S., Hu, J., Carpick, B. and Kirkitadze, M. (2017) 'Differential Scanning Calorimetry; A Method for Assessing the Thermal Stability and Conformation of Protein Antigen', *Journal of Visualized Experiments*, (121). doi: 10.3791/55262.
Eeckhout, W. and De Paepe, M. (1994) 'Total phosphorus, phytate-phosphorus and phytase activity in plant feedstuffs', *Animal Feed Science and Technology*, 47(1–2), pp. 19–29. doi: 10.1016/0377-8401(94)90156-2.
Eichinger, L., Pachebat, J. A., Glöckner, G., Rajandream, M.-A., Sucgang, R., Berriman, M., Song, J., Olsen, R., Szafranski, K., Xu, Q., Tunggal, B., Kummerfeld, S., Madera, M., Konfortov, B. A., Rivero, F., Bankier, A. T., Lehmann, R., Hamlin, N., Davies, R., *et al.* (2005) 'The genome of the social amoeba Dictyostelium discoideum', *Nature*, 435(7038), pp. 43–57. doi: 10.1038/nature03481.
Ellestad, L. E., Angel, R. and Soares, J. H. (2002) 'Intestinal phytase II: A comparison of activity and in vivo phytate hydrolysis in three teleost species with differing digestive strategies', *Fish Physiology and Biochemistry*, 26(3), pp. 259–273. doi: 10.1023/A:1026231624543.
Van Etten, R. L., Davidson, R., Stevis, P. E., MacArthur, H. and Moore, D. L. (1991) 'Covalent structure, disulfide bonding, and identification of reactive surface and active site residues of human prostatic acid phosphatase', *Journal of Biological Chemistry*, 266(4), pp. 2313–2319.
Falconer, R. J. (2016) 'Applications of isothermal titration calorimetry ??? the research and technical developments from 2011 to 2015', *Journal of Molecular Recognition*, (May), pp. 504–515. doi:

10.1002/jmr.2550.

Fathallh Eida, M., Nagaoka, T., Wasaki, J. and Kouno, K. (2013) 'Phytate Degradation by Fungi and Bacteria that Inhabit Sawdust and Coffee Residue Composts', *Microbes and Environments*, 28(1), pp. 71–80. doi: 10.1264/jsme2.ME12083.

Fei, B., Xu, H., Zhang, F., Li, X., Ma, S., Cao, Y., Xie, J., Qiao, D. and Cao, Y. (2013) 'Relationship between Escherichia coli AppA phytase's thermostability and salt bridges', *Journal of Bioscience and Bioengineering*. Elsevier Ltd, 115(6), pp. 623–627. doi: 10.1016/j.jbiosc.2012.12.010.

Fontaínhas-Fernandes, A., Gomes, E., Reis-Henriques, M. A. and Coimbra, J. (1999) 'Replacement of Fish Meal by Plant Proteins in the Diet of Nile Tilapia: Digestibility and Growth Performance', *Aquaculture International*, 7(1), pp. 57–67. doi: 10.1023/A:1009296818443.

Fredua-Agyeman, M. and Gaisford, S. (2015) 'Comparative survival of commercial probiotic formulations: Tests in biorelevant gastric fluids and real-time measurements using microcalorimetry', *Beneficial Microbes*, 6(1), pp. 141–151. doi: 10.3920/BM2014.0051.

Fu, D., Li, Z., Huang, H., Yuan, T., Shi, P., Luo, H., Meng, K., Yang, P. and Yao, B. (2011) 'Catalytic efficiency of HAP phytases is determined by a key residue in close proximity to the active site', *Applied Microbiology and Biotechnology*, 90(4), pp. 1295–1302. doi: 10.1007/s00253-011-3171-0.

Fujita, J., Shigeta, S., Yamane, Y.-I., Fukuda, H., Kizaki, Y., Wakabayashi, S. and Ono, K. (2003) 'Production of Two Types of Phytase from Aspergillus oryzae during Industrial Koji Making', *Journal of Bioscience and Bioengineering*, 95(5), pp. 460–465. doi: 10.1263/jbb.95.460.

Gibson, D. M. and Ullah, A. H. J. (1988) 'Purification and characterization of acid phosphatase from cotyledons of germinating soybean seeds.', *Archives of biochemistry and biophysics*, 260(2), pp. 503–513. doi: 10.1016/0003-9861(88)90476-6.

Gilbert, N. (2009) 'Environment: The disappearing nutrient', *Nature*, 461(7265), pp. 716–718. doi: 10.1038/461716a.

Giles, C., Cade-Menun, B. and Hill, J. (2011) 'The inositol phosphates in soils and manures: Abundance, cycling, and measurement', *Canadian Journal of Soil Science*, 91(3), pp. 397–416. doi: 10.4141/cjss09090.

Glick, B. R., Pasternak, J. J. and Patten, C. L. (2010) *Molecular Biotechnology : Principles and Applications of Recombinant DNA*. 4th edn. American Society for Microbiology.

Goel, M. and Sharma, C. B. (1979) 'Multiple forms of phytase in germinating cotyledons of Cucurbita maxima', *Phytochemistry*, 18(12), pp. 1939–1942. doi: 10.1016/S0031-9422(00)82707-7.

Goldsmith, S. J. (1975) 'Radioimmunoassay: review of basic principles', *Semin Nucl Med*, 5(2), pp. 125–152. Available at: http://www.ncbi.nlm.nih.gov/pubmed/164695.

Greiner, R., Carlsson, N. and Larsson, M. (2000) 'Stereospecificity of myo -inositol hexakisphosphate dephosphorylation by a phytate-degrading enzyme of Escherichia coli', 84, pp. 53–62.

Greiner, R. and Egli, I. (2003) 'Determination of the activity of acidic phytate-degrading enzymes in cereal seeds', *Journal of Agricultural and Food Chemistry*, 51(4), pp. 847–850. doi: 10.1021/jf0204405.

Greiner, R. and Farouk, A. E. (2007) 'Purification and characterization of a bacterial phytase whose properties make it exceptionally useful as a feed supplement', *Protein Journal*, 26(7), pp. 467–474. doi: 10.1007/s10930-007-9086-z.

Greiner, R., Haller, E. and Konietzny, U. (1997) 'Purification and characterization of a phytase from Klebsiella

terrigena.', *Archives of Biochemistry and Biophysics*, 341(2), pp. 201–206. doi: 10.1006/abbi.1997.9942.
Greiner, R., Konietzny, U. and Jany, K. D. (1993) 'Purification and characterization of two phytases from Escherichia coli.', *Archives of biochemistry and biophysics*, pp. 107–113. doi: 10.1006/abbi.1993.1261.
Griessler, R., D'Auria, S., Tanfani, F. and Nidetzky, B. (2000) 'Thermal denaturation pathway of starch phosphorylase from Corynebacterium callunae: oxyanion binding provides the glue that efficiently stabilizes the dimer structure of the protein.', *Protein science : a publication of the Protein Society*, 9(6), pp. 1149–61. doi: 10.1110/ps.9.6.1149.
Gruninger, R. J., Thibault, J., Capeness, M. J., Till, R., Mosimann, S. C., Sockett, R. E., Selinger, B. L. and Lovering, A. L. (2014) 'Structural and biochemical analysis of a unique phosphatase from Bdellovibrio bacteriovorus reveals its structural and functional relationship with the protein tyrosine phosphatase class of phytase', *PLoS ONE*, 9(4). doi: 10.1371/journal.pone.0094403.
Gutteridge, A. and Thornton, J. (2004) 'Conformational change in substrate binding, catalysis and product release: An open and shut case?', *FEBS Letters*, 567(1), pp. 67–73. doi: 10.1016/j.febslet.2004.03.067.
György, H., József, K., Mihály, K. and Al., E. (2013) 'Spectrophotometry and protein concentration measurements', *Introduction to Practical Biochemistry*, pp. 42–59. doi: TÁMOP-4.1.2.A/1-11/1-2011-0073.
Ha, N. C., Oh, B. C., Shin, S., Kim, H. J., Oh, T. K., Kim, Y. O., Choi, K. Y. and Oh, B. H. (2000) 'Crystal structures of a novel, thermostable phytase in partially and fully calcium-loaded states.', *Nature structural biology*, 7(2), pp. 147–153. doi: 10.1038/72421.
Hammes, G. G. (2002) 'Multiple conformational changes in enzyme catalysis', *Biochemistry*, 41(26), pp. 8221–8228. doi: 10.1021/bi0260839.
Hammes, G. G., Chang, Y.-C. and Oas, T. G. (2009) 'Conformational selection or induced fit: A flux description of reaction mechanism', *Proceedings of the National Academy of Sciences*, 106(33), pp. 13737–13741. doi: 10.1073/pnas.0907195106.
Harland, B. F. and Morris, E. R. (1995) 'Phytate: A good or a bad food component?', *Nutrition Research*, pp. 733–754. doi: 10.1016/0271-5317(95)00040-P.
Haros, M., Bielecka, M., Honke, J. and Sanz, Y. (2007) 'Myo-inositol hexakisphosphate degradation by Bifidobacterium infantis ATCC 15697', *International Journal of Food Microbiology*, 117(1), pp. 76–84. doi: 10.1016/j.ijfoodmicro.2007.02.021.
Haros, M., Bielecka, M. and Sanz, Y. (2005) 'Phytase activity as a novel metabolic feature in Bifidobacterium', *FEMS Microbiology Letters*, 247(2), pp. 231–239. doi: 10.1016/j.femsle.2005.05.008.
Haros, M., Carlsson, N. G., Almgren, A., Larsson-Alminger, M., Sandberg, A. S. and Andlid, T. (2009) 'Phytate degradation by human gut isolated Bifidobacterium pseudocatenulatum ATCC27919 and its probiotic potential', *International Journal of Food Microbiology*, 135(1), pp. 7–14. doi: 10.1016/j.ijfoodmicro.2009.07.015.
Hart, E. B. and Tottingham, W. E. (1909) 'The nature of the acid soluble phosphorus compounds of some important feeding materials', *Journal of Biological Chemistry*, 6(5), pp. 431–444.
Hayes, J. E., Richardson, A. E. and Simpson, R. J. (1999) 'Phytase and acid phosphatase activities in extracts from roots of temperate pasture grass and legume seedlings', *Australian Journal of Plant Physiology*, 26(8), pp. 801–809. doi: 10.1071/PP99065.
Hayward, S. and Berendsen, H. J. (1998) 'Systematic analysis of domain motions in proteins from

conformational change: new results on citrate synthase and T4 lysozyme.', *Proteins*, 30(2), pp. 144–54. Available at: http://www.ncbi.nlm.nih.gov/pubmed/9489922.

Hayward, S. and Berendsen, H. J. C. (1998) *DynDom - Protein Domain Motion Analysis*. Available at: http://fizz.cmp.uea.ac.uk/dyndom/runDyndom.jsp.

Hegeman, C. E. and Grabau, E. A. (2001) 'A novel phytase with sequence similarity to purple acid phosphatases is expressed in cotyledons of germinating soybean seedlings.', *Plant physiology*, 126(4), pp. 1598–608. doi: 10.1104/pp.126.4.1598.

Hidaka, K., Kanematsu, T., Caffrey, J. J., Takeuchi, H., Shears, S. B. and Hirata, M. (2003) 'The importance to chondrocyte differentiation of changes in expression of the multiple inositol polyphosphate phosphatase', *Experimental Cell Research*, 290(2), pp. 254–264. doi: 10.1016/S0014-4827(03)00337-9.

Holm, P. B., Kristiansen, K. N. and Pedersen, H. B. (2002) 'Transgenic approaches in commonly consumed cereals to improve iron and zinc content and bioavailability', *Journal of Nutrition*, 132(3), p. 514s–516s.

Huang, H., Shi, P., Wang, Y., Luo, H., Shao, N., Wang, G., Yang, P. and Yao, B. (2009) 'Diversity of beta-propeller phytase genes in the intestinal contents of grass carp provides insight into the release of major phosphorus from phytate in nature', *Applied and Environmental Microbiology*, 75(6), pp. 1508–1516. doi: 10.1128/AEM.02188-08.

Huang, H., Zhang, R., Fu, D., Luo, J., Li, Z., Luo, H., Shi, P., Yang, P., Diao, Q. and Yao, B. (2011) 'Diversity, abundance and characterization of ruminal cysteine phytases suggest their important role in phytate degradation', *Environmental Microbiology*, 13(3), pp. 747–757. doi: 10.1111/j.1462-2920.2010.02379.x.

Huang, R. and Lau, B. L. T. (2016) 'Biomolecule-nanoparticle interactions: Elucidation of the thermodynamics by isothermal titration calorimetry', *Biochimica et Biophysica Acta - General Subjects*, 1860(5), pp. 945–956. doi: 10.1016/j.bbagen.2016.01.027.

Idriss, E. E., Makarewicz, O., Farouk, A., Rosner, K., Greiner, R., Bochow, H., Richter, T. and Borriss, R. (2002) 'Extracellular phytase activity of Bacillus amyloliquefaciens FZB45 contributes to its plant-growth-promoting effect', *Microbiology*, 148(7), pp. 2097–2109. doi: 10.1099/00221287-148-7-2097.

Ingram, D. L. and Legge, K. F. (1970) 'Variations in deep body temperature in the young unrestrained pig over the 24 hour period.', *The Journal of physiology*, 210(4), pp. 989–98. doi: 10.1113/jphysiol.1970.sp009253.

Iqbal, T. H., Lewis, K. O. and Cooper, B. T. (1994) 'Phytase activity in the human and rat small intestine.', *Gut*, 35(9), pp. 1233–1236. doi: 10.1136/gut.35.9.1233.

Irvine, R. F. and Schell, M. J. (2001) 'Back in the Water: the Return of The Inositol Phosphates', *Nature Reviews: Molecular Cell Biology*, 2(May), pp. 327–338. doi: 10.1038/35073015.

Irving, G. C. J. and Cosgrove, D. J. (1974) 'Inositol phosphate phosphatases of microbiological origin - Some properties of partially purified phosphatases of Aspergillus-ficuum NRRL-3135', *Australian Journal of Biological Sciences*, 27(4), pp. 361–368.

Ishikawa, K., Mihara, Y., Gondoh, K., Suzuki, E. and Asano, Y. (2000) 'X-ray structures of a novel acid phosphatase from Escherichia blattae and its complex with the transition-state analog molybdate.', *The EMBO journal*, 19(11), pp. 2412–2423. doi: 10.1093/emboj/19.11.2412.

Islam, S. U. (2016) 'Clinical Uses of Probiotics', *Medicine*, 95(5), p. e2658. doi: 10.1097/MD.0000000000002658.

'IUPAC-IUB Joint Commission on Biochemical Nomenclature (JCBN). Nomenclature and symbolism for amino acids and peptides. Recommendations 1983.' (1984) *European journal of biochemistry*, 138(1), pp. 9–37. Available at: http://www.ncbi.nlm.nih.gov/pubmed/6692818.

Jackson, S. and Duke, G. E. (1995) 'Intestine fullness influences feeding behaviour and crop filling in the domestic turkey', *Physiology and Behavior*, 58(5), pp. 1027–1034. doi: 10.1016/0031-9384(95)00151-8.

Jain, J., Sapna and Singh, B. (2016) 'Characteristics and biotechnological applications of bacterial phytases', *Process Biochemistry*. Elsevier Ltd, 51(2), pp. 159–169. doi: 10.1016/j.procbio.2015.12.004.

Jameson, D. M. (2011) 'Fluorescence Polarisation/Anisotropy in Diagnostics and Imaging', *Burns*, 110(5), pp. 2685–2708. doi: 10.1021/cr900267p.Fluorescence.

Jog, S. P., Garchow, B. G., Mehta, B. D. and Murthy, P. P. N. (2005) 'Alkaline phytase from lily pollen: Investigation of biochemical properties.', *Archives of biochemistry and biophysics*, 440(2), pp. 133–40. doi: 10.1016/j.abb.2005.05.029.

Johnson, C. M. (2013) 'Differential scanning calorimetry as a tool for protein folding and stability', *Archives of Biochemistry and Biophysics*, 531(1–2), pp. 100–109. doi: 10.1016/j.abb.2012.09.008.

Kalsi, H. K., Singh, R., Dhaliwal, H. S. and Kumar, V. (2016) 'Phytases from Enterobacter and Serratia species with desirable characteristics for food and feed applications', *3 Biotech*. Springer Berlin Heidelberg, 6(1), pp. 1–13. doi: 10.1007/s13205-016-0378-x.

Kapuscinski, J. (1995) 'DAPI: a DNA-specific fluorescent probe.', *Biotechnic & histochemistry : official publication of the Biological Stain Commission*, 70(5), pp. 220–33. doi: 10.3109/10520299509108199.

Kennefick, S. and Cashman, K. D. (2000) 'Inhibitory effect of wheat fibre extract on calcium absorption in Caco-2 cells: Evidence for a role of associated phytate rather than fibre per se', *European Journal of Nutrition*, 39(1), pp. 12–17. doi: 10.1007/s003940050071.

Kerovuo, J., Lauraeus, M., Nurminen, P., Kalkkinen, N. and Apajalahti, J. (1998) 'Isolation, characterization, molecular gene cloning, and sequencing of a novel phytase from Bacillus subtilis', *Applied and Environmental Microbiology*, 64(6), pp. 2079–2085.

Kerovuo, J., Ruovinen, J. and Hatzack, F. (2000) 'Analysis of myo-inositol hexakisphosphate hydrolysis by Bacillus phytase: indication of a novel reaction mechanism.', *Biochemical Journal*, 352, pp. 623–628. doi: 10.1042/0264-6021:3520623.

Khan, M. S. K., Siddique, M. A. M. and Zamal, H. (2013) 'Replacement of fish meal by plant protein sources in Nile tilapia (Oreochromis niloticus) diet: growth performance and utilization', *IFRO*, 12(4), p. 864–872 KW Rice polish KW mustard oil cake KW plan. Available at: http://jifro.ir/article-1-1345-en.html.

Kim, Y. O., Kim, H. K., Bae, K. S., Yu, J. H. and Oh, T. K. (1998) 'Purification and properties of a thermostable phytase from Bacillus sp. DS11', *Enzyme and Microbial Technology*, 22(1), pp. 2–7. doi: 10.1016/S0141-0229(97)00096-3.

Kim, Y. O., Lee, J. K., Kim, H. K., Yu, J. H. and Oh, T. K. (1998) 'Cloning of the thermostable phytase gene (phy) from Bacillus sp. DS11 and its overexpression in Escherichia coli', *FEMS Microbiology Letters*, 162(1), pp. 185–191. doi: 10.1016/S0378-1097(98)00119-0.

Kolozsvari, B., Parisi, F. and Saiardi, A. (2014) 'Inositol phosphates induce DAPI fluorescence shift.', *The Biochemical journal*, 460(3), pp. 377–85. doi: 10.1042/BJ20140237.

Kong, Y., Li, X., Ma, J., Li, W., Yan, G. and Zhang, C. (2014) 'GmPAP4, a novel purple acid phosphatase gene

isolated from soybean (Glycine max), enhanced extracellular phytate utilization in Arabidopsis thaliana', *Plant Cell Reports*, 33(4), pp. 655–667. doi: 10.1007/s00299-014-1588-5.

Konietzny, U. and Greiner, R. (2002) 'Molecular and catalytic properties of phytate-degrading enzymes (phytases)', *International Journal of Food Science and Technology*, pp. 791–812. doi: 10.1046/j.1365-2621.2002.00617.x.

Konietzny, U. and Greiner, R. (2004) 'Bacterial phytase: Potential application, in vivo function and regulation of its synthesis', *Brazilian Journal of Microbiology*, 35(1–2), pp. 11–18. doi: 10.1590/S1517-83822004000100002.

Koshland, D. E. (1963) 'Correlation of structure and function in enzyme action.', *Science (New York, N.Y.)*, 142(3599), pp. 1533–41. Available at: http://www.ncbi.nlm.nih.gov/pubmed/14075684.

Koshland, D. E. (1995) 'The Key–Lock Theory and the Induced Fit Theory', *Angewandte Chemie International Edition in English*, 33(23–24), pp. 2375–2378. doi: 10.1002/anie.199423751.

Kostrewa, D., Wyss, M., D'Arcy, A. and van Loon, A. P. G. . (1999) 'Crystal structure of Aspergillus niger pH 2.5 acid phosphatase at 2.4 Å resolution', *Journal of Molecular Biology*, 288(5), pp. 965–974. doi: 10.1006/jmbi.1999.2736.

Kumar, V., Sinha, A. K., Makkar, H. P. S. and Becker, K. (2010) 'Dietary roles of phytate and phytase in human nutrition: A review', *Food Chemistry*. Elsevier Ltd, 120(4), pp. 945–959. doi: 10.1016/j.foodchem.2009.11.052.

Kumar, V., Yadav, A. N., Verma, P., Sangwan, P., Saxena, A., Kumar, K. and Singh, B. (2017) 'β-Propeller phytases: Diversity, catalytic attributes, current developments and potential biotechnological applications', *International Journal of Biological Macromolecules*. Elsevier B.V., 98, pp. 595–609. doi: 10.1016/j.ijbiomac.2017.01.134.

Kushwaha, M. P. (2013) 'Replacement of fish meal by soybean (Glycine max) in the formulation of fish feed ingredients essential for Immunostimulation and growth performance of carps', *International Journal of Fauna and Biological Studies*, 1(2), pp. 35–38.

Laboure, a M., Gagnon, J. and Lescure, a M. (1993) 'Purification and characterization of a phytase (myo-inositol-hexakisphosphate phosphohydrolase) accumulated in maize (Zea mays) seedlings during germination.', *The Biochemical journal*, 295 (Pt 2, pp. 413–419.

Lacount, M. W., Handy, G. and Lebioda, L. (1998) 'Structural Origins of L (⅄) -Tartrate Inhibition of Human Prostatic Acid Phosphatase *', *Biochemistry*, 273(46), pp. 30406–30409.

Lakowicz, J. R. (2006) *Principles of Fluorescence Spectroscopy Principles of Fluorescence Spectroscopy*, *Principles of fluorescence spectroscopy, Springer, New York, USA, 3rd edn, 2006.* doi: 10.1007/978-0-387-46312-4.

Lan, G. Q., Abdullah, N., Jalaludin, S. and Ho, Y. W. (2011) 'Purification and characterization of a phytase from Mitsuokella jalaludinii, a bovine rumen bacterium', *African Journal of Biotechnology*, 10(59), pp. 12796–12806. doi: 10.5897/AJB11.294.

Lazali, M., Louadj, L., Ounane, G., Abadie, J., Amenc, L., Bargaz, A., Lullien-Pellerin, V. and Drevon, J. J. (2014) 'Localization of phytase transcripts in germinating seeds of the common bean (Phaseolus vulgaris L.)', *Planta*, 240(3), pp. 471–478. doi: 10.1007/s00425-014-2101-7.

Lebowitz, J., Lewis, M. S. and Schuck, P. (2002) 'Modern analytical ultracentrifugation in protein science: a

tutorial review.', *Protein science : a publication of the Protein Society*, 11(9), pp. 2067–2079. doi: 10.1110/ps.0207702.proaches.

Lee, D. C., Cottrill, M. A., Forsberg, C. W. and Jia, Z. (2003) 'Functional insights revealed by the crystal structures of Escherichia coli glucose-1-phosphatase', *Journal of Biological Chemistry*, 278(33), pp. 31412–31418. doi: 10.1074/jbc.M213154200.

Lee, S. A., Dunne, J., Mottram, T. and Bedford, M. R. (2017) 'Effect of diet phase change, dietary Ca and P level and phytase on bird performance and real-time gizzard pH measurements', *British Poultry Science*, 58(3), pp. 290–297. doi: 10.1080/00071668.2017.1293799.

Lei, X. G., Weaver, J. D., Mullaney, E., Ullah, A. H. and Azain, M. J. (2013) 'Phytase, a New Life for an "Old" Enzyme', *Annual Review of Animal Biosciences*, 1(1), pp. 283–309. doi: 10.1146/annurev-animal-031412-103717.

Lejeune, A., Vanhove, M., Lamotte-Brasseur, J., Pain, R. H., Frére, J. M. and Matagne, A. (2001) 'Quantitative analysis of the stabilization by substrate of Staphylococcus aureus PC1 α-lactamase', *Chemistry and Biology*, 8(8), pp. 831–842. doi: 10.1016/S1074-5521(01)00053-9.

Li, A. W. H. (2014) *Structure-function studies of multiple inositol polyphosphate phosphatases from gut commensal bacteria*. University of East Anglia.

Li, M., Osaki, M., Rao, I. M. and Tadano, T. (1997) 'Secretion of phytase from the roots of several plant species under phosphorus-deficient conditions', *Plant and Soil*, 195(1), pp. 161–169. doi: 10.1023/A:1004264002524.

Li, Z., Huang, H., Zhao, H., Meng, K., Zhao, J., Shi, P., Yang, P., Luo, H., Wang, Y. and Yao, B. (2014) 'Genetic diversity and expression profiles of cysteine phytases in the sheep rumen during a feeding cycle', *Letters in Applied Microbiology*, 59(6), pp. 615–620. doi: 10.1111/lam.12318.

Lim, B. L., Yeung, P., Cheng, C. and Hill, J. E. (2007) 'Distribution and diversity of phytate-mineralizing bacteria', *The ISME Journal*, pp. 321–330. doi: 10.1038/ismej.2007.40.

Lim, D., Golovan, S., Forsberg, C. W. and Jia, Z. (2000) 'Crystal structures of Escherichia coli phytase and its complex with phytate.', *Nature structural biology*, 7(2), pp. 108–113. doi: 10.1038/72371.

Lim, P. E. and Tate, M. E. (1971a) 'The phytases. I. Lysolecithin-activated phytase from wheat bran.', *Biochimica et biophysica acta*, 250(1), pp. 155–64. Available at: http://www.ncbi.nlm.nih.gov/pubmed/4334854.

Lim, P. E. and Tate, M. E. (1971b) 'The phytases. I. Lysolecithin-activated phytase from wheat bran.', *Biochimica et biophysica acta*, 250(1), pp. 155–64.

Lim, P. E. and Tate, M. E. (1973) 'Phytases. 2. Properties of phytase fractions F 1 and F 2 from wheat bran and the myoinositol phosphates produced by fraction F 2', *Biochimica et biophysica acta*, 302(2), pp. 316–328. doi: 10.1016/0005-2744(73)90160-5.

Lin, P.-H., Chen, R.-H., Lee, C.-H., Chang, Y., Chen, C.-S. and Chen, W.-Y. (2011) 'Studies of the binding mechanism between aptamers and thrombin by circular dichroism, surface plasmon resonance and isothermal titration calorimetry', *Colloids and Surfaces B: Biointerfaces*. Elsevier B.V., 88(2), pp. 552–558. doi: 10.1016/j.colsurfb.2011.07.032.

Lindqvist, Y., Schneider, G. and Vihko, P. (1994) 'Crystal structures of rat acid phosphatase complexed with the transition state analogs vanadate and molybdate: Implications for the reaction mechanism', *European*

Journal of Biochemistry, 221(1), pp. 139–142. doi: 10.1111/j.1432-1033.1994.tb18722.x.

Liu, B. L., Rafiq, A., Tzeng, Y. M. and Rob, A. (1998) 'The induction and characterization of phytase and beyond', *Enzyme and Microbial Technology*, 22(5), pp. 415–424. doi: 10.1016/S0141-0229(97)00210-X.

Liu, Q., Huang, Q., Lei, X. G. and Hao, Q. (2004) 'Crystallographic snapshots of Aspergillus fumigatus phytase, revealing its enzymatic dynamics', *Structure*, 12(9), pp. 1575–1583. doi: 10.1016/j.str.2004.06.015.

Lorenz, U. (2011) 'Protein Tyrosine Phosphatase Assays', *Curr Protoc Immunol.*, (434), pp. 1–14. doi: 10.1002/0471142735.im1107s93.Protein.

Madsen, C. K., Dionisio, G., Holme, I. B., Holm, P. B. and Brinch-Pedersen, H. (2013) 'High mature grain phytase activity in the Triticeae has evolved by duplication followed by neofunctionalization of the purple acid phosphatase phytase (PAPhy) gene', *Journal of Experimental Botany*, 64(11), pp. 3111–3123. doi: 10.1093/jxb/ert116.

Majumder, A. and Biswas, B. B. (2006) *Biology of Inositols and Phosphoinositides*, *PhD Proposal*. doi: 10.1017/CBO9781107415324.004.

Mandal, N. C., Burman, S. and Biswas, B. B. (1972) 'Isolation, purification and characterization of phytase from germinating mung beans', *Phytochemistry*, 11(2), pp. 495–502. doi: 10.1016/0031-9422(72)80003-7.

Mattarelli, P., Bonaparte, C., Pot, B. and Biavati, B. (2008) 'Proposal to reclassify the three biotypes of Bifidobacterium longum as three subspecies: Bifidobacterium longum subsp. longum subsp. nov., Bifidobacterium longum subsp. infantis comb. nov. and Bifidobacterium longum subsp. suis comb. nov.', *International journal of systematic and evolutionary microbiology*, 58(Pt 4), pp. 767–72. doi: 10.1099/ijs.0.65319-0.

Maugenest, S., Martinez, I. and Lescure, a M. (1997) 'Cloning and characterization of a cDNA encoding a maize seedling phytase.', *The Biochemical journal*, 322 (Pt 2, pp. 511–7.

McCoy, A. J., Grosse-Kunstleve, R. W., Adams, P. D., Winn, M. D., Storoni, L. C. and Read, R. J. (2007) 'Phaser crystallographic software.', *Journal of applied crystallography*, 40(Pt 4), pp. 658–674. doi: 10.1107/S0021889807021206.

Mehta, B. D., Jog, S. P., Johnson, S. C. and Murthy, P. P. N. (2006) 'Lily pollen alkaline phytase is a histidine phosphatase similar to mammalian multiple inositol polyphosphate phosphatase (MINPP)', *Phytochemistry*, 67(17), pp. 1874–1886. doi: 10.1016/j.phytochem.2006.06.008.

Menezes-Blackburn, D., Gabler, S. and Greiner, R. (2015) 'Performance of Seven Commercial Phytases in an in Vitro Simulation of Poultry Digestive Tract', *Journal of Agricultural and Food Chemistry*, 63(27), pp. 6142–6149. doi: 10.1021/acs.jafc.5b01996.

Miller, C. W. and Taylor, A. E. (1914) 'On reduction of ammonium molybdate in acid solution', *Journal of Biological Chemistry*, 17, p. 531.

Million, M., Diallo, A. and Raoult, D. (2017) 'Gut microbiota and malnutrition', *Microbial Pathogenesis*. Elsevier Ltd, 106, pp. 127–138. doi: 10.1016/j.micpath.2016.02.003.

Minch, M. J. (1999) 'An Introduction to Hydrogen Bonding', *Journal of Chemical Education*, 76(6), p. 759. doi: 10.1021/ed076p759.1.

Mocz, G. (2006) 'Information content of fluorescence polarization and anisotropy', *Journal of Fluorescence*, 16(4), pp. 511–524. doi: 10.1007/s10895-006-0095-7.

Morar-Mitrica, S., Nesta, D. and Crotts, G. (2013) 'Differential Scanning Calorimetry (DSC) for

Biopharmaceutical Development: Old concepts, new applications', *BioPharma Asia*, (July/August), pp. 46–55.

Mozhaev, V. V, Berezin, I. V, Martinek, K. and Nosoh, Y. (1988) 'Structure-Stability Relationship in Proteins: Fundamental Tasks and Strategy for the Development of Stabilized Enzyme Catalysts for Biotechnolog', *Critical Reviews in Biochemistry*. Taylor & Francis, 23(3), pp. 235–281. doi: 10.3109/10409238809088225.

Mukhametzyanova, A. D., Akhmetova, A. I. and Sharipova, M. R. (2012) 'Microorganisms as phytase producers', *Microbiology*, 81(3), pp. 267–275. doi: 10.1134/S0026261712030095.

Mullaney, E. J., Daly, C. B., Kim, T., Porres, J. M., Lei, X. G., Sethumadhavan, K. and Ullah, A. H. J. (2002) 'Site-directed mutagenesis of Aspergillus niger NRRL 3135 phytase at residue 300 to enhance catalysis at pH 4.0', *Biochemical and Biophysical Research Communications*, 297(4), pp. 1016–1020. doi: 10.1016/S0006-291X(02)02325-2.

Mullaney, E. J. and Ullah, A. H. J. (2005) 'Conservation of cysteine residues in fungal histidine acid phytases', *Biochemical and Biophysical Research Communications*, 328(2), pp. 404–408. doi: 10.1016/j.bbrc.2004.12.181.

Mullaney, E., Sethumadhavan, K., Boone, S., Lei, X. G. and Ullah, A. H. J. (2012) 'Elimination of a disulfide bridge in Aspergillus niger NRRL 3135 Phytase (PhyA) enhances heat tolerance and optimizes its temperature versus activity profile', 2012(November), pp. 372–378. doi: 10.4236/abc.2012.24046.

Nagai, Y. and Funahashi, S. (1962) 'Phytase (myoinositolhexaphosphate phosphohydrolase) from Wheat Bran', *Agricultural and Biological Chemistry*, 26(12), pp. 794–803. doi: 10.1080/00021369.1962.10858050.

Nagul, E. A., McKelvie, I. D., Worsfold, P. and Kolev, S. D. (2015) 'The molybdenum blue reaction for the determination of orthophosphate revisited: Opening the black box', *Analytica Chimica Acta*. Elsevier Ltd, 890, pp. 60–82. doi: 10.1016/j.aca.2015.07.030.

Neal, A. L., Rossmann, M., Brearley, C., Akkari, E., Guyomar, C., Clark, I. M., Allen, E. and Hirsch, P. R. (2017) 'Land-use influences phosphatase gene microdiversity in soils', *Environmental Microbiology*, 19(7), pp. 2740–2753. doi: 10.1111/1462-2920.13778.

Niesen, F. H. (2007) 'Differential Scanning Fluorimetry (DSF) Instrumentation & Method Principle', *SGC Oxford*, pp. 1–6. doi: 10.1081/CI-200056075.

Niu, C., Luo, H., Shi, P., Huang, H., Wang, Y., Yang, P. and Yao, B. (2016) 'N -Glycosylation Improves the Pepsin Resistance of HAP Phytases by Enhancing Their Stability at Acidic pH and Reducing the pepsin Accessibility to Cleavage Sites', *Applied and Environmental Microbiology*, 82(4), pp. 1004–1014. doi: 10.1128/AEM.02881-15.

Niu, C., Yang, P., Luo, H., Huang, H., Wang, Y. and Yao, B. (2017) 'Engineering the residual side chains of HAP phytases to improve their pepsin resistance and catalytic efficiency', *Scientific Reports*. Nature Publishing Group, 7(January), p. 42133. doi: 10.1038/srep42133.

Nomenclature Committee of the International Union of Biochemistry and Molecular Biology (2017) *EC 3.1.3 Phosphoric Monoester Hydrolases*. Available at: http://www.chem.qmul.ac.uk/iubmb/enzyme/EC3/1/3/ (Accessed: 13 September 2017).

O'Sullivan, M. G., Thornton, G., O'Sullivan, G. C. and Collins, J. K. (1992) 'Probiotic bacteria: myth or reality?', *Trends in Food Science & Technology*, 3(December), pp. 309–314. doi: 10.1016/S0924-2244(10)80018-4.

Ognalaga, M., Frossard, E. and Thomas, F. (1994) 'Glucose-1-phosphate and Myo-inositol Hexaphosphate Adsorption Mechanisms on Goethite', *Soil Science Society of America Journal*, 58(2), p. 332. doi: 10.2136/sssaj1994.03615995005800020011x.

Oh, B. C., Choi, W. C., Park, S., Kim, Y. O. and Oh, T. K. (2004) 'Biochemical properties and substrate specificities of alkaline and histidine acid phytases', *Applied Microbiology and Biotechnology*, 63(4), pp. 362–372. doi: 10.1007/s00253-003-1345-0.

Ooi, T., Oobatake, M., Nemethy, G. and Scheraga, H. a (1987) 'Accessible surface areas as a measure of the thermodynamic parameters of hydration of peptides.', *Proceedings of the National Academy of Sciences*, 84(10), pp. 3086–3090. doi: 10.1073/pnas.84.10.3086.

Ostanin, K. and Van Etten, R. L. (1993) 'Asp304 of Escherichia coli acid phosphatase is involved in leaving group protonation.', *The Journal of biological chemistry*, 268(28), pp. 20778–84. Available at: http://www.ncbi.nlm.nih.gov/pubmed/8407904.

Ostanin, K., Harms, E. H., Stevis, P. E., Kuciel, R., Zhou, M. M. and Van Etten, R. L. (1992) 'Overexpression, site-directed mutagenesis, and mechanism of Escherichia coli acid phosphatase.', *The Journal of biological chemistry*, 267(32), pp. 22830–6. Available at: http://www.ncbi.nlm.nih.gov/pubmed/1429631.

Pandey, A., Negi, S. and Socco, C. (2016) *Current Developments in Biotechnology and Bioengineering: Production, Isolation and Purification of Industrial Products*. Available at: https://www.elsevier.com/books/current-developments-in-biotechnology-and-bioengineering/pandey/978-0-444-63662-1.

Peers, F. G. (1953) 'The phytase of wheat.', *The Biochemical journal*, 53(1), pp. 102–110. doi: 10.1042/bj0530102.

Perez Corona, M. E., van der Klundert, I. and Verhoeven, J. T. (1996) 'Availability of organic and inorganic phosphorus compounds as Phosphorus sources for \textit{Carex} Species', *New Phytologist*, 133(2), pp. 225–231. doi: 10.1111/j.1469-8137.1996.tb01889.x.

Phillippy, B. Q. and Bland, J. M. (1988) 'Gradient ion chromatography of inositol phosphates.', *Analytical biochemistry*, 175(1), pp. 162–6.

Pinto-Sanchez, M. I., Hall, G. B., Ghajar, K., Nardelli, A., Bolino, C., Lau, J. T., Martin, F. P., Cominetti, O., Welsh, C., Rieder, A., Traynor, J., Gregory, C., De Palma, G., Pigrau, M., Ford, A. C., Macri, J., Berger, B., Bergonzelli, G., Surette, M. G., *et al.* (2017) 'Probiotic Bifidobacterium longum NCC3001 Reduces Depression Scores and Alters Brain Activity: A Pilot Study in Patients With Irritable Bowel Syndrome', *Gastroenterology*. Elsevier, 153(2), p. 448–459.e8. doi: 10.1053/j.gastro.2017.05.003.

Plaza-Díaz, J., Ruiz-Ojeda, F. J., Vilchez-Padial, L. M. and Gil, A. (2017) 'Evidence of the anti-inflammatory effects of probiotics and synbiotics in intestinal chronic diseases', *Nutrients*, 9(6). doi: 10.3390/nu9060555.

Porvari, K. S., Herrala, A. M., Kurkela, R. M., Taavitsainen, P. A., Lindqvist, Y., Schneider, G. and Vihko, P. T. (1994) 'Site-directed mutagenesis of prostatic acid phosphatase. Catalytically important aspartic acid 258, substrate specificity, and oligomerization', *Journal of Biological Chemistry*, 269(36), pp. 22642–22646. Available at: http://www.ncbi.nlm.nih.gov/pubmed/8077215.

Pronk, S., Páll, S., Schulz, R., Larsson, P., Bjelkmar, P., Apostolov, R., Shirts, M. R., Smith, J. C., Kasson, P. M., van der Spoel, D., Hess, B. and Lindahl, E. (2013) 'GROMACS 4.5: a high-throughput and highly parallel open source molecular simulation toolkit.', *Bioinformatics (Oxford, England)*, 29(7), pp. 845–54. doi:

10.1093/bioinformatics/btt055.

Puhl, A. a, Greiner, R. and Selinger, L. B. (2009) 'Stereospecificity of myo-inositol hexakisphosphate hydrolysis by a protein tyrosine phosphatase-like inositol polyphosphatase from Megasphaera elsdenii.', *Applied microbiology and biotechnology*, 82(1), pp. 95–103. doi: 10.1007/s00253-008-1734-5.

Qvirist, L., Carlsson, N.-G. and Andlid, T. (2015) 'Assessing phytase activity–methods, definitions and pitfalls', *Journal of Biological Methods*, 2(1), p. 16. doi: 10.14440/jbm.2015.58.

Raboy, V. (1997) 'Accumulation and Storage of Phosphate and Minerals', in, pp. 441–477. doi: 10.1007/978-94-015-8909-3_12.

Raboy, V. (2003) 'myo-Inositol-1,2,3,4,5,6-hexakisphosphate', *Phytochemistry*, 64(6), pp. 1033–1043. doi: 10.1016/S0031-9422(03)00446-1.

Rasmussen, S., Sorensen, M. and Johansen, K. (2007) 'Polynucleotides encoding phytase polypeptides'. doi: 10.1016/j.(73).

Reale, A., Konietzny, U., Coppola, R., Sorrentino, E. and Greiner, R. (2007) 'The importance of lactic acid bacteria for phytate degradation during cereal dough fermentation', *Journal of Agricultural and Food Chemistry*, 55(8), pp. 2993–2997. doi: 10.1021/jf063507n.

Reddy, C. S., Achary, V. M. M., Manna, M., Singh, J., Kaul, T. and Reddy, M. K. (2015) 'Isolation and Molecular Characterization of Thermostable Phytase from Bacillus subtilis (BSPhyARRMK33)', *Applied Biochemistry and Biotechnology*, 175(6), pp. 3058–3067. doi: 10.1007/s12010-015-1487-4.

Reddy, C. S., Kim, S. C. and Kaul, T. (2017) 'Genetically modified phytase crops role in sustainable plant and animal nutrition and ecological development: a review', *3 Biotech*. Springer Berlin Heidelberg, 7(3). doi: 10.1007/s13205-017-0797-3.

Reddy, N. R., Pierson, M. D., Sathe, S. K. and Salunkhe, D. K. (1989) *Phytates in Cereals and Legumes*. CRC Press.

Riahi-Madvar, A. and Hosseinkhani, S. (2009) 'Design and characterization of novel trypsin-resistant firefly luciferases by site-directed mutagenesis', *Protein Engineering, Design and Selection*, 22(11), pp. 655–663. doi: 10.1093/protein/gzp047.

Richardson, A. E. and Hadobas, P. A. (1997) 'Soil isolates of Pseudomonas spp. that utilize inositol phosphates.', *Canadian Journal of Microbiology*, 43(6), pp. 509–516. doi: 10.1139/m97-073.

Richardson, A. E., Hadobas, P. A. and Hayes, J. E. (2000) 'Acid phosphomonoesterase and phytase activities of wheat (Triticum aestivum L.) roots and utilization of organic phosphorus substrates by seedlings grown in sterile culture', *Plant, Cell and Environment*, 23(4), pp. 397–405. doi: 10.1046/j.1365-3040.2000.00557.x.

Richardson, A. E., Hadobas, P. A. and Hayes, J. E. (2001) 'Extracellular secretion of Aspergillus phytase from Arabidopsis roots enables plants to obtain phosphorus from phytate', *Plant Journal*, 25(6), pp. 641–649. doi: 10.1046/j.1365-313X.2001.00998.x.

Rigden, D. J. (2008) 'The histidine phosphatase superfamily: structure and function.', *The Biochemical journal*, 409(2), pp. 333–48. doi: 10.1042/BJ20071097.

Riley, A. M., Windhorst, S., Lin, H. Y. and Potter, B. V. L. (2014) 'Cellular internalisation of an inositol phosphate visualised by using fluorescent InsP5', *ChemBioChem*, 15(1), pp. 57–67. doi: 10.1002/cbic.201300583.

Rivera-Solís, R. A., Peraza-Echeverria, S., Echevarría-Machado, I. and Herrera-Valencia, V. A. (2014)

'Chlamydomonas reinhardtii has a small family of purple acid phosphatase homologue genes that are differentially expressed in response to phytate', *Annals of Microbiology*, 64(2), pp. 551–559. doi: 10.1007/s13213-013-0688-8.

Rodriguez, F., Lillington, J., Johnson, S., Timmel, C. R., Lea, S. M. and Berks, B. C. (2014) 'Crystal structure of the Bacillus subtilis phosphodiesterase PhoD reveals an iron and calcium-containing active site', *Journal of Biological Chemistry*, 289(45), pp. 30889–30899. doi: 10.1074/jbc.M114.604892.

Romano, P. R., Wang, J., O'Keefe, R. J., Puzas, J. E., Rosier, R. N. and Reynolds, P. R. (1998) 'HiPER1, a phosphatase of the endoplasmic reticulum with a role in chondrocyte maturation.', *Journal of cell science*, 111 (Pt 6, pp. 803–813.

Rumsey, G. L. (1993) 'Fish Meal and Alternate Sources of Protein in Fish Feeds', *Fisheries*, 18(7), pp. 14–19.

Sajjadi, M. and Carter, C. G. (2004) 'Effect of phytic acid and phytase on feed intake, growth, digestibility and trypsin activity in Atlantic salmon (Salmo salar, L.)', *Aquaculture Nutrition*, 10(2), pp. 135–142. doi: 10.1111/j.1365-2095.2003.00290.x.

Sanchez-Romero, I., Ariza, A., Wilson, K. S., Skjøt, M., Vind, J., De Maria, L., Skov, L. K. and Sanchez-Ruiz, J. M. (2013) 'Mechanism of protein kinetic stabilization by engineered disulfide crosslinks.', *PloS one*, 8(7), p. e70013. doi: 10.1371/journal.pone.0070013.

Sandberg, A., Rossander, L. and Turk, M. (1996) 'Human and Clinical Nutrition Dietary Aspergillus niger Phytase Increases Iron Absorption in Humans1 â€™ 2', (June 1995), pp. 476–480.

Sandberg, A. S. and Andlid, T. (2002) 'Phytogenic and microbial phytases in human nutrition', *International Journal of Food Science and Technology*, 37(7), pp. 823–833. doi: 10.1046/j.1365-2621.2002.00641.x.

Sawaya, M. R. and Kraut, J. (1997) 'Loop and subdomain movements in the mechanism of Escherichia coli dihydrofolate reductase: Crystallographic evidence', *Biochemistry*, 36(3), pp. 586–603. doi: 10.1021/bi962337c.

Schell, M. A., Karmirantzou, M., Snel, B., Vilanova, D., Berger, B., Pessi, G., Zwahlen, M.-C., Desiere, F., Bork, P., Delley, M., Pridmore, R. D. and Arigoni, F. (2002) 'The genome sequence of Bifidobacterium longum reflects its adaptation to the human gastrointestinal tract.', *Proceedings of the National Academy of Sciences of the United States of America*, 99(22), pp. 14422–7. doi: 10.1073/pnas.212527599.

Schenk, G., Korsinczky, M. L. J., Hume, D. A., Hamilton, S. and Dejersey, J. (2000) 'Purple acid phosphatases from bacteria: similarities to mammalian and plant enzymes', *Gene*, 255(2), pp. 419–424. doi: 10.1016/S0378-1119(00)00305-X.

Schneider, G., Lindqvist, Y. and Vihko, P. (1993) 'Three-dimensional structure of rat acid phosphatase', 12(7), pp. 2609–2615. Available at: https://www-ncbi-nlm-nih-gov.libaccess.lib.mcmaster.ca/pmc/articles/PMC413507/pdf/emboj00079-0037.pdf.

Secco, D., Bouain, N., Rouached, A., Prom-u-thai, C., Hanin, M., Pandey, A. K. and Rouached, H. (2017) 'Phosphate, phytate and phytases in plants: from fundamental knowledge gained in Arabidopsis to potential biotechnological applications in wheat', *Critical Reviews in Biotechnology*. Informa Healthcare USA, Inc, 37(7), pp. 898–910. doi: 10.1080/07388551.2016.1268089.

Shamsuddin, A. M. (2002) 'Anti-cancer function of phytic acid', *International Journal of Food Science and Technology*, 37(7), pp. 769–782. doi: 10.1046/j.1365-2621.2002.00620.x.

Shamsuddin, R., Doktorova, M., Jaswal, S., Lee-St John, A. and McMenimen, K. (2014) 'Computational

prediction of hinge axes in proteins', *BMC Bioinformatics*, 15(Suppl 8), p. S2. doi: 10.1186/1471-2105-15-S8-S2.

Sharma, A. and Trivedi, S. (2015) 'Evaluation of in vitro probiotic potential of phytase-producing bacterial strain as a new probiotic candidate', *International Journal of Food Science and Technology*, 50(2), pp. 507–514. doi: 10.1111/ijfs.12697.

Sharpley, A. (1999) 'Symposium: Reducing the environmental impact of poultry production: Focus on phosphorus: Agricultural phosphorus, water quality, and poultry production: Are they compatible?', *Poultry Science*, 78(5), pp. 660–673.

Shieh, T. R. and Ware, J. H. (1968) 'Survey of Microorganisms for the Production of Extracellular Phytase', 16(9), pp. 1348–1351.

Shimizu, M. (1992) 'Purification and Characterization of Phytase from *Bacillus suhtilis* (*natto*) N–77', *Bioscience, Biotechnology, and Biochemistry*, 56(8), pp. 1266–1269. doi: 10.1271/bbb.56.1266.

Shin, S., Ha, N. C., Oh, B. C., Oh, T. K. and Oh, B. H. (2001) 'Enzyme mechanism and catalytic property of β propeller phytase', *Structure*, 9(9), pp. 851–858. doi: 10.1016/S0969-2126(01)00637-2.

Shivange, A. V. and Schwaneberg, U. (2017) 'Recent Advances in Directed Phytase Evolution and Rational Phytase Engineering', in *Recent Advances in Directed Phytase Evolution and Rational Phytase Engineering*. Cham: Springer International Publishing, pp. 145–172. doi: 10.1007/978-3-319-50413-1_6.

Simpson, C. J. and Wise, A. (1990) 'Binding of zinc and calcium to inositol phosphates (phytate) in vitro', *British Journal of Nutrition*, 64(1), pp. 225–232. doi: 10.1079/BJN19900024.

Singh, B. and Satyanarayana, T. (2010) 'Applications of phytase of thermophilic mould, Sporotrichum thermophile: A review', *Journal of Scientific and Industrial Research*. Elsevier Ltd, 69(6), pp. 411–414. doi: 10.1016/j.biortech.2008.10.025.

Spolar, R. S., Ha, J. H. and Record, M. T. (1989) 'Hydrophobic effect in protein folding and other noncovalent processes involving proteins', *Proceedings of the National Academy of Sciences of the United States of America*, 86(21), pp. 8382–8385. doi: 10.1073/pnas.86.21.8382.

Sreeramulu, G., Srinivasa, D. S., Nand, K. and Joseph, R. (1996) 'Lactobacillus amylovorus as a phytase producer in submerged culture', *Letters in Applied Microbiology*, 23(6), pp. 385–388. doi: 10.1111/j.1472-765X.1996.tb01342.x.

Sridharan, R., Zuber, J., Connelly, S. M., Mathew, E. and Dumont, M. E. (2014) 'Fluorescent approaches for understanding interactions of ligands with G protein coupled receptors', *Biochimica et Biophysica Acta - Biomembranes*. Elsevier B.V., 1838(1 PARTA), pp. 15–33. doi: 10.1016/j.bbamem.2013.09.005.

Steen, I. (1998) 'Phosphorus availability in the 21st century: management of a non-renewable resource.', *Phosphorus and Potassium*, 217, pp. 25–31.

Stentz, R., Osborne, S., Horn, N., Li, A. W. H., Hautefort, I., Bongaerts, R., Rouyer, M., Bailey, P., Shears, S. B., Hemmings, A. M., Brearley, C. A. and Carding, S. R. (2014) 'A Bacterial Homolog of a Eukaryotic Inositol Phosphate Signaling Enzyme Mediates Cross-kingdom Dialog in the Mammalian Gut', *Cell Reports*, 6(4), pp. 646–656. doi: 10.1016/j.celrep.2014.01.021.

Sturtevant, J. M. (1977) 'Heat capacity and entropy changes in processes involving proteins.', *Proceedings of the National Academy of Sciences*, 74(6), pp. 2236–2240. doi: 10.1073/pnas.74.6.2236.

Sun, J., Ding, S. Y. and Peterson, J. D. (2013) *Biological Conversion of Biomass for Fuels and Chemicals:*

Explorations from Natural Utilization Systems. Royal Society of Chemistry (Energy and Environment Series). Available at: https://books.google.co.uk/books?id=bXYoDwAAQBAJ.

Sun, M., Alikhani, J., Massoudieh, A., Greiner, R. and Jaisi, D. P. (2017) 'Phytate Degradation by Different Phosphohydrolase Enzymes: Contrasting Kinetics, Decay Rates, Pathways, and Isotope Effects', *Soil Science Society of America Journal*, 0(0), p. 0. doi: 10.2136/sssaj2016.07.0219.

Sutardi and Buckle, K. A. (1988) 'Characterization of extra- and intracellular phytases from Rhizopus oligosporus used in tempeh production.', *International journal of food microbiology*, 6(1), pp. 67–79. Available at: http://www.ncbi.nlm.nih.gov/pubmed/2856346.

Svihus, B. (2014) 'Function of the digestive system', *Journal of Applied Poultry Research*, 23(2), pp. 306–314. doi: 10.3382/japr.2014-00937.

Svihus, B., Hetland, H., Choct, M. and Sundby, F. (2002) 'Passage rate through the anterior digestive tract of broiler chickens fed on diets with ground and whole wheat', *British Poultry Science*, 43(5), pp. 662–668. doi: 10.1080/0007166021000025037.

Svihus, B., Lund, V. B., Bjorgen, B., Bedford, M. R. and Bakken, M. (2013) 'Effect of intermittent feeding, structural components and phytase on performance and behaviour of broiler chickens', *British Poultry Science*, 54(2), pp. 222–230. doi: 10.1080/00071668.2013.772952.

Taha, M., e Silva, F. A., Quental, M. V, Ventura, S. P. M., Freire, M. G. and Coutinho, J. A. P. (2014) 'Good's buffers as a basis for developing self-buffering and biocompatible ionic liquids for biological research', *Green chemistry : an international journal and green chemistry resource : GC*, 16(6), pp. 3149–3159. doi: 10.1039/C4GC00328D.

Tamayo-Ramos, J. A., Sanz-Penella, J. M., Yebra, M. J., Monedero, V. and Haros, M. (2012) 'Novel phytases from Bifidobacterium pseudocatenulatum ATCC 27919 and bifidobacterium longum subsp. infantis ATCC 15697', *Applied and Environmental Microbiology*, 78(14), pp. 5013–5015. doi: 10.1128/AEM.00782-12.

Tambe, S. M., Kaklij, G. S., Kelkar, S. M. and Parekh, L. J. (1994) 'Two distinct molecular forms of phytase from Klebsiella aerogenes: Evidence for unusually small active enzyme peptide', *Journal of Fermentation and Bioengineering*, 77(1), pp. 23–27. doi: 10.1016/0922-338X(94)90202-X.

Tang, J., Leung, A., Leung, C. and Lim, B. L. (2006) 'Hydrolysis of precipitated phytate by three distinct families of phytases', *Soil Biology and Biochemistry*, 38(6), pp. 1316–1324. doi: 10.1016/j.soilbio.2005.08.021.

Tarafdar, J. C. and Marschner, H. (1995) 'Dual inoculation with Aspergillus fumigatus and Glomus mosseae enhances biomass production and nutrient uptake in wheat (Triticum aestivum L.) supplied with organic phosphorus as Na-phytate', *Plant and Soil*, 173(1), pp. 97–102. doi: 10.1007/BF00155522.

Tarayre, C., De Clercq, L., Charlier, R., Michels, E., Meers, E., Camargo-Valero, M. and Delvigne, F. (2016) 'New perspectives for the design of sustainable bioprocesses for phosphorus recovery from waste', *Bioresource Technology*, 206, pp. 264–274. doi: 10.1016/j.biortech.2016.01.091.

Taylor, D., Cawley, G. and Hayward, S. (2014) 'Quantitative method for the assignment of hinge and shear mechanism in protein domain movements', *Bioinformatics*, 30(22), pp. 3189–3196. doi: 10.1093/bioinformatics/btu506.

Tseng, Y. H., Fang, T. J. and Tseng, S. M. (2000) 'Isolation and characterization of a novel phytase from Penicillium simplicissimum', *Folia Microbiologica*, 45(2), pp. 121–127. doi: 10.1007/BF02817409.

Turner, B. L., Richardson, A. E. and Mullaney, E. J. (2007) *Inositol phosphates: linking agriculture and the environment*, *World*. Edited by B. L. Turner, A. E. Richardson, and E. J. Mullaney. Wallingford: CABI. doi: 10.1079/9781845931520.0000.

Ullah, A. H. J., Cummins, B. J. and Dischinger, H. C. (1991) 'Cyclohexanedione modification of arginine at the active site of Aspergillus ficuum phytase', *Biochemical and Biophysical Research Communications*, 178(1), pp. 45–53. doi: 10.1016/0006-291X(91)91777-A.

Ullah, A. H. J. and Mullaney, E. J. (1996) 'Disulfide Bonds Are Necessary for Structure and Activity inAspergillus ficuumPhytase', *Biochemical and biophysical research communications*, 227(2), pp. 311–317.

Understanding the value chain of phytate (2017). Available at: https://www.abvista.com/news/May-2017/Understanding-the-value-chain-of-phytate.aspx (Accessed: 9 September 2017).

Veiga, N., Torres, J., Macho, I., Gómez, K., González, G. and Kremer, C. (2014) 'Coordination, microprotonation equilibria and conformational changes of myo-inositol hexakisphosphate with pertinence to its biological function.', *Dalton transactions (Cambridge, England : 2003)*, 43(43), pp. 16238–51. doi: 10.1039/c4dt01350f.

Vohra, A. and Satyanarayana, T. (2002) 'Purification and characterization of a thermostable and acid-stable phytase from Pichia anomala', *World Journal of Microbiology and Biotechnology*, 18(7), pp. 687–691. doi: 10.1023/A:1016850121719.

Vohra, A. and Satyanarayana, T. (2003) 'Phytases : Microbial Sources , Production , Purification , and Potential Biotechnological', 23(1), pp. 29–60. doi: 10.4061/2011/217861.

Wang, H., Lee, I. S., Braun, C. and Enck, P. (2016) 'Effect of probiotics on central nervous system functions in animals and humans: A systematic review', *Journal of Neurogastroenterology and Motility*, 22(4), pp. 589–605. doi: 10.5056/jnm16018.

Wang, X.-Y., Meng, F.-G. and Zhou, H.-M. (2004) 'The role of disulfide bonds in the conformational stability and catalytic activity of phytase.', *Biochemistry and cell biology = Biochimie et biologie cellulaire*, 82(2), pp. 329–34. doi: 10.1139/o03-082.

Watson, P. J., Millard, C. J., Riley, A. M., Robertson, N. S., Wright, L. C., Godage, H. Y., Cowley, S. M., Jamieson, A. G., Potter, B. V. L. and Schwabe, J. W. R. (2016) 'Insights into the activation mechanism of class I HDAC complexes by inositol phosphates.', *Nature communications*, 7, p. 11262. doi: 10.1038/ncomms11262.

Wu, P., Tian, J. C., Walker, C. E. and Wang, F. C. (2009) 'Determination of phytic acid in cereals - A brief review', *International Journal of Food Science and Technology*, 44(9), pp. 1671–1676. doi: 10.1111/j.1365-2621.2009.01991.x.

Wynne, C. J., Hamilton, S. E., Dionysius, D. A., Beck, J. L. and Dejersey, J. (1995) 'Studies on the Catalytic Mechanism of Pig Purple Acid Phosphatase', *Archives of Biochemistry and Biophysics*, 319(1), pp. 133–141. doi: https://doi.org/10.1006/abbi.1995.1275.

Wyss, M., Brugger, R., Kronenberger, A., Rémy, R., Fimbel, R., Oesterhelt, G., Loon, A. P. G. M. Van, Re, R. and Lehmann, M. (1999) 'Biochemical Characterization of Fungal Phytases (myo -Inositol Hexakisphosphate Phosphohydrolases): Catalytic Properties Biochemical Characterization of Fungal Phytases (myo -Inositol Hexakisphosphate Phosphohydrolases): Catalytic Properties', 65(2), pp. 367–373.

Xia, X., Longo, L. M. and Blaber, M. (2015) 'Mutation choice to eliminate buried free cysteines in protein

therapeutics', *Journal of Pharmaceutical Sciences*. Elsevier Masson SAS, 104(2), pp. 566–576. doi: 10.1002/jps.24188.

Xu, J. (2003) 'A Genomic View of the Human-Bacteroides thetaiotaomicron Symbiosis', *Science*, 299(5615), pp. 2074–2076. doi: 10.1126/science.1080029.

Yanke, L. J., Bae, H. D., Selinger, L. B. and Cheng, K. J. (1998) 'Phytase activity of anaerobic ruminal bacteria', *Microbiology*, 144(6), pp. 1565–1573. doi: 10.1099/00221287-144-6-1565.

Yanke, L. J., Selinger, L. B. and Cheng, K. J. (1999) 'Phytase activity of Selenomonas ruminantium: A preliminary characterization', *Letters in Applied Microbiology*, 29(1), pp. 20–25. doi: 10.1046/j.1365-2672.1999.00568.x.

Yao, M.-Z., Zhang, Y.-H., Lu, W.-L., Hu, M.-Q., Wang, W. and Liang, a-H. (2012) 'Phytases: crystal structures, protein engineering and potential biotechnological applications.', *Journal of applied microbiology*, 112(1), pp. 1–14. doi: 10.1111/j.1365-2672.2011.05181.x.

Yu, S., Cowieson, A., Gilbert, C., Plumstead, P. and Dalsgaard, S. (2012) 'Interactions of phytate and myo-inositol phosphate esters (IP1-5) including IP5 isomers with dietary protein and iron and inhibition of pepsin', *Journal of Animal Science*, 90(6), pp. 1824–1832. doi: 10.2527/jas.2011-3866.

Yu, X.-W., Tan, N.-J., Xiao, R. and Xu, Y. (2012) 'Engineering a Disulfide Bond in the Lid Hinge Region of Rhizopus chinensis Lipase: Increased Thermostability and Altered Acyl Chain Length Specificity', *PLoS ONE*. Edited by E. A. Permyakov, 7(10), p. e46388. doi: 10.1371/journal.pone.0046388.

Zamudio, M., González, A. and Medina, J. A. (2001) 'Lactobacillus plantarum phytase activity is due to non-specific acid phosphatase', *Letters in Applied Microbiology*, 32(3), pp. 181–184. doi: 10.1046/j.1472-765X.2001.00890.x.

Zeller, E., Schollenberger, M., Kühn, I. and Rodehutscord, M. (2015a) 'Hydrolysis of phytate and formation of inositol phosphate isomers without or with supplemented phytases in different segments of the digestive tract of broilers', *Journal of Nutritional Science*, 4, p. e1. doi: 10.1017/jns.2014.62.

Zeller, E., Schollenberger, M., Kühn, I. and Rodehutscord, M. (2015b) 'Hydrolysis of phytate and formation of inositol phosphate isomers without or with supplemented phytases in different segments of the digestive tract of broilers', *Journal of Nutritional Science*, 4, p. e1. doi: 10.1017/jns.2014.62.

Zeller, E., Schollenberger, M., Kühn, I. and Rodehutscord, M. (2016) 'Dietary effects on inositol phosphate breakdown in the crop of broilers', *Archives of Animal Nutrition*. Taylor & Francis, 70(1), pp. 57–71. doi: 10.1080/1745039X.2015.1112622.

Zeller, E., Schollenberger, M., Witzig, M., Shastak, Y., Kühn, I., Hoelzle, L. E. and Rodehutscord, M. (2015) 'Interactions between supplemented mineral phosphorus and phytase on phytate hydrolysis and inositol phosphates in the small intestine of broilers', *Poultry Science*, 94(5), pp. 1018–1029. doi: 10.3382/ps/pev087.

Zhang, W., Gruszewski, H. A., Chevone, B. I. and Nessler, C. L. (2007) 'An Arabidopsis Purple Acid Phosphatase with Phytase Activity Increases Foliar Ascorbate', *Plant Physiology*, 146(2), pp. 431–440. doi: 10.1104/pp.107.109934.

Zhang, W. and Lei, X. G. (2008) 'Cumulative improvements of thermostability and pH-activity profile of Aspergillus niger PhyA phytase by site-directed mutagenesis', *Applied Microbiology and Biotechnology*, 77(5), pp. 1033–1040. doi: 10.1007/s00253-007-1239-7.

9 Appendices

9.1 Appendix 1. Protein sequences of Bp, Bt and Bl phytases.

MAHHHHHHSSGLEVLFQGPGEGTARYYSSKQPYVAPASTSYSAIPSRYHLAYTESVARH
GSRGLSSYKYDALLALMAQSAAENNYAGFVSPEVGKEFINNVNAITAANVGNGYGMLS
GQGAIQHQGIGERIYQRDADLFANAAKQGLRVSYQSSGEPRATESGENFKLGFDQASN
GLLANAVVAPNNPADNNSGKNFDKNTTTLYFHKTDNPDGTQKTGEAKERAERYQQFV
ANDGGIAEAEENVTNDPSMTTASHNLLSQIFTDDFLASIGKEEGQRIWYNTADGTKKG
AANCAAGADPAKDANACGDAKKKIASEQDAAMDLYNLYIIAADMEQENTGSHTFNFD
QYFQGQHAQEAKTFAWSLDAEDFYEKGPGRAGQDETYRIAQPLLDDFFNAIDTRERAG
TAATFRFAHAETIIPFAALLKLPGSQQQASELYTYENNPWRGESVTPMAANVQWDVVV
RDGTDVSGQPYQPLVRMLYNEKEIGFNDSCTPIADGSTWYKESELKSCLNGKGTTVDA
RL

Figure 9.1 Amino acid sequence of the Bifidobacterium pseudocatenulatum phytase. Showing the construct used for expression of the protein. His-tag insert is highlighted in yellow. The active site motif HAE is highlighted in blue.

MAHHHHHHSSGLEVLFQGPMEADGRYYSSKQPYVAPNDATASSYSKAPKGYGPIYTES
MARHGSRGLSSYKYDALLMRMAETAARDGGFKSEAIKAEFVKNLSGITAANVENGYG
MLTGQGAQQHYGIGERAYQRNRSLFDQAAADGGTIAYQSSGEARATESGENFEKGFN
EASGGRLIGNVSAPTNPADSGNGKDFQKNPDTLYFHKVQNPDGTSKVPGTKAYDIANN
YQNFVANDATIAGAEKTIGDNVDVKRASHDLLSQIFTEEFLAKLENGEYKWYNTTDGTK
KGGKNCAPGADASKDPDACGEVSKKIKSEYDAAMDLYNLYIIAADMHNENTGDHTFAF
DQYFQGAYADDARMFAWALDAEDFYEKGPSYAGQNETYSIAQPLLDDFLNTIDARVN
GGSTVATFRFAHAETMMPFAALLGLPGSTQQAPASTTDVYTYGNNEWRGESVTPMA
ANVQWDVYARKGEDPATGQRYTPIVRMLYNENEVPFRSECTPVADGSTWYKLTELKS

Figure 9.2 Amino acid sequence of the Bifidobacterium longum phytase. Showing the construct used for expression of the protein. His-tag insert is highlighted in yellow. The active site motif HAE is highlighted in blue.

MGSSHHHHHHSSGLVPRGSHMQTKIQKYAGTAMPYPNRTDSSITFRDGMTPFYINHL
GRHGARFPTSRKALDKVEKVLVSAQQENGLTSEGMALLSMIRRLSRLFDGQWGKLSKL
GETEQEGIAGRMIRNYPQLFSNSAKIEAIATYVPRSINSMDAFLSCMIRHNPALQVQRSE
GKQYNHILRFFDLNKSYVNYKEKGDWLPIYKAFVHKKISPVPIMKKFLLNPEQYLDKEAE
EFVMALFSVAAILPDTSIPLNLEDLFTLDEWHRYWQTQNLRQYMSKSSAPVGKMLPVAI
AWPLLSEFIRSAQEVISGKSDYQANFRFAHAETVIPFVSLMGIEKTDVQVCRPDSVSVY
WKDYEISPMAANVQWLFYRDRDQRIWVKILLNEEAAALPISTACFPYYSWEKTRIFFNQ
RIEMAKKTLSVFNE

Figure 9.3 Amino acid sequence of the Bacteroides thetaiotaomicron phytase. Showing the construct used for expression of the protein. His-tag insert is highlighted in yellow. The active site motif HAE is highlighted in blue.

9.2 Appendix 2. Sequence alignments.

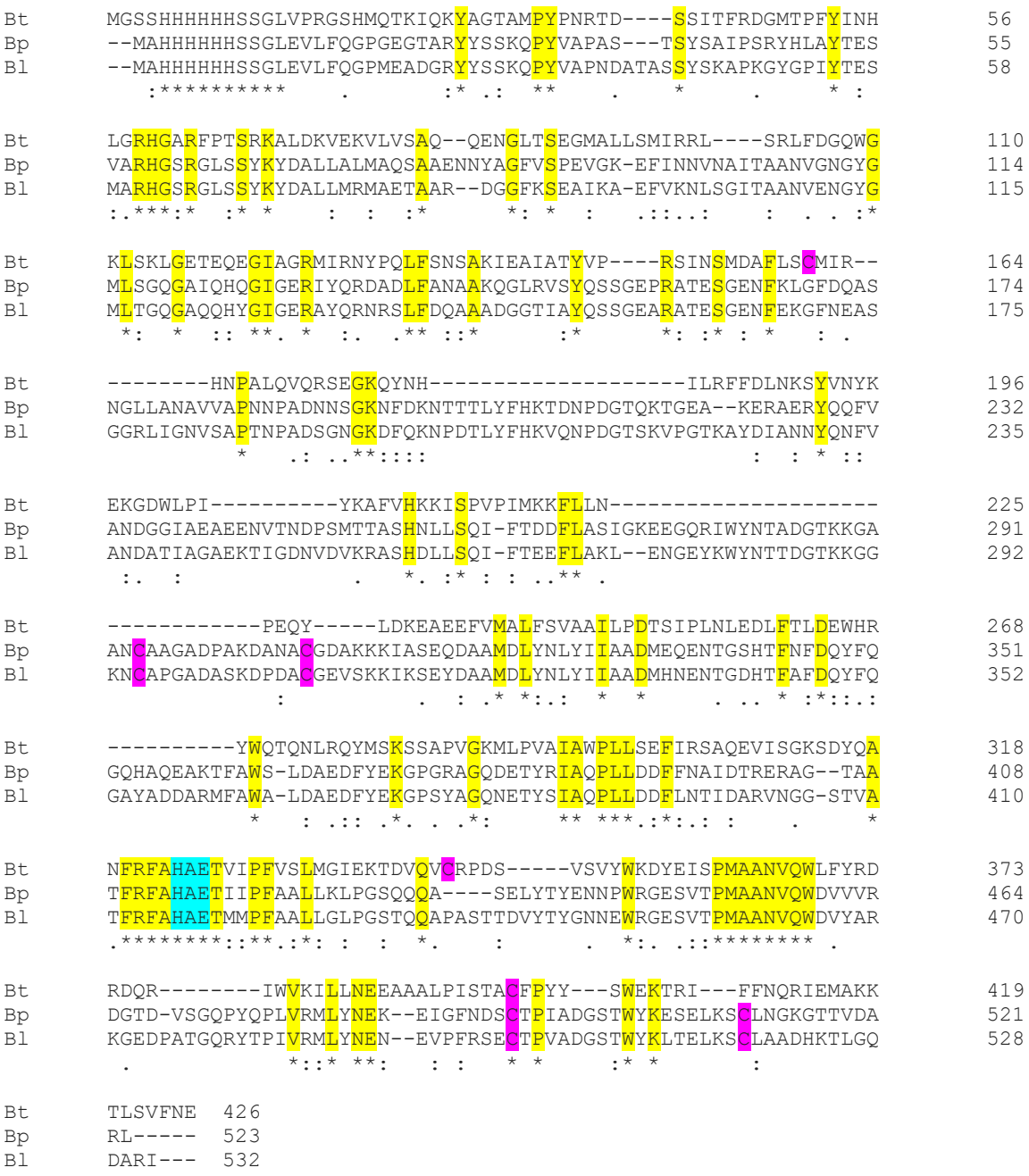

Figure 9.4 Protein sequence alignment of Bt, Bp and Bl Minpp phytases.

Created using the online tool Clustal Omega. Showing the sequences of the constructs used for expression. The catalytic motif HAE is highlighted in blue. Cysteines are highlighted in pink. Other conserved sequences are highlighted in yellow, omitting the His-tag sequence.

```
lily          --------MAFS--L-HALIFALL------LAAAAANDEPFDVRRHLSTVSSYDAAKNVI    43
barley        -MAPLGTRLPFLLLLATLLAAAPL------SPPAAAEPEPFDVRRHLSTVTRYDVARESN    53
wheat         -MSPPATPLPFLL-LATLLAAAPL------LPPAAAEPEAFDVRRHLSTVTRYDVSRASN    52
Chicken       ----------------------MAPCRAACLLPLLVAVASAGLGGYFGTKSRYEEVNPHL    38
human         ------------------------------------------------------------    0
rat           MLRGARSHLSASVALAAVLAAALLSSFARCSLPGRGDPVASVLSPYFGTKTRYEDVNPWL    60
Bt            -MGSSHHHHHHSS-----------------GLVPRGSHMQTKIQKYAGTAMPYPNRTD--    40
Bp            ---MAHHHHHHSS-----------------GLEVLFQGPGEGTARYYSSKQPYVAPAS--    38
Bl            ---MAHHHHHHSS-----------------GLEVLFQGPMEADGRYYSSKQPYVAPNDAT    40

lily          LG-------SFVPSSVPDGCRAIHLNLVARHGTRAPTKKRIKEMDQLAIRLDALLTDAKE    96
barley        IV-------DAA-PAISDECRVIHLNLVARHGTRAPTKKRIKELNTLSVRLGALVEEAKQ    105
wheat         SV-------VSA-PSISDECRVIHLNLVARHGTRAPTKKRIKELDRLAVRLGTLVDEAKQ    104
Chicken       AEDPLSLGPHAAAARLPAACAPLQLRRVVRHGTRYPTAGQIRRLAELHGRLRRAA---AP    95
human         ------------------------------------------------------------    0
rat           LGDPVA--PRRDPELLAGTCTPVQLVALIRHGTRYPTTKQIRKLRQLQGLLQTRESV-DG    117
Bt            -----------SSITFRDGMTPFYINHLGRHGARFPTSRKALDKVEKVLVSAQ--QENGL    87
Bp            ----------TSYSAIPSRYHLAYTESVARHGSRGLSSYKYDALLALMAQSAAENNYAGF    88
Bl            A---------SSYSKAPKGYGPIYTESMARHGSRGLSSYKYDALLMRMAETAAR--DGGF    89

lily          KTHDSSLPPNIPSWLSGWQSPWKGRQTGGELISKGEDELYHLGTRIRERFPDLFDEEYHP    156
barley        GSD-SDSLKRLPSWMKGWESRWKGRVKGGELVSEGEEELFSFANRVKERFQDLFDEEYHP    164
wheat         GSD-TASLKKIPSWMKGWESRWKGRVKGGELVSEGEEELFNFANRVKERFQDLFDEEYHP    163
Chicken       SCPAAAALAAWPMWYEES--------LDGRLAPRGRRDMEHLARRLAARFPALFAAR--R    145
human         ------------------------------------------------------------    0
rat           GSRVAAALDQWPLWYDDW--------MDGQLVEKGRQDMRQLALRLAALFPDLFCRENYG    169
Bt            TSEGMALLSMI-RRL----SRLF-DGQWGKLSKLGETEQEGIAGRMIRNYPQLFSNSAKI    141
Bp            VSPEVGK-EFI-NNVNAITAANV-GNGYGMLSGQGAIQHQGIGERIYQRDADLFANAAKQ    145
Bl            KSEAIKA-EFV-KNLSGITAANV-ENGYGMLTGQGAQQHYGIGERAYQRNRSLFDQAAAD    146

lily          HI-YSIRATQVPRASASAVAFGIGLFSGRGHLGPGKNRAFSVI----------------    198
barley        DV-YSIRATQVPRASASAVAFGLGLLSGKGRLGAGKNRAFSVL----------------    206
wheat         DV-YSIRATQVPRASASAVAFGLGLLSGKGKLGAGNNRAFSVL----------------    205
Chicken       RL-ALAS-SSKHRCLQSGAAFRRGLGPSLSLG--------ADE----------------    178
human         -----------MCL----------FQ------LCGLVRYMEF----------------    15
rat           RL-RLIT-SSKHRCVDSSAAFLQGLWQHYHPGLPPPDVSDMEC----------------    210
Bt            EAIATYVP----RSINSMDAFLSCMIR----------HNPALQVQRSEGKQYNH------    181
Bp            GLRVSYQSSGEPRATESGENFKLGFDQASNGLLANAVVAPNNPADNNSGKNFDKNTTTLY    205
Bl            GGTIAYQSSGEARATESGENFEKGFNEASGGRLIGNVSAPTNPADSGNGKDFQKNPDTLY    206
                         .

lily          ----S--ESRASDTCLRFFDSCETYKEYRKHEEPAVSKLK--------EPVLDGIVVALV    244
barley        ----S--ESRASDICRRFFDSCKTYKDYRKRKEPDVDKQK--------EPILEHVTSALV    252
wheat         ----S--ESRASDICLRFFDSCKTYKDYRKRKEPDVDKQK--------EPILEHVTSALV    251
Chicken       ----T--EIEVNDALMRFFDHCDKFVAFVEDNDTAMYQVNAFKEGPEMRKVLEKVASALC    232
human         ----G--PPTVNDKLMRFFDHCEKFLTEVEKNATALYHVEAFKTGPEMQNILKKVAATLQ    69
rat           ----D--PPRVNDKLMRFFDHCEKFLTEVERNATALYHVEAFKTGPEMQTVLKKVAATLQ    264
Bt            --------------ILRFFDLNKSYVNYKEKGDWLPI----------YKAFVHKKISPVP    217
Bp            FHKTDNPDGTQKTGEA--KERAERYQQFVANDGGIAEAEENVTNDPSMTTASHNLLSQI-    262
Bl            FHKVQNPDGTSKVPGTKAYDIANNYQNFVANDATIAGAEKTIGDNVDVKRASHDLLSQI-    265
                            :  . :                              .    :

lily          --SRYQLNFTRQDVASLWFLC----------------------------------------    263
barley        --NRYHLNFITQDVSSLWFLC----------------------------------------    271
wheat         --SRYHLKFTTQDVSSLWFLC----------------------------------------    270
Chicken       --L-PASELNADLVQVAFLTC----------------------------------------    250
human         --V-PVNDLNADLIQVAFFTC----------------------------------------    87
rat           --V-PVNNLNADLIQVAFFTC----------------------------------------    282
Bt            IMKKFLLN-----------------------------------PEQY-----LDKEAEEFVM    239
Bp            FTDDFLASIGKEEGQRIWYNTADGTKKGAANCAAGADPAKDANACGDAKKKIASEQDAAM    322
Bl            FTEEFLAKL--ENGEYKWYNTTDGTKKGGKNCAPGADASKDPDACGEVSKKIKSEYDAAM    323
                     .
```

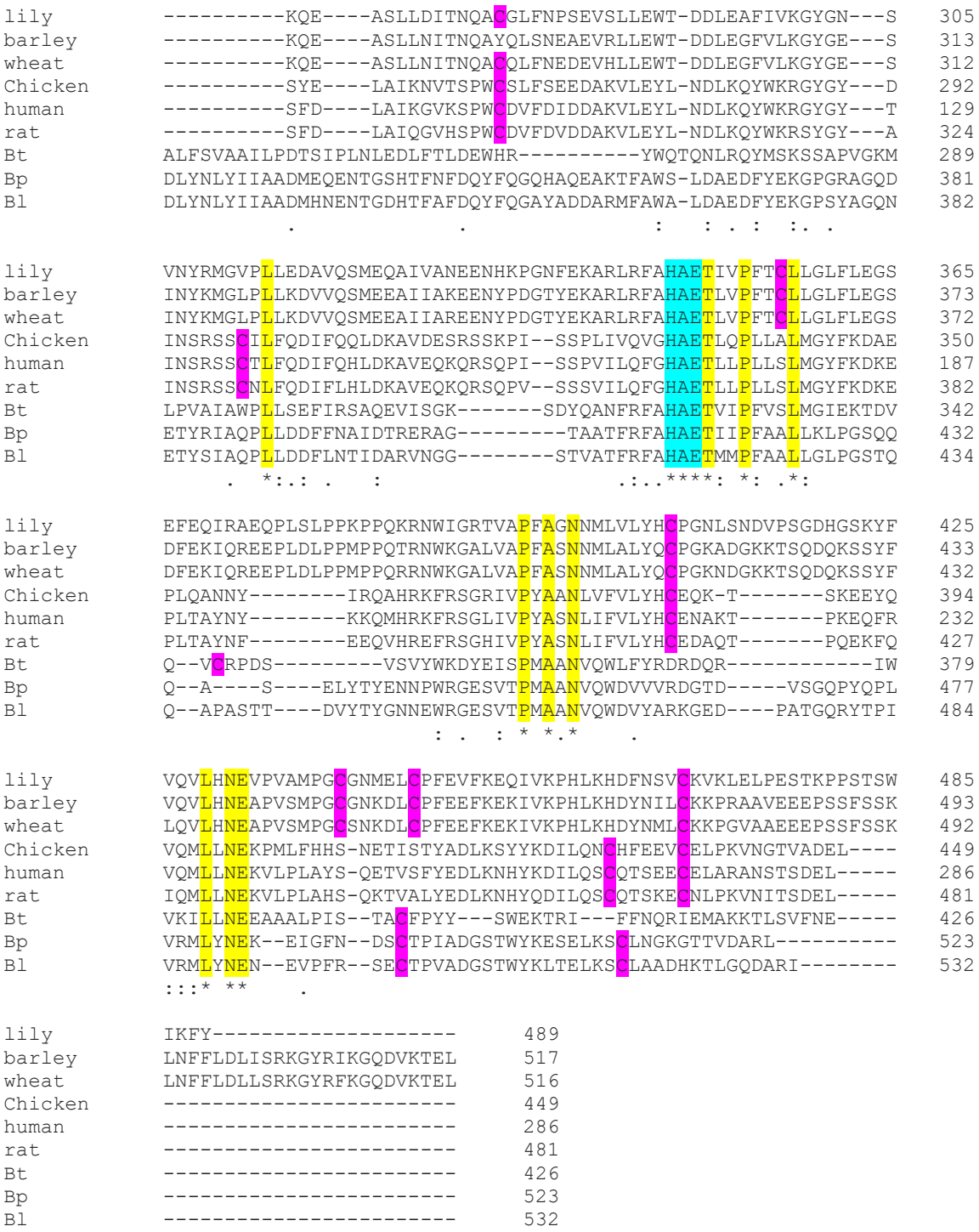

Figure 9.5 Protein sequence alignment of Minpp phytases from Bt, Bp, Bl, lilly, barley, wheat, chicken, human and rat.

Created using the online tool Clustal Omega. The catalytic motifs HAE are highlighted in blue. Cysteines are highlighted in pink. Other fully conserved sequences are highlighted in yellow.

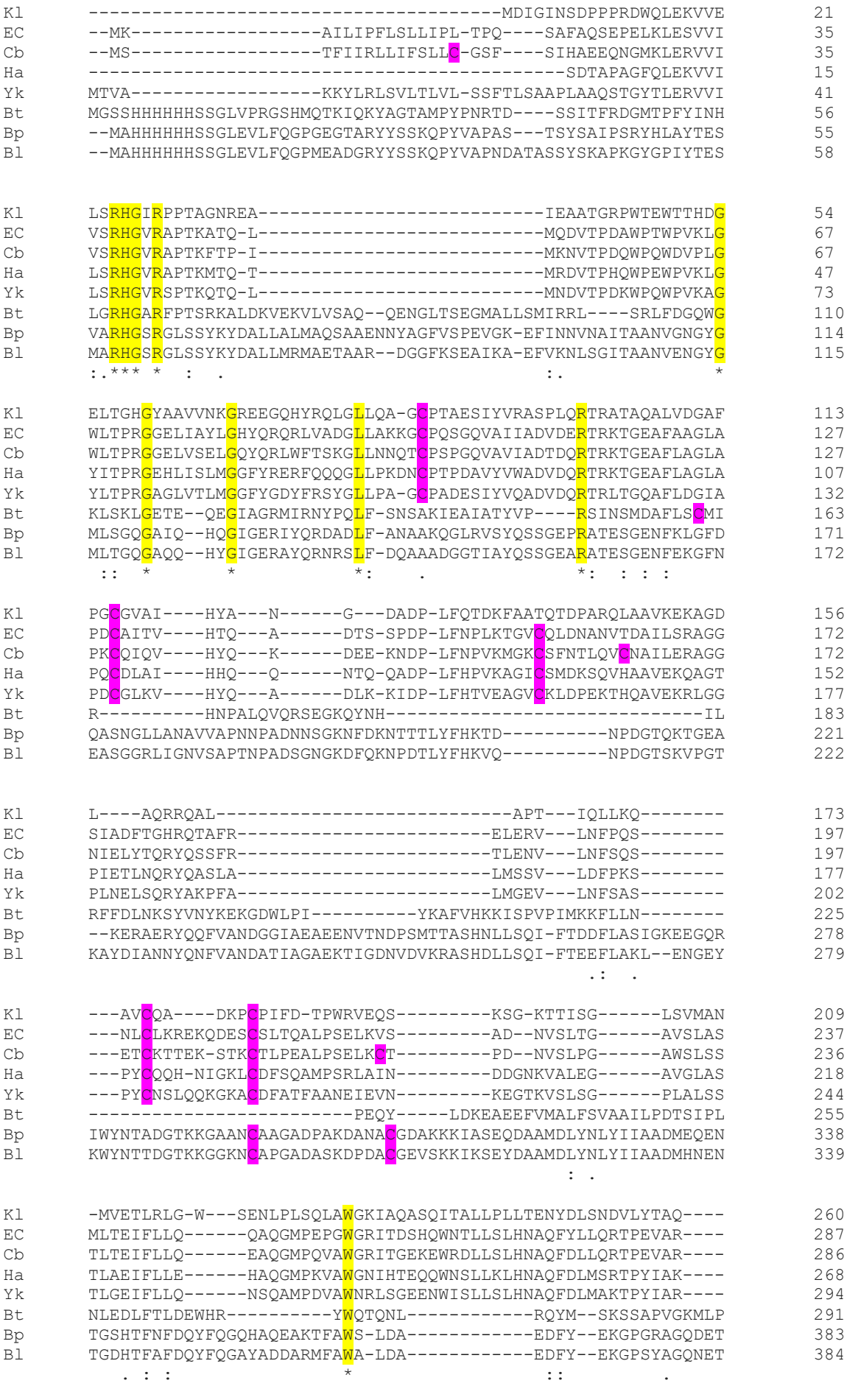
Kl -----------------------------------MDIGINSDPPPRDWQLEKVVE 21
EC --MK-----------------AILIPFLSLLIPL-TPQ----SAFAQSEPELKLESVVI 35
Cb --MS-----------------TFIIRLLIFSLLC-GSF----SIHAEEQNGMKLERVVI 35
Ha ---SDTAPAGFQLEKVVI 15
Yk MTVA-----------------KKYLRLSVLTLVL-SSFTLSAAPLAAQSTGYTLERVVI 41
Bt MGSSHHHHHHSSGLVPRGSHMQTKIQKYAGTAMPYPNRTD----SSITFRDGMTPFYINH 56
Bp --MAHHHHHHSSGLEVLFQGPGEGTARYYSSKQPYVAPAS---TSYSAIPSRYHLAYTES 55
Bl --MAHHHHHHSSGLEVLFQGPMEADGRYYSSKQPYVAPNDATASSYSKAPKGYGPIYTES 58
Kl LSRHGIRPPTAGNREA---------------------------IEAATGRPWTEWTTHDG 54
EC VSRHGVRAPTKATQ-L---------------------------MQDVTPDAWPTWPVKLG 67
Cb VSRHGVRAPTKFTP-I---------------------------MKNVTPDQWPQWDVPLG 67
Ha LSRHGVRAPTKMTQ-T---------------------------MRDVTPHQWPEWPVKLG 47
Yk LSRHGVRSPTKQTQ-L---------------------------MNDVTPDKWPQWPVKAG 73
Bt LGRHGARFPTSRKALDKVEKVLVSAQ--QENGLTSEGMALLSMIRRL----SRLFDGQWG 110
Bp VARHGSRGLSSYKYDALLALMAQSAAENNYAGFVSPEVGK-EFINNVNAITAANVGNGYG 114
Bl MARHGSRGLSSYKYDALLMRMAETAAR--DGGFKSEAIKA-EFVKNLSGITAANVENGYG 115
Kl ELTGHGYAAVVNKGREEGQHYRQLGLLQA-GCPTAESIYVRASPLQRTRATAQALVDGAF 113
EC WLTPRGGELIAYLGHYQRQRLVADGLLAKKGCPQSGQVAIIADVDERTRKTGEAFAAGLA 127
Cb WLTPRGGELVSELGQYQRLWFTSKGLLNNQTCPSPGQVAVIADTDQRTRKTGEAFLAGLA 127
Ha YITPRGEHLISLMGGFYRERFQQQGLLPKDNCPTPDAVYVWADVDQRTRKTGEAFLAGLA 107
Yk YLTPRGAGLVTLMGGFYGDYFRSYGLLPA-GCPADESIYVQADVDQRTRLTGQAFLDGIA 132
Bt KLSKLGETE--QEGIAGRMIRNYPQLF-SNSAKIEAIATYVP----RSINSMDAFLSCMI 163
Bp MLSGQGAIQ--HQGIGERIYQRDADLF-ANAAKQGLRVSYQSSGEPRATESGENFKLGFD 171
Bl MLTGQGAQQ--HYGIGERAYQRNRSLF-DQAAADGGTIAYQSSGEARATESGENFEKGFN 172
Kl PGCGVAI----HYA---N------G---DADP-LFQTDKFAATQTDPARQLAAVKEKAGD 156
EC PDCAITV----HTQ---A------DTS-SPDP-LFNPLKTGVCQLDNANVTDAILSRAGG 172
Cb PKCQIQV----HYQ---K------DEE-KNDP-LFNPVKMGKCSFNTLQVCNAILERAGG 172
Ha PQCDLAI----HHQ---Q------NTQ-QADP-LFHPVKAGICSMDKSQVHAAVEKQAGT 152
Yk PDCGLKV----HYQ---A------DLK-KIDP-LFHTVEAGVCKLDPEKTHQAVEKRLGG 177
Bt R----------HNPALQVQRSEGKQYNH-----------------------------IL 183
Bp QASNGLLANAVVAPNNPADNNSGKNFDKNTTTLYFHKTD----------NPDGTQKTGEA 221
Bl EASGGRLIGNVSAPTNPADSGNGKDFQKNPDTLYFHKVQ----------NPDGTSKVPGT 222
Kl L----AQRRQAL----------------------------APT---IQLLKQ-------- 173
EC SIADFTGHRQTAFR-------------------------ELERV---LNFPQS-------- 197
Cb NIELYTQRYQSSFR-------------------------TLENV---LNFSQS-------- 197
Ha PIETLNQRYQASLA-------------------------LMSSV---LDFPKS-------- 177
Yk PLNELSQRYAKPFA-------------------------LMGEV---LNFSAS-------- 202
Bt RFFDLNKSYVNYKEKGDWLPI----------YKAFVHKKISPVPIMKKFLLN-------- 225
Bp --KERAERYQQFVANDGGIAEAEENVTNDPSMTTASHNLLSQI-FTDDFLASIGKEEGQR 278
Bl KAYDIANNYQNFVANDATIAGAEKTIGDNVDVKRASHDLLSQI-FTEEFLAKL--ENGEY 279
Kl ---AVCQA----DKPCPIFD-TPWRVEQS---------KSG-KTTISG------LSVMAN 209
EC ---NLCLKREKQDESCSLTQALPSELKVS---------AD--NVSLTG------AVSLAS 237
Cb ---ETCKTTEK-STKCTLPEALPSELKCT---------PD--NVSLPG------AWSLSS 236
Ha ---PYCQQH-NIGKLCDFSQAMPSRLAIN---------DDGNKVALEG------AVGLAS 218
Yk ---PYCNSLQQKGKACDFATFAANEIEVN---------KEGTKVSLSG------PLALSS 244
Bt ------------------------PEQY-----LDKEAEEFVMALFSVAAILPDTSIPL 255
Bp IWYNTADGTKKGAANCAAGADPAKDANACGDAKKKIASEQDAAMDLYNLYIIAADMEQEN 338
Bl KWYNTTDGTKKGGKNCAPGADASKDPDACGEVSKKIKSEYDAAMDLYNLYIIAADMHNEN 339
Kl -MVETLRLG-W---SENLPLSQLAWGKIAQASQITALLPLLTENYDLSNDVLYTAQ---- 260
EC MLTEIFLLQ------QAQGMPEPGWGRITDSHQWNTLLSLHNAQFYLLQRTPEVAR---- 287
Cb TLTEIFLLQ------EAQGMPQVAWGRITGEKEWRDLLSLHNAQFDLLQRTPEVAR---- 286
Ha TLAEIFLLE------HAQGMPKVAWGNIHTEQQWNSLLKLHNAQFDLMSRTPYIAK---- 268
Yk TLGEIFLLQ------NSQAMPDVAWNRLSGEENWISLLSLHNAQFDLMAKTPYIAR---- 294
Bt NLEDLFTLDEWHR----------YWQTQNL------------RQYM--SKSSAPVGKMLP 291
Bp TGSHTFNFDQYFQGQHAQEAKTFAWS-LDA------------EDFY--EKGPGRAGQDET 383
Bl TGDHTFAFDQYFQGAYADDARMFAWA-LDA------------EDFY--EKGPSYAGQNET 384

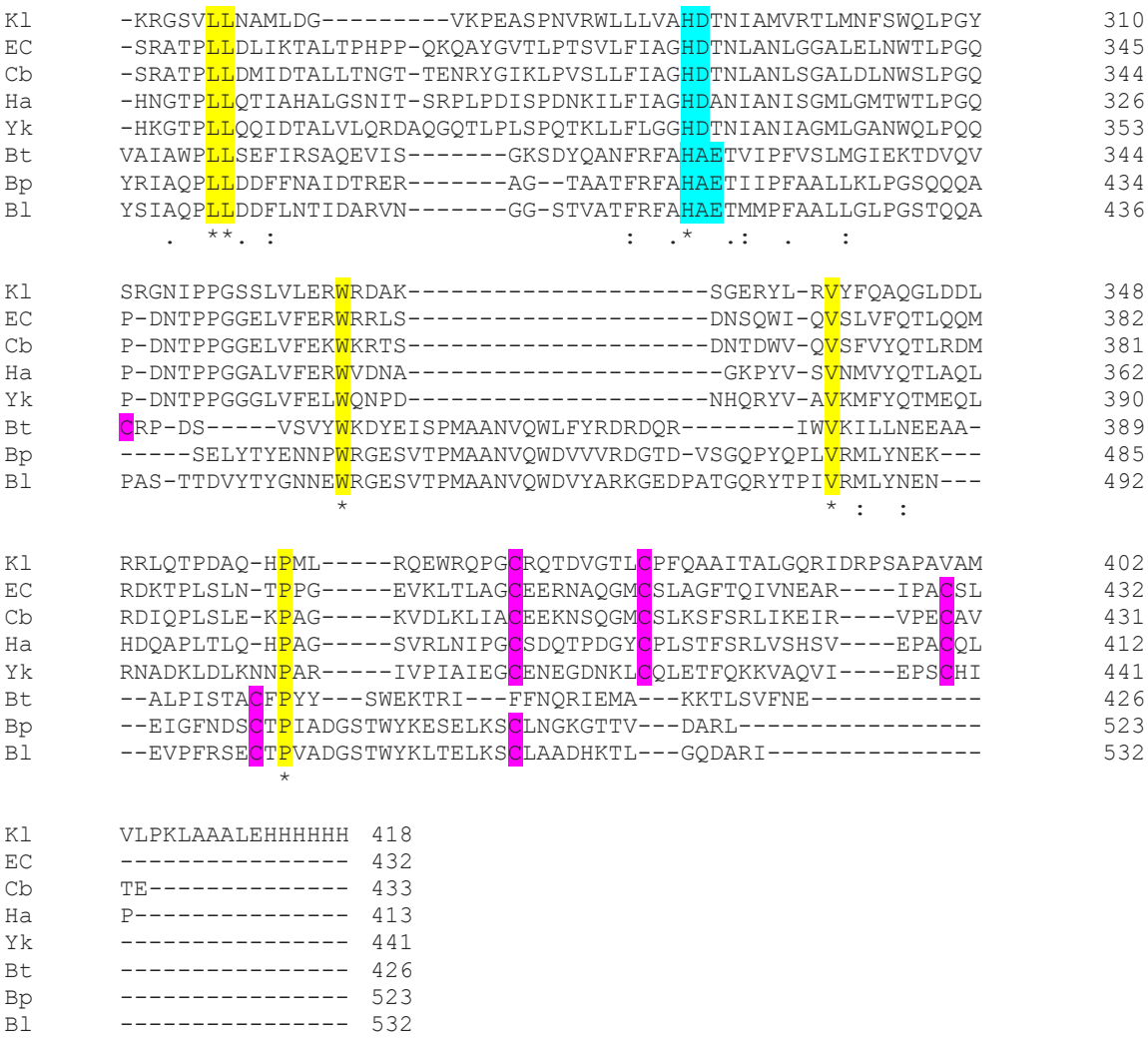

Figure 9.6 Protein sequence alignment of bacterial HAP phytases

Kl: *Klebsiella* sp ASR1; Ec: *E.coli*; Cb: *C.braakii*; Ha: *H.alvei*; Yk: Y.*kristensenii*; Bt: *B.thetaiotaomicron*; Bp: B.*pseudocatenulatum*; Bl: *B.longum*. Created using the online tool Clustal Omega. The catalytic motifs HAE and HD are highlighted in blue. Cysteines are highlighted in pink. Other fully conserved sequences are highlighted in yellow.

9.3 Appendix 3. Protein purification images.

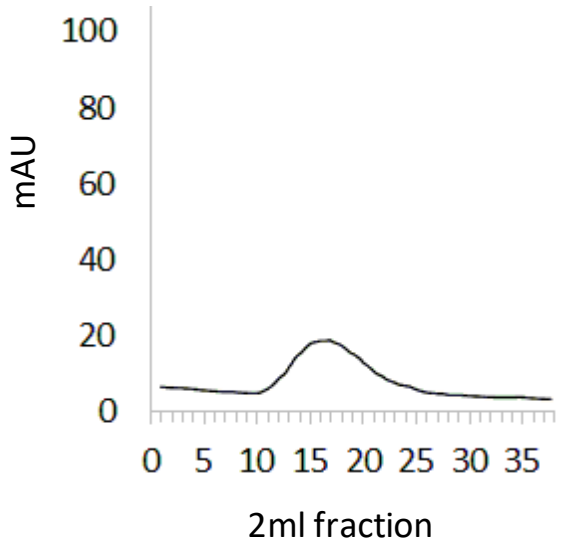

Figure 9.7 Bifidobacterium pseudocatenulatum phytase His-tag purification using imidazole elution.

Fractions 15-18 were collected and used for further purification.

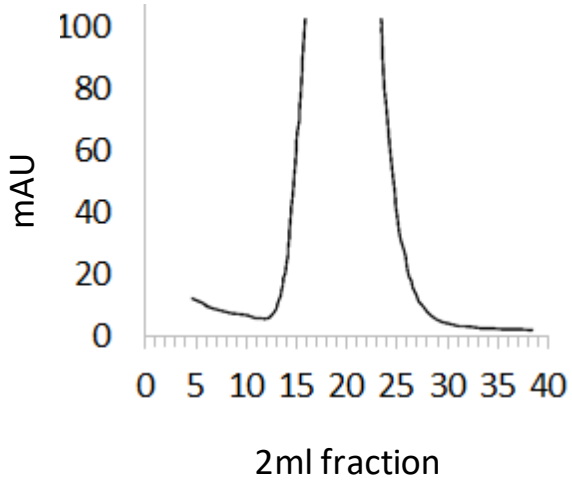

Figure 9.8 Bacteroides thetaiotaomicron phytase His-tag purification using imidazole elution.

Fractions 16-25 were collected and used for further purification.

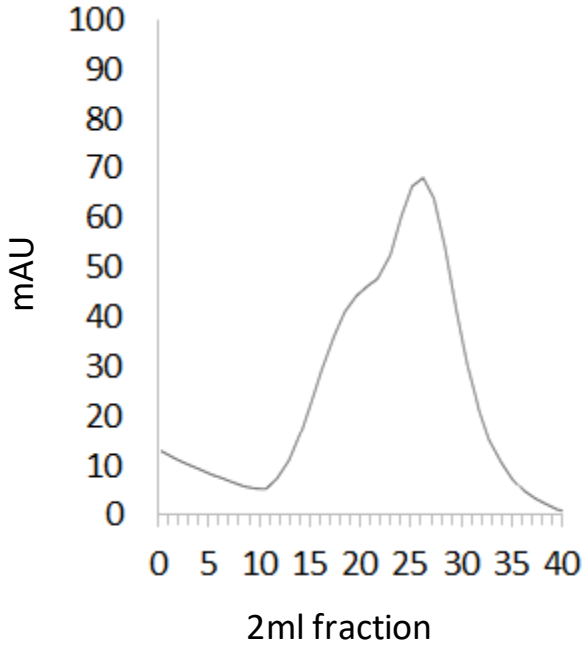

Figure 9.9 Active site mutant E401Q of the Bifidobacterium longum phytase His-tag purification using imidazole elution.

Fractions 23 – 40 were collected and used for further purification.

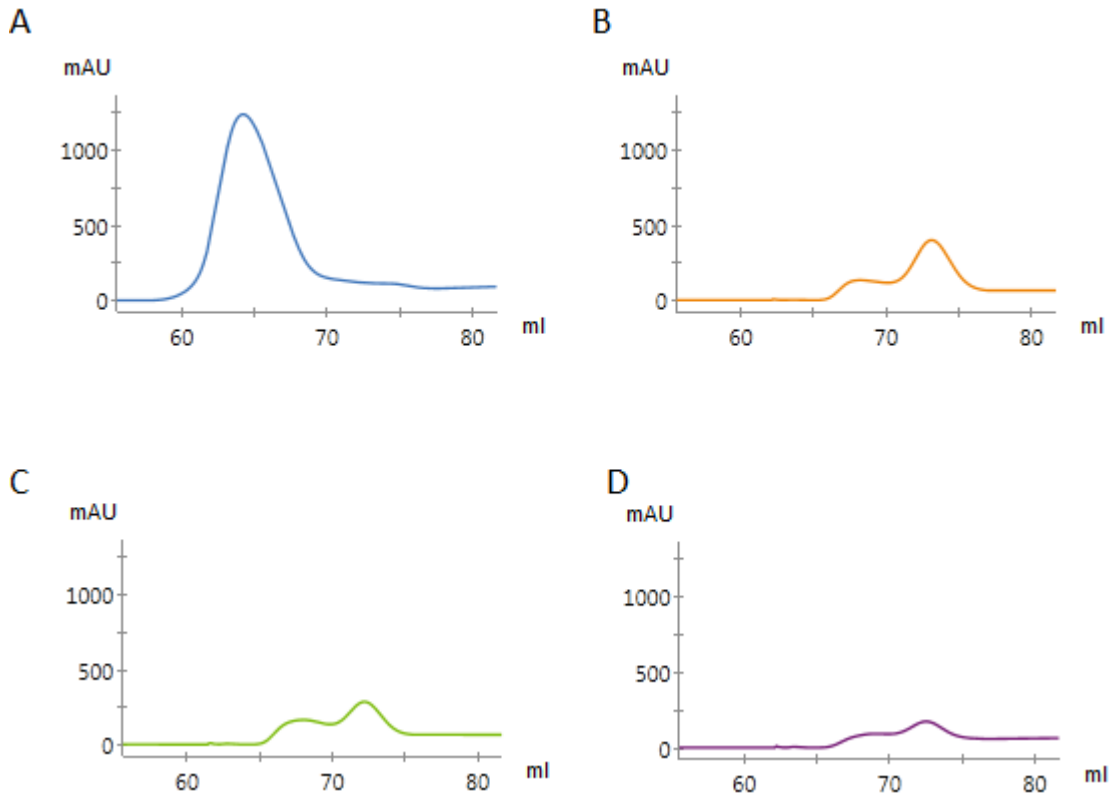

Figure 9.10 Bifidobacterium longum phytase variants His-tag purification using imidazole elution.

A. Wild-type phytase. Fractions from 62-68 ml were collected and used for further purification. B. Disulphide knockout mutant D1. Fractions from 72-76 ml were collected and used for further purification. C. Disulphide knockout mutant D2. Fractions from 72-76 ml were collected and used for further purification. D. Double disulphide knockout mutant D1D2. Fractions from 72-76 ml were collected and used for further purification.

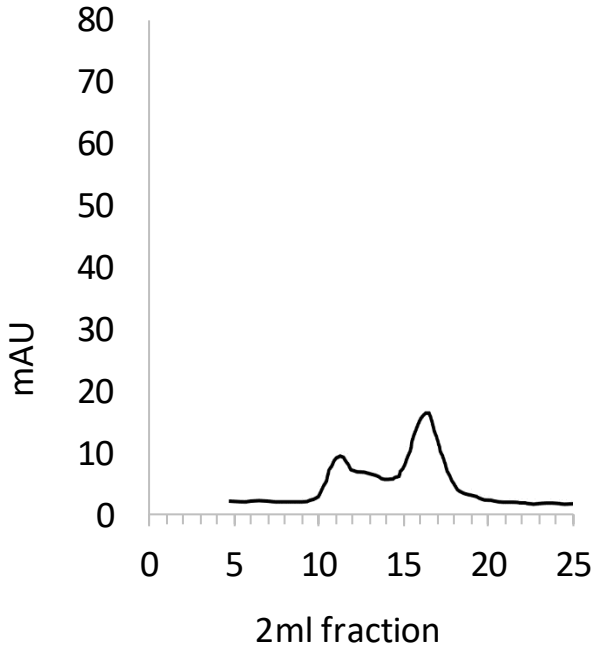

Figure 9.11 Bifidobacterium pseudocatenulatum phytase gel filtration purification.

Fractions 15-18 were collected, concentrated and used for experiments.

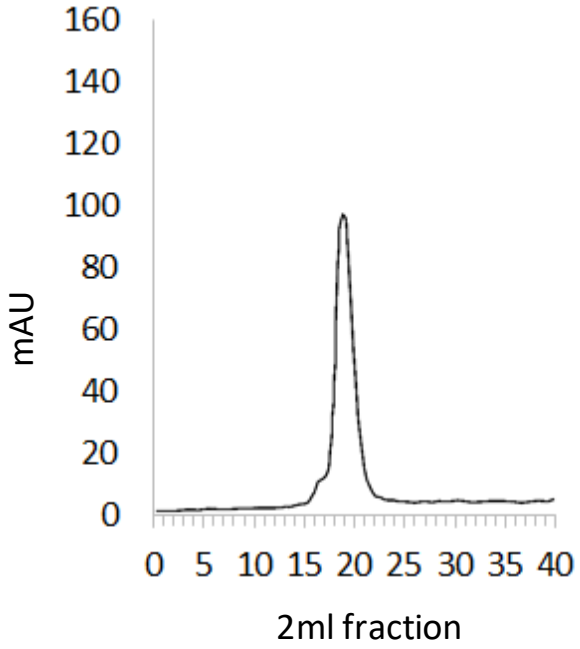

Figure 9.12 Bacteroides thetaiotaomicron phytase gel filtration purification.

Fractions 17-21 were collected, concentrated and used for experiments.

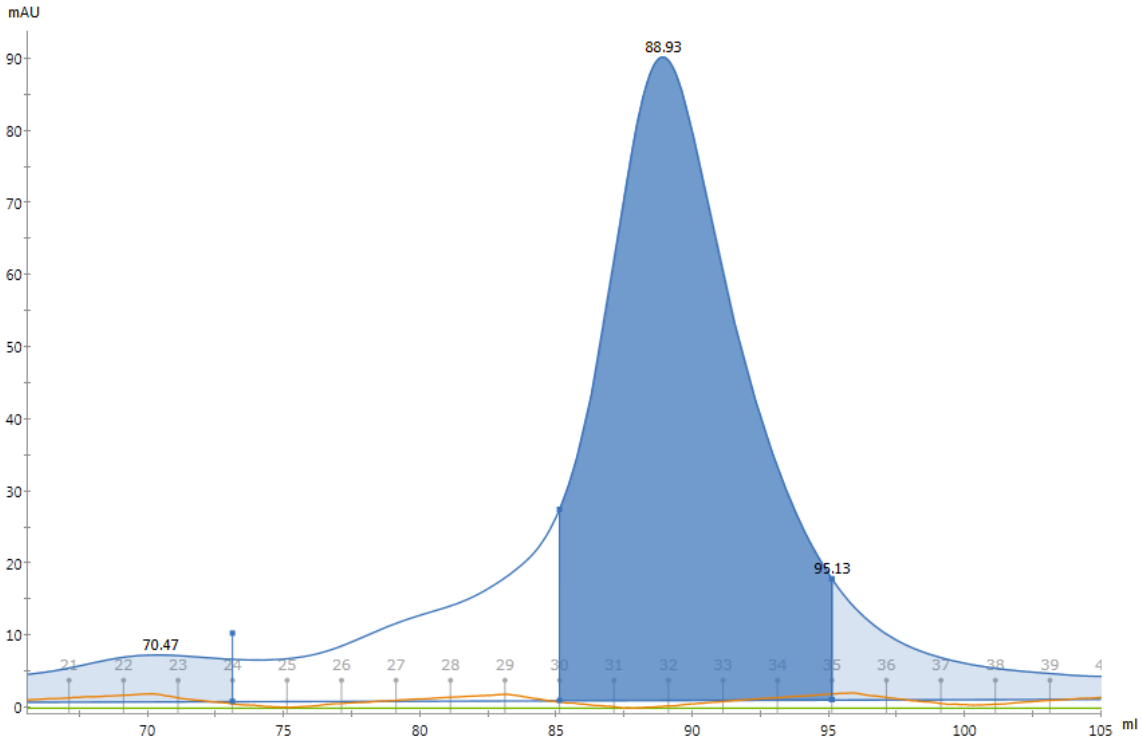

Figure 9.13 Active site mutant E401Q of the Bifidobacterium longum phytase gel filtration purification.

Fractions 30-35 were collected, concentrated and used for experiments.

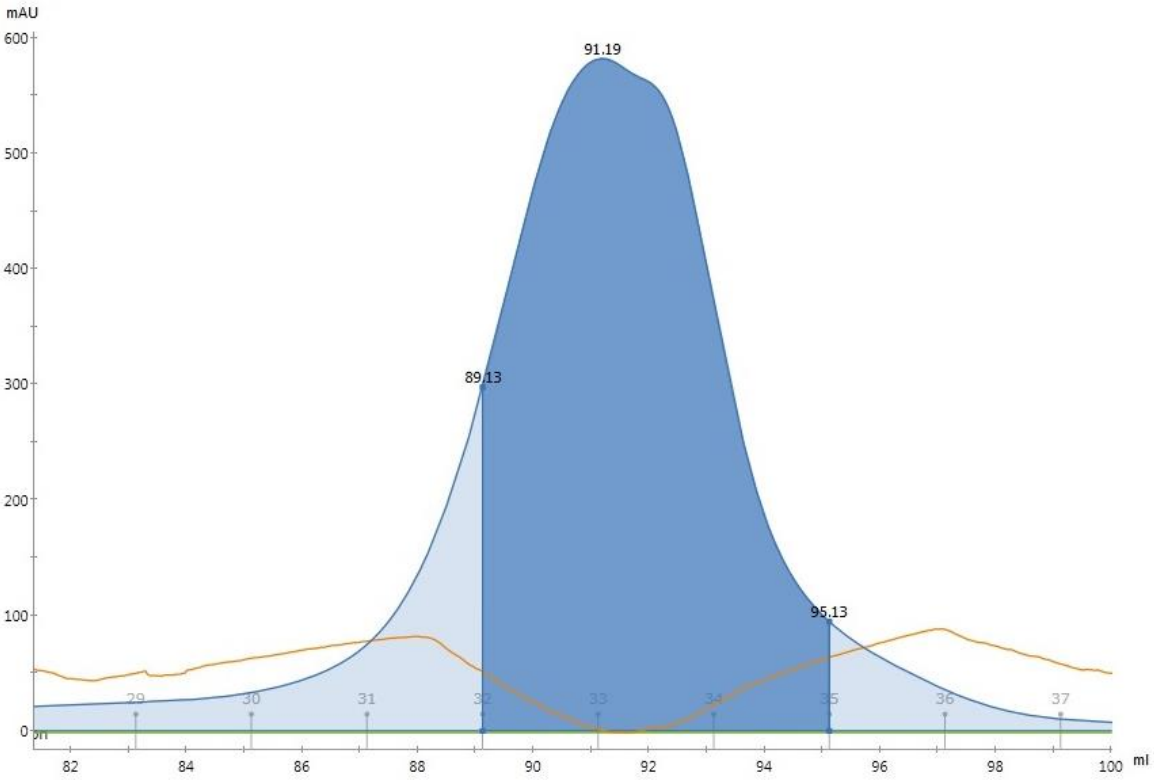

Figure 9.14 Wild-type Bifidobacterium longum phytase gel filtration purification.

Fractions 32-35 were collected, concentrated and used for experiments.

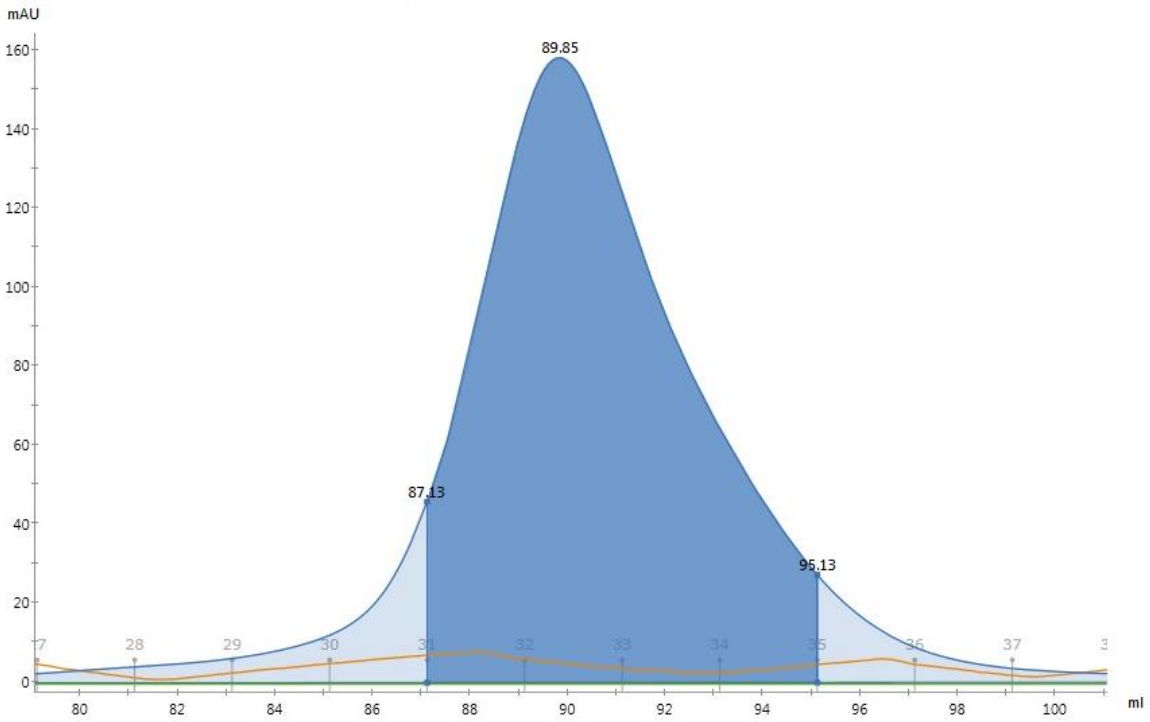

Figure 9.15 Disulphide knockout D1 mutant of Bifidobacterium longum phytase gel filtration purification.

Fractions 31-35 were collected, concentrated and used for experiments.

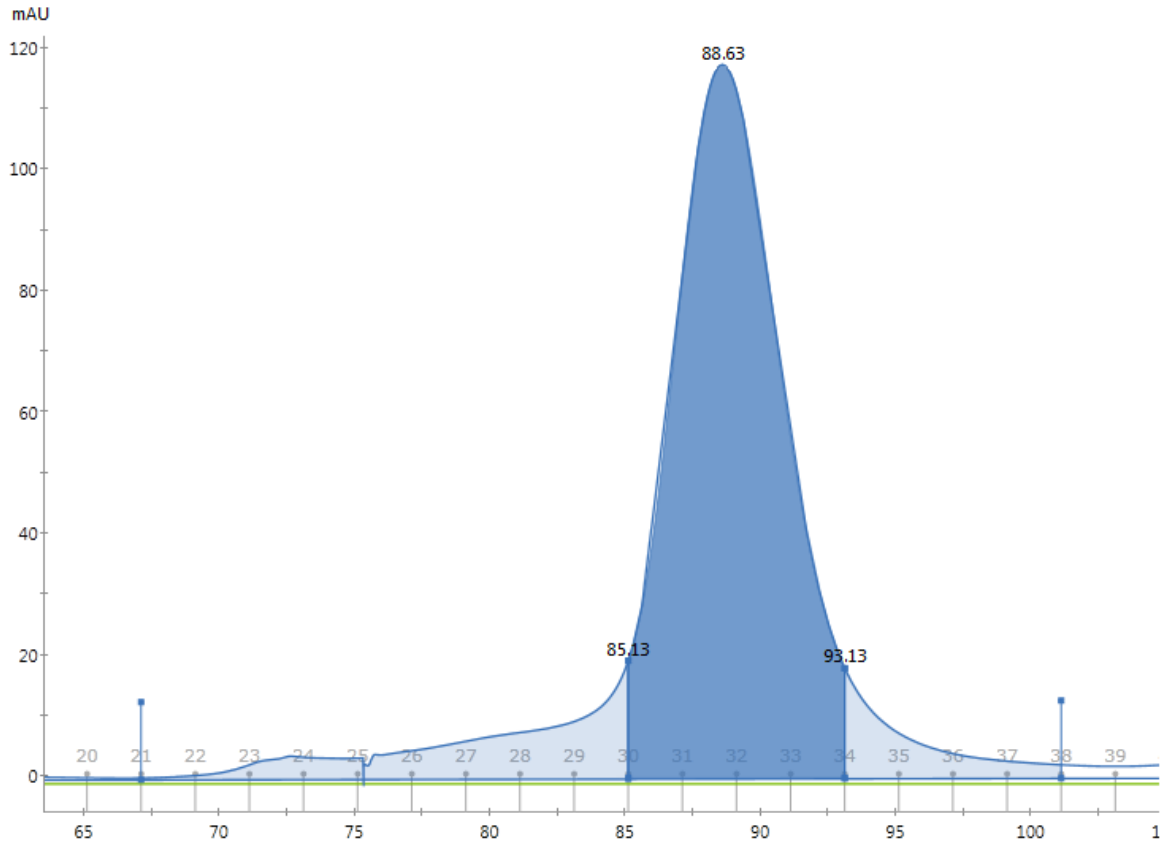

Figure 9.16 Disulphide knockout D2 mutant of Bifidobacterium longum phytase gel filtration purification.

Fractions 30-34 were collected, concentrated and used for experiments.

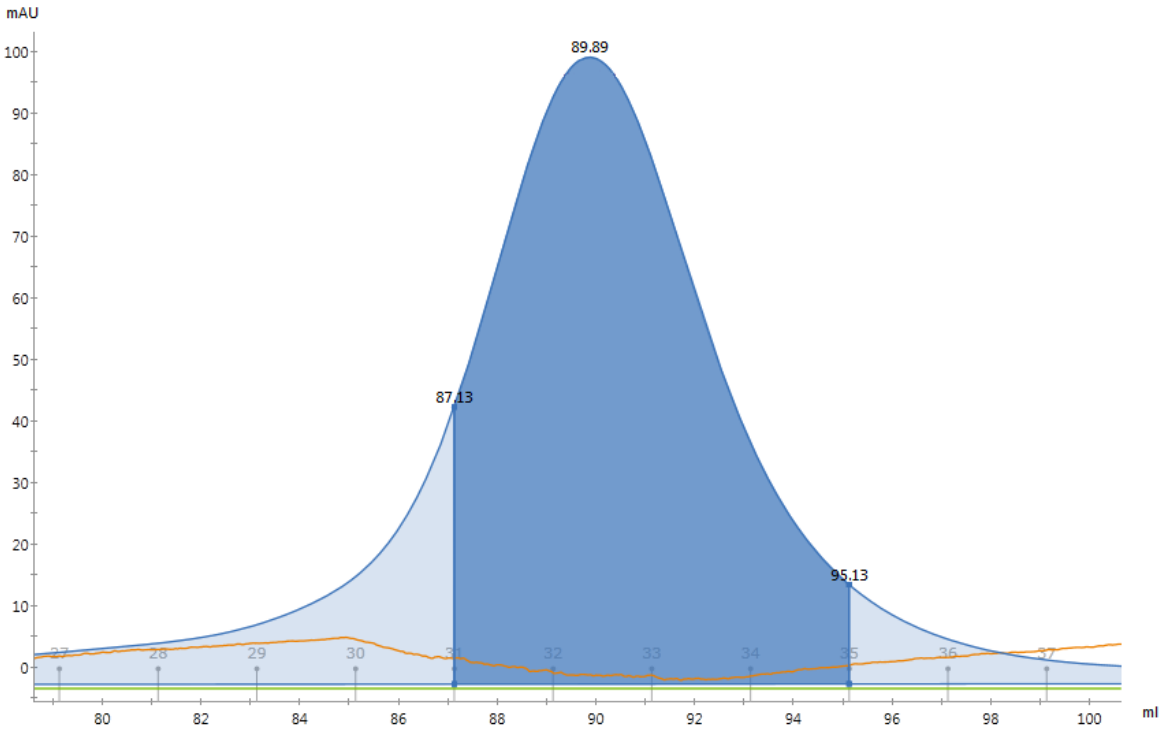

Figure 9.17 Double disulphide knockout D1D2 mutant of Bifidobacterium longum phytase gel filtration purification.

Fractions 31-35 were collected, concentrated and used for experiments.

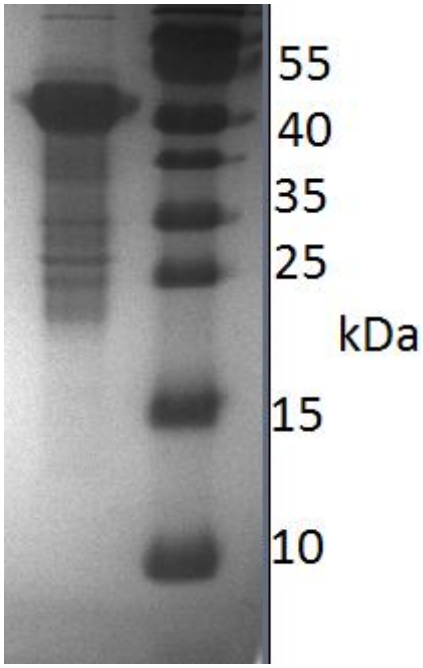

Figure 9.18 SDS-PAGE gel image of the purified Bifidobacterium pseudocatenulatum phytase.

Lane 1: 23 µg of the purified and concentrated protein. Lade 2: Molecular weight ladder used was PageRuler Prestained Protein Ladder (ThermoScientific).

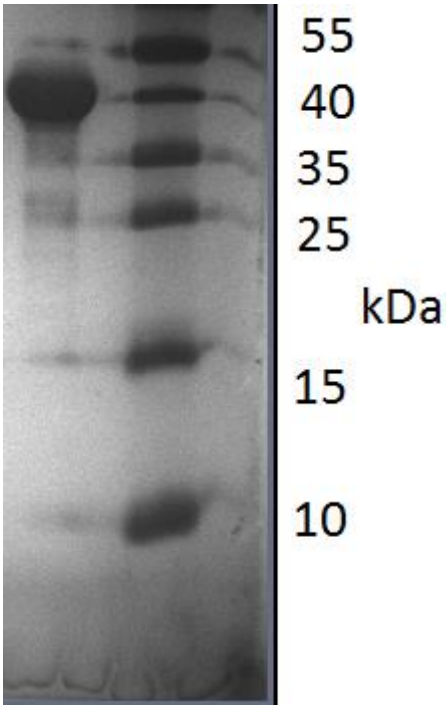

Figure 9.19 SDS-PAGE gel image of the purified Bacteroides thetaiotaomicron phytase.

Lane 1: 9 µg of the purified and concentrated protein. Lade 2: Molecular weight ladder used was PageRuler Prestained Protein Ladder (ThermoScientific).

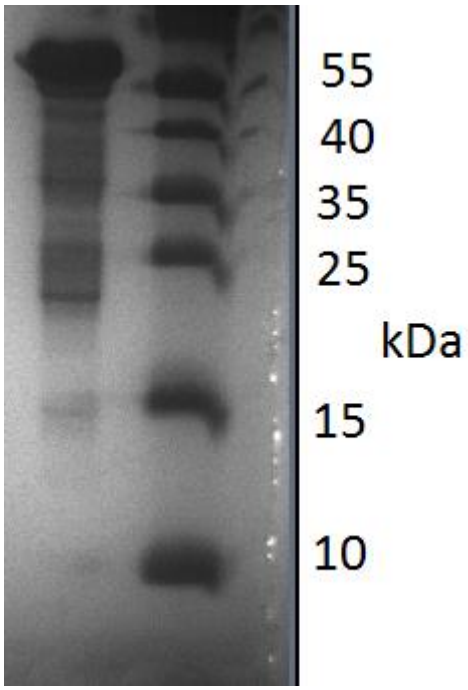

Figure 9.20 SDS-PAGE gel image of the purified Bifidobacterium longum phytase.
Lane 1: 45 µg of the purified and concentrated protein. Lade 2: Molecular weight ladder used was PageRuler Prestained Protein Ladder (ThermoScientific).

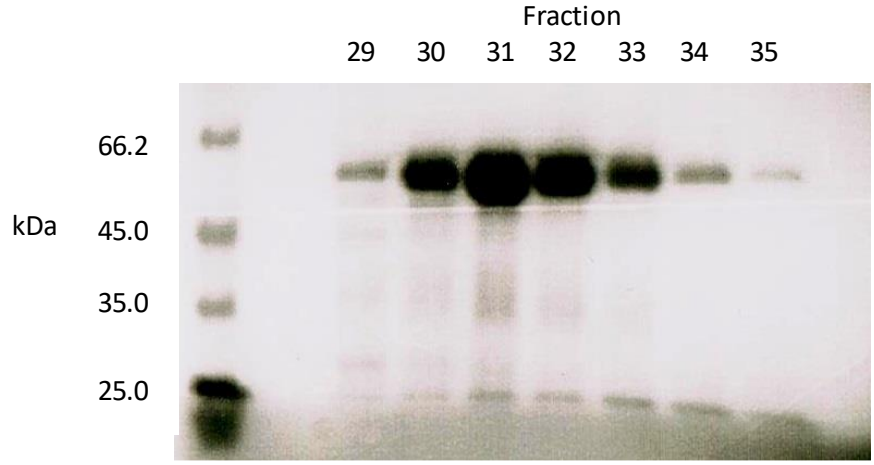

Figure 9.21 SDS-PAGE gel image of the gel purification fractions of the D1 disulphide mutant of the Bifidobacterium longum phytase.
Lane 1: Molecular weight ladder used was NEB Protein Marker Broad Range. Fractions 30-33 were concentrated and used for experiments.

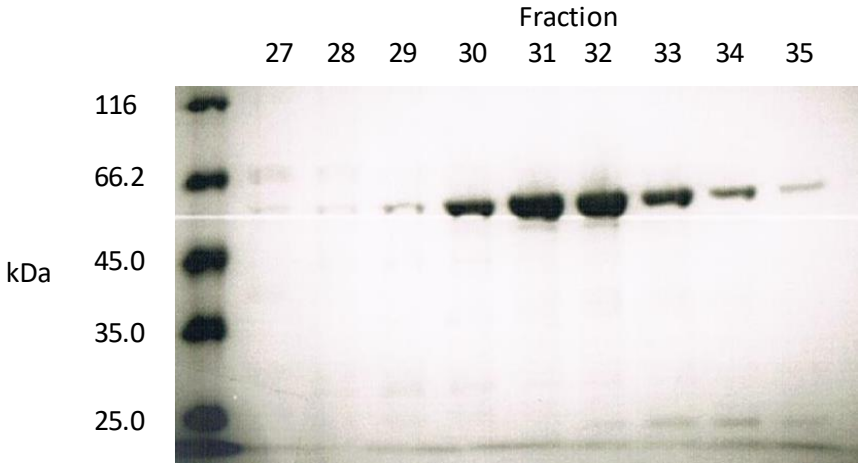

Figure 9.22 SDS-PAGE gel image of the gel purification fractions of the D2 disulphide mutant of the Bifidobacterium longum phytase.

Lane 1: Molecular weight ladder used was NEB Protein Marker Broad Range. Fractions 30-33 were concentrated and used for experiments.

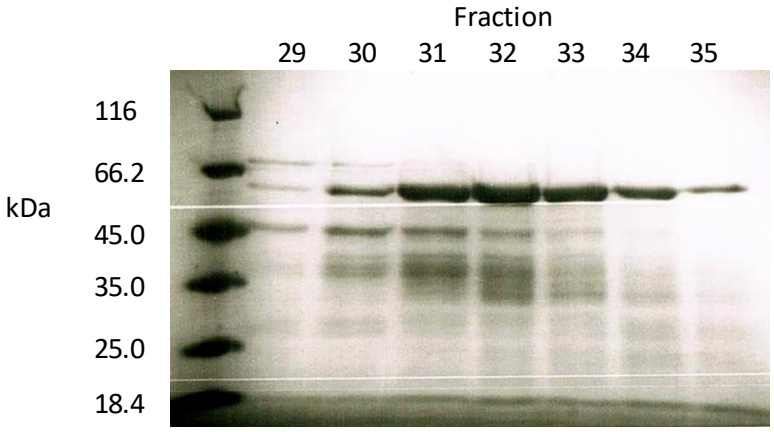

Figure 9.23 SDS-PAGE gel image of the gel purification fractions of the double D1D2 disulphide mutant of the Bifidobacterium longum phytase.

Lane 1: Molecular weight ladder used was NEB Protein Marker Broad Range. Fractions 31-35 were concentrated and used for experiments.